Coffin, M.F., Frey, F.A., Wallace, P.J., et al., 2000
Proceedings of the Ocean Drilling Program, Initial Reports Volume 183

9. Sites 1141 and 1142[1]

Shipboard Scientific Party[2]

BACKGROUND AND OBJECTIVES

Sites 1141 and 1142 are situated near the crest of Broken Ridge ~350 km east of Deep Sea Drilling Project (DSDP) Site 255 and Ocean Drilling Program (ODP) Sites 752, 753, 754, and 755 (Fig. F1). Flanked to the south by Eocene and earlier oceanic crust of the Australia-Antarctic Basin and to the north by Cretaceous oceanic crust of the Wharton Basin, Broken Ridge appears to have formed during Late Cretaceous time as a result of Kerguelen hot spot magmatism (Duncan, 1991; Duncan and Storey, 1992). Subsequently, Broken Ridge and the Kerguelen Plateau began to separate along the nascent Southeast Indian Ridge at ~40 Ma. Igneous basement of Broken Ridge has not been sampled previously by drilling; dredge samples from three locations along the feature's southern faulted boundary yield dates of ~62, ~83, and 88–89 Ma (Duncan, 1991). Because of the scatter in ages of the dredged rocks and the absence of in situ basement samples from Broken Ridge, knowledge of Broken Ridge's age and composition remains extremely limited. We located Sites 1141 and 1142 on *JOIDES Resolution* single-channel seismic line JR183-101 (Fig. F2). Sites 1141 and 1142 lie at depths of 1197 and 1201 m, respectively, ~3–4 km north of the crest of Broken Ridge. We chose this location primarily on the basis of its thin sedimentary section (Fig. F3). The top of acoustic basement is flat lying at Site 1141 but has an apparent dip of 2.5° to the north-northeast at Site 1142. A sediment sequence ~100 m thick overlies igneous basement at both sites.

Summary of Objectives

The main objectives at this site were to

1. Characterize the petrography and compositions of the lavas;

F1. Satellite-derived free-air gravity map of Broken Ridge, **p. 43.**

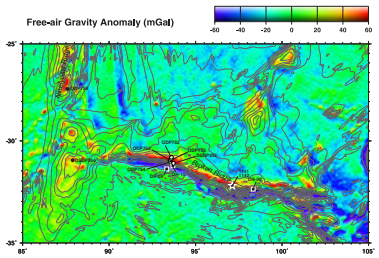

F2. Location of Sites 1141 and 1142 relative to site-survey data, **p. 44.**

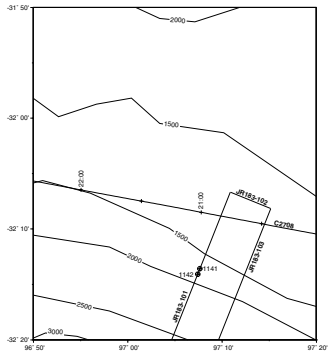

F3. *JOIDES Resolution* JR183-101 single-channel seismic profile across Sites 1141 and 1142, **p. 45.**

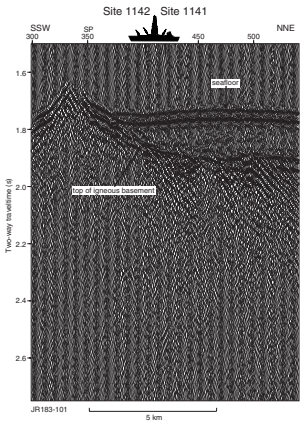

[1]Examples of how to reference the whole or part of this volume.
[2]Shipboard Scientific Party addresses.

2. Determine the age of the lavas, testing the hypothesis that the uppermost igneous basement of eastern Broken Ridge is ~85 Ma, similar to that of the central Kerguelen Plateau (CKP) (Duncan, 1991; Duncan and Storey, 1992; Pringle et al., 1994; Storey et al., 1996).
3. Determine the physical characteristics of the lava flows;
4. Identify the environment of eruption (subaerial or submarine);
5. Obtain minimum estimates for the age of basement from overlying sediment;
6. Estimate the duration of possible subaerial and shallow marine environments from the sedimentary and igneous record;
7. Determine the facies of the seismic stratigraphic sequences;
8. Define the ages of seismic sequence boundaries;
9. Determine the paleoceanographic history of this temperate latitude site.

OPERATIONS

Site 1141

The 2880-km transit from Site 1140 on the northern Kerguelen Plateau to the starting point of the seismic survey on Broken Ridge was made in 135.7 hr at an average speed of 11.5 kt. At 1915 hr on 2 February 1999, we slowed to deploy the seismic equipment, and, at 2015 hr, we crossed over the first way point of the desired seismic line. Before selecting the Site 1141 drill site, a 85-km (7 hr) seismic survey was conducted using the ship's single-channel seismic streamer. By 0215 hr on 3 February 1999, the survey was completed. The ship continued on course until the seismic gear was recovered and then resumed full speed for the selected drilling location. Within 1.3 hr, the ship arrived at the new location. At 0330 hr on 3 February 1999, we deployed a beacon on the precise Global Positioning System (GPS) coordinates for Site 1141.

Hole 1141A

We spudded Hole 1141A at 0815 hr on 3 February 1999. The seafloor depth adjusted to the rig floor was estimated at 1209.0 m below rig floor (mbrf) based on a hard "tag" indication by the driller. This yields a seafloor depth of 1196.9 m below sea level (mbsl). The 3.5-kHz precision depth recorder (PDR) had indicated an adjusted seafloor depth of 1212.4 mbrf.

The first two cores contained foraminifer nannofossil ooze largely composed of sand-sized foraminifers. Recovery was low in this material. Continuous wireline coring proceeded without incident through Core 183-1141A-10R to a depth of 94.2 meters below seafloor (mbsf). After the first two cores, recovery averaged 72% but was quite variable, ranging from 0% to 104%. The formation then graded into foraminifer chalk with abundant scattered chert through Core 183-1141A-11R. Core 183-1141A-12R contained no recovery. Core 183-1141A-13R contained only a few centimeter-sized pieces of gabbro. The next interval (Core 183-1141A-14R) cored slowly and marked the first contact with the volcanic basement rocks at a depth of 113.5 mbsf. Coring operations were temporarily interrupted at 0500 hr on 4 February 1999 when the core winch electrically shut down. After repairing the electrical problem, coring proceeded through five separate flows of aphyric to

sparsely plagioclase-phyric basalt to a depth of 185.6 mbsf. Recovery in basement averaged 55% (cutting half cores), and the rate of penetration (ROP) averaged 2.9 m/hr. At this point, hole conditions were excellent. Summaries of core numbers, depths, and recovery are given in Tables T1 and T2.

T1. Coring summary for Sites 1141 and 1142, p. 120.

T2. Expanded coring summary for Sites 1141 and 1142, p. 121.

While drilling Core 183-1141A-24R, a 20-bbl sweep of sepiolite mud was circulated and displaced out of the hole. The sinker bars were installed, and the core was retrieved without incident. After laying out the core, a fresh barrel was dropped, the drill string was made up, and circulation was established. Immediately upon picking the drill string up off the elevators, the pipe was stuck. Attempts to gain rotation were unsuccessful and circulating pressure was ~500 psi higher than normal. The drill bit was at 179.0 mbsf, or 6.6 m above the bottom of the hole, when the drill string became stuck.

A 60-bbl sepiolite sweep was circulated while we attempted to work the drill string free. Initial attempts to free the drill string were made by setting the pipe in compression and applying 700 A of torque. After numerous unsuccessful attempts to break the string free, overpulls were applied in gradual 20,000-lb increments up to 100,000 lb of overpull with 700 A of torque. Torque was released and overpull was gradually increased to 300,000 lb. A single joint of drill pipe was slowly worked out of the hole and laid out. As we were able to move the drill string slowly upward, we decided not to expend the wireline time required to retrieve the empty core barrel, as this would have resulted in minimal circulation and could have jeopardized further drill-string movement. Another 2.5 m was pulled up with 300,000 lb overpull before the pipe became totally stuck at 166.9 mbsf. While we attempted to free the drill string, 180 bbl of bentonite gel mud was swept at 140 strokes per minute at 2500 psi. Circulating pressures were higher than normal, indicating that there was some packing off of the drill string. While attempting to free the pipe, 1000 A of rotary torque was applied. The maximum overpull used, with no torque in the drill string, was 300,000 lb. With all efforts at freeing the drill string unsuccessful, there was no other alternative left but to explosively sever the pipe. This ended coring operations at a total depth of 185.6 mbsf, or 71.1 m into basement. A total of 96.79 m of core was recovered from the hole for an overall average of 52.2%.

The severing charge was run in and was fired at the box end of the transition drill collar, which was at 53.6 mbsf. Drill string overpull was 100,000 lb above the new calculated string weight of 240,000 lb when the severing charge was fired. A loss of 100,000 lb was immediately noticed upon detonation, and the remaining string came free. The wireline was then retrieved and rigged down, and the drill string was pulled clear of the seafloor at 1330 hr on 5 February 1999.

While the drill string was being tripped, the positioning beacon was released and recovered. A new drill site was identified by the co-chief scientists, and the vessel was moved using the dynamic positioning system thrusters ~800 m to Site 1142. This move took ~30 min and was completed before the drill string trip was completed. Hole 1141A officially ended at 1615 hr on 5 February 1999 when the severed end of the lower 5½-in drill-pipe transition joint cleared the rotary table.

Hole 1142A

The positioning beacon was deployed on this site while the pipe was still being tripped back to the drill ship. The beacon was deployed at

1500 hr on 5 February 1999 on the precise GPS coordinates for Site 1142.

We spudded Hole 1142A at 2330 hr on 5 February 1999. The seafloor depth adjusted to the rig floor was estimated at 1213.0 mbrf based, once again, on a hard "tag" indication by the driller. This yields a seafloor depth of 1200.8 mbsl. The 3.5-kHz PDR had indicated an adjusted seafloor depth of 1216.4 mbrf.

Because the objective was basalt and the sedimentary sequence had already been cored in Hole 1141A, we were given permission from ODP headquarters at Texas A&M University to drill through the overlying sediments. The driller washed/drilled with a wash barrel in place for 119 min rotating time (45.9 m/hr) until the formation became firm at a depth of 91.0 mbsf. The wash barrel (1W) was recovered and Core 183-1142A-2R was cut in aphyric to moderately plagioclase-phyric basalt. Coring continued in this formation, with much of the recovered basalt totally altered to brown clay. Recovery was highly variable and generally low (13.0% to 84.4%). Even cutting half cores only resulted in an overall recovery of 34.4% for the section. The ROP was also highly variable, ranging from 2.3 to 7.7 m/hr, and averaging 3.7 m/hr overall.

Before completion of Core 183-1142A-10R, a 20-bbl sweep of sepiolite mud was circulated and displaced out of the hole. The sinker bars were installed and the core was retrieved without incident. After laying out the core, the drill string was immediately made up and circulation was established. As in the last hole, upon picking the drill string up off the elevators, the pipe became stuck. This time rotation was possible but upward travel of the drill string was not possible. The drill bit was at ~6.0 m above the bottom of the hole when the drill string became stuck.

The stuck pipe was worked from 125.6 to 106.3 mbsf. Circulation and rotation were possible with high, erratic torque. We were unable to come up without stalling the top drive. Maximum amperage on the top drive was 1000 and maximum overpull used was 80,000 lb. The pipe was eventually worked free by going gradually down with the bit. At that point, <3 hr of coring time remained in the schedule, so further coring operations were suspended. Total depth of the hole was 141.9 mbsf, or 50.9 m into basement. A total of 17.54 m of core was recovered from the hole for an overall average of 34.4%. Summaries of core numbers, depths, and recovery are given in Tables **T1** and **T2.**

The pipe was pulled out of the hole using the top drive, clearing the seafloor at 0400 hr on 7 February 1999. The forward core line was subsequently run in the hole and coated with compound L corrosion inhibitor. The core barrels were stored away, and the drill string was tripped the remaining distance out of the hole while corrosion inhibitor was applied. During the pipe trip, the positioning beacon was released and recovered at 0615 hr. The bottom-hole assembly was broken down and all drill collars racked and secured in the forward collar rack. With the bit at the rig floor at 1055 hr, the remaining thrusters were pulled and the rig was secured for transit.

At 1100 hr on 7 February 1999, we were under way for Fremantle, Australia.

LITHOSTRATIGRAPHY

Introduction

Site 1141 is located in 1197 m of water near the crest of Broken Ridge. Hole 1141A was rotary cored continuously to a depth of 185.60 mbsf. Sediments were recovered from 0 to 103.80 mbsf. Altered and relatively fresh basalts were recovered from the lower 72.1 m of the hole (Fig. **F4;** Table **T3**). The sedimentary section above igneous basement, lithologic Unit I, consists entirely of pelagic sediments. The basement volcanic rocks are designated lithologic Unit II and are subdivided into basement Units 1–6 (Fig. **F4,** Table **T3**) (see **"Igneous Petrology,"** p. 22, **"Physical Volcanology,"** p. 12, and **"Alteration and Weathering,"** p. 30, for descriptions). Core recovery in Hole 1141A ranged from excellent to poor (Fig. **F4**).

F4. Composite stratigraphic section for Site 1141, **p. 46.**

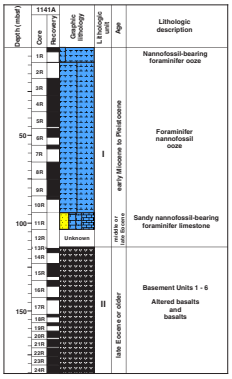

T3. Summary of lithologic units at Sites 1141 and 1142, **p. 124.**

T4. XRD results and carbonate contents for Hole 1141A, **p. 125.**

Unit I

Interval: 183-1141A-1R-1, 0 cm, to 11R-CC, 6 cm
Depth: 0 to 113.50 mbsf
Age: Pleistocene to late or middle Eocene

Unit I consists predominantly of homogeneous white (N9) foraminifer nannofossil ooze of Pleistocene to middle Miocene age (Fig. **F4;** Table **T3**). The $CaCO_3$ content of Unit I is uniformly high and ranges from 95 to 96 wt% (Table **T4**). Rare black sand is disseminated throughout Cores 183-1141A-4R and 5R. X-ray diffraction (XRD) analyses show that only calcite is present, except for Section 183-1141A-1R-1, which is ~1% aragonite (Table **T4**). Drilling disturbance is generally minimal, except for short soupy and slightly disturbed intervals in Cores 183-1141A-1R through 4R.

Core 183-1141A-1R consists of light pale brown nannofossil-bearing foraminifer ooze that is predominantly composed of sand-sized foraminifers and rare shell fragments. Clay- to silt-sized foraminifers (juveniles) and other particles constitute <10% of the sediment. Interval 183-1141A-1R-1, 0 cm, to 2R-2, 26 cm, appears to be a single bed that displays slight normal size grading. Interval 183-1141A-1R-2, 26 cm, to 1R-CC, 16 cm, contains the top of a second bed that appears to display slight normal size-grading. In the top few centimeters of this interval, fine-grained white ooze with abundant nannofossils grades downward into light pale brown ooze composed mostly of sand-sized foraminifers.

The base of Unit I is marked by a layer of sandy nannofossil-bearing foraminifer limestone of late or middle Eocene age. The thickness of this layer is uncertain as only two small fragments were recovered (interval 183-1141A-11R-CC, 0–6 cm). This sediment has an indurated matrix composed of foraminifer tests and lesser amounts of silt- to sand-sized calcareous test fragments and particles. This matrix contains abundant sand- to pebble-sized rock fragments and mineral grains. The sand-sized grains are mainly quartz. Subrounded to well-rounded pebbles, as much as 1 cm in diameter, are composed mainly of chert, silicified sedimentary rock, ferromanganese-encrusted light gray porcellanite, and rare altered basalt. One of the core fragments is partially covered by a ferromanganese crust at least 1 cm thick. Small pockets in this crust are filled with white nannofossil foraminifer ooze of early Miocene age. A thin section of the limestone (Sample 183-1141A-11R-CC, 1–4 cm) shows ~25% foraminifers (mainly planktonic), crinoids

(1%), bryozoans (1%), shell fragments (3%), ostracodes (<1%), and sand- to pebble-sized lithic fragments (17%). The pebbles are well-rounded and consist mainly of quartz, microquartz, and volcanic rock. One pebble has phenocrysts. The sand fraction includes quartz and alkali feldspar. Grains are angular. The remainder of the matrix (~45%) mainly consists of micrite and silt-sized bioclasts.

There was no official recovery in Core 183-1141A-12R (cored interval 103.80–113.50 mbsf); however, several 0.25- to 0.75-cm-diameter subrounded pebbles of chert similar to those in Core 183-1141A-11R were in the core catcher along with a tubular-shaped fossil (2 mm in diameter and 3 mm long). Because the original stratigraphic location of these pebbles is uncertain, we can not definitely interpret the composition of this interval; however, we include it as part of Unit I (Fig. **F4**).

In Hole 1142A, rock fragments of similar lithology to those of Section 183-1141A-11R-CC in Unit I were recovered from interval 183-1142A-1W-1 (Pieces 1 and 2, 0–10 cm). These are light pale brown sandy, pebbly foraminifer limestone with echinoid spines and bivalve(?) shells. Nannofossils indicate an Oligocene or Eocene age for the sediment. Some echinoderm fragments have a syntaxial overgrowth of idiomorphic clear calcite. The surface of a rounded basalt pebble (Piece 5 in Core 183-1142A-1W-1) is coated with sandy packstone containing bryozoans and echinoid spines. A second basalt fragment (Piece 7) has an altered, oxidized surface. A thin layer of pale brown calcareous sandstone with well-sorted, rounded, medium sand is attached to this altered surface. Because these sediments from Hole 1142A were found in a wash core and represent an interval from 0 to 91 mbsf (Fig. **F5**), the stratigraphic interval from which they were recovered is uncertain.

F5. Composite stratigraphic section for Site 1142, **p. 47.**

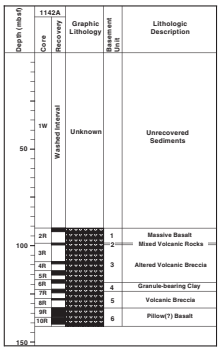

Unit II

Interval: 183-1141A-13R-1, 0 cm, to 24R-CC, 18 cm
Depth: 113.50 to 185.60 mbsf
Age: late Eocene or older

Lithologic Unit II is composed of basalts, which are highly altered in the upper portion of the section (Fig. **F4;** Table **T3**). Unit II is subdivided into 6 basement units, which are described in the **"Igneous Petrology,"** p. 22, **"Physical Volcanology,"** p. 12, and **"Alteration and Weathering,"** p. 30, sections.

Discussion

The rather homogeneous pelagic sedimentary succession (Unit I) recovered at Site 1141 indicates that Broken Ridge has been at bathyal water depths since at least early Miocene time. The sequence of sediments recovered in Site 1141 is very similar to Unit I of Site 755 (Leg 121, Peirce, Weissel, et al., 1989), also close to the crest of Broken Ridge. In contrast to the sites drilled during Leg 121 on Broken Ridge (Peirce, Weissel, et al., 1989), older sedimentary successions were not recovered between Unit I and basement at Site 1141. Thus, we have no record of the erosional/depositional history of sedimentation prior to early Miocene time. The sediments of lithologic Unit I offer no evidence for the alteration environment (e.g., subaerial or submarine) of the extensively altered basalts of the basement units.

The short interval of sediment at the top (interval 183-1141A-1R-1, 0 cm, to 2R-CC, 16 cm) of Unit I appears to represent a local deposit em-

placed by gravity-controlled processes or bottom-current reworking. In the coarse nannofossil-bearing foraminifer ooze, the low abundance of fine particles and normal size-grading suggests deposition by turbidity currents or related gravity-controlled flows. Localized carbonate turbidites and debris-flow deposits are commonly generated by local mass wasting on the sides of seamounts, abyssal hills, and basement ridges, such as the crest of Broken Ridge, which is only a few kilometers from Sites 1141 and 1142. Alternatively, removal of the fine sediment fraction by currents impinging on Broken Ridge may account for this bed.

The nannofossil-bearing foraminifer limestone in the bottom interval (interval 183-1141A-11R-CC, 0–6 cm) with randomly distributed rock and mineral pebbles and sand grains may also represent a debris-flow deposit. However, ferromanganese coatings around pebbles and an in situ ferromanganese crust in the limestone fragments imply a period of very low sedimentation rates and nondeposition, possibly caused by bottom-current activity. Winnowing of fine-grained sediments could explain the high percentage of coarse-grained material. A long period of nondeposition and simultaneous pore-water flushing by bottom currents could also explain the strong cementation of this layer. A possible hiatus of as much as 15 Ma is indicated by the age difference between the limestone (late or middle Eocene) and the overlying ooze (early Miocene).

The occurrence of similar limestone covering a pebble of basalt and similar calcareous sandstone attached to the surface of a basalt fragment in interval 183-1142A-1W, 0–10 cm, suggest that these sedimentary rocks were deposited on top of a basalt layer. Bryozoans, bivalves, and echinoids may indicate shallow marine environments; however, the high abundance of planktonic foraminifers indicates redeposition of these shallow-water organisms to a bathyal environment.

BIOSTRATIGRAPHY

The objective at Sites 1141 and 1142 on eastern Broken Ridge was to sample basaltic basement to discern its relationship to the CKP. Broken Ridge and the CKP formed as one entity, and then separated by rifting and seafloor spreading during the middle Eocene. During its subsequent journey north as part of the Australian Plate, Broken Ridge passed from the high latitudes to its present mid-latitude setting as the Earth's global climate cooled. This change in latitude has been noted in concomitant changes in the microfaunas and microfloras (Pierce, Weissel, et al., 1989). The fossil assemblages changed progressively from those with high-latitude, Southern Ocean affinities in the Eocene to more temperate ones in the Miocene. Pliocene–Pleistocene assemblages contain some subtropical elements. As a consequence, we adopted primarily temperate zonations for the Miocene–Quaternary section cored at Site 1141 but used a number of low-latitude index fossils for the Neogene section (see Fig. **F5,** p. 59, in the "Explanatory Notes" chapter). Nevertheless, some of the more tropical marker taxa are missing.

Sediments were cored only from Hole 1141A because Hole 1142A was washed to basement. Ten of the first eleven rotary cores recovered nannofossil ooze in variable amounts. We only examined core-catcher samples on board ship, and these suggest an average sedimentation rate of 6 m/m.y. for the entire carbonate ooze section (Fig. **F6**), although several hiatuses are probably present in this section. Coarse-grained unconsolidated to poorly consolidated foraminifer–nannofossil ooze

F6. Site 1141 age-depth plot, **p. 48.**

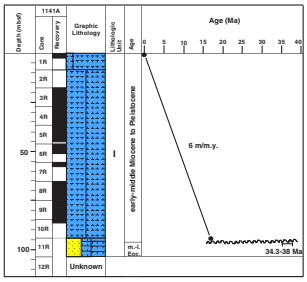

(lithologic Unit I) suggests an unusually high percentage of planktonic foraminifers, perhaps concentrated because of winnowing of nannofossils by currents passing along or across the ridge crest. If so, some reworking in the assemblages might be expected.

Nannofossils

Sample 183-1141A-1R-CC yielded a characteristic Pleistocene assemblage with *Ceratolithus cristatus, Ceratolithus simplex, Rhabdosphaera stylifer/claviger, Scapholithus fossilis,* various gephyrocapsids, and small (2.5 to 3 µm) forms that may be *Emiliania huxleyi*. If scanning electron–microscope study shows that the latter is present, the sample's age would be <0.248 Ma (Zone CN15). Preservation is good, although some specimens show etching.

The subjacent core catcher (Sample 183-1141A-2R-CC) contains a Pliocene assemblage including common *Discoaster pentaradiatus, Discoaster brouweri,* few *Discoaster triradiatus,* and a few possible *Discoaster surculus* (strongly overgrown by secondary calcite), plus *Oolithotus fragilis, Ceratolithus rugosus,* and a single specimen of *Sphenolithus abies*. Assuming that the latter is reworked, the assemblage probably belongs to Zone CN12.

Sample 183-1141A-3R-CC yielded a variety of *Amaurolithus* species, including *Amaurolithus primus, Amaurolithus delicatus,* and some forms with small apical horns characteristic of *Amaurolithus tricorniculatus*. Also present are *Reticulofenestra pseudoumbilicus, S. abies, D. surculus, D. pentaradiatus,* and *D. brouweri*. *Ceratolithus* spp., *Discoaster quinqueramus/berggrenii,* or *Triquetrorhabdulus rugosus/farnsworthii* were not observed. Ordinarily we would readily assign such an assemblage to the lowest Pliocene Zone CN10b because of the absence of *D. quinqueramus* and *T. rugusus*. Some caution should be exercised in making this age interpretation, however, because none of the *D. quinqueramus–D. berggrenii* lineage has been found on Broken Ridge or in this region south of ODP Site 757 (Leg 121) on Ninetyeast Ridge (now at 17°S; see Shipboard Scientific Party, 1989b).

Abundant *T. farnsworthii* is present in Sample 183-1141A-4R-CC, however, along with abundant *D. pentaradiatus,* few *D. veriabilis* (including large, three-rayed forms and overgrown specimens with stellate bosses but diminished ray tips); however, amauroliths are absent. As *Amaurolithus* species are present in the uppermost Miocene at ODP Site 754 (Leg 121; Shipboard Scientific Party, 1989a), we assumed that their absence here is not a result of ecological exclusion, although the absence of *D. quinqueramus–D. berggrenii* probably is (see discussion above). Based on this reasoning and the presence of abundant *D. pentaradiatus,* we assigned this sample to the uppermost Miocene Zone CN9, probably the lower part (CN9a).

Preservation diminishes in Sample 183-1141A-5R-CC in that many nannoliths are fragmented and some discoasters are heavily overgrown. Some massive discoasters that resemble *Discoaster kugleri* might have been reworked. *Discoaster pentaradiatus* continues to be abundant along with abundant *Calcidiscus leptoporus/macintyrei;* the assemblage is joined by abundant representatives of the cool-water *Reticulofenestra perplexa/gelida* plexus. We also assign this sample to the lower part of Zone CN9.

We attributed a few large (up to 15 µm), smoothly overgrown five-rayed discoasters in Sample 183-1141A-6R-CC to *Discoaster hamatus,* although we could not distinguish their characteristic ray-tip spurs. A few

six-rayed discoasters with indications of such features were assigned to *Discoaster neohamatus*. The sample was, therefore, tentatively assigned to Zone CN7 (*D. hamatus* Zone). These two index taxa were not noted by Leg 121 shipboard scientists at their Broken Ridge sites; however, they were detected at Site 757 on Ninetyeast Ridge to the northwest (Shipboard Scientific Party, 1989b). Their occurrence at Site 1141, therefore, probably represents the southernmost limits of their range, and some of their more distinctive features may not be well expressed here. Alternatively, the smallish *D. hamatus* may be in the lowest part of their biostratigraphic range. Parker et al. (1985, p. 568) noted that this taxon starts out small and becomes larger with time, as recorded in DSDP Hole 558 (Leg 82). This is a common trend among nannofossils. We observed no catinasters in Sample 183-1141A-6R-CC, in keeping with observations by Leg 121 shipboard scientists, who reported them absent as far north as Site 757 (Shipboard Scientific Party, 1989b). The barrel for Core 183-1141A-7R returned no sediment.

We noted the first downhole occurrence of *Cyclicargolithus floridanus/abisectus* in Sample 183-1141A-8R-CC, along with large, long-rayed discoasters attributed to *Discoaster exilis*. Also present are large (12 µm) elliptical *C. macintyrei,* abundant *S. moriformis, R. pseudoumbilicus* (up to 10 µm), and pointed six-rayed discoasters that may be *D. intercalaris*. This and the subjacent Sample 183-1141A-9R-CC belong to Subzone CN5a, based on the presence of the *Cyclicargolithus* plexus in the absence of *Sphenolithus heteromorphus*. Also present in the latter sample are *Coronocyclus nitescens, Geminilithella rotula, Helicosphaera granulata,* and common heavily overgrown discoasters that resemble illustrations of *Discoaster woodringii*.

Sphenolithus heteromorphus is present in Samples 183-1141A-10R-CC and 11R-CC, indicating that we reached the combined Zones CN4/CN3 in this hole. As this index taxon and its probable ancestor, *Sphenolithus belemnos,* have both been identified during previous drilling at Broken Ridge Sites 255 (Leg 26) and 754 (Leg 121) (Thierstein, 1974, and Shipboard Scientific Party, 1989a, respectively), we assumed that the stratigraphic range of neither taxa was restricted for ecological reasons at this site. Discoasters are even more heavily overgrown in Sample 183-1141A-11R-CC than in overlying cores; however, those present appear to be predominantly relatively short-rayed *Discoaster deflandrei,* rather than the longer-rayed *D. exilis*. If this is correct, then the last carbonate-ooze core belongs to Zone CN3, which spans the early/middle Miocene time boundary. Unfortunately, Core 183-1141A-11R only recovered 0.06 m of sediment, and the next core attempt (12R) recovered none, so little is known about this part of the section.

Besides a small amount of carbonate ooze, however, Sample 183-1141A-11R-CC also contained a well-cemented, manganese-coated, orange-colored conglomeratic foraminiferal limestone with various kinds of pebbles and clasts (see **"Lithostratigraphy,"** p. 5). Nannofossils are rare in this rock and most are poorly preserved; however, *Reticulofenestra bisecta, Zygrhablithus bijugatus, Coccolithus eopelagicus* (up to 20 µm), large (up to 12 µm) *Coccolithus formosus* are rare to common, and a single specimen of *Discoaster saipanensis* (seven rayed) was also observed. If in situ, this assemblage ranges from late middle to late Eocene in age. A similar-looking limestone from wash core Section 183-1142A-1W-1 also contained small *R. bisecta,* which ranges in age from the late middle Eocene to Oligocene; this assemblage is probably of a similar age to that of Sample 183-1141A-11R-CC.

A white streak of nannofossil chalk within Sample 183-1141A-11R-CC contained a nannofossil assemblage with *C. floridanus, C. abisectus, Coccolithus pelagicus,* and *Discoaster* sp. The assemblage looks similar to those in the lower part of the Miocene carbonate ooze section above.

Planktonic Foraminifers

Planktonic foraminifers recovered from the Neogene carbonate ooze at Site 1141 are abundant and very well preserved. Compared to those from the Kerguelen Plateau, these assemblages show high species diversity and are virtually identical to assemblages recovered from Broken Ridge Site 754 (Leg 121). Pliocene and Pleistocene faunas reflect temperate conditions with some affinities to subtropical assemblages. Upper Miocene assemblages are rich in species associated with temperate waters with forms characteristic of the high latitudes becoming increasingly important in lower and middle Miocene sediment. This gradual change in faunal composition, also observed by Leg 121 shipboard scientists during drilling on Broken Ridge (Pierce, Weissel, et al., 1989), reflects warming of surface waters associated with the post–mid-Eocene northward motion of the Broken Ridge drill sites from higher latitudes to lower latitudes. Thus, for this site we were able to employ the more detailed temperate planktonic foraminifer zonation of Srinivasan and Kennett (1981). This zonal scheme is largely based on species of *Globorotalia,* reflecting the importance of these evolutionary lineages in temperate areas (Kennett and Srinivasan, 1983).

Quaternary

The Quaternary is represented by one core of Pleistocene, winnowed, nannofossil-bearing foraminifer ooze. Sample 183-1141A-1R-CC contains a rich assemblage of foraminifers with pristine preservation of tests and wall textures. The assemblage is dominated by *Globorotalia inflata* and *Globorotalia truncatulinoides,* which are species typical of temperate water masses. However, the assemblage also contains the tropical to subtropical forms such as *Orbulina* spp., *Globigerinoides ruber,* and *Globorotalia menardii.* More cosmopolitan species, including *Globigerina bulloides* and *Globigerina falconensis* are also present. We assign this sample to the upper Pleistocene *G. truncatulinoides* Zone owing to the common occurrence of the nominate taxon and absence of *Globorotalia tosaensis,* from which the latter evolved. This Broken Ridge Pleistocene fauna contrasts markedly to Kerguelen Plateau and other high-latitude assemblages that show extremely low diversity, as well as dominance by *Neogloboquadrina pachyderma.*

Neogene

Cores 183-1141A-2R to 11R contain well-preserved planktonic-foraminifer assemblages that contain a mixture of Southern Ocean and subtropical elements. Sample 183-1141A-2R-CC is below the last appearance datum (LAD) of *G. truncatulinoides*. *Globorotalia tosaensis* is present in this sample, and we therefore assign it to the uppermost Pliocene zone bearing that name. Other elements of this fauna include cool-water *Globigerina woodi, G. falconensis,* and *G. bulloides* plus the warmer water–loving taxa *Orbulina, Globigerinella siphonifera, G. inflata, G. menardii,* and *G. ruber.* As noted at Site 754 by the Leg 121 Shipboard Scientific Party (1989a), fully tropical species such as *Globorotalia tu-*

mida, Sphaeroidinella dihiscens, and *Pulleniatina obliquiloculata* are absent.

The next three samples contain conical forms belonging to the *Globorotalia miozea-conoidea* plexus. In Sample 183-1141A-3R-CC, we found the short-ranging species *Globorotalia conomiozea* and the first downhole occurrence of *Globoquadrina altispira,* indicating an early Pliocene or late Miocene age. At Site 754, the first appearance datum (FAD) of *Globorotalia puncticulata* and *Globorotalia margaritae* was used to approximate the Miocene/Pliocene boundary (Leg 121 Shipboard Scientific Party, 1989a). We did not find these species during preliminary examination of core-catcher samples and were thus unable to delineate the *G. puncticulata–G. conomiozea* Zones. More detailed sampling during shore-based studies should allow us to locate this boundary more precisely.

Upper Miocene assemblages are characterized by *G. conoidea, G. miozea, Globorotalia panda, G. woodi, Globigerina nepenthes, G. falconensis, Globigerina bulloides, Globquadrina altispira, Dentiglobigerina* sp., *Globigerinella aequilateralis, Orbulina* sp., *Globigerina trilobus,* and *G. menardii.* The downhole FAD of *G. conomiozea* occurs in Sample 183-1141A-4R-CC. *Neogloboquadrina continuosa,* the last appearance datum (LAD) of which marks the lower boundary of the late Miocene *G. nepenthis* Zone, is rare or absent in Hole 1141A. Therefore, we assign Samples 183-1141A-4R-CC to 6R to the combined *G. nepenthes–N. continuosa* Zones. Core 183-1141A-7R was empty, so no paleontological sample was available.

In addition to abundant *G. miozea,* we noted *Globorotalia mayeri* in Sample 183-1141A-8R-CC and accordingly assigned it to the mid-Miocene zone bearing that name. In Sample 183-1141A-9R-CC, we recognized a small, inflated, six-chambered form, identified as *Globorotalia peripheroacuta,* that allowed us to place this sample in the *Globorotalia peripheronda–G. peripheroacuta* Zone. We did not find this form in the subjacent sample and therefore placed it in the lower mid-Miocene *Orbulina suturalis* Zone.

Globoquadrina sp., *Dentigloboquadrina* sp., and *G. miozea* dominate planktonic foraminifer assemblages from the last core catcher, Sample 183-1141A-11R-CC. This sample occurs below the FAD of *O. suturalis* and above the LAD of *Catapsydrax dissimilis*. We did not distinguish *Preaorbulina glomerosa curva,* indicative of uppermost lower Miocene strata, and therefore assign this sample to the *G. miozea* Zone, suggesting a minimum age of 16–18 Ma for the last carbonate ooze sediments above basement.

In addition to the unconsolidated Miocene carbonate ooze described above, the core catcher of Core 183-1141A-11R contained pebbles of a sandy foraminiferal limestone. We could not isolate individual planktonic foraminifers from these pebbles but were able to recognize foraminifers in petrographic thin section. Postcruise examination of thin sections (I. Premoli Silva, pers. comm., 1999) confirmed that limestone Sample 183-1141A-11R-CC contained abundant planktonic and benthic foraminifers. Among the planktonic forms we recognize biserial *Chiloguembelina* spp. and possible *Globigerinatheka index*. Acarininids appear to be absent, indicating a late Eocene age (~34.3–38 Ma). Chips of similar sandy foraminifer limestone were recovered from between basalts at Site 1142. In postcruise studies of thin sections (Sample 183-1142A-3R-1, 1–6 cm), we also found planktonic foraminifers indicative of a middle–late Eocene in age.

Basal Sediment

The age date for the oldest sediment in these sites (late middle to late Eocene, 34.3–38 Ma) probably does not provide a date close to the age of basaltic basement. Sites 1141 and 1142 were chosen to avoid Cretaceous limestones interpreted from seismic lines that lie to the north; thus, the holes penetrated only the youngest overlying sediment. This strategy was to avoid drilling problems that prevented sampling of Broken Ridge's igneous basement during Legs 26 and 121. Indeed, this strategy worked to the point that basement was cored. Eventually, however, Hole 1141A collapsed, and Broken Ridge claimed yet another bottom-hole assembly to add to its collection (see "Operations," p. 2).

The basal sediments in Hole 1141A are late middle to late Eocene in age, which dates from the time that Broken Ridge rifted from the Kerguelen Plateau. Conglomeratic in nature with pebbles that include pieces of altered basalt (see "Igneous Petrology," p. 22), these sediments apparently record processes of erosion and redeposition that accompanied that tectonic episode (see Pierce, Weissel, et al., 1989, for further details of this event).

PHYSICAL VOLCANOLOGY

We drilled Hole 1141A 72.1 m into basement. The igneous rocks recovered were divided into six units interpreted to represent five mafic lava flows overlain by a coarse-grained sedimentary deposit made up of gabbroic pebbles (Table T5). Hole 1142A penetrated 50.9 m into basement and the rocks recovered were divided into six units (Table T6). These units include a very diverse range of lithologies, including possible pillow basalts, subaerial deeply weathered (felsic?) lavas and volcanic sediments, rhyolite lava flows, and olivine-phyric basalt lava flows. Despite the close proximity of Sites 1141 and 1142 (~1 km), the recovered basement sections show very large differences.

T5. Basement units at Site 1141, p. 126.

T6. Basement units at Site 1142, p. 127.

We describe each unit first, then provide unit-by-unit interpretations in the following section. The rationale for placing the unit boundaries in the locations we chose is also explained in the interpretive section.

Hole 1141A Unit Descriptions

Lithologic Units

Unit I

The sedimentary sequence overlying basement contains a very small amount of disseminated volcanic detritus, including dispersed black sand-sized lithic grains in Cores 183-1141A-4R and 5R and rare, altered sand- to pebble-sized basalt clasts in interval 183-1141A-11R-CC, 0–6 cm (see "Lithostratigraphy," p. 5).

Basement Units

Unit 1 (Interval 183-1141A-13R-1, 0 cm, to 14R-1, 0 cm)

The recovered material from Unit 1 consists of three angular pebbles of gabbro (see "Igneous Petrology," p. 22 for description).

Unit 2 (Interval 183-1141A-14R-1, 0 cm, to 16R-2, 19 cm)

The 7.36 m of material recovered from Unit 2 consists of highly altered and locally intensely oxidized lava (see **"Alteration and Weathering,"** p. 30). Only the lowermost 19 cm of the unit (the top of Section 183-1141A-16R-2) is relatively unaltered. Table **T7** describes the few patches with recognizable vesicles. In the better preserved part of Unit 2, vesicularity generally decreases with depth but vesicle size increases. The least-altered rocks in the lowermost part of Unit 2 range from moderately to highly vesicular with near-spherical vesicles (Fig. **F7**).

Unit 3 (Interval 183-1141A-16R-2, 19 cm, to 17R-1, 35 cm)

Recovered rocks from Unit 3 consist of 2.29 m of altered mafic lava. The alteration is complete in most of the unit, but the bottom of Unit 3 (the top 30 cm of Core 183-1141A-17R) consists of relatively unaltered loose pieces. The top of Unit 3 is also strongly oxidized (Fig. **F7;** see **"Alteration and Weathering,"** p. 30).

Despite the generally complete alteration, the >1-mm vesicle fillings are commonly well preserved, allowing the distribution of larger vesicles to be determined in several locations (Fig. **F8**). Recognizable vesicularity is ~7% until interval 183-1141A-16R-3, 40–53 cm, where a zone of 1- to 2-cm-diameter vesicles appears (Fig. **F9**). Below this, vesicularity grades down to ~3% and into a zone of 3- to 10-mm horizontally elongate blebs (Fig. **F10**). Below the blebs the vesicularity becomes too low to detect in these altered rocks except for thin horizontal sheets of vesicles in the core catcher from Core 183-1141A-16R at 36 and 42.5 mm. The loose pieces at the top of Core 1831-1141A-17R consist of a mix of dense (~2% vesicles) and highly vesicular (~30% vesicles) lava.

Unit 4 (Interval 183-1141A-17R-3, 35 cm, to 20R-1, 79 cm)

The recovered rocks from Unit 4 consist of 5.92 m of variably altered mafic lava. The vesicularity pattern (Figure **F11**) generally changes from a vesicular flow top to a massive interior and back to a thinner vesicular base. Domains of vesicle-rich mesostasis material are found in the dense interior, including a 3-mm-wide inclined sheet (Fig. **F12**), 8-mm-wide vertical pipes (Fig. **F13**), and ~20-cm-thick irregular pods. The groundmass texture of the massive interior in the vicinity of the inclined vesicle sheet is finer grained than in the vesicular flow top (Fig. **F12**). The base of the unit is highly vesicular and the lowermost 6 cm is variably altered (Fig. **F14**). This alteration makes the primary features of the base difficult to discern, especially because the alteration includes millimeter-scale rounded blebs that are both subhorizontal and spherical.

Unit 5 (Interval 183-1141A-20R-1, 79 cm, to 21R-3, 130 cm)

The 6.37 m of recovered rocks from Unit 5 are variably altered coherent basalt. The vesicle distribution is shown in Figure **F15,** and the familiar pattern of a thicker vesicular upper part, massive interior, and vesicular base is repeated. The uppermost centimeter of Unit 5 is a somewhat altered, smooth, undulating surface that contains abundant <1-mm rounded, horizontally elongated vesicles. There is a pair of identical parallel but slightly inclined surfaces 10–12 cm down into Unit 5 (Fig. **F14**). Within the vesicular upper portion of Unit 5, brecciation in the form of collapsed larger vesicles is common. Small vesicle trains are common in the lower part of the upper vesicular zone (Section 183-1141A-20R-2). The transition from vesicular to massive lava is marked by a megavesicle horizon with a horizontal sheet of vesicular material (Fig. **F16**). The bottom 2–3 cm of Unit 5 (Fig. **F17**) is more heavily al-

T7. Vesicle distribution in Unit 2 at Site 1141, **p. 128.**

F7. Close-up photograph of interval 183-1141A-16R-2, 13–25 cm, **p. 49.**

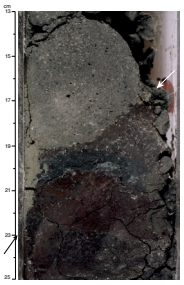

F8. Vesicularity and vesicle density as a function of depth in basement Unit 3, Site 1141, **p. 50.**

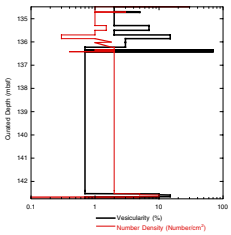

F9. Close-up photograph of interval 183-1141A-16R-3, 40–56 cm, **p. 51.**

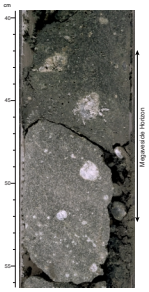

F10. Close-up photograph of interval 183-1141A-16R-CC, 4–16 cm, **p. 52.**

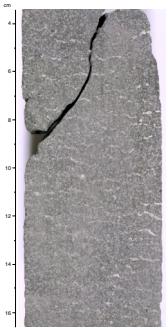

tered and appears sheared (see "Alteration and Weathering," p. 30). Few vesicles are visible.

Unit 6 (Interval 183-1141A-21R-3, 130 cm, to 24R-CC, 17 cm)

The recovered rocks from Unit 6 include an upper breccia, a thick massive interior, and a small amount of breccia at the base. The breccias are pervasively altered to clays and are intensely disturbed, making it difficult to discern primary textures in most places. However, local features can be described (Fig. F17). Figure F18 plots vesicularity vs. depth for Unit 6 and shows data for several intervals. Interval 183-1141A-21R-4, 3–30 cm, appears to be a single coherent lobe with abundant large vesicles in the interior and a denser exterior. Interval 183-1141A-22R-1, 65–142 cm, contains the best preserved portion of the breccia (Fig. F19). In this interval, 80% of the breccia consists of clasts 1–7 cm in size. The remainder consists of subequal proportions of 1- to 10-mm rounded to subangular fragments and the clay matrix. The smaller fragments are in ~10-cm pods and as halos around larger clasts. The vesicularities and vesicle morphologies of the clasts are variable (Fig. F18) but generally rather dense (3%–10%). The remainder of the disturbed and altered breccia appears to be broadly similar to this interval but includes 5%–10% clay-filled voids in the uppermost part of the breccia.

The coherent interior starts in Section 183-1141A-22R-2, 72 cm, with no recovered transition. The vesicle patterns are patchy across 4- to 7-cm spheroidal and subplanar domains in interval 183-1141A-22R-2, 72–136 cm. Below this, vesicularity gradually decreases with depth until just above the base of the flow (Fig. F19). The largest step in vesicularity is marked by a horizon of megavesicles (Fig. F20). There are two unusual types of features within the interior of Unit 6. The first is an interweaving of lava with different groundmass textures. Figures F21 and F22 show two examples of this texture. The other unusual class of features is sheets of nonvesicular segregated material (Fig. F23).

The core catcher from the last core contains 17 cm of altered, disturbed breccia broadly similar to that at the top of Unit 6.

Hole 1141A Interpretation

Unit 1 (Gabbroic Pebbles)

These loose pieces are presumed to be eroded intrusive rocks that have been transported to this site. Their relationship to the lava flows underneath is not known. The angular shapes suggest limited transport but could also be a result of fracturing during drilling.

Unit 1/Unit 2 Boundary

No contact between the gabbroic pebbles and the altered lava was recovered.

Unit 2 (Lava Flow, Type Unknown)

The patches of recognizable vesicles in Unit 2 are not diagnostic (or even strongly suggestive) of any particular type of lava flow.

Unit 2/Unit 3 Boundary

The change from relatively unoxidized to intensely oxidized lava marks the boundary between Units 2 and 3. Given the patchy nature of

F11. Vesicularity and vesicle number density as a function of depth in basement Unit 4, Site 1141, p. 53.

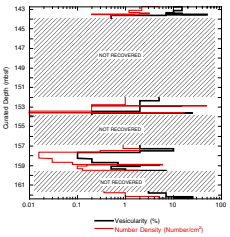

F12. Close-up photograph of interval 183-1141A-18R-2, 9–19 cm, p. 54.

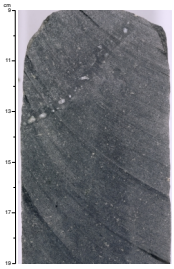

F13. Close-up photograph of interval 183-1141A-19R-2, 60–70 cm, p. 55.

F14. Close-up photograph of interval 183-1141A-20R-1, 71–91 cm, p. 56.

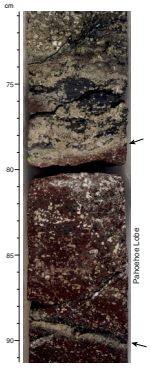

the oxidation in the overlying recovered rocks, this does not necessarily represent a significant time break or even a physical break between two flows. However, we have interpreted this as the relatively less altered base of the flow in Unit 2 over the weathered and altered vesicular top of Unit 3.

Unit 3 (Inflated Pahoehoe? Flow)

The vesicle distribution, a megavesicle horizon grading into a massive interior, and the horizontal vesicle sheets with associated mesostasis blebs are all characteristics of an inflated pahoehoe lava flow. However, some transitional lava flows seen at previous sites on Leg 183 also have similar interiors. The loose pieces of relatively unaltered rock at the base of Unit 3 show no evidence of brecciation and are likely to come from a smooth, coherent, lower vesicular crust. Such a basal surface strongly suggests a pahoehoe flow.

Unit 3/Unit 4 Boundary

The change from relatively unaltered to completely altered lava marks the boundary between Units 3 and 4. We have interpreted this as the relatively less altered base of the flow in Unit 3 over the weathered and altered vesicular top of Unit 4.

Unit 4 (Inflated Pahoehoe Flow)

The distribution and morphology of vesicle features in Unit 4 are diagnostic of an inflated flow. The consistently round vesicle shapes and smooth base are strong indicators of a pahoehoe flow. The fine-grained massive interior of the flow has been hypothesized to be a dike (see **"Igneous Petrology,"** p. 22), but the vesicle features are completely consistent with being part of the interior of a thick, inflated pahoehoe flow. The fine-grained nature of the interior is difficult to explain, but variations in groundmass textures in thick flows are not documented.

Unit 4/Unit 5 Boundary

The surfaces with small, stretched vesicles near the boundary between Units 4 and 5 are interpreted to be altered glassy chill margins. However, the precise location of the basal chill of Unit 4 is difficult to pinpoint because of the alteration, possible tectonic shearing, and the topography on the top of Unit 5. The 10-cm-thick lobe between the two thicker flows could belong to either unit. However, based on the identical oxidation of the thin lobe and the rest of Unit 5, it is placed with Unit 5. The deep oxidation of the upper part of Unit 5 suggests a substantial time break, but there is little evidence for extensive erosion or weathering of the top of Unit 5.

Unit 5 (Compound Inflated Pahoehoe Flow)

Multiple lobes of pahoehoe define a compound pahoehoe flow. The features within the thick lobe are diagnostic of inflation. This indicates that the underlying ~7-m-thick lobe started as a lobe similar to the ≥10-cm-thick lobe on top. The zone of irregular vesicle trains and relatively low vesicularity record a time during which the flow began to stagnate. The underlying horizontal vesicular zone indicates that the flow was reactivated with injections of fresh, bubble-laden lava. The lower vesicu-

F15. Vesicularity and vesicle number density as a function of depth in basement Unit 5, Site 1141, **p. 57.**

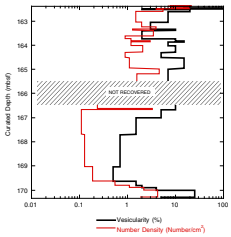

F16. Close-up photograph of interval 183-1141A-21R-1, 20–34 cm, **p. 58.**

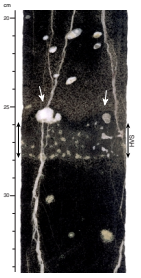

F17. Close-up photograph of interval 183-1141A-21R-3, 120–140 cm, **p. 59.**

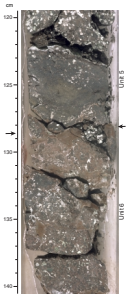

F18. Vesicularity and vesicle number density as a function of depth in basement Unit 6, Site 1141, **p. 60.**

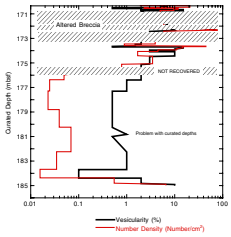

lar crust and the morphology of the basal contact are also typical of inflated pahoehoe flows.

Unit 5/Unit 6 Boundary

The contact between the pahoehoe base of Unit 5 and the brecciated top of Unit 6 is well preserved and easy to locate. However, the alteration and disturbance is sufficient to make it impossible to determine the amount of weathering and reworking the breccia was subjected to before being covered by Unit 5.

Unit 6 (Breccia-Topped Transitional Lava Flow)

The patchy vesicular domains in the upper part of the coherent lava are interpreted to be remelted entrained breccia clasts. This and the irregular, angular morphology of many of the vesicles are strong evidence that the lava flow in Unit 6 was emplaced with a disrupted, brecciated flow top. A vesicular ≥30-cm-thick coherent lobe in the upper part of the breccia indicates that this was not an aa flow.

The intermixing of lavas with grossly different groundmass textures seen in Unit 6 is a feature we have not noted in any other lava flows. It is possible that this is actually quite common in lava flows that have remelted entrained material but is not visible without a style of alteration that enhances these features. The relationship between the different groundmass textures and the nonvesicular sheets of segregated material is also unclear. The breccia at the base of Unit 6 is equally likely to be the basal breccia of Unit 6 or the flow-top breccia of the underlying lava.

Hole 1142A Unit Descriptions

Unit 1 (Interval 183-1142A-1W, 11 cm, to 3R-1, 0 cm), Massive Basalt

The recovered rocks from Unit 1 consist of 1.91 m of massive basalt. The uppermost pieces are pebbles and cobbles with a 0.5-cm oxidation rim and have calcareous sediments cemented to their margins. Although the smallest pebbles are well rounded, the original shapes of the larger cobbles cannot be determined because of drilling disturbance. There is no visible difference between the larger cobbles and the underlying coherent massive lava. The massive lava contains 0.3%–0.5% round vesicles and is remarkably featureless. The few pieces of calcareous sediments above Unit 1 are described in "Lithostratigraphy," p. 5.

Unit 2 (Interval 183-1142A-3R-1, 0 cm, to 3R-1, 73 cm), Mixed Volcanic Rocks

The 1.03 m of rock recovered from Unit 2 consist of a highly altered breccia overlying a mixture of different volcanic rocks. The uppermost pieces in Core 183-1142A-3R are pieces of calcareous sediment identical to those found above Unit 1. The breccia of Unit 2 contains ~25 vol% clasts in the 1- to 5-cm size range and 40%–60% clay matrix (Fig. F24). The remainder is sand- to silt-sized fragments. Clasts are subangular to well rounded and consist of variably altered and oxidized lava. Most lava appears dense. However, the largest clast is a loose 1 cm × 1.5-cm spheroidal piece of secondary vesicle fill.

F19. Close-up photograph of interval 183-1141A-22R-1, 105–120 cm, p. 61.

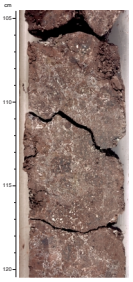

F20. Close-up photograph of Sample 183-1141A-22R-3 (Piece 2, 10–24 cm), p. 62.

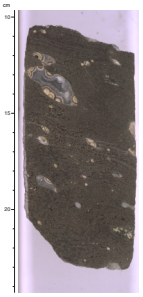

F21. Close-up photograph of interval 183-1141A-22R-2, 89–101 cm, p. 63.

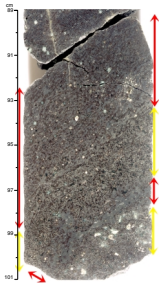

F22. Close-up photograph of interval 183-1141A-22R-3, 111–119 cm, p. 64.

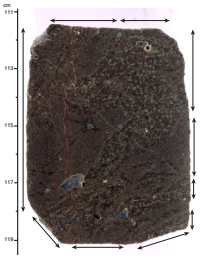

The rocks below the breccia are poorly recovered with ≤10-cm-long pieces, of which only one can be oriented. Lithologies are varied, including pieces that include large olivine phenocrysts and others with quartz and possible pumice fragments (see "Igneous Petrology," p. 22). Interval 183-1142A-3R-1, 73–93 cm, consists of 1- to 7-cm pieces of an altered breccia. The clasts within the breccia are subrounded pieces of sparsely vesicular and moderately olivine? phyric lava that have a halo of smaller fragments embedded in a clay matrix (Fig. F25).

Subunit 3A (Interval 183-1142A-3R-CC, 0 cm, to 5R-1, 0 cm), Disturbed Volcanic Rock

Unit 3A contains 1.31 m of completely altered and highly disturbed broken rubble and clay-sized material. Zones within the disturbed material preserve angular broken rock fragments. These are either massive, nonvesicular lava fragments with devitrification textures (e.g., interval 183-1142A-4R-1, 0–3 cm), or red, altered, massive, clay-rich material (e.g., interval 183-1142A-4R-1, 9.5–12 cm).

Unit 3B (Interval 183-1142A-5R-1, 0 cm, to 6R-1, 0 cm), Lava and Volcanic Breccia

In the upper part of Unit 3B, pieces of altered, relatively massive, dark reddish gray, moderately indurated (basalt?) lava were recovered (interval 183-1142A-5R-1 [Pieces 1–4, 0–23 cm]). Below this interval, the altered volcanic rock is dark brown and massive (interval 183-1142A-5R-1 [Pieces 5–7, 23–47 cm]) to brecciated (interval 183-1142A-5R-1 [Pieces 7 and 8, 47–57 cm]). Brecciation in this interval appears to be caused by brittle deformation. Angular pebble-sized clasts sit in a matrix of dark red (oxidized) clay-sized material and coarse sand to small granule-sized, variably oxidized, angular, lava fragments (Fig. F26). Lower in Section 183-11442A-5R-1 there is another interval of dark reddish gray, relatively massive, altered basalt? lava (interval 183-1142A-5R-1 [Pieces 9–17, 57–66 cm]). In most pieces an internal texture ~30° from horizontal is defined by a coalescence of thin (<1 mm), orange, elongate domains of altered material in the mesostasis (e.g., interval 183-1142A-5R-1 [Piece 12, 70–80 cm]) (Fig. F27). In one interval the orange altered domains are up to 0.6 cm × 2 cm (interval 183-1142A-5R-1 [Pieces 13–14, 103–118 cm]). In some places the altered domains have coalesced into long narrow trains that define a pseudobreccia texture in the rock (interval 183-1142A-5R-1 [Pieces 15–16, 118–131 cm]) (Fig. F28).

At the top of interval 183-1142A-5R-2, 0–12 cm, and in interval 183-1142A-5R-2, 24–28 cm, there is some dark reddish gray pebble-sized rubble. This rubble has the same texture as material at the base of Section 183-1142A-5R-1, and lower in Section 183-1142A-5R-2, and probably fell downhole during drilling. Within the same lithology, a breccia with dark red, flattened clasts in a reddish brown clay matrix is found in interval 183-1142A-5R-2 (Piece 2, 12–24 cm) (Fig. F29). Olivine was recognized in three cobble-sized pieces of dark reddish gray, altered, (basalt?) lava (interval 183-1142A-5R-1 [Pieces 4–6, 28–48 cm]) below the breccia interval (see "Igneous Petrology," p. 22). Similar dark reddish gray altered (basalt?) lava continues to the bottom of the section (interval 183-1142A-5R-2 [Piece 7, 48–75 cm]). These rocks have an internal fabric ~30° from horizontal defined by an in situ brecciation tex-

F23. Close-up photograph of interval 183-1141A-23R-1, 105–115 cm, p. 65.

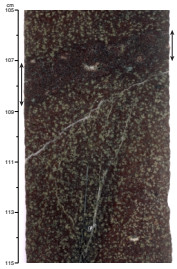

F24. Close-up photograph of interval 183-1142A-3R-1, 16–24 cm, p. 66.

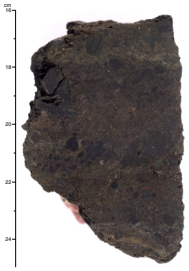

F25. Close-up photograph of interval 183-1142A-3R-1, 76–83 cm, p. 67.

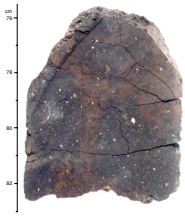

F26. Close-up photograph of Sample 183-1142A-5R-1 (Piece 7, 38–52 cm), p. 68.

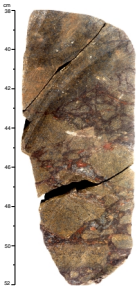

ture with alignment of slightly flattened subrounded clasts. This may be an alteration texture, after a primary flow fabric.

Subunit 3C (Interval 183-1142A-6R-1, 0 cm, to 6R-2, 0 cm), Lava and Volcanic Breccia

The upper 28 cm of Core 183-1142A-6R-1 contains mixed volcanic rubble reworked from higher in the hole during drilling. Lithologies present include altered, resinous, clay-rich, porphyritic volcanic rock (rhyolite?); dark reddish gray lava (Unit 3B); greenish gray altered basalt pebbles; and red brown indurated clay pebbles. Below this, a pale brown to brown, indurated, altered, relatively massive lava with an internal fabric ~30° from horizontal defined by thin (<1 mm), pale brown, elongate domains of altered material in the mesostasis (Sample 183-1142A-6R-1 [Pieces 5A-5D, 28–52 cm]). This seems to be an alteration texture in otherwise massive lava. Interval 183-1142A-6R-1, 52–67 cm, includes one dark reddish gray pebble similar to Subunit 3B and an interval of broken rock that was highly disturbed by drilling.

A brownish gray, altered, relatively massive (basalt?) lava is located in interval 183-1142A-6R-1 (Pieces 8 and 9, 67–114 cm). This lava also has an internal fabric ~30° from horizontal, but it is defined by thin (<1 mm), pale orange, elongate domains of altered material, separated by whiter devitrified zones in the mesostasis. Although the texture in this rock is similar to the textures of rocks in interval 183-1142A-5R-1 (Piece 4, 28–52 cm), less olivine was identified in this rock. Another interval of highly disturbed volcanic rock (drilling fragmentation) is interval 183-1142A-6R-1, 114–146 cm. Two dark gray, massive pebbles with aligned, elongate domains of orange altered material, forming a 1-cm-wide zone around their perimeter, were preserved at the base of the disturbed material.

Unit 4 (Interval 183-1142A-6R-2, 0 cm, to 7R-1, 92 cm), Granule–Bearing Clay

Unit 4 is a normally graded (intervals 183-1142A-6R-2, 27–40 cm, and 40–46 cm; Fig. F30) to matrix-supported (intervals 183-1142A-6R-2, 0–27 cm, and 46-49 cm; interval 183-1142A-7R-1, 9–92 cm; Fig. F31), red (oxidized), very coarse sand to granule-bearing clay. Coarse to very coarse sand-sized clasts are dominantly angular, and very coarse sand to small granule-sized clasts are dominantly rounded, indicating the incorporation of more than one clast population. The clasts include quartz, kaolinitized feldspar, variably altered volcanic lithic fragments, and feldspar crystals. The red clay matrix is homogeneous and massive and does not preserve pedogenic features. In interval 183-1142A-7R-1, 0–9 cm, there is some brownish gray, altered, pebble-sized rubble with a subparallel internal texture that is similar to material in interval 183-1142A-6R-1 (Piece 8, 67–104 cm) higher in the sequence.

Unit 5 (Interval 183-1142A-7R-1, 92 cm, to 9R-1, 0 cm), Volcanic Breccia

A relatively coherent brownish gray lava is preserved in interval 183-1142A-7R-1, 100–137 cm. It has an arcuate alteration front along one side that reflects a round lobe shape in the core. Within the more altered zone, there is alignment of small, elongate, altered zones, possibly altered phenocrysts or variolites, in the mesostasis. Within the less al-

F27. Close-up photograph of interval 183-1142A-5R-1, 70–80 cm, p. 69.

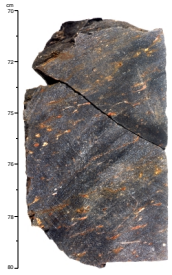

F28. Close-up photograph of interval 183-1142A-5R-1, 118–126 cm, p. 70.

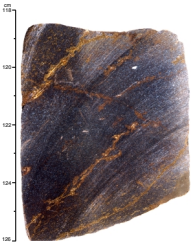

F29. Close-up photograph of interval 183-1142A-5R-2, 12–23 cm, p. 71.

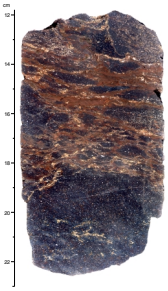

F30. Close-up photograph of interval 183-1142A-6R-2, 28–40 cm, p. 72.

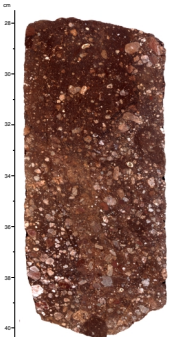

tered zone, the internal texture is massive. Pieces above and below this interval are brecciated (intervals 183-1142A-7R-1 [Piece 8, 92–100 cm] and 183-1142A-7R-1, 137–151 cm). The breccia has dark reddish gray clasts in a red clay matrix, with incorporated coarse sand- to granule-sized, angular to subrounded and partially flattened, spalled lava fragments (Fig. F32). A few of the larger lava clasts show irregular to fluidal margins, and there is some evidence of flattening. All of the pieces in Core 183-1142A-7R-2 are brecciated. Piece 1 is massive, dark-red, altered material with a 1 cm × 1.5 cm included clast, and Piece 2 contains clasts with either chilled or oxidized margins that are possibly joined along a suture. Pebbles in interval 183-1142A-7R-2, 12–22 cm, are subangular to subrounded dark red and dark gray breccia fragments. The lower part of interval 183-1142A-7R-2, 22–48 cm, is a dark reddish gray breccia with a subhorizontal texture and possibly some clast flattening (Fig. F33). This breccia texture may have been enhanced during alteration. Section 183-1142A-8R-1 is almost totally disturbed by drilling, but domains of less broken rock are similar to the breccia in interval 183-1142A-7R-2 (Piece 4, 22–48 cm).

Unit 6 (Interval 183-1142A-9R-1, 0 cm, to 10R-3, 74 cm)

The 8.27 m of recovered rock from Unit 6 consists of less altered, generally massive basalt. The lava also contains abundant veins and oxidation halos (Fig. F34; see "Alteration and Weathering," p. 30) and small faults (Fig. F35). The veins in intervals 183-1142A-9R-2, 58–61 cm, and 9R-4, 0–5 cm, have a thick, altered margin with a distinctly finer grained groundmass (Figs. F36, F37). The lava is remarkably nonvesicular; we were unable to find a single macroscopic vesicle in the recovered rocks from Unit 6.

Hole 1142A Interpretation

Unit 1 (Lava Flow, Type Unknown)

The massive featureless lava from Unit 1 is interpreted to be from the interior of a thick lava flow. The sparse vesicularity and oxidized top tentatively suggest a subaerial flow rather than a submarine flow.

Unit 1/Unit 2 Boundary

The change from a relatively unaltered massive lava to a highly altered breccia marks the change from Unit 1 to 2. The breccia appears to be extensively reworked and suggests a major time break between these two units.

Unit 2 (Breccia, Origin Unknown)

The wide range of lithologies within Core 183-1142A-3R cannot be all in place. However, the lack of a visible matrix and the presence of a clast that contains a breccia are difficult to explain in a debris flow or sedimentary breccia. We tentatively suggest that Unit 2 is a reworked talus pile that was covered by the flow of Unit 1.

Several observations suggest that breccia at the top of Unit 2 was extensively reworked. The scarcity of larger clasts and the wide mixture of different types of fine-grained lava fragments are distinctly different from the primary flow-top breccias seen earlier during Leg 183 (see

F31. Close-up photograph of interval 183-1142A-7R-1, 10–20 cm, p. 73.

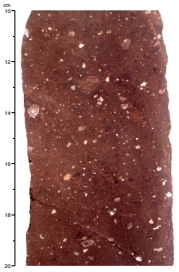

F32. Close-up photograph of interval 183-1142A-7R-1, 137–148 cm, p. 74.

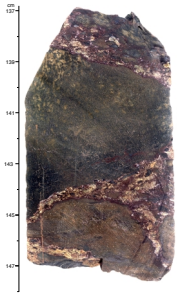

F33. Close-up photograph of interval 183-1142A-7R-2, 21–40 cm, p. 75.

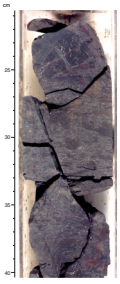

F34. Close-up photograph of interval 183-1142A-9R-1, 71–93 cm, p. 76.

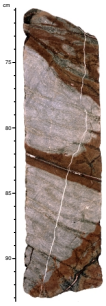

"Physical Volcanology," p. 10, in the "Site 1136" chapter, "Physical Volcanology," p. 13, in the "Site 1137" chapter, and "Physical Volcanology," p. 22, in the "Site 1138" chapter). The loose piece of vesicle fill is also evidence that this breccia at the top of Unit 2 is composed of lava that was completely disaggregated.

Unit 2/Unit 3 Boundary

A transition from relatively unaltered rocks to a completely altered and disturbed rock and the top of a new core mark the change from Unit 2 to Unit 3.

Subunit 3A (Weathered Basalt?)

Extensive drilling disturbance in these highly altered rocks make it difficult to interpret the volcanological aspects of this unit.

Subunit 3B

Subunit 3B is composed of intervals of altered coherent (basaltic?) lava and at least two associated breccias. The upper breccia (interval 183-1142A-5R-1 [Pieces 7–8, 47–57 cm]) (Fig. F26) has angular clasts and formed because of brittle deformation of volcanic rock. There is no evidence of welding, and a partially pulverized matrix indicates clast/clast contact during breccia formation. This is a tectonic breccia, probably formed after the lava was emplaced and had cooled. The lava is aphanitic, has low vesicularity, and is internally massive (Figs. F27, F28). A secondary fabric of coalesced, elongate, altered domains may follow a primary flow alignment. These domains may originate as altered phenocrysts or variolites in the rock that are later modified during alteration. It is not clear whether the lava has been emplaced in a subaerial or subaqueous environment.

The lower breccia (interval 183-1142A-5R-2 [Piece 2, 12–24 cm]) (Fig. F29) has a subhorizontal fabric that could be the result of either shearing or flattening. The clasts are similar to the lava material above and below. It is difficult to flatten solid lava; hence, this is either a shear zone or a zone where clasts were flattened while hot. There are no chilled margins on clasts or welding textures preserved and no other evidence of heat in this breccia, implying that the breccia probably has elongated clasts because it has been sheared.

Subunit 3C

This unit is dominated by two intervals of altered brown to brownish gray, sparsely olivine-phyric basaltic? lava (intervals 183-1142A-6R-1, 28–52 cm, and 6R-1, 67–114 cm). Both are relatively massive although they have secondary alteration textures that highlight a fabric ~30° from horizontal. This fabric is delineated by aligned and coalesced, elongate alteration/devitrification domains within the lavas that may relate to primary flow in the lavas. It is not clear whether the lava was emplaced in a subaerial or subaqueous environment. The balance of the unit is composed of material that has probably fallen down the hole during drilling (e.g., interval 183-1142A-6R-1, 0–28 cm) and highly disturbed intervals, broken and mixed during drilling (e.g., interval 183-1142A-6R-1, 114–146 cm).

F35. Close-up photograph of interval 183-1142A-10R-1, 42–63 cm, p. 77.

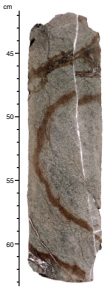

F36. Close-up photograph of interval 183-1142A-9R-2, 58–68 cm, p. 78.

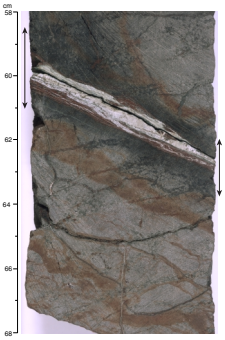

F37. Close-up photograph of interval 183-1142A-9R-4, 0–13 cm, p. 79.

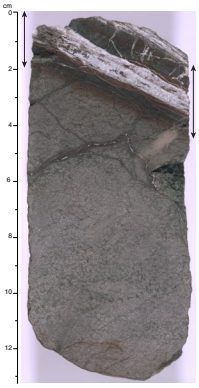

Subunit 3C/Unit 4 Boundary

The transition from highly disturbed material at the base of Subunit 3C to a (baked?) clay with disseminated granules marks the transition into Unit 4. The Unit 4 sediment is red (oxidized) and pervasively weathered, implying a significant time break at this boundary.

Unit 4

The mixture of incorporated clast lithologies and morphologies as well as the normal grading in the very coarse sand to granule-bearing clay indicates that this is a reworked interval. The high concentration of fine-grained material and the disseminated crystal feldspar? content in this unit suggest that it is a resedimented volcanic ash that has been pervasively altered. The transition from normal-graded to matrix-supported textures is consistent with mass-flow resedimentation of the clay-rich sediment, and it is probably a mudflow deposit. The uniform red oxidation color throughout this unit more likely results from deep weathering in a subaerial environment rather than baking in either a subaerial or subaqueous environment. However, no other regolith features are preserved in this interval to confirm a subaerial weathering history. Alternatively, the red matrix could have been derived by erosion of intensely weathered clay-rich material, with no post emplacement weathering.

Unit 4/Unit 5 Boundary

The boundary between Units 5 and 6 is located at the change from indurated granule-bearing clay into a massive aphyric volcanic breccia.

Unit 5

Unit 5 is largely composed of brecciated rocks with one >35-cm-diameter lobe of coherent lava near the top. The breccia materials vary from tightly juxtaposed clasts, which may show contacts along sutures (interval 183-1142A-7R-1, 92–100 cm), to a breccia with sheared and/or flattened clasts in a granule-bearing red clay matrix (interval 183-1142A-7R-1, 137–151 cm) to an in situ breccia with polygonal fracture networks separating clasts (interval 183-1142A-8R-1, 44–48 cm). These breccias may show transitional states in an autobreccia carapace, in which there is both brittle deformation of earlier-formed cooled rock and interaction of clasts and lobes that may have been hot. Examples of the latter include the suture textures in the upper breccia and enhanced alteration around perimeter of the intrusive lobe. The matrix in the breccia with more sheared and flattened clasts is similar in composition to the overlying granule-bearing red clay, implying some interaction between intrusive lobes or lava material and sediment. The flattening of clasts may be caused by hot emplacement and welding, variable alteration and load flattening, or shearing through the breccia zone. Lack of evidence of heating of the breccia materials and the observation that larger clasts seem altered to a similar degree suggest some shearing of this breccia after emplacement. The lava lobe in this interval is massive and aphyric and has zoned alteration. The secondary fabric is defined by coalescence of elongate, millimeter-scale, altered domains in the lava.

Unit 5/Unit 6 Boundary

The change from highly disturbed altered rock at the base of Unit 5 to a relatively coherent massive lava (and the top of a new core) mark the change from Unit 5 to Unit 6. It is possible that parts of Unit 5 are the deeply weathered and highly altered upper part of Unit 6.

Unit 6 (Pillow? Basalt)

The most distinguishing feature of Unit 6 is its complete lack of vesiculation. The patterns delineated by the veins are reminiscent of the pattern of chill margins seen in pillow basalts (cf. Figs. **F36** and **F37** to Figs. **F6,** p. 42, and **F13,** p. 49, in the "Site 1140" chapter), but the identification of chilled margins remains equivocal (see **"Alteration and Weathering,"** p. 30). Chilled margins are diagnostic of emplacement in a subaqueous environment, and the lack of vesicles would suggest eruption in relatively deep water. The two possible chill margins could be simply altered veins.

Interpretive Summary

All the lavas seen in Hole 1141A are consistent with being subaerially emplaced, and there is no evidence for interaction with water during emplacement. Without downhole logging data, we are cautious about estimating flow thicknesses. However, these flows are probably all between 5 and 20 m thick. These thicknesses are greater than are typical for historical Hawaiian flows but thinner than typical continental flood basalt flows. Instead, they are most similar to the largest recent Icelandic lava flows.

Unit 6 in Hole 1142A is possibly submarine and the features in the other lavas are inconclusive with regard to the environment into which they were emplaced. However, the alteration and weathering suggests that the rocks were exposed for some time in a subaerial environment (see **"Alteration and Weathering,"** p. 30).

The differences between Sites 1141 and 1142 are rather striking, considering that they are only 800 m apart. These differences demonstrate the complex geologic history of this part of Broken Ridge.

IGNEOUS PETROLOGY AND GEOCHEMISTRY

Site 1141

Introduction

Drilling at Site 1141 recovered material from 72.1 m of igneous basement (see **"Operations,"** p. 2, and **"Physical Volcanology,"** p. 12). We did not recover the contact with the overlying sedimentary section, but the lowermost sedimentary rock recovered above basement is a sandy nannofossil-bearing foraminifer limestone that contains microfossils of middle to late Eocene age (see **"Biostratigraphy,"** p. 7, and **"Lithostratigraphy,"** p. 5). Thus, the minimum age of basement at this site (and Site 1142; see **"Lithostratigraphy,"** p. 5) is near the age inferred for rifting between Broken Ridge and the Kerguelen Plateau (e.g., Mutter and Cande, 1983).

The basement section is divided into six units (Cores 183-1141A-13R through 24R); Figure **F38** contains a summary of unit boundaries, cu-

F38. Interpretive log for Hole 1141A, **p. 80.**

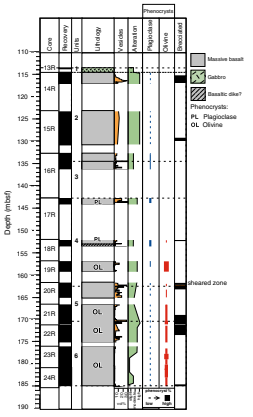

rated depths and thicknesses, and recovery (see also Table T5). All but the first unit are basaltic lavas that appear to have been emplaced subaerially. We have defined the basaltic lava units on the basis of marked differences in flow structure, oxidation, and/or vesicularity (see "Physical Volcanology," p. 12). The most diagnostic criteria for stratigraphic classification at Site 1141 were distinctive red or green color (e.g., the Unit 2/3 boundary) accompanied by a change from massive structure (interpreted to correspond to flow interiors) to brecciated structure (interpreted to correspond to flow margins) (e.g., the Unit 5/6 boundary) and/or a change in vesicularity and vesicle shape and size (e.g., the Unit 4/5 boundary). Units 5 and 6 are also distinguished by macroscopic differences in phenocryst content. Each lava unit corresponds to what we provisionally interpret to be a single eruption event. Note, however, that Unit 4 may contain an additional flow boundary and possibly a dike (Section 183-1141A-18R-2), but a definite identification of either is precluded by limited recovery (Table T5) and requires detailed shore-based study.

Macroscopic Features of Basement Lithology

Unit 1 (1.0 m curated thickness) is represented by only three small pieces (2–3 cm) of angular, rough-surfaced, moderately altered, medium-grained, plagioclase-clinopyroxene-olivine gabbro, which could be originally from a dike or sill but could also have been collected from a gravel bed. Because the rocks are likely to have been broken during drilling, the shapes and surfaces of the pieces provide no insight into which of these possibilities is correct.

Large portions of Units 2 and 3 are altered to clay and were disturbed considerably by drilling. Unit 2 (20.0 m curated thickness) is dominantly clay, with the exception of a few pebble- to small cobble-sized pieces of soft, completely altered basalt near the bottom of the unit. From these pieces, we determined that the protolith was aphanitic to fine-grained aphyric basalt. Most of Unit 3 (8.3 m curated thickness) is also clay; however, pieces recovered from the lower ~0.5 m of the unit are only moderately altered. The basalt in these pieces is fine to medium grained and sparsely plagioclase-phyric.

Unit 4 (19.6 m curated thickness) varies from completely altered to locally slightly altered, aphyric to moderately plagioclase- or plagioclase-olivine-phyric basalt. Alteration in most of the massive interior portion of the unit is moderate. The basalt in Section 183-1141A-18R-2 and in the bottom of Section 183-1141A-18R-1 is notably fresher, finer grained, and denser than that above or below in Unit 4. This interval could simply be a dense, better-preserved zone within the interior of the flow. Alternatively, it could be a portion of a dike intruded into Unit 4; however, no contacts were recovered. As with the entire basement sequence, the magnetic polarity of this zone is normal (see "Paleomagnetism," p. 35). The top piece of Section 183-1141A-18R-1 is brecciated and could represent part of a flow top, but, again, no contact was recovered.

Alteration in Unit 5 (8.0 m curated thickness) is high to complete in the upper portion of the unit but decreases to moderate in the lower portion (Sections 183-1141A-21R-1 through 21R-3) (see "Alteration and Weathering," p. 30). The basalt is sparsely olivine-phyric. Most of Unit 6 (15.3 m curated thickness) is also sparsely olivine-phyric, but a range from aphyric to moderately olivine-plagioclase-phyric basalt is

present. Alteration ranges from complete to moderate and, in Sections 183-1141A-23R-1 and 23R-2, to locally slight.

Petrography

Table T8 summarizes the thin-section mineralogy and textures of samples from Sites 1141 and 1142. All basalt samples studied from these sites have relatively uniform mineralogical compositions and textures.

Site 1141 samples from Units 2, 3, and most of 4 are aphyric to plagioclase-phyric basalts. Plagioclase phenocrysts commonly exhibit sieve textures as well as overgrowths (Fig. F39). In the lower part of Unit 4 and in Units 5 and 6, partially altered olivine is a persistent phenocryst phase (Fig. F40). The groundmass consists of plagioclase, clinopyroxene, titanomagnetite, and altered glass. In the lower part of Unit 4, and throughout Units 5 and 6, olivine is present in the groundmass. Another minor but common groundmass phase is apatite, which is found as minute needles concentrated in interstitial glassy regions. These two features suggest that the basalts are alkalic, an observation that is confirmed by geochemistry.

Textures in the groundmass range from intergranular to intersertal or trachytic, but in coarser-grained interiors of the larger flows, subophitic to ophitic textures have developed (Fig. F41). Samples from the margins of Units 5 and 6 are vesicular and finer grained, but have essentially the same mineralogy as the more slowly cooled flow interiors.

The degree of alteration as observed in thin section is moderate to high from the top of Unit 1 to the upper part of Unit 6. In this interval, the mafic minerals and groundmass glass are completely replaced by fine-grained carbonate (Fig. F42), clay, and iron oxides. Crystalline goethite is present and is an alteration product of titanomagnetite (Fig. F43). However, even in these rocks, a large proportion of plagioclase has escaped alteration. In contrast, portions of the middle to lower part of Unit 6 are well preserved and samples from this interval retain a large proportion of fresh phenocryst and groundmass olivine (Fig. F40).

Site 1142

Introduction

Drilling at Site 1142 penetrated 50.9 m of basement. Four pieces of basalt, totaling 0.3 m in curated thickness, were recovered from the bottom of the interval above the basement sequence (interval 183-1142A-1W-1, 0–41 cm) (see "Operations," p. 2). The contact between igneous basement and the overlying sedimentary sequence was not recovered, but Section 183-1142A-1W-1 includes two pieces of the middle to late Eocene, sandy, nannofossil-bearing foraminifer limestone similar to that found at Site 1141 (see "Biostratigraphy," p. 7, and "Lithostratigraphy," p. 5). Moreover, small amounts of this limestone are cemented onto the weathered surfaces of the basalt pieces in this section; thus, the basalt and limestone were in contact before drilling, although the contact was not necessarily a conformable one. Within the basement sequence, many of the volcanological features that were useful in determining unit boundaries at the other Leg 183 sites are not present in the material recovered at Site 1142 (see "Physical Volcanology," p. 12); however, major lithologic changes define six distinct basement units. The upper five units provide no evidence for submarine emplacement; however, Unit 6 contains basalts that were possibly emplaced in

T8. Summary of petrographic characteristics of Sites 1141 and 1142 basement units, p. 129.

F39. Two examples from Unit 3 of plagioclase phenocrysts exhibiting a sieve texture, p. 81.

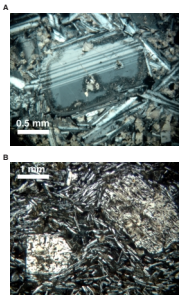

F40. Altered olivine phenocryst from Unit 6 with fresh cores, p. 82.

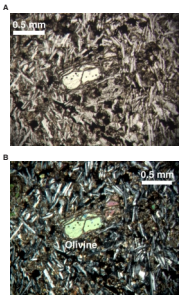

F41. Subophitic texture with olivine phenocrysts, clinopyroxene, and plagioclase, p. 83.

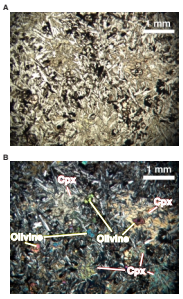

F42. Carbonate pseudomorph (in cross-polarized light) of a mafic phenocryst, p. 84.

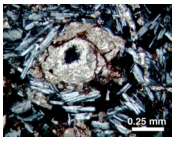

water (see "Physical Volcanology," p. 12). Table T6 presents a summary of the unit boundaries, curated depths and thicknesses, and recovery (see also Fig. F44).

Macroscopic Features of Basement Lithology

Unit 1 is massive basalt with a recovered thickness of 1.9 m and an estimated thickness of 8.8 m (Fig. F44). There is no curated thickness for this unit. We began coring within the unit (see Table T6; Fig. F44). The basalt is slightly to moderately altered, fine grained, and aphyric to sparsely plagioclase-olivine-phyric. The basalt fragments from the upper portion of the unit (Section 183-1142A-1W-1) have prominent (~0.3 to 5 cm thick) oxidation halos at their margins. The presence of oxidation halos and adhering limestone suggests periods of both subaerial and submarine exposure and weathering, possibly related to the Eocene rifting of Broken Ridge from the Kerguelen Plateau. Basalt from the lower portion of the unit (Sections 183-1142A-2R-1 and 2R-2) lacks oxidation halos (and associated limestone).

Unit 2 (1.2 m curated thickness) consists of a single section (Section 183-1142A-3R-1) containing 20 moderately to completely altered cobble-sized pieces of genetically unrelated rock types. With the exception of material in the core-catcher of this section, these rocks represent all that was recovered of a 9.6-m interval. The rocks include volcanic breccia (see "Physical Volcanology," p. 12, for description), clinopyroxene-phyric basalt, plagioclase-phyric basalt, olivine-phyric basalt, aphyric basalt, and feldspar- and feldspar-quartz-phyric felsic volcanic rocks. Approximately half of the pieces are round to subround, with abraded, slightly weathered surfaces; this feature, together with the mixture of rock types present, may indicate that we sampled some type of immature, uncemented sedimentary deposit, perhaps a near-source debris flow or a talus pile. The felsic rocks demonstrate that a wider range of igneous lithologies is present in the upper levels of basement in this region of Broken Ridge than represented by the basaltic lavas drilled at either Site 1141 or 1142.

Unit 3 (19.3 m curated thickness) is a completely altered brecciated aphanitic basalt; the upper portions are aphyric (Sections 183-1142A-3R-CC through 5R-1) and the lower portion (Sections 183-1142A-5R-2 through 6R-1) is aphyric to moderately olivine-plagioclase-phyric. Much of the unit is highly disturbed by drilling, but the lower portion contains more massive and coherent breccia and thin (~0.1 m) lava lobes. A description of the textural features used to subdivide the unit into three subunits is in "Physical Volcanology," p. 12.

Unit 4 (4.3 m curated thickness) is a well-indurated, normally graded claystone or mudstone. The red clay matrix supports very coarse sand-sized to small-granule-sized clasts of very highly to completely altered lithic fragments and crystals of quartz and altered feldspar. This unit is interpreted as a mudflow deposit (see detailed description and discussion in "Physical Volcanology," p. 12).

Unit 5 (8.8 m curated thickness) is composed of aphanitic, aphyric volcanic breccia. Alteration is nearly complete, except near the base of the unit (Section 183-1142A-8R-1), where some very highly altered material is preserved (see "Physical Volcanology," p. 12, and "Alteration and Weathering," p. 30). The only hint of the original rock type is provided by very rare quartz crystals in Section 183-1142A-7R-2, suggesting an evolved composition.

F43. Two examples of crystalline goethite replacing titanomagnetite, p. 85.

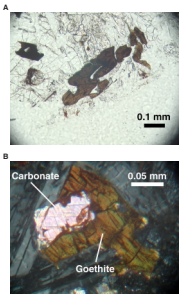

F44. Interpretive log for Hole 1142A, p. 86.

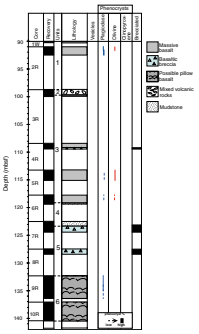

Evidence of possible eruption into water is provided by Unit 6. This unit is composed of ≥8.5 m of nonvesicular, massive, and possibly pillowed basalt. The portion we recovered contains at least two possible glassy margins, now altered to clay. The basalt is aphyric and fine-grained to aphanitic. Rare plagioclase phenocrysts are present in Sections 183-1142A-9R-2 through 9R-4. Alteration varies from high to moderate in most of the unit, although portions of Section 183-1142A-10R-1 are only slightly altered. In addition to the presence of possible glassy margins (Figs. F36, F37), the pattern of veining (see "Alteration and Weathering," p. 30) is consistent with that of pillow lavas. The near absence of vesicles (see "Physical Volcanology," p. 12) suggests eruption of the unit in relatively deep water. Distinctive, curved, and commonly roughly concentric brown to orange oxidation bands are abundant in all but the lowermost section of the unit (Section 183-1142A-10R-3); these bands are similar to those in weathered pillow lava lobes. However, such bands are not typical of submarine alteration and probably represent subaerial weathering during the period of uplift and rifting of Broken Ridge from the Kerguelen Plateau.

Petrography

The general petrographic characteristics of the basement units from Site 1142 are presented in Table T8. Unit 1 of Site 1142 is sparsely olivine-phyric basalt with an intergranular texture. Although relatively fresh, with large proportions of all silicate minerals including unaltered olivine (Fig. F45), it contains large patches of carbonate in the groundmass. Thin sections from the best-preserved parts of the underlying Units 2, 3, and 6 all show moderate to high alteration. Of the primary phases, only a portion of the plagioclase and magnetite has not been replaced by secondary minerals. Textures, however, are well preserved. Unit 3 is a moderately olivine-plagioclase-phyric basalt with plagioclase that exhibits sieve textures and olivine that is completely altered to clay (Fig. F46). A Unit 6 sample from a possible pillow margin (183-1142A-9R-4, 3–7 cm) contains an apparent outer glassy rind. The rind is brecciated, replaced by cryptocrystalline goethite and clay, and intruded by multiple calcite veins; despite this, it retains the appearance of relict glass (Fig. F47). Adjacent to the rind, the rock consists of fine, well-oriented plagioclase laths and lesser amounts of granular clinopyroxene and titanomagnetite, all altered to clay and secondary iron oxide. As in the region farther from the margin (e.g., Sample 183-1142A-10R-1, 38–40 cm), which has similar texture and mineralogy, this portion of the rock is sparsely plagioclase-phyric, with plagioclase phenocrysts that exhibit sieve-textured rims (Fig. F48).

Sites 1141 and 1142 Geochemistry

We report X-ray fluorescence (XRF) analyses for eleven lavas, nine from Site 1141 and two from Site 1142, in Table T9. The samples are generally olivine-normative basalts, although three samples (two from Site 1141 and one from Site 1142) are quartz normative. Compositions are generally slightly alkalic (Fig. F49), with data for all but two samples (one from Site 1141, a trachybasalt, and one from Site 1142, a basaltic andesite) plotting in the basalt field. For this discussion, all samples will be referred to as basalts.

The samples exhibit moderate compositional variations (Site 1141: SiO_2 = 45.3–51.6 wt%; MgO = 3.16–6.45 wt%; Mg#, assuming 80% of

F45. Corroded olivine microphenocrysts with fresh cores in an intergranular groundmass, p. 87.

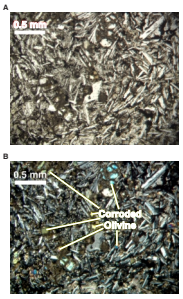

F46. Sieve-textured plagioclase and altered olivine phenocrysts in an intergranular groundmass, p. 88.

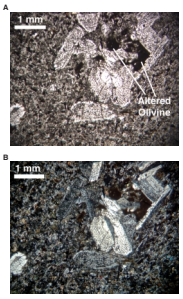

F47. Altered, possibly originally glassy, pillow margin, p. 89.

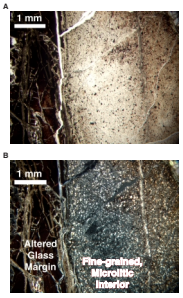

F48. Interior of probable pillow lava showing corroded plagioclase phenocrysts in an intergranular groundmass, p. 90.

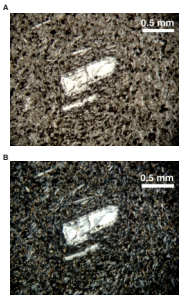

the total iron is FeO, = 0.38–0.55. Site 1142: SiO_2 = 46.7–53.9 wt%; MgO = 2.77–6.56 wt%; Mg# = 0.39–0.55). At Site 1141, the three units sampled generally exhibit limited variations in TiO_2, Al_2O_3, Na_2O, and K_2O from Unit 4 to Unit 6 (Table **T9;** Fig. **F50**), except for the uppermost sample from Unit 4 (183-1141A-17R-1, 27–31 cm), which contains notably higher abundances of these elements. Silica exhibits little variation in Units 4 and 5 (47.2–48.2 wt%; Table **T9**), but in Unit 6, it shows a range from 45.3 to 51.6 wt%. This may reflect variable alteration but the samples with different SiO_2 have similar Na_2O and K_2O contents (Fig. **F50**). The MgO contents steadily increase from the top of Unit 4 to the base of Unit 5, then markedly decrease at the top of Unit 6 before steadily increasing down through this unit. This pattern is generally paralleled by that of CaO. Fe_2O_3 varies more in Unit 4 (9.54–12.9 wt%), with a maximum value in the center of the flow, than in the other two units (10.8–12.3 wt%).

Minor and trace elements show similar downhole patterns to those of the major elements, with P_2O_5, Nb, Ba, Rb, and Zr (not shown) contents decreasing downhole markedly from the uppermost Unit 4 sample to similar abundances throughout the remainder of Unit 4 and Units 5 and 6 (Fig. **F51**). Chromium increases from 125 ppm near the top of Unit 4 to 292 ppm at the base but varies less through Units 5 and 6 (296–344 ppm). Primitive mantle-normalized $(Nb/Zr)_N$ varies little in Unit 6 (~1.7–1.8) compared to Units 4 and 5, where it decreases from ~2.5 at the top of Unit 4 to ~1.7 in the middle of the unit, then increases downward to ~1.9 within Unit 5. Variation in $(Zr/Y)_N$ broadly parallels and $(Zr/Ti)_N$ is opposite to that displayed by $(Nb/Zr)_N$.

In terms of the geochemistry, no compositional differences in Unit 4 correlate with the composite nature of this unit observed in the cores. The downhole compositional variation can be explained by igneous fractionation and alteration processes. For example, Samples 183-1141A-22R-3, 94–96 cm, and 22R-3, 142–146 cm, of Unit 6 are quartz normative (Table **T9**) yet contain olivine as phenocrysts and as a groundmass phase. Their quartz-normative character may be explained by the secondary silica present as vesicle fill (see **"Alteration and Weathering,"** p. 30). Variations in TiO_2, MgO, and CaO, (Fig. **F50**), along with P_2O_5, Ni, and Cr (Fig. **F51**), are consistent with two inputs of fresh, comparatively primitive magma at the beginning of the Unit 5 and Unit 6 eruptions. For example, at the top of Unit 6, MgO has decreased to 3.19 wt%, from 6.45 wt% at the base. At the base of Unit 5, MgO is again more than 6 wt%. We suggest these changes represent pulses of new, more primitive magma, rather than crystal accumulation at the base of the flows. We observed no increase in the proportion of phenocrysts at the bases of flow units in thin section. From the Al_2O_3 and CaO variations, it appears that olivine was joined by clinopyroxene, rather than plagioclase, as a fractionating phase because CaO increases then decreases upward (i.e., as each magma evolved) (Fig. **F50F**), whereas Al_2O_3 generally increases up the core (Fig. **F50C**). Also, clinopyroxene fractionation can affect incompatible element ratios (i.e., 30% fractional crystallization of clinopyroxene results in an increase of 1 unit in $[Zr/Y]_N$, it results in an increase of <0.08 for $[Nb/Zr]_N$). However, clinopyroxene is not observed as a phenocryst phase in thin section. Rather, sieve textured plagioclase phenocrysts are present. Resorption of plagioclase could be the result of the influx of more primitive magma. The range of incompatible element ratios may reflect open-system fractional crystallization and/or magma mixing.

T9. Major and trace element XRF data for Sites 1141 and 1142 basalts, **p. 130.**

F49. Sites 1141 and 1142 igneous rock compositions, **p. 91.**

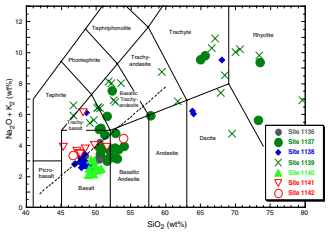

F50. Downhole variations of major elements through basement Units 4–6 at Site 1141, **p. 92.**

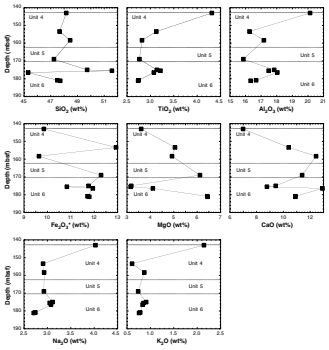

F51. Downhole variations of selected minor and trace elements through basement Units 4–6 at Site 1141, **p. 93.**

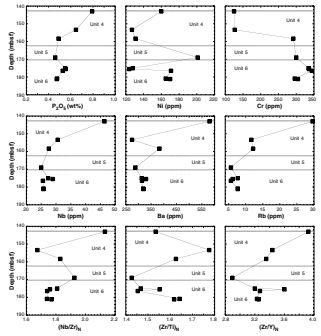

At Site 1142, the two samples analyzed demonstrate compositional differences between Units 1 (basalt) and 6 (basaltic andesite). Compositional variations between the samples from Site 1142 suggest that the two units represented are not related by simple closed-system fractional crystallization. For example, although the sample with the highest MgO content (interval 183-1142A-2R-1, 50–53 cm, of Unit 1, with 6.56 wt% vs. interval 183-1142A-10R-1, 37–40 cm, of Unit 6, with 2.77 wt%) has the highest Ni and Cr abundances (184 vs. 34 ppm and 303 vs. 21 ppm, respectively), it also contains the highest TiO_2, Nb, and Zr abundances (2.77 vs. 2.46 wt%, 26.3 vs. 16.1 ppm and 233 vs. 220 ppm, respectively). In addition, primitive mantle–normalized incompatible element ratios differ significantly between the Unit 1 and Unit 6 samples, which have, respectively, $(Nb/Zr)_N$ = 1.8 and 1.2, $(Zr/Ti)_N$ = 1.6 and 1.8, and $(Zr/Y)_N$ = 3.2 and 2.3. As with Site 1141 basalts, clinopyroxene fractionation can affect these ratios, but it is not observed as a phenocryst phase.

As Sites 1141 and 1142 are only ~800 m apart, establishing similarities between the two basement sections was difficult on the basis of core descriptions or petrography. Whole-rock geochemistry demonstrates interval 183-1142A-2R-1, 50–53 cm, of Unit 1 has a similar composition to those from Unit 6 from Site 1141 (Figs. **F52, F53, F54;** Table **T9**). This suggests that Site 1142 Unit 6 is from beneath the recovered sequence at Site 1141. The analyzed sample from Unit 6 (interval 183-1142A-10R-1, 37–40 cm) has a composition similar to other Kerguelen Plateau basalts and it is tholeiitic (Fig. **F49**).

Comparison with Other Broken Ridge Samples

Mahoney et al. (1995) reported geochemical data for dredge samples from the central and eastern Broken Ridge and concluded that at least some of these samples contained evidence of a continental lithospheric, possibly crustal, influence in their genesis especially for the eastern part of Broken Ridge. These data are presented on primitive mantle–normalized diagrams in Fig. **F55,** where they are compared with those from Sites 1141 and 1142. It is evident that the dredge and drill-core samples generally have different compositions. For example, the Leg 183 samples have subparallel profiles with $(Nb/Ce)_N$ ratios generally >1, distinct from the dredge samples, which have $(Nb/Ce)_N$ <1. Only interval 183-1142A-10R-1, 37–40 cm, has a $(Nb/Ce)_N$ ratio < 1. This sample appears to be similar to the dredge samples from Broken Ridge (Fig. **F55**). Overall, the other Sites 1141 and 1142 samples are enriched in the incompatible minor and trace elements relative to the dredge samples and lack evidence of any obvious continental influence. General distinctions between the Broken Ridge drill and dredge samples are further emphasized in Figures **F52, F53,** and **F54.**

Comparison with Kerguelen Plateau Sites

The basalts from Sites 1141 and 1142 are compared with those from sites on the Kerguelen Plateau, as well as the dredge samples from Broken Ridge in Figures **F52** and **F53.** Except for lavas from Site 1139, samples from Sites 1141 and 1142 have lower MgO and higher Al_2O_3, TiO_2, P_2O_5, Zr, Nb, Ti, and Ni contents relative to lavas from other sites. The generally alkaline composition of Site 1141 and 1142 basalts is supported by the presence of apatite in the groundmass, which is consis-

F52. Major and minor element compositions of Sites 1141 and 1142 basalts, **p. 94.**

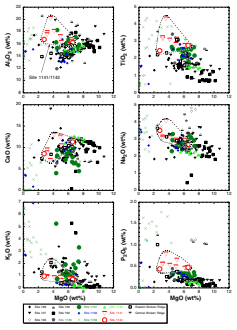

F53. Trace element compositions of Sites 1141 and 1142 basalts, **p. 95.**

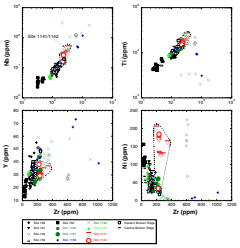

F54. Variations of minor and trace element abundances with primitive mantle–normalized Nb/Zr ratio for Sites 1141 and 1142 basalts, **p. 96.**

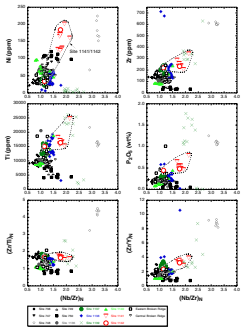

F55. Primitive mantle–normalized plots of Sites 1141 and 1142 basalts, **p. 97.**

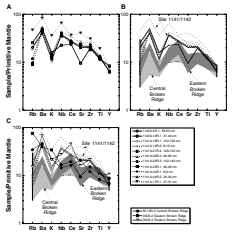

tent with their elevated P_2O_5 contents relative to most Kerguelen Plateau and other Broken Ridge samples (Figs. F52, F54). Data for one of the two basalts analyzed from Site 1142 (183-1142A-2R-1, 50–53 cm, the sample with the higher MgO content) fall within the range of the Site 1141 data, whereas the other sample plots with the majority of Kerguelen Plateau and Broken Ridge basalts (Fig. F53). In terms of Zr, Ti, and Nb, the Leg 183 Broken Ridge basalts are similar to those from Site 1139 and the alkali basalt from Site 748, but they contain lower Y contents for a given Zr abundance, having similar $(Zr/Y)_N$ ratios to those of Site 1137 basalts (Fig. F54). In terms of Ni, basalts from Sites 1141 and 1142 are distinct (Figs. F53, F54). The elevated Ni contents are consistent with the presence of olivine both as a phenocryst and groundmass phase in some of the Site 1141 basalts. The only other samples exhibiting such elevated Ni abundances are from the Site 748 alkali basalt. Curiously, lavas with hot Ni content at Sites 748, 1141, and 1142 have high $(Nb/Zr)_N$ (Fig. F54).

Summary and Conclusions

At Sites 1141 and 1142, six basement units were identified. On the basis of macroscopic and microscopic features, these units cannot be correlated, even though Site 1142 is only ~800 m to the south of Site 1141. From geochemical evidence, however, we suggest that Unit 1 of Site 1142 is equivalent to Unit 6 of Site 1141. This is consistent with seismic data that suggest basement in this area has a persistent northerly dip (see "Background and Objectives," p. 1). The observed differences could also be a result of paleotopographic control on the deposition of the lavas and other basement units, or locally different erosion rates.

Compared to most basement lavas from the Kerguelen Plateau and Broken Ridge, basement lavas at Sites 1141 and 1142 have higher abundances of Ni and incompatible elements. The relatively high Zr and Nb contents result in $(Nb/Zr)_N$ and $(Zr/Y)_N$ ratios similar to Site 1139 basement lavas; only samples from the Site 748 alkali basalt have higher values (Fig. F54). We infer that Site 1141 and 1142 basalts were generated by lower degrees of partial melting than basement lavas from Leg 183 Sites 1136, 1137, 1138, and 1140. The elevated Ni contents, however, indicate that they experienced lower amounts of olivine fractional crystallization. The ranges in incompatible element ratios suggest fractional crystallization did not occur in a closed system (especially as clinopyroxene is not observed as a phenocryst phase). Sieve-textured plagioclase phenocrysts suggest that fractional crystallization was accompanied by magma mixing.

Given that drilling at Sites 1141 and 1142 penetrated only the uppermost few tens of meters of basement from this many kilometers thick edifice, the rocks recovered clearly represent the terminal stages of volcanism on this portion of Broken Ridge. The igneous activity recorded in the drill cores was alkalic and may reflect lower degrees of partial melting under the influence of a waning heat source. Only the base of Site 1142 penetrated beneath this terminal alkalic sequence of lava flows into the general tholeiitic sequence. This lowermost unit at Site 1142 is compositionally distinct from other Site 1141 and 1142 basalts in that it exhibits $(Nb/Ce)_N < 1$, similar to the dredge samples from Broken Ridge (Fig. F55), a result that is consistent with contamination by a continental component (Mahoney et al., 1995). All other Site

1141 or 1142 lavas do not exhibit evidence of this contamination (i.e., they have $[Nb/Ce]_N > 1$).

ALTERATION AND WEATHERING

Hole 1141A

A lithic pebble conglomerate characterized by chert and basalt pebbles within a calcareous foraminifer-rich matrix directly overlies the basement in Hole 1141A. The conglomerate is coated with a 1-cm-thick manganese crust, suggesting submarine exposure for an extended time. The six basement units below the conglomerate include gabbroic rocks (Unit 1) and subaerial basalt flows (Units 2–6) (see "Physical Volcanology," p. 12, and "Igneous Petrology," p. 22). All basement units in Hole 1141A have been variably affected by secondary processes. These include subaerial weathering and fluid/rock interaction, as indicated by the abundance of clay in flow tops and secondary minerals that partly to completely replace mesostasis and fill veins, vesicles, and open spaces between breccia clasts (see the "Supplementary Materials" contents list for the alteration and vein structure logs; see also Fig. F56A). Detailed analysis of structural data was not performed, but orientations were measured for most planar features observed in these cores.

F56. The distribution of secondary minerals in Holes 1141A and 1142A, p. 98.

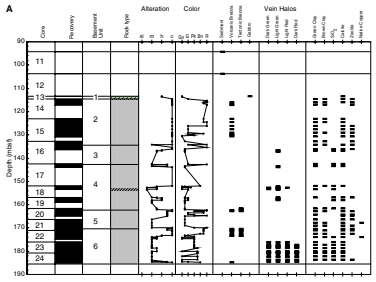

Unit 1

The two gabbroic pebbles comprising Unit 1 are dark green and highly to completely altered. Small orange halos are present around oxidized clinopyroxene phenocrysts, and the groundmass has been pervasively replaced by calcite. The pebbles contain one 0.2-mm calcite vein.

Unit 2

The basalt flow comprising Unit 2 has a curated thickness of 20 m and is completely altered to clay, although the core is still coherent and many intervals have not been disturbed by drilling. We observed distinct color variations in Unit 2 that suggest a general decrease in oxidation with depth. Various shades of red characterize the color of the upper part of the unit from the top of Section 183-1141A-14R-1 to the bottom of Section 183-1141A-15R-2. The middle portion of the flow (Interval 183-1141A-15R-3 through 15R-5, 114 cm) is light gray to brown gray, and color gradually changes to light green and greenish gray with depth toward the bottom of the unit. Although the flow has been completely altered, some primary igneous features are still discernible. Vesicles are particularly well preserved and are completely filled with dark green clay, carbonate, and zeolite (Table T10). In addition, possible late-stage, more highly vesicular segregations are present near the top of the flow (e.g., intervals 183-1141A-14R-1, 90–93 cm, and 14R-1, 126–134 cm), and some intervals have brecciated textures (e.g., interval 183-1141A-15R-5, 0–30 cm). Veins are not present.

T10. XRD identification of alteration minerals from Hole 1141A, p. 131.

Unit 3

The intensity of alteration within Unit 3 varies from complete near the top of the flow to moderate at the base. This corresponds to a large

increase in competency with depth, from soft clay easily penetrated by the probe to solid rock (see "Alteration and Weathering," p. 25, in the "Explanatory Notes" chapter). A brick red interval, completely altered to clay, is present in the uppermost 9 cm of the flow (interval 183-1141A-16R-2, 19–28 cm). Below this interval, color gradually changes from dark to light greenish gray and finally to light gray at the base of the flow, consistent with a decrease in oxidation with depth and similar to the alteration patterns we observed in Unit 2. Primary variolitic textures are visible, even in the completely altered basalts, and tend to be accentuated by replacement of igneous minerals with light green clay. A pronounced mesostasis is also visible in the less altered intervals and is replaced by light green clay and calcite within the halos of calcite veins. Vesicles are locally abundant (as much as 7%) and are filled with dark green clay, calcite, zeolite, and, rarely, quartz. Rare amorphous silica replaces possible late-stage magmatic segregations (e.g., interval 183-1141A-16R-CC, 40–41 cm). Calcite veins are common and are generally <0.5 mm wide, some with light brown carbonate-rich halos.

Unit 4

Unit 4 is variably altered fine-grained basalt with only slight to moderate change in some intervals within the interior of the flow and complete alteration near the top. Color varies from greenish gray to dusky red in the highly to completely altered flow top and gradually changes to green and greenish gray with depth through the unit. Thus, a distinctive oxidized flow top, such as those present in the uppermost parts of basement Units 1–3, appears to be less well developed in Unit 4. Primary igneous features, including glassy mesostasis and variolitic textures, have been altered to green clay, and calcite locally replaces the groundmass (e.g., Sample 183-1141A-19R-21, Piece 21). Vesicle morphology is preserved because the vesicles are completely filled with brown and green clay, calcite, and amorphous silica, and some vesicles have colloform textures (Fig. F57). We observed a trace of native copper in vesicles and the groundmass. Secondary minerals filling veins include green, brown, and red clay, calcite, zeolite, and, more rarely, quartz. Dark green alteration halos <10 mm wide are common around veins and tend to be much more highly altered to clay than adjacent regions. Red oxidation vein halos or bands, not always associated with veins or fractures, are present and are typically crosscut by late calcite veins. Light green alteration halos associated with these calcite veins replace the oxidized halos (Fig. F56A). Slickensides are numerous along some fractured surfaces, and brecciated wall rock is present in some veins.

F57. Color close-up photograph of interval 183-1141A-18R-1 (Piece 11B, 74–85 cm), p. 100.

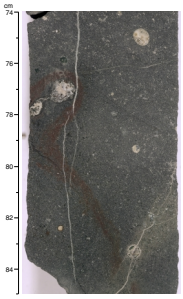

Unit 5

The flow top of the basalt comprising Unit 5 is red, highly vesicular (15%), and completely altered to clay with abundant slickensides on clay-lined fractures. Color gradually changes to pinkish gray and greenish gray with depth, suggesting a decrease in oxidation. Intensity of alteration correspondingly decreases with depth, but all intervals are at least moderately altered, with clay replacing the fine-grained groundmass. The least-altered basalt is in the massive, sparsely vesicular flow interior. The flow base is highly vesicular and completely altered to red clay. Secondary minerals filling vesicles include green clay, calcite, zeolite, and (more rarely) amorphous silica. Veins are extremely common,

generally <1 mm wide, and filled with calcite, zeolite, and (more rarely) green and blue clay. Zeolite is the most abundant mineral filling veins in the upper portion of the unit to the bottom of Section 183-1141A-20R-3. Below this depth, and continuing to the bottom of Unit 5, veins filled with calcite and green clay are common. We observed one fracture lined with calcite, green clay, and abundant native copper that comprises ~10% of the fracture surface (Sample 183-1141A-21R-2 [Piece 5, 39–44 cm]). Slickensides are also common, particularly along fractures lined with red clay.

Unit 6

The flow top of the lowermost basalt flow in Hole 1141A (Unit 6) is brecciated and completely altered to red-brown clay (Fig. F58). The brecciation may be related to primary volcanic processes, but slickensides on clay-lined fractured surfaces suggest that tectonic processes may also be involved. Unlike other basement units in Hole 1141A, color does not vary consistently with depth in Unit 6 because of the presence of complex alteration halos of different color surrounding subvertical veins. Like other basement units, the intensity of alteration and vesicularity both decrease with depth; the freshest rocks are moderately altered and sparsely vesicular. The basalt in the lowermost section of Hole 1141A (Section 183-1141A-24R-CC) is highly to completely altered to brown clay; this may be a highly altered flow base. Alteration accentuates primary igneous textures, including a prominent mesostasis altered to green and, more rarely, light red clay, variolitic textures, and late-stage magmatic segregations (Fig. F59). Vesicles are filled with green clay, calcite, and amorphous silica. Multiple generations of these secondary minerals produce colloform textures (Fig. F20). Perhaps the most noteworthy aspect of the alteration within Hole 1141A in general, and Unit 6 in particular, is the abundant and very well-developed halos that surround subvertical veins filled with quartz, calcite, and green clay. In some instances, a single quartz vein can be followed for >120 cm (e.g., Sample 183-1141A-24R-1 [Piece 2, 24–144 cm]) with multiple symmetrical alteration halos progressively altering the surrounding wall rock (Fig. F60). The color of these halos varies from dark green at the vein margin to light green, dark red, and light red grading into dark red-gray basalt. A general decrease in alteration intensity is associated with this color change. Calcite veins lacking distinctive halos crosscut the quartz-rich veins, indicating multiple generations of fracturing with quartz formation before calcite. We observed similarly complex alteration halos around networks of calcite and quartz veins that locally incorporate brecciated wall rock fragments (Fig. F61).

The alteration patterns observed in Hole 1141A suggest that the upper part of the basement (Units 2 and 3) was weathered in a subaerial environment long enough to deeply and completely weather these flows to clay. Units 4–6 also have highly or completely altered flow tops, but the presence of only moderately altered flow interiors may suggest subaerial exposure for shorter lengths of time. All the units were also affected by hydrothermal alteration at low to moderate temperatures (probably <200°C), but the relative timing of weathering and hydrothermal processes is not clear.

F58. Color close-up photograph of interval 183-1141A-22R-1 (Piece 2, 105–120 cm), p. 101.

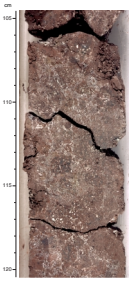

F59. Color close-up photograph of interval 183-1141A-23R-1, 105–115 cm, p. 102.

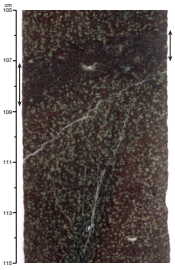

F60. Color close-up photograph of interval 183-1141A-24R-1 (Piece 2H, 85–101 cm), p. 103.

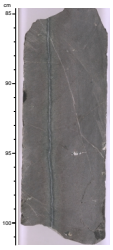

F61. Color close-up photograph of interval 183-1141A-23R-2 (Piece 1, 98–120 cm), p. 104.

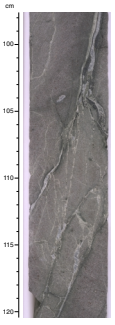

Hole 1142A

Six basement units have been defined in Hole 1142A, including a granule-bearing clay (Unit 4) and five volcanic units of unknown origin (Units 1, 2, 3, 5, and 6). All basement units have been variably altered by fluid/rock interaction at low to moderate temperatures, as indicated by secondary minerals that replace primary igneous phases, partly line fractures, and partly to completely fill veins and vesicles. The distribution of secondary phases is recorded in the alteration and vein structure logs for Hole 1142A (see the **"Supplementary Materials"** contents list) and plotted in Figure **F56B.**

Unit 1

Unit 1 is a massive basalt that is relatively fresh compared to other basement units in Hole 1142A (and Hole 1141A, which is only 0.8 km away). The flow is gray, sparsely vesicular, and only slightly altered. Calcite, zeolite, and minor green clay fill vesicles. Green and red-brown halos as much as 10 mm wide are common around veins filled with green clay and calcite.

Unit 2

The mixed volcanic rocks comprising Unit 2 have different compositions and textures and have been altered to varying degrees. Chocolate brown volcanic breccias completely altered to clay were recovered (Sample 183-1142A-3R-1 [Pieces 3 and 4 and 12–15]). Other lithologies present include variably altered microcrystalline to fine-grained mixed volcanic rocks. Highly altered pieces are blue green (Sample 183-1142A-3R-1 [Pieces 5 and 8–10]) and are moderately vesicular with white clay and calcite-filling vesicles. Moderately altered pieces are light gray (Sample 183-1142A-3R-1 [Pieces 6, 7, and 11]) with few or no vesicles present. The lowermost pieces recovered from this unit include dark green plagioclase-phyric basalt (Sample 183-1142A-3R-1 [Pieces 16–18]) and a light gray plagioclase-phyric volcanic rock (Sample 183-1142A-3R-1 [Pieces 19–20]). Quartz(?) phenocrysts may be present in the latter, suggesting a relatively felsic composition. All of these lowermost pieces are completely altered to clay, and the groundmass of Pieces 19 and 20 are also replaced by calcite. Sparse carbonate veins, <1 mm wide, are in the unit.

Unit 3

Unit 3 has been divided into three subunits that include disturbed volcanic rock (Subunit 3A) and mixed lava, and volcanic breccias (Subunits 3B and 3C, respectively). Subunit 3A is dusky red and completely altered to clay. Some units are relatively coherent, whereas others have been highly disturbed by drilling. The volcanic rocks comprising Subunit 3B are dusky red, variably brecciated, and highly to completely altered to red-brown clay. Sparse vesicles are filled with brown clay. Slickensides are present on some fractured surfaces. Subunit 3C includes moderately to highly altered volcanic rubble and dusky red volcanic rocks that are completely altered to clay. The latter are variably disturbed by drilling, although some coherent pieces are present. Primary igneous textures are still visible and are accentuated by the re-

placement of feldspar by light green clay and mafic minerals by red-brown clay.

Unit 4

The granule-bearing clay comprising Unit 4 probably represents reworked volcanic debris (see "Physical Volcanology," p. 12). Subangular to rounded matrix-supported lithic pebbles are supported by a red clay matrix and become more abundant near the bottom of the unit. The pebbles are highly altered to clay minerals of variable color.

Unit 5

Unit 5 is volcanic breccia that is highly to completely altered to clay and variably disturbed by drilling, particularly near the base of the unit. The breccia is clast supported and varies from greenish brown near the top of the unit to reddish brown near the base. We observed pyrite and slickensides on some fracture surfaces lined with brown clay. Flow banding is present on some clasts, and quartz was tentatively identified, implying that this unit may be relatively silicic in composition.

Unit 6

The lowermost unit in Hole 1142A (Unit 6) is a nonvesicular basalt flow that may be either subaerial or submarine. Color varies from red to green to gray and alteration intensity varies from slight to high, depending on the abundance of red-brown oxidation and alteration halos around veins. Calcite ± hematite and brown clay veins are associated with red-oxidized halos that penetrate the wall rock to a greater extent along mesostasis trails (Fig. F34). Calcite veins clearly crosscut and locally offset red oxidation halos (Figs. F34, F35), meaning that calcite veins formed after the rock was variably oxidized. Some calcite veins in Unit 6 are associated with multiple alteration halos of varying color and alteration intensity (Fig. F62). Highly altered basalt is present as relatively narrow, very dark greenish black alteration halos immediately adjacent to calcite veins and comprises <1% of the rock. Dark green alteration halos produce moderately to highly altered basalt with moderately altered light green and red-brown halos at even greater distances from vein margins. These halos typically grade into slightly altered gray basalt.

Unit 6 has a number of alteration features that suggest the basalts may be pillows formed in a subaqueous environment. These include semicircular red-brown oxidation halos that could reflect progressive oxidation fronts into pillow-shaped lava and narrow dark green to black intervals associated with carbonate veins that may be completely altered glassy pillow margins.

The oxidation fronts are extremely common in Unit 6. Some are not connected with veins or fractures, indicating fluid migration through the rock along grain boundaries. However, close examination of these red-brown bands indicates that many of them are simply linear alteration halos cutting through the core along veins and fractures (e.g., Fig. F35). Moreover, based on our observations of numerous subaerial and submarine basalt flows on Leg 183, oxidation fronts typically have variable geometries that appear to be unrelated to macroscopic structures. They are, instead, probably more related to the complexities of fluid flow along grain boundaries. The dark green to black intervals associ-

F62. Color close-up photograph of interval 183-1142A-9R-2, 56–58 cm, p. 105.

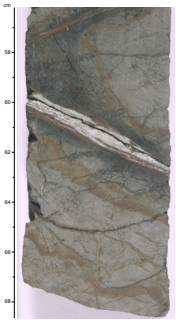

ated with carbonate veins perhaps provide a more compelling argument for glassy pillow margins (e.g., Figs. F37, F62). Superficially, they look very much like completely altered analogs of the fresh glassy margins recovered from the pillow basalts in Hole 1140A. Close examination of some of these zones (e.g., Fig. F62) reveals that primary igneous textures extend from the relatively unaltered basalt through the dark green to black alteration zones. If this is the case, these features simply represent intense alteration halos around calcite veins. Other examples may be more compelling (e.g., F37). Thin-section analysis, however, indicates that grain size does not decrease toward the margin of the highly altered zones, an observation that is not consistent with the presence of glassy pillow margins (see "Igneous Petrology," p. 22).

PALEOMAGNETISM

We measured the natural remanent magnetization (NRM) of most archive halves from Holes 1141A and 1142A with the pass-through cryogenic magnetometer using measurement intervals of 5 and 2.5 cm for sediments and basement rocks, respectively. Subsequently, sediment and basement core sections were demagnetized with peak alternating fields (AF) at 20 and 50 mT, respectively. We did not analyze highly disturbed sections of sediments. Discrete sediment samples were stepwise AF demagnetized up to 30 mT; however, no discrete basement samples were analyzed by stepwise demagnetization because of limited time for measurement.

Sediment was recovered only in Hole 1141A. With Cores 183-1141A-8R and 9R, we obtained reliable remanent magnetizations and correlated normal and reversed polarities with middle Miocene Chrons C5 through C5AD. However, the upper part of the sediment section from Hole 1141A provides only a limited paleomagnetic record as a result of weak magnetizations and highly disturbed cores. We obtained reliable paleomagnetic directions from basement rocks from both Holes 1141A and 1142A that showed normal polarity. We observed no significant differences in average susceptibility and NRM intensity in the lava flows of Hole 1141A. In Hole 1142A, we observed the highest average susceptibility in basement Unit 6, the strongest NRM intensity in Unit 1, and the lowest average NRM intensity and susceptibility in basement Unit 4.

Sediments

One archive section of most cores was demagnetized stepwise up to 30 mT. We took one or two discrete samples per section, and 12 samples were stepwise AF demagnetized up to 30 mT to confirm the reliability of whole-core measurements. We obtained reliable results from Cores 183-1141A-8R and 9R and correlated normal and reversed segments with biostratigraphic zones (see "Biostratigraphy," p. 7). Cores 183-1141A-8R and 9R generally have a stable magnetization, which was obtained after AF demagnetization at 10 mT. Most discrete samples from Cores 183-1141A-8R and 9R have a high median destructive field (MDF), and the remanent direction is stable in demagnetization steps between 10 and 30 mT (Fig. F63). Therefore, we used the remanent magnetization, after AF demagnetization at 20 mT, to correlate the paleomagnetic record with the geomagnetic chrons. Furthermore, we used the data selection criteria as described in "Paleomagnetism," p. 27, in

F63. AF demagnetization of a discrete sediment sample from Hole 1141A, p. 106.

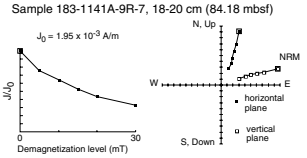

the "Explanatory Notes" chapter for magnetostratigraphic studies of Hole 1141A (Fig. F64). The selection criteria were that (1) the intensity of remanent magnetization after AF demagnetization at 20 mT was >2 × 10^{-4} A/m, (2) the inclination was >±20°, (3) at least two consecutive values (which corresponds to a 10-cm length of split core) had the same polarity, and (4) there was no significant core disturbance. Characteristic inclinations from discrete samples generally agree well with selected inclinations from whole-core measurements (Fig. F64).

Correlation of biostratigraphic data and polarity reversals (Fig. F64) suggests that the reversed and normal chrons in Cores 183-1141A-8R and 9R are middle Miocene in age (see "Biostratigraphy," p. 7). We obtained short normal and reversed segments between 66 and 86 mbsf in the lower part of Unit I (see "Lithostratigraphy," p. 5). The upper part of the unit provides only a limited paleomagnetic record as a result of weak magnetizations and highly disturbed cores. However, we propose some correlations with paleontological data from the core catcher of each core (see "Biostratigraphy," p. 7). The normal and reversed segments between 66 and 86 mbsf probably lie within middle Miocene Chrons C5 through C5AD.

We observed negative susceptibilities (whole-core multisensor track [MST] measurements; see "Physical Properties," p. 37) (Fig. F65) and weak NRM intensities in Unit I (nannofossil ooze; see "Lithostratigraphy," p. 5) (Fig. F64). In the lower part of Unit I, we observed stronger NRM intensities and, thus, obtained a more reliable paleomagnetic record than in the upper part.

Basement Rocks

Hole 1141A

We determined the magnetic properties of each basement unit (see "Igneous Petrology," p. 22, and "Physical Volcanology," p. 12) and the variation of magnetic properties within each unit of Hole 1141A (Fig. F66). Three independent types of susceptibility measurements, MST, AMST (see "Paleomagnetism," p. 27, in the "Explanatory Notes" chapter), and discrete samples, generally show consistent results. We observed no significant differences in average susceptibility and NRM intensity in the lava flows (basement Units 2 to 6; Figs. F65, F66). Average NRM intensities range from 4.40 (basement Unit 5) to 0.49 (basement Unit 2) A/m. Average susceptibilities range from 1.54 × 10^{-3} (basement Unit 3) to 1.04 × 10^{-3} (basement Unit 5) SI units.

We found negative inclinations, indicating a normal magnetic polarity, in all basement units after AF demagnetization at 40 mT. We observed scattered negative inclinations in Units 2 and 3. Scattered inclinations are probably related to alteration (see "Igneous Petrology," p. 22, and "Physical Volcanology," p. 12). Basement Units 4, 5, and 6 have more reliable (less scattered) negative inclinations. Within basement Unit 4, we observed lower NRM intensities and susceptibilities in the bottom part than the upper part. We found higher NRM intensities and susceptibilities at the upper part of basement Unit 5 than in the lower part of the unit. In the lower part of basement Unit 6, we observed a reversed overprint, which was probably not caused by the recent (Brunhes normal epoch) magnetic field. The reversed magnetic component may be secondary, acquired during alteration or as a result of drilling effects.

F64. Inclination, intensity of remanent magnetization, and susceptibility of Hole 1141A sediments, p. 107.

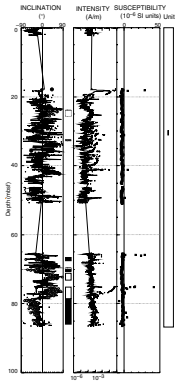

F65. Average NRM intensity and MST susceptibility of all units, p. 108.

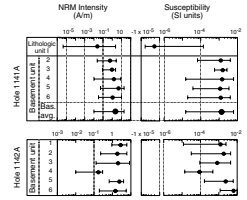

F66. Inclination, intensity of remanent magnetization, and susceptibility of Hole 1141A basement rocks, p. 109.

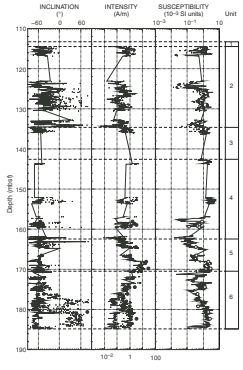

Stepwise AF demagnetization up to 50 mT was applied to all the basement archive-half sections to analyze their behavior during demagnetization. For analysis, we selected data points in rock pieces that are longer than the effective sensitivity of the pass-through magnetometer (~15 cm). We found two different types of magnetic behavior. The upper part of basement Unit 6 has a stable single-component magnetization (Fig. F67A) and a high MDF. The magnetization of the lower part of basement Unit 6 is characterized by a two-component magnetization (Fig. F67B) and a low MDF. The soft reversed component is probably related to alteration or drilling effects, as mentioned above.

F67. AF demagnetization of basement archive halves from Hole 1141A, p. 110.

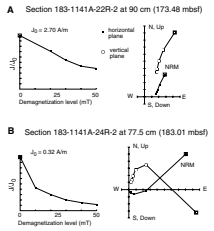

1142A

We observed the magnetic properties of each basement unit (see "Igneous Petrology," p. 22, and "Physical Volcanology," p. 12) and the variation of magnetic properties within each unit of Hole 1142A (Fig. F68). Average NRM intensities range from 2.65 (basement Unit 1) to 0.16 (basement Unit 4) A/m. Average susceptibilities range from 6.25 × 10^{-3} (basement Unit 6) to 8.84 × 10^{-5} (basement Unit 4) SI units (Fig. F65). We observed the highest average susceptibility in basement Unit 6, the strongest NRM intensity in basement Unit 1, and the lowest average NRM intensity and susceptibility in basement Unit 4 (granule-bearing clay; see "Physical Volcanology," p. 12).

We found negative inclinations, indicating a normal magnetic polarity, in all units after AF demagnetization at 40 mT. We observed scattered negative inclinations in basement Units 2 and 3. Scattered inclinations are probably related to alteration (see "Igneous Petrology," p. 22, and "Physical Volcanology," p. 12). Basement Units 4, 5, and 6 have more reliable (less scattered) negative inclinations. Within basement Unit 6, we observed lower NRM intensities in the bottom part than in the upper part (Fig. F68). In the upper part of basement Unit 6, we observed a reversed overprint, which was probably not caused by the recent (Brunhes normal epoch) magnetic field. As in basement Unit 6 of Hole 1141A, the reversed magnetic component may be secondary, acquired during basement alteration or as a result of drilling effects.

F68. Inclination, intensity of remanent magnetization, and susceptibility of Hole 1142A basement rocks, p. 111.

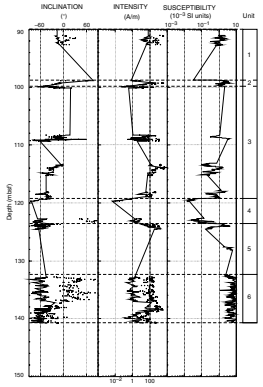

Stepwise AF demagnetization up to 50 mT was applied to all basement archive-half sections of Hole 1142A to analyze behavior during demagnetization. For analysis, we selected data points in rock pieces that are longer than the effective sensitivity of the pass-through magnetometer (~15 cm). The lower part of basement Unit 6 has a stable single-component magnetization (Fig. F69A) and a low MDF. The magnetic overprint was removed by AF demagnetization at 20 mT. Piece 7 in Section 183-1142A-5R-2 (Unit 3) has a very high MDF (Fig. F69B), and the intensity of the remanent magnetization remaining after AF demagnetization at 50 mT is >95% of the NRM intensity.

F69. AF demagnetization of basement archive halves from Hole 1142A, p. 112.

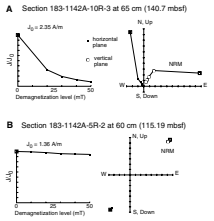

PHYSICAL PROPERTIES

Introduction

We determined the physical properties of whole-core sections from Hole 1141A, where sediments and basement rocks were recovered, and from Hole 1142A, where only basement was cored. Measurements obtained from the MST included magnetic susceptibility, gamma-ray attenuation porosity evaluator (GRAPE) bulk density, and natural gamma

radiation (NGR). We determined compressional wave velocities (V_p) from the split cores in transverse directions (x) for soft sediments in liners and for hard-rock pieces without the liner. Measurements in the longitudinal (z) and transverse (x and y) directions on cut samples of consolidated sediment and hard rock allowed us to investigate velocity anisotropy. Index properties determinations included bulk density, water content, porosity, and grain density. We calculated index properties from wet and dry sample weights and dry volumes. We also determined thermal conductivity for sediment and basalt.

Index Properties

We determined index properties by using gravimetric methods on discrete samples from Sites 1141 and 1142 (Table T11). The general trends exhibited by the index properties data at both sites reflect downhole variations in lithology (Figs. F70, F71, F72).

Site 1141

Between ~20 and ~51 mbsf in Unit I, bulk densities change little, varying from 1.6 to 1.7 g/cm³, averaging 1.7 g/cm³. Porosity ranges from 57% to 65% with a mean of 62%. Grain densities also exhibit small scatter in this interval, with values between 2.6 and 2.7 g/cm³. Sediments in this interval consist of foraminifer nannofossil ooze (see "Lithostratigraphy," p. 5).

From ~67 to ~86 mbsf, still within Unit I, bulk density increases slightly, from 1.7 to 1.8 g/cm³. The grain density changes between 2.5 and 2.7 g/cm³. Porosity decreases from 62% to 54% with a mean of 58% (Fig. F70C). Sediments in this depth interval also change little, from generally fine-grained white ooze with abundant nannofossils grading downward into light pale brown ooze composed mostly of sand-sized foraminifers.

Below the boundary between Units I and II (~114 mbsf), index properties change abruptly (Figs. F70, F71). From 115.8 to 116.7 mbsf in the upper part of basement Unit 2, which consists of reddish, loosely consolidated altered basalt (see "Physical Volcanology," p. 12), bulk densities increase to a mean value ~2.0 g/cm³, grain densities increase to 2.9 g/cm³, and porosities decrease to 48%. In this interval, the degree of alteration is moderate to high, and the mafic minerals are almost completely replaced by fine-grained carbonate, clay, and Fe-oxides (see "Igneous Petrology," p. 22).

From 123.2 to 130.0 mbsf, in the middle to lower parts of basement Unit 2, bulk density slightly decreases to 1.8 g/cm³, grain density also decreases to a mean 2.7 g/cm³, and porosity increases to a mean of 49%.

From 132.9 to 135.8 mbsf, all index properties change markedly near the boundary between basement Units 2 and 3 because the base of Unit 2 and top of Unit 3 are relatively less altered (see Fig. F38). As will be discussed in the later sections, natural gamma ray and compressional wave velocities also change significantly at this interval. Bulk density and grain density increase downhole with mean values of 2.0 and 2.8 g/cm³, respectively, and porosity decreases to a mean value of 44%.

Between 158.1 and 169.7 mbsf in basement Units 4 and 5, recovered rocks are basalts with relatively uniform mineralogical compositions and textures. Index properties in this interval reflect this change in li-

T11. Index properties data from Sites 1141 and 1142, p. 132.

F70. Downhole index properties and V_p at Site 1141, p. 113.

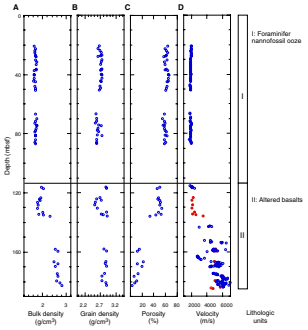

F71. Downhole index properties profiles of basement Units 1–6 in Hole 1141A, p. 114.

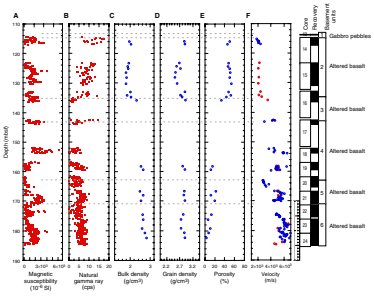

F72. Downhole index properties and V_p at Site 1142, p. 115.

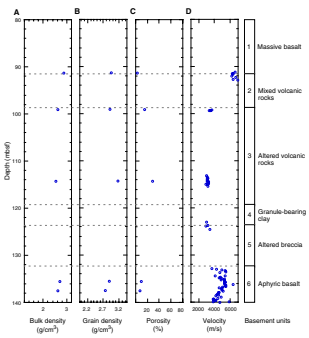

thology—bulk density varies from 2.5 to 2.7 g/cm³, grain density increases from 2.8 to 2.9 g/cm³, and porosity decreases to 16%.

In the lowermost basement unit (Unit 6, 174.4 to 184.5 mbsf), bulk densities vary from 2.6 to 2.9 g/cm³ with a mean of 2.7 g/cm³, grain density approaches a mean of 2.8 g/cm³, and porosity varies from 16% to 3% (Fig. F71). The lithologies in this interval are relatively fresh basalts.

Site 1142

Because of limited time, we were only able to determine index properties for five representative samples from basement Units 1, 2, 3, and 6 (Table T11; Fig. F72). The index properties show that massive basalt in Sample 183-1142A-2R-1, 28–30 cm (91.28 mbsf) from basement Unit 1 has a bulk density of 2.87 g/cm³, grain density of 2.92 g/cm³, and porosity of 2.6%. In Sample 183-1142A-3R-1, 39–41 cm, which is from the basaltic breccia in basement Unit 2, the bulk density is 2.60 g/cm³, grain density is 2.89 g/cm³, and porosity is 15%. The index properties in the massive basalt Sample 183-1142A-5R-1, 107–109 cm, of basement Unit 3 are distinctly different, with bulk density of 2.53 g/cm³, grain density of 3.13 g/cm³, and porosity of 28%. Two samples from the possible pillow basalt in basement Unit 6 show that from 135.6 to 137.5 mbsf, bulk densities are 2.62 to 2.70 g/cm³; grain density, 2.75 to 2.87 g/cm³; and porosity, 7% to 9%. These basalts are relatively altered and contain large patches of carbonate in the groundmass (see "Alteration and Weathering," p. 30).

MST Measurements

GRAPE Density

Bulk density was measured by the GRAPE every 4 cm on whole sections of cores recovered from Holes 1141A and 1142A. For Hole 1141A, the maximum (right side of the bulk densities profile) (Fig. F73) values of GRAPE densities correspond very well with wet bulk densities determined from discrete samples in the sedimentary section (Unit I; 0 to 103.8 mbsf). Below ~103.8 mbsf, bulk densities are much more scattered than in overlying sediments. As previously noted, the larger scatter in the GRAPE bulk density data for the deeper units results from empty space between pieces of core and the core's fractured nature, whereas the generally lower maximum GRAPE values are because of the smaller diameters of the cores.

In Hole 1142A, the aphyric basalts in basement Unit 6 exhibited highest maximum values of GRAPE densities, followed by the mixed volcanic rocks in Unit 2 (Fig. F74). The maximum GRAPE bulk densities for the remaining units are quite uniform, although the data are highly scattered (Fig. F74).

Natural Gamma Radiation

We measured NGR every 12 cm on unsplit sections of cores from Sites 1141 and 1142. At Site 1141, the NGR count in Unit I (between the seafloor and ~103 mbsf) is uniform. Between ~116 and ~130 mbsf, within basement Units 1 and 2, NGR values are constantly greater than 7 counts per second (cps) (Fig. F71B), reflecting the relatively higher clay content in these intervals. Gamma-ray values decrease near the

F73. Downhole profiles of MST measurements along with discrete determinations, p. 116.

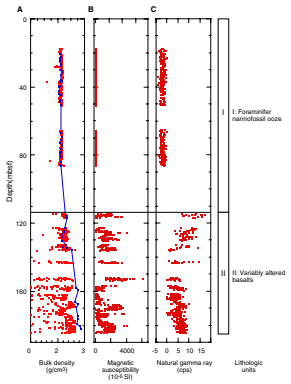

F74. Downhole profiles of MST measurements, including whole-core measurements, p. 117.

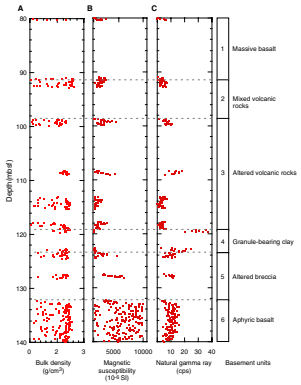

boundary between basement Units 2 and 3, with an associated increase in bulk and grain densities, as mentioned previously. The remaining basement Units have values of ~6 cps. Note that the downhole natural gamma-ray profile exhibit fluctuations associated with those of downhole magnetic susceptibility data (see Fig. F71A, F71B).

NGR measurements in basement sections of Hole 1142A also reflect lithologic changes (Fig. F74C). Between ~80 and ~119 mbsf in basement Units 1 through 3, gamma-ray values average 5 cps. NGR count increase distinctively at a depth of ~108 mbsf, with an average value 14 cps and corresponding to the clay-rich Subunit 3A (Section 183-1142A-3R-2) (Fig. 56B). The highest count (average >30 cps) is in the granule-bearing clay (basement Unit 4) at a depth of 119.3–119.7 mbsf. Between 132.3 and 140.7 mbsf, gamma-ray values reached an average value of 11 cps, corresponding to the altered breccia in basement Unit 5 (see "Igneous Petrology," p. 22). In basement Unit 6 (aphyric basalt; 132.3–140.7 mbsf), NGR values fluctuate between 4 and 16 cps, with a mean value of 10 cps.

Magnetic Susceptibility

We routinely determined magnetic susceptibility on all cores from Sites 1141 and 1142 (Figs. F71A, F73B, F74B). The results are discussed in "Paleomagnetism," p. 35.

Compressional Wave Velocity

We determined compressional wave velocities from split-core sections from Sites 1141 and 1142, and on discrete samples at Site 1141 (Figs. F70, F71, F74).

The compressional wave velocity data for Unit I of Hole 1141A (20.4 to ~86 mbsf), which consist of foraminifer-bearing nannofossil ooze, show very little scatter, with a mean value of ~1860 m/s (Table T12; Fig. F70). Below the boundary between Unit I and basement at ~114 mbsf (Fig. F71), compressional wave velocities start to increase with depth. Velocity from 115.8 to 116.7 mbsf increases from 1723 to 2353 m/s, with a mean of 2018 m/s, corresponding to a change in lithology from coarse-grained sedimentary deposit (gabbro pebbles) in basement Unit 1 to the altered basalt in basement Unit 2. Compressional wave velocities are fairly uniform between 123.2 and 130.0 mbsf (middle part of basement Unit 2), ranging between 2013 and 2213 m/s and corresponding to the clay-rich altered basalt in this interval.

Velocities gradually increase between 132.9 and 135.8 mbsf, from 2099 to 3422 m/s. Core 183-1141A-16R in this interval is altered basalt at the boundary between basement Units 2 and 3.

Velocities in basement Units 4 and 5 (~144 to ~170 mbsf) range from 4550 to 5180 m/s, with a mean around 4900 m/s. Compressional wave velocities in basement Unit 6 also increase gradually with depth, from 4276 to 6902 m/s. Velocities above 6000 m/s seem high and may be a consequence of the calibration method (see "Physical Properties," p. 31, in the "Explanatory Notes" chapter), but the general differences are probably valid. These changes correspond to a decrease in porosity and an increase in bulk and grain densities, as mentioned above. Changes in velocity, bulk density, and porosity in this unit correlate well.

Velocities for the basement units at Site 1142 vary considerably downhole (Table T13; Fig. F72). The highest velocities of >6000 m/s

T12. V_p measured in discrete samples, Site 1141, p. 133.

T13. V_p measured in discrete samples, Site 1142, p. 135.

correspond to massive basalt forming basement Unit 1 and the top of basement Unit 2 (from 91.1 to 92.8 mbsf). Velocities in the altered volcanic rocks and breccia of basement Units 3 and 5 decrease significantly, ranging between 2840 and 3640 m/s. Compressional wave velocities for the aphyric basalts in basement Unit 6 (132.8–140.8 mbsf) vary from 3600 to 6370 m/s, with a mean value of 4725 m/s.

Thermal Conductivity

At Site 1141 thermal conductivity values for sediments from Unit I are commonly between 1.0 and 1.3 W/(m·K), with a mean value of 1.1 W/(m·K), and show little scatter (Fig. **F75;** Table **T14**). The mean value is similar to values in sedimentary units at other Leg 183 sites. For the basement unit, thermal conductivity values vary quite widely, from a low of 0.7 W/(m·K) to a high of 2.4 W/(m·K) between ~154 and ~184 mbsf, with a mean value of 1.6 W/(m·K).

At Site 1142, thermal conductivity values for basement Units 1–4 average 1.6 W/(m·K) (Fig. **F76;** Table **T14**), similar to the mean value in basement rocks at Site 1141 (Fig. **F75**). Between ~133 and ~138 mbsf (aphyric basalt of basement Unit 6), thermal conductivity averages 1.5 W/(m·K). The highest values (2.4 W/[m·K]) were in Section 183-1142A-6R-2 (~119 mbsf), which is the reddish clay and granule-bearing mudstone in basement Unit 4. The mudstone also yields the highest gamma-ray value in Hole 1142A, as described earlier.

ORGANIC AND INORGANIC GEOCHEMISTRY

We determined concentrations of carbonate in six sediment samples from Hole 1141A (Table **T15**). Three of these samples were analyzed for organic carbon, total nitrogen, sulfur, and hydrogen. The results of the analyses are discussed in **"Lithostratigraphy,"** p. 5. We also determined total carbon, total nitrogen, sulfur, and hydrogen in two highly altered basalts using the CNS analyzer (Table **T15**).

F75. Site 1141 downhole profile of thermal conductivity, **p. 118.**

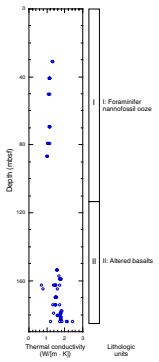

T14. Thermal conductivity values for Sites 1141 and 1142, **p. 136.**

F76. Downhole profile of whole-core measurements of thermal conductivity, **p. 119.**

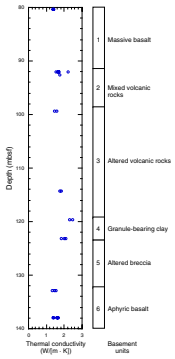

T15. Carbon, nitrogen, sulfur, and hydrogen analyses of sediments and altered volcanic rocks from Site 1141, **p. 137.**

REFERENCES

Duncan, R.A., 1991. Age distribution of volcanism along aseismic ridges in the eastern Indian Ocean. *In* Weissel, J., Peirce, J., Taylor, E., Alt, J., et al., *Proc. ODP, Sci. Results,* 121: College Station, TX (Ocean Drilling Program), 507–517.

Duncan, R.A., and Storey, M., 1992. The life cycle of Indian Ocean hotspots. *In* Duncan, R.A., Rea, D.K., Kidd, R.B., von Rad, U., and Weissel, J.K. (Eds.), *Synthesis of Results from Scientific Drilling in the Indian Ocean.* Geophys. Monogr., Am. Geophys. Union, 70:91–103.

Fisher, R.L., 1997. Bathymetry of the Southern Indian Ocean. *General Bathymetric Chart of the Oceans*. GEBCO, Sheet 97.1.

Kennett, J.P., and Srinivasan, M.S., 1983. *Neogene Planktonic Foraminifera: A Phylogenetic Atlas:* Stroudsburg, PA (Hutchinson Ross).

Le Bas, M.J., Le Maitre, R.W., Streckeisen, A., and Zanettin, B., 1986. A chemical classification of volcanic rocks based on the total alkali-silica diagram. *J. Petrol.,* 27:745–750.

Macdonald, G.A., and Katsura, T., 1964. Chemical composition of Hawaiian lavas. *J. Petrol.,* 5:82–133.

Mahoney, J.J., Jones, W.B., Frey, F.A., Salters, V.J.M., Pyle, D.G., and Davies, H.L., 1995. Geochemical characteristics of lavas from Broken Ridge, the Naturaliste Plateau and southernmost Kerguelen Plateau: Cretaceous plateau volcanism in the Southeast Indian Ocean. *Chem. Geol.,* 120:315–345.

Mutter, J.C., and Cande, S.C., 1983. The early opening between Broken Ridge and Kerguelen Plateau. *Earth Planet. Sci. Lett.,* 65:369–376.

Parker, M.E., Clark, M., and Wise, S.W., Jr., 1985. Calcareous nannofossils of Deep Sea Drilling Project Sites 558 and 563, North Atlantic Ocean: biostratigraphy and the distribution of Oligocene braarudosphaerids. *In* Bougault, H., Cande, S.C., et al., *Init. Repts. DSDP,* 82: Washington (U.S. Govt. Printing Office), 559–589.

Peirce, J., Weissel, J., et al., 1989. *Proc. ODP, Init. Repts.,* 121: College Station, TX (Ocean Drilling Program).

Pringle, M.S., Storey, M., and Wijbrans, J., 1994. $^{40}Ar/^{39}Ar$ geochronology of mid-Cretaceous Indian ocean basalts: constraints on the origin of large flood basalt. *Eos,* 75:728.

Sandwell, D.T., and Smith, W.H.F., 1997. Marine gravity anomaly from Geosat and ERS-1 satellite altimetry. *J. Geophys. Res.,* 102:10039–10054.

Shipboard Scientific Party, 1989a. Site 754. *In* Peirce, J., Weissel, J., et al., *Proc. ODP, Init. Repts.,* 121: College Station, TX (Ocean Drilling Program), 191–236.

Shipboard Scientific Party, 1989b. Site 757. *In* Peirce, J., Weissel, J., et al., *Proc. ODP, Init. Repts.,* 121: College Station, TX (Ocean Drilling Program), 305–358.

Srinivasan, M.S., and Kennett, J.P., 1981. Neogene planktonic foraminiferal biostratigraphy and evolution: equatorial to subantarctic, South Pacific. *Mar. Micropaleontol.,* 6:499–533.

Storey, M., Pringle, M.S., Coffin, M.F., and Wijbrans, J., 1996. Geochemistry and geochronology of Kerguelen Plateau basalts: results from ODP Legs 119 and 120. *Eos,* 76:123.

Sun, S.-S., and McDonough, W.F., 1989. Chemical and isotopic systematics of oceanic basalts: implications for mantle composition and processes. *In* Saunders, A.D., and Norry, M.J. (Eds.), *Magmatism in the Ocean Basins*. Geol. Soc. Spec. Publ. London, 42:313–345.

Thierstein, H.R., 1974. Calcareous nannoplankton, Leg 26, Deep Sea Drilling Project. *In* Davies, T.A., Luyendyk, B.P., et al., *Init. Repts. DSDP,* 26: Washington (U.S. Govt. Printing Office), 619–667.

Figure F1. Satellite-derived free-air gravity map of Broken Ridge (after Sandwell and Smith, 1997). Current (Leg 183) and previous (Legs 26 and 121) DSDP and ODP sites are indicated by stars and circles, respectively (solid = basement sites). Solid squares indicate dredge sites where igneous rocks were recovered.

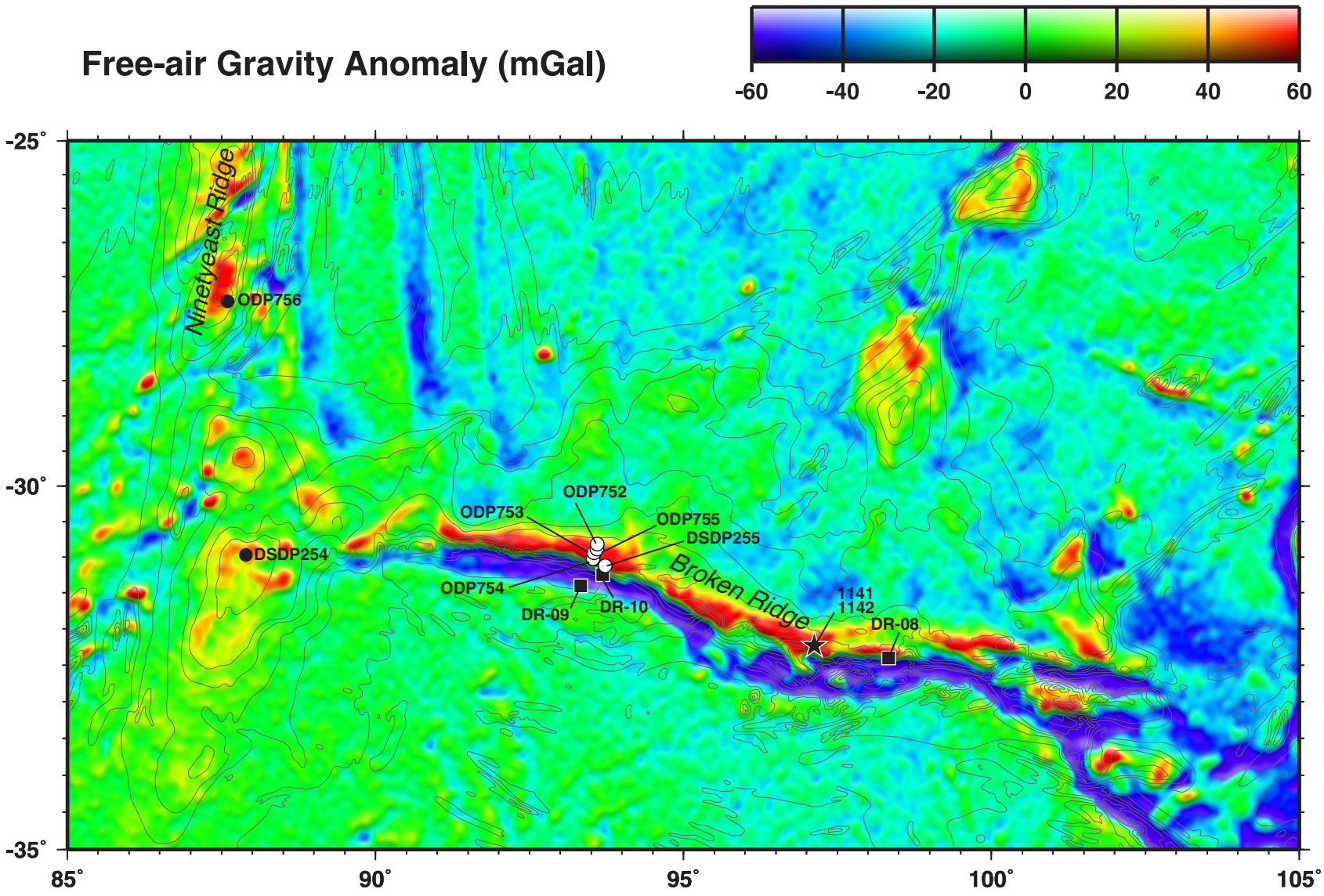

Figure F2. Location of Sites 1141 and 1142 relative to site-survey data. Navigation for *JOIDES Resolution* Leg 183, lines 101–103, and *Robert D. Conrad* survey 2708 are shown in hours:minutes. Bathymetric control for Broken Ridge is meager; note that the water depths of Sites 1141 (1209 m) and 1142 (1213 m) indicate that the most recent published bathymetry requires revision. Bathymetric contour interval = 500 m (Fisher, 1997).

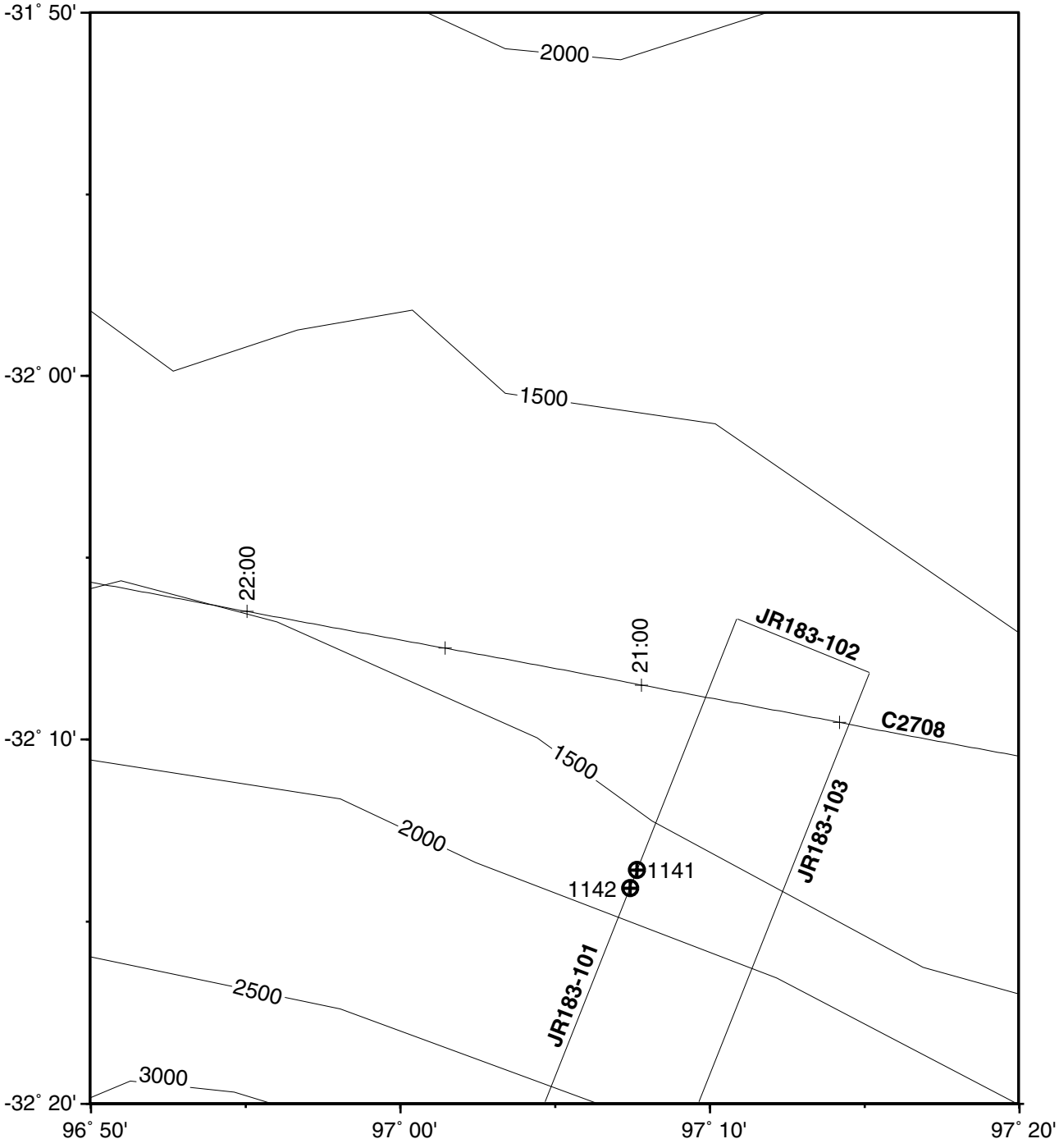

Figure F3. *JOIDES Resolution* JR183-101 single-channel seismic profile across Sites 1141 and 1142. Vertical exaggeration = ~20 at the seafloor.

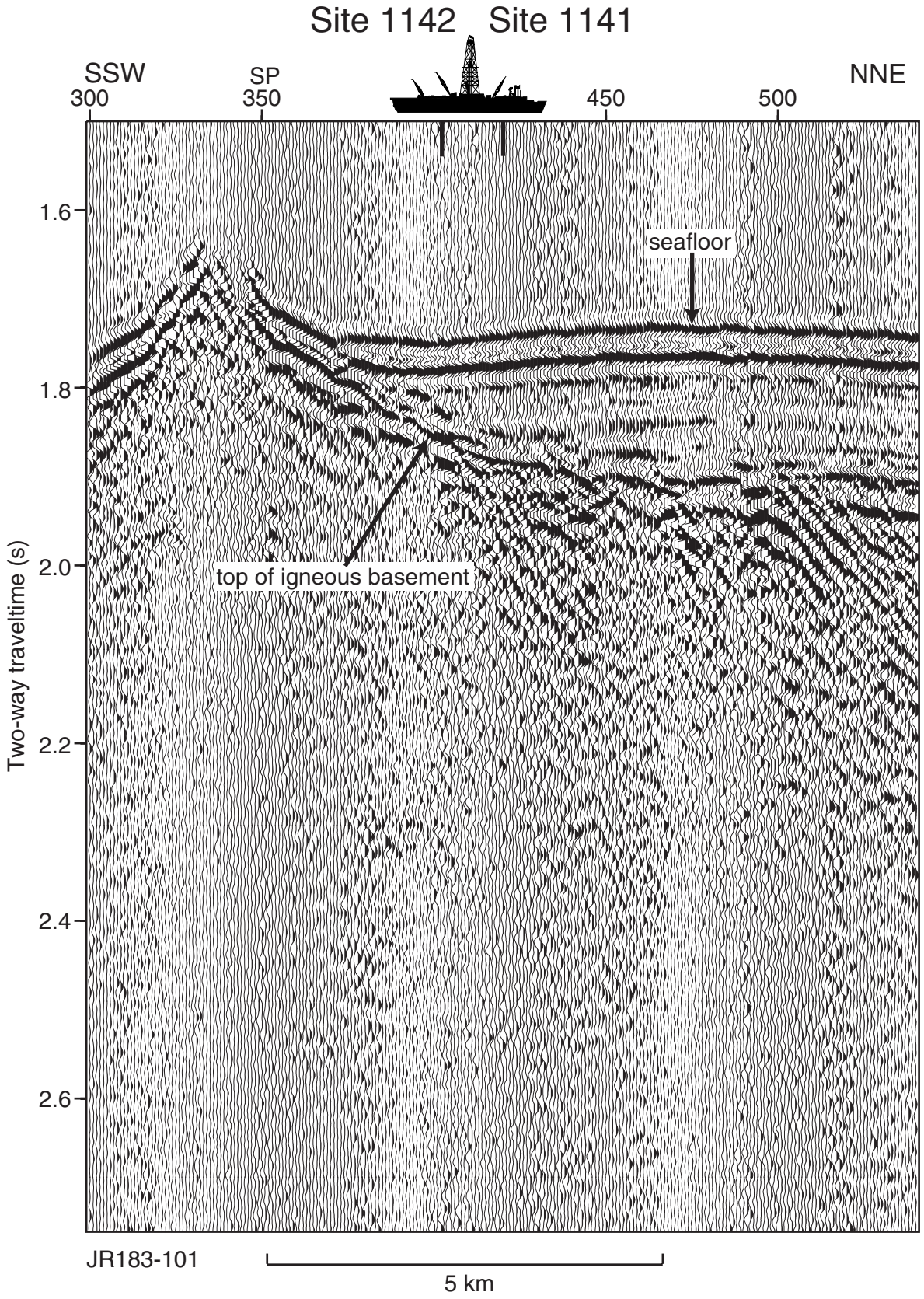

Figure F4. Composite stratigraphic section for Site 1141 showing core recovery, a simplified summary of lithology, lithologic unit boundaries, ages of units, and names of lithologies. The lithologic symbols are explained in Figure F3, p. 57, of the "Explanatory Notes" chapter.

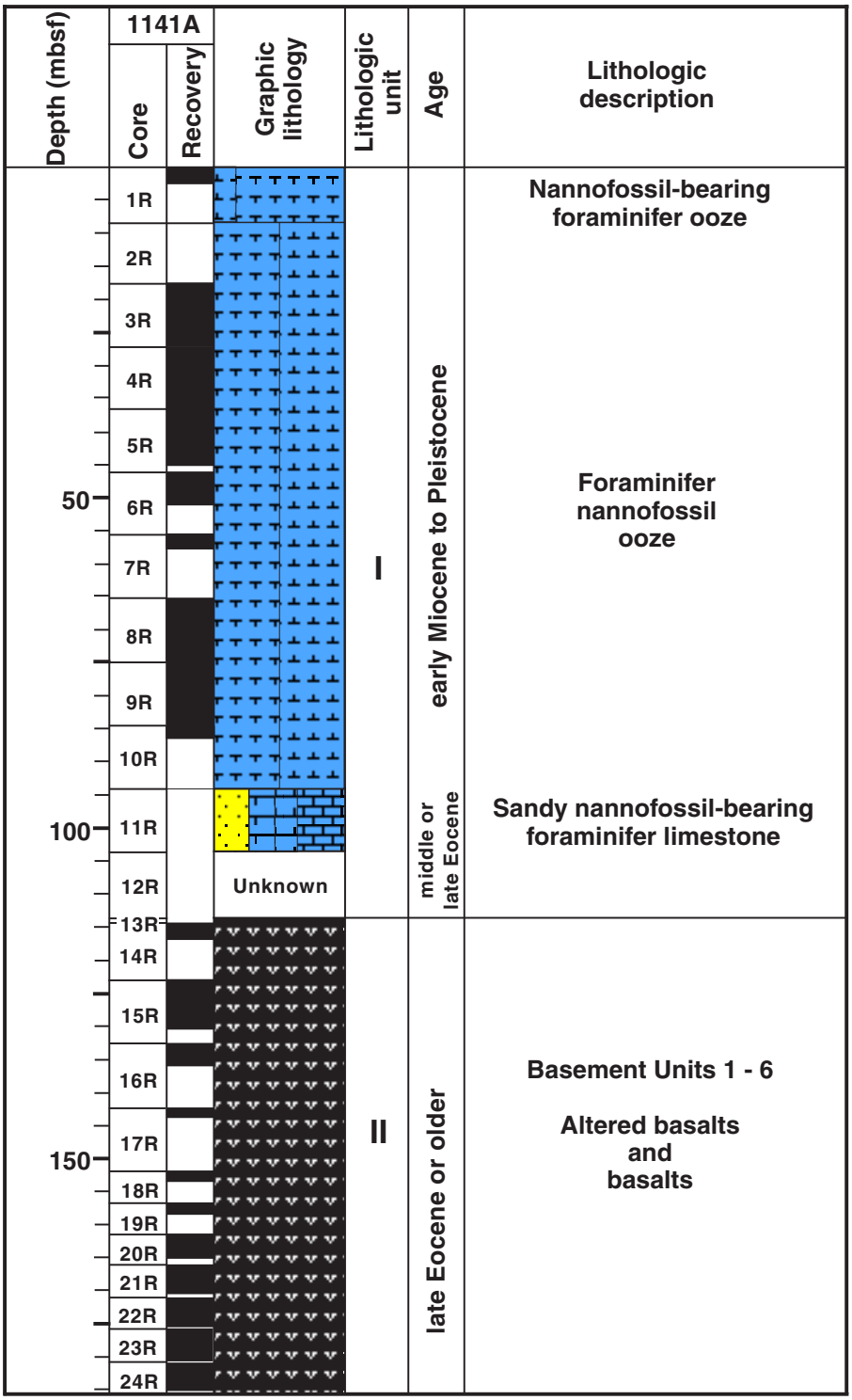

Figure F5. Composite stratigraphic section for Site 1142 showing core recovery, a simplified summary of basement lithology, basement unit boundaries, and names of basement lithologies. The interval from the seafloor to the top of basement rocks was washed, and the sedimentary section was not cored. The lithologic symbols are explained in Figure F3, p. 57, of the "Explanatory Notes" chapter.

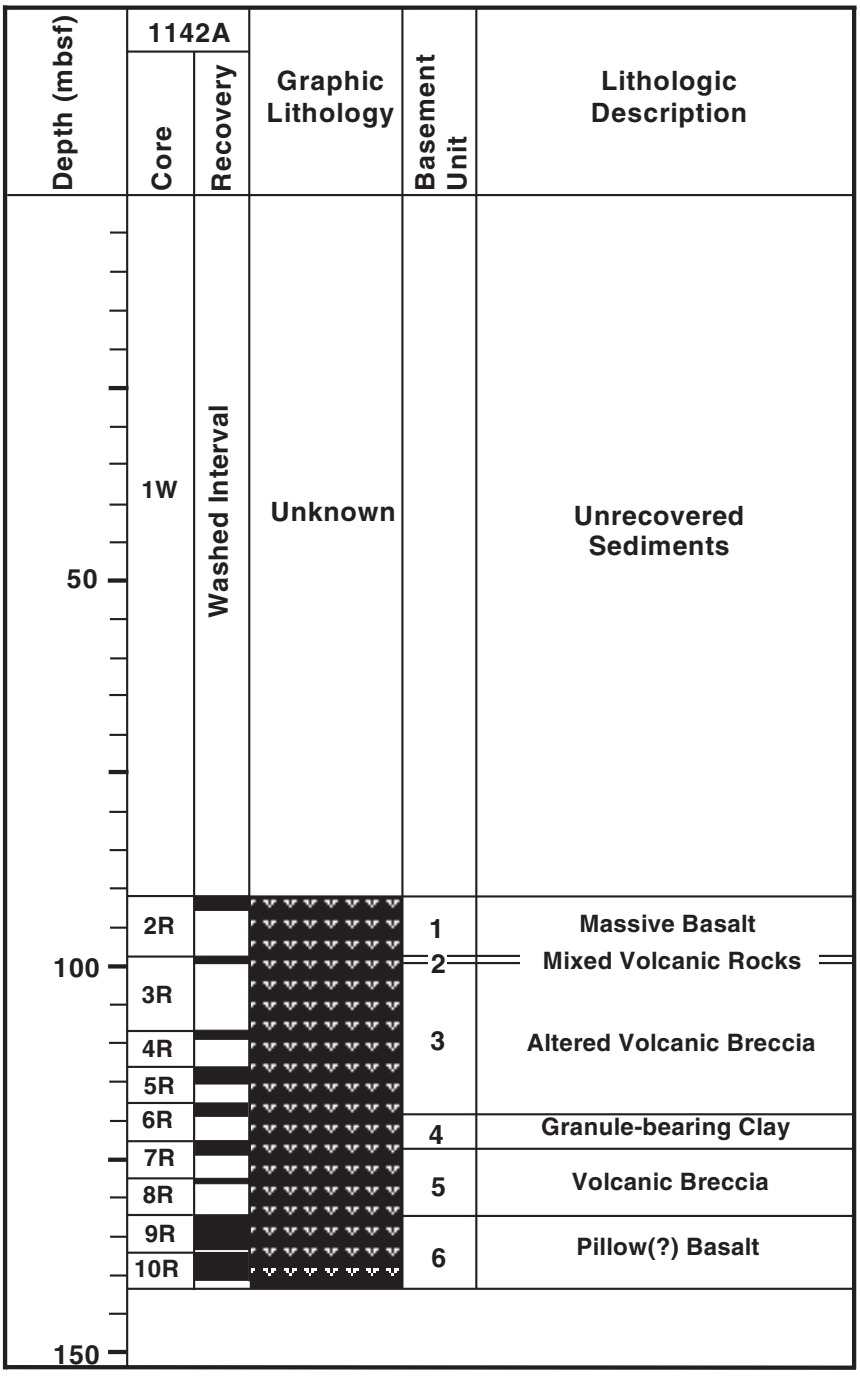

Figure F6. Site 1141 age-depth plot.

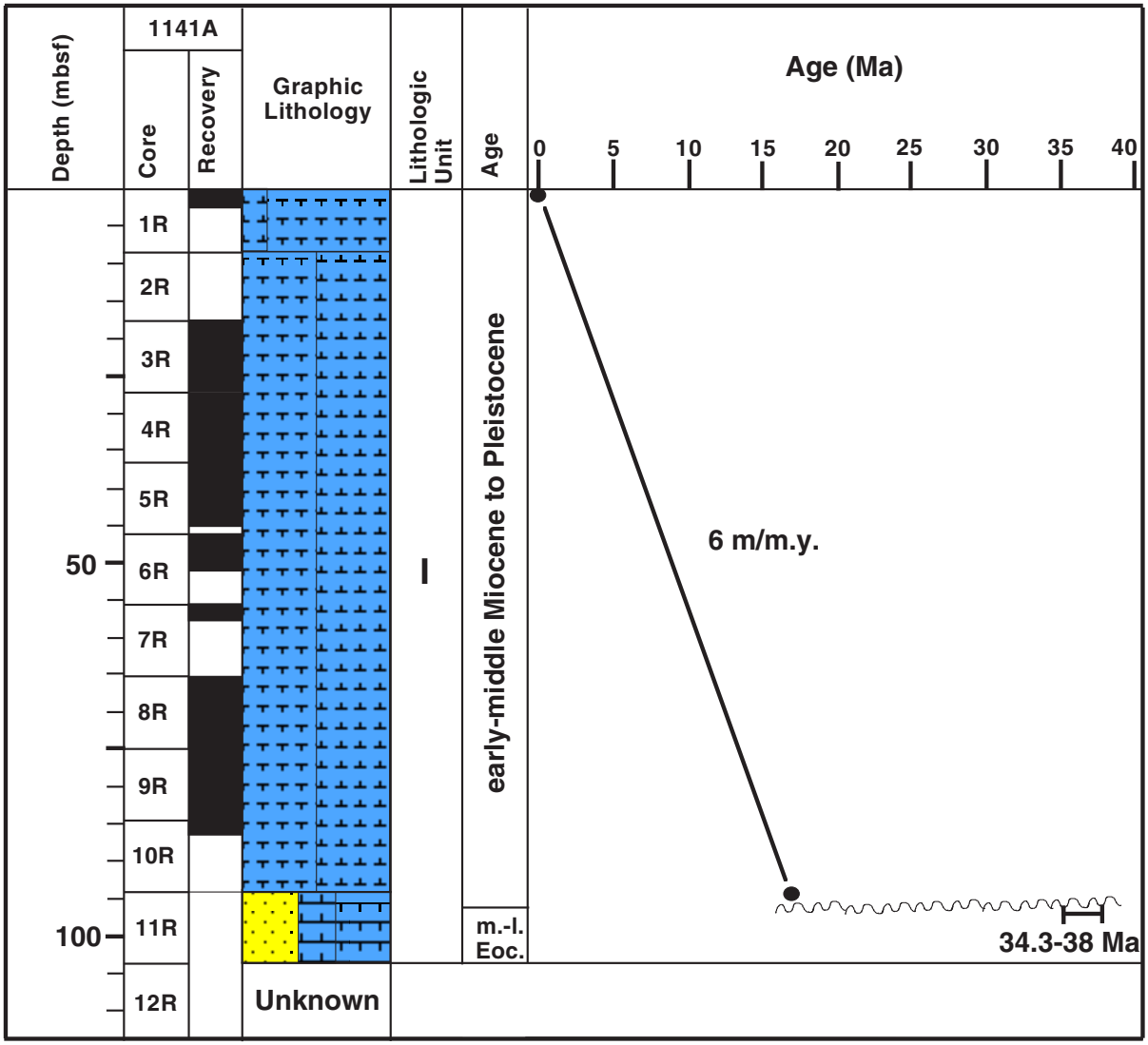

Figure F7. Close-up photograph of interval 183-1141A-16R-2, 13–25 cm, showing the boundary between basement Units 2 and 3. Note the relatively unaltered bottom of basement Unit 2 and its locally high vesicularity.

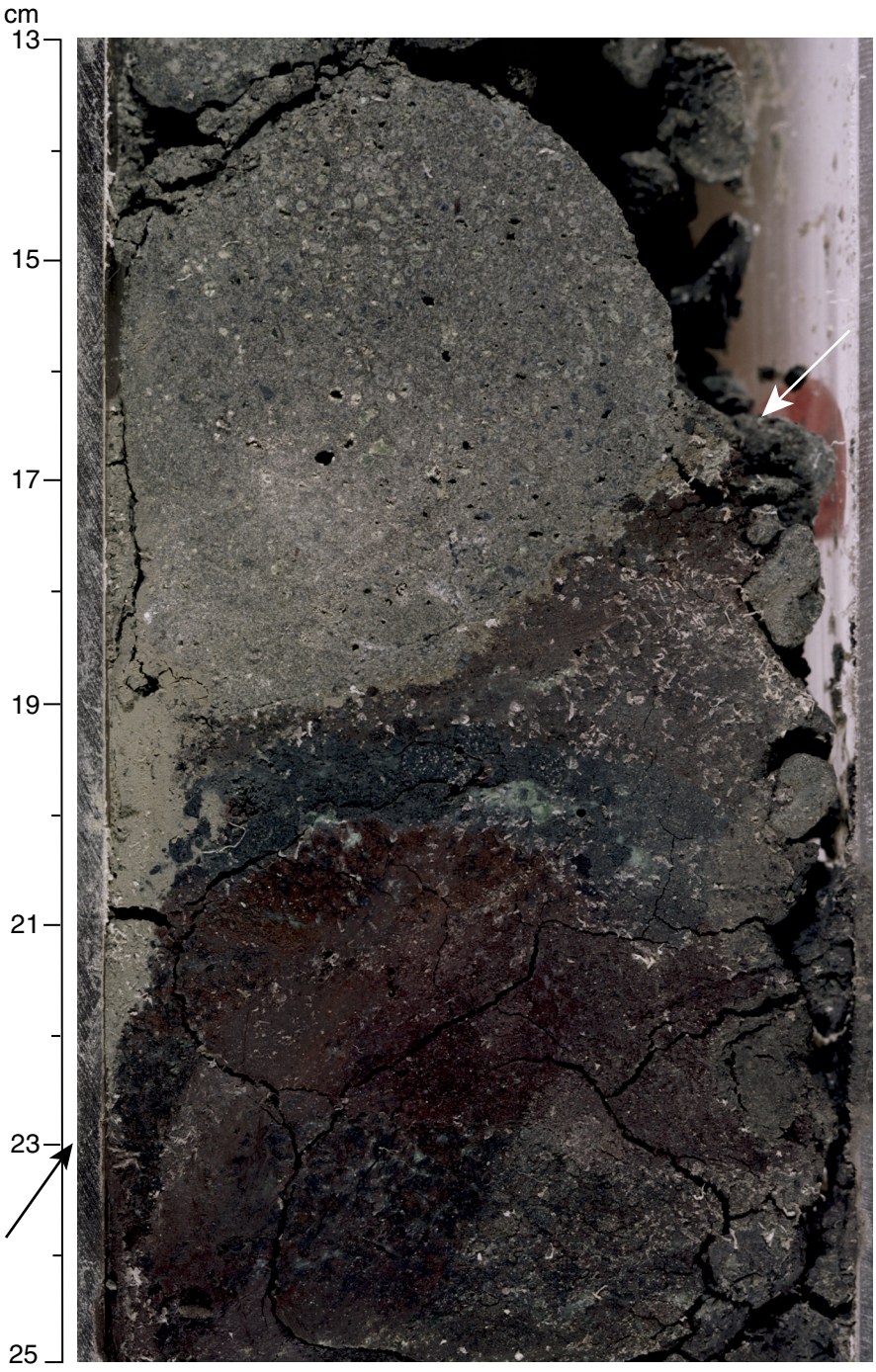

Figure F8. Vesicularity and vesicle density as a function of depth in basement Unit 3, Site 1141.

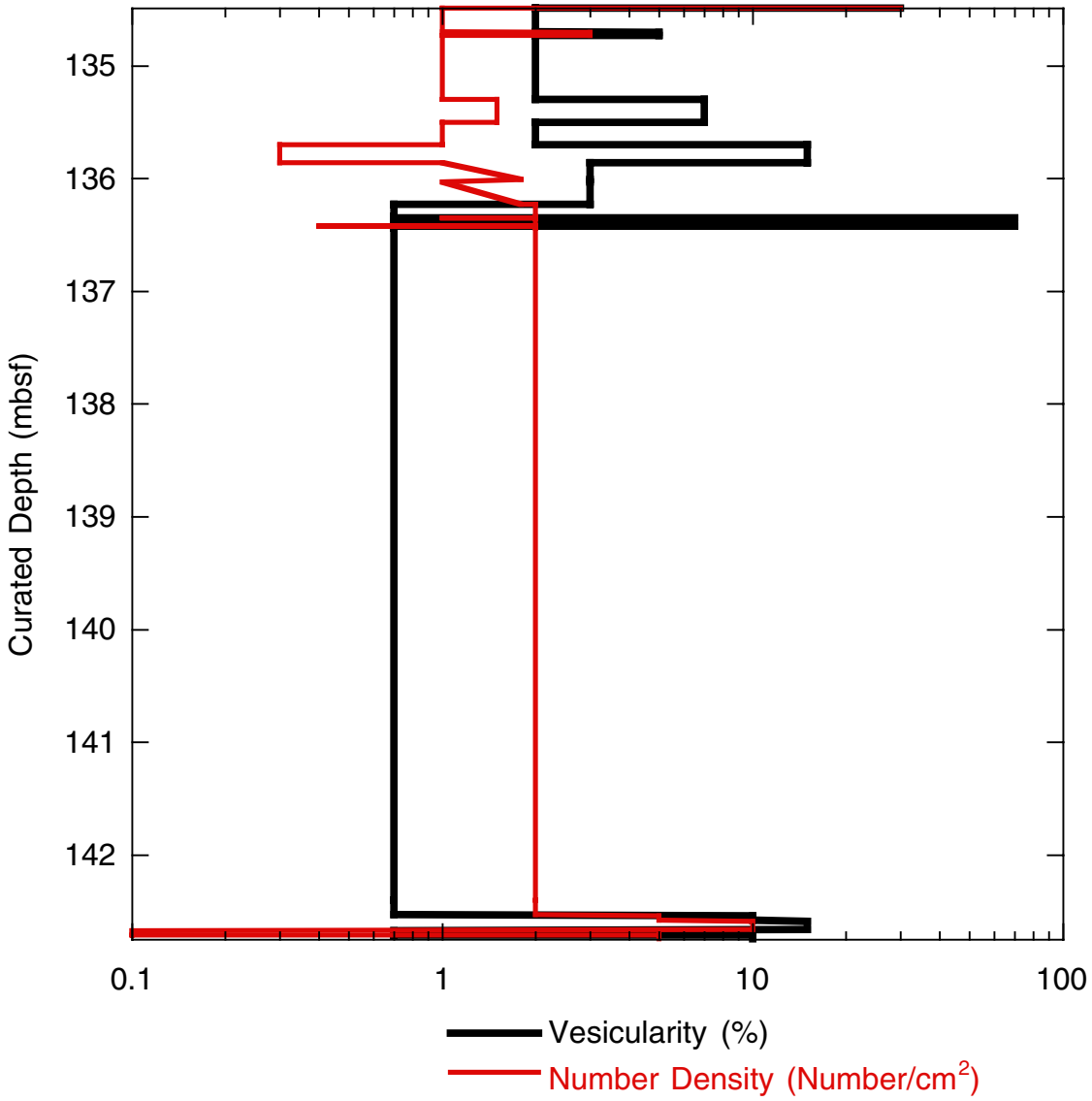

Figure F9. Close-up photograph of interval 183-1141A-16R-3, 40–56 cm, from the base of the upper vesicular crust of basement Unit 3. Note the coarsening upward of the vesicles within the megavesicle horizon.

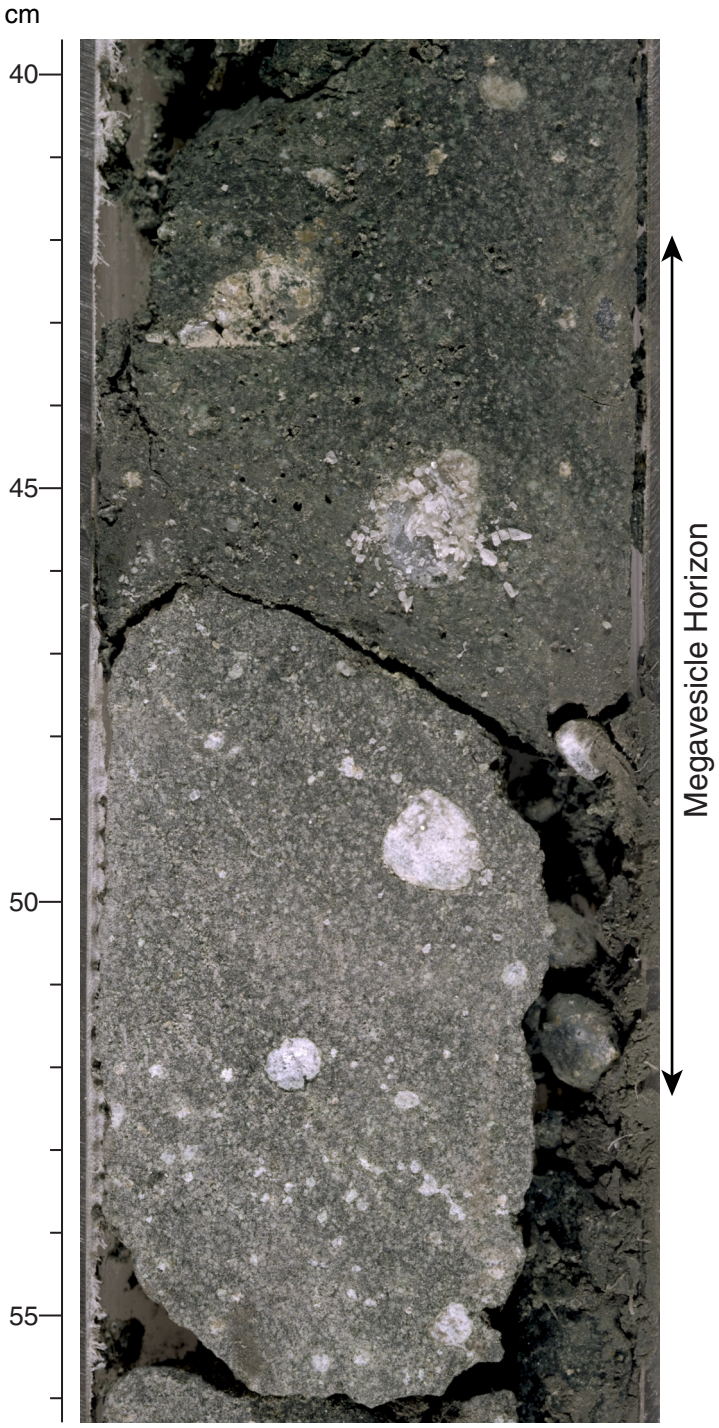

Figure F10. Close-up photograph of interval 183-1141A-16R-CC, 4–16 cm, from the top of the massive interior of basement Unit 3. The elongated streaks are interpreted to have been vesicle-rich mesostasis blebs.

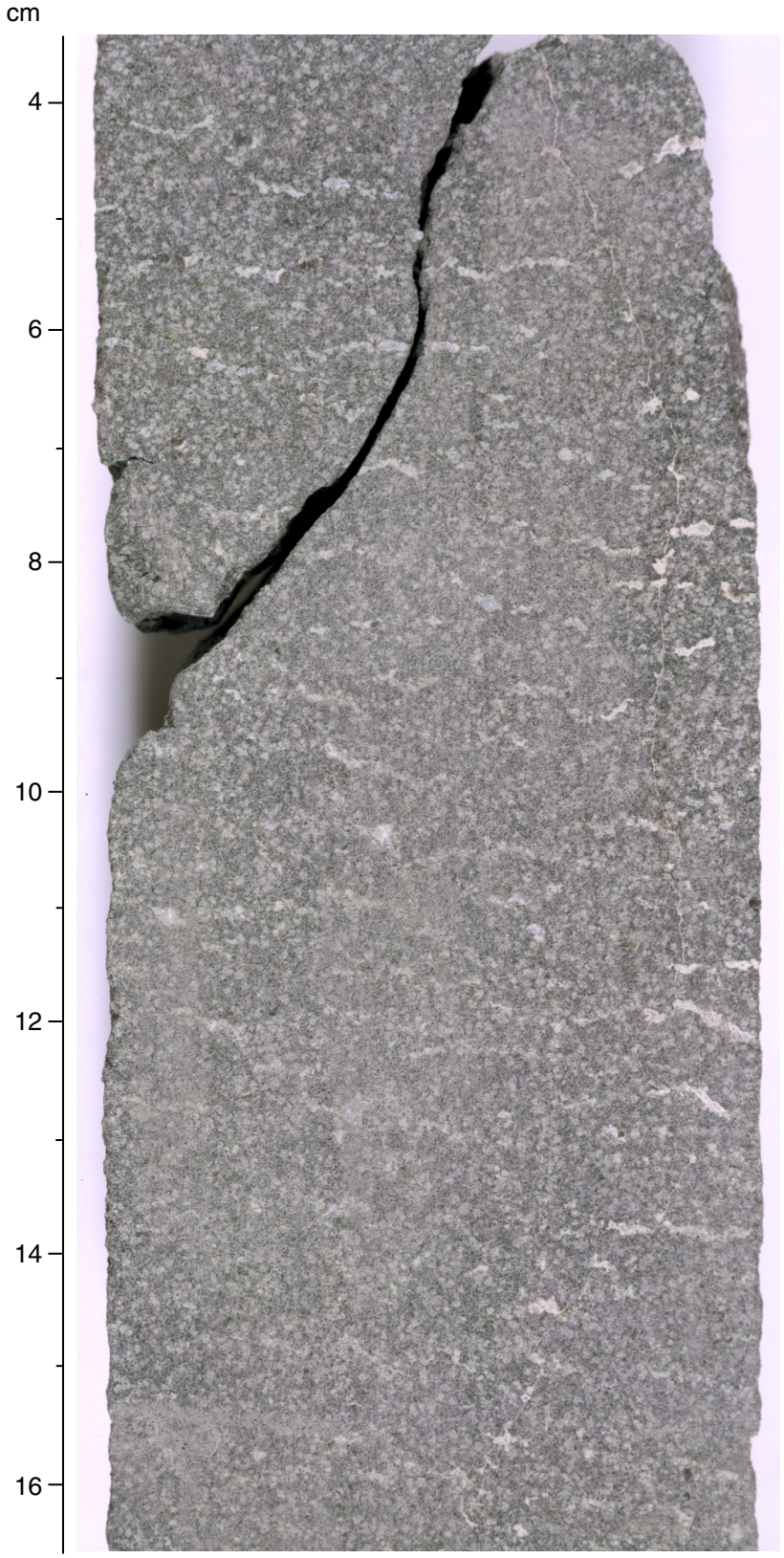

Figure F11. Vesicularity and vesicle number density as a function of depth in basement Unit 4, Site 1141.

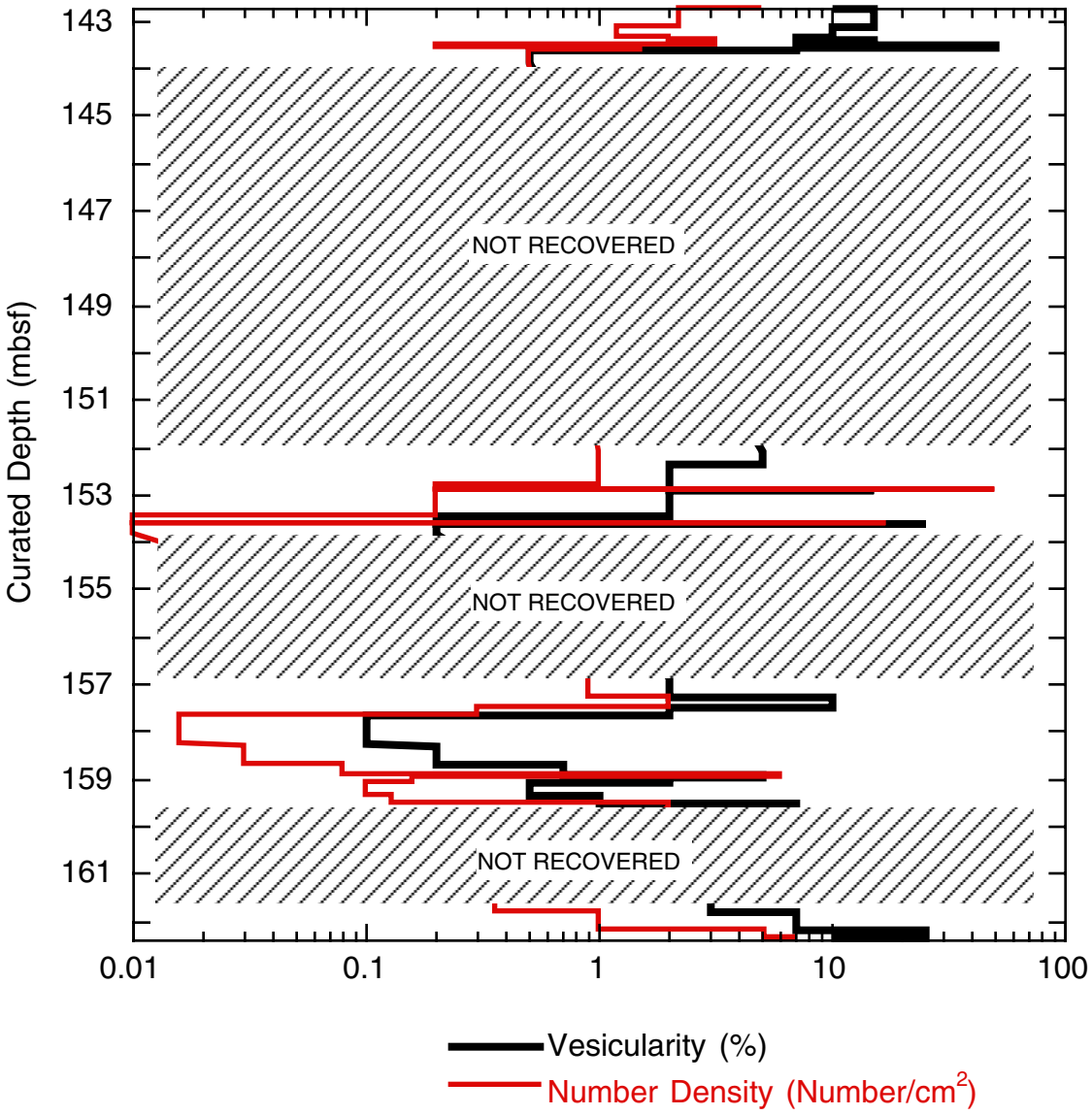

Figure F12. Close-up photograph of interval 183-1141A-18R-2, 9–19 cm, from the dense interior of basement Unit 4. The groundmass in this interval appears finer grained upon visual inspection of the core, leading to the suggestion that this is a dike. However, the presence of vesicles and the sheet of segregated material, from 13.5 cm on the left to 9.5 cm at the top surface of the core on the right, are more consistent with the massive interior of a thick inflated flow.

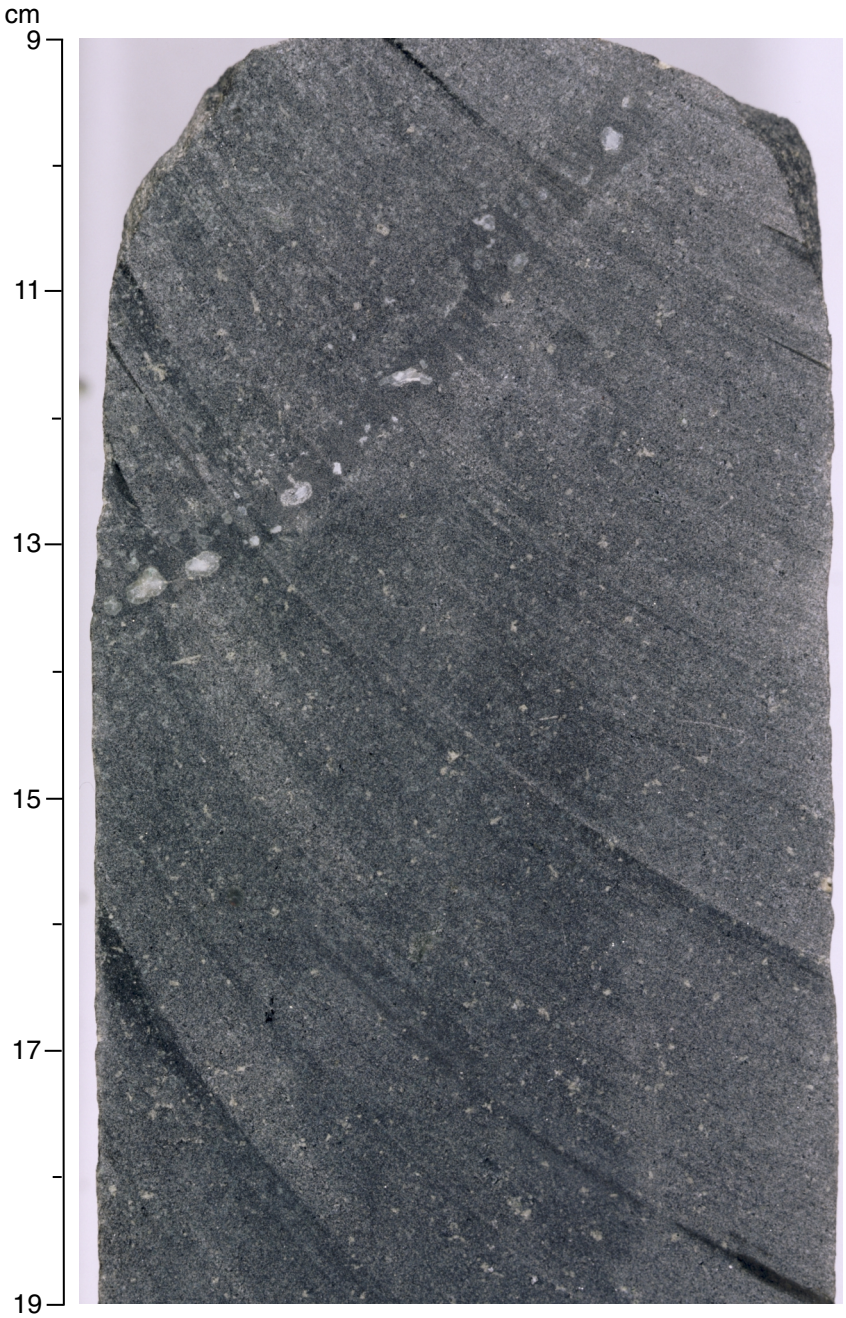

Figure F13. Close-up photograph of interval 183-1141A-19R-2, 60–70 cm, from the dense interior of basement Unit 4. Note the thin, vertical vesicle cylinders with distinct groundmass color.

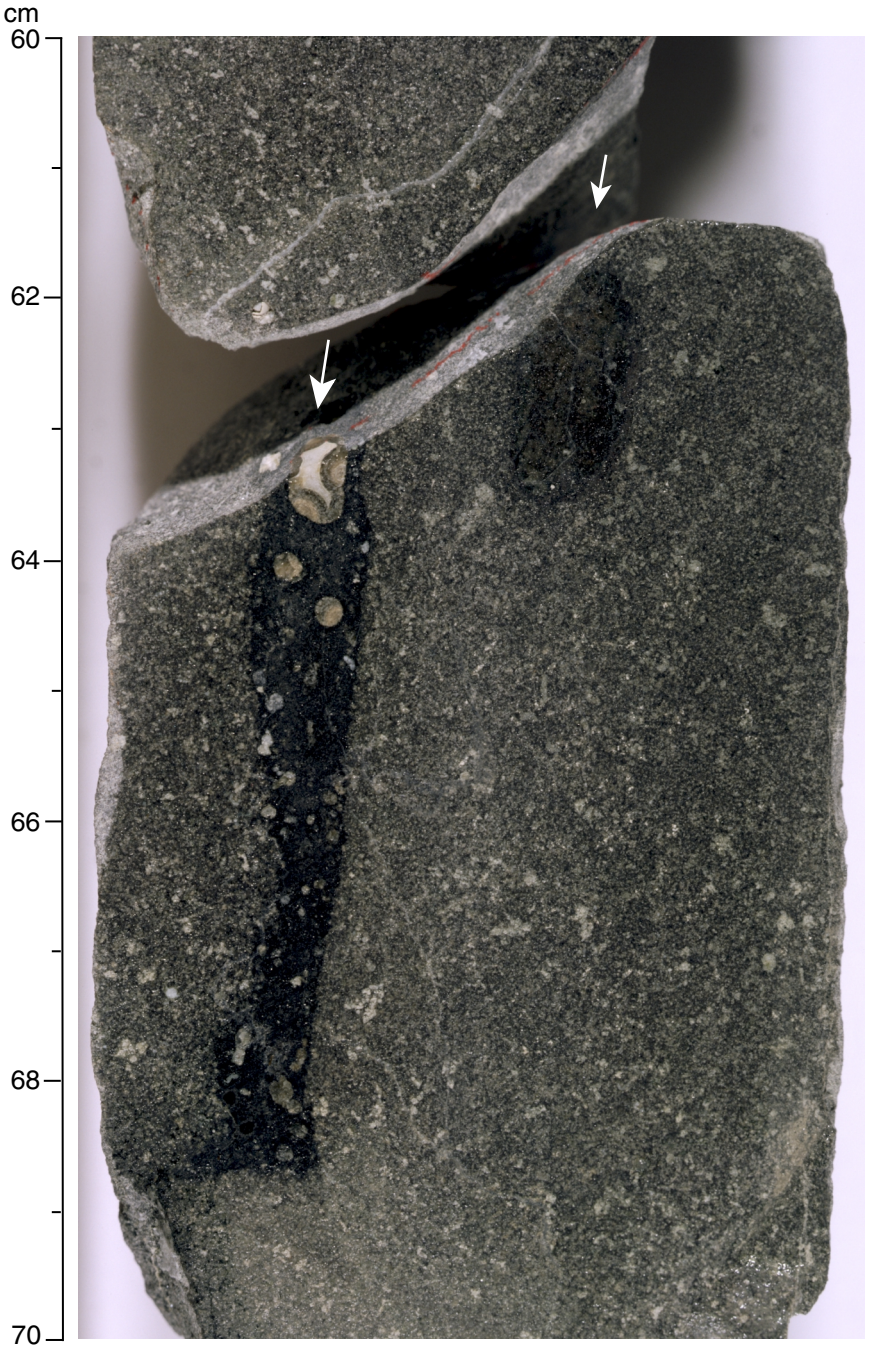

Figure F14. Close-up photograph of interval 183-1141A-20R-1, 71–91 cm, showing the contact between basement Units 4 and 5. Note the altered glassy chill margins (arrows) at the contact and defining the 10-cm-thick pahoehoe lobe at the top of Unit 5. When the whole core is examined, it is apparent that the contact between Units 4 and 5 has 5-cm-scale topography, and the cut surface of the core obliquely intersects a pocket of Unit 4 lava filling a gap in the top of Unit 5.

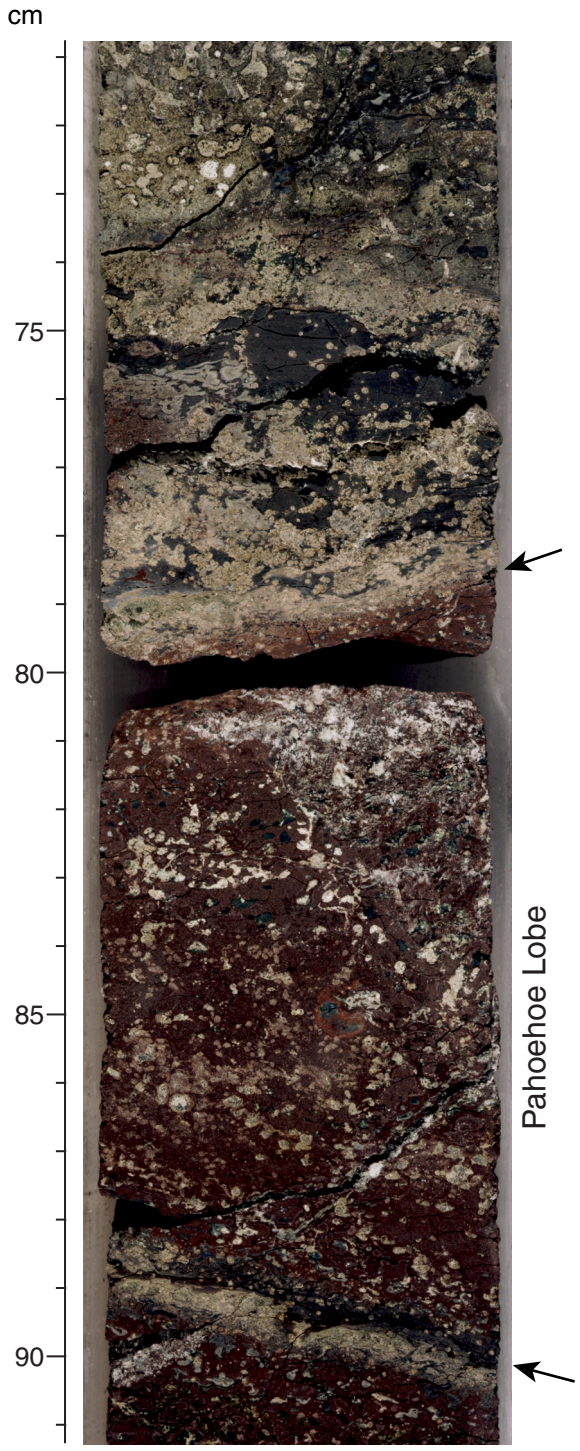

Figure F15. Vesicularity and vesicle number density as a function of depth in basement Unit 5, Site 1141.

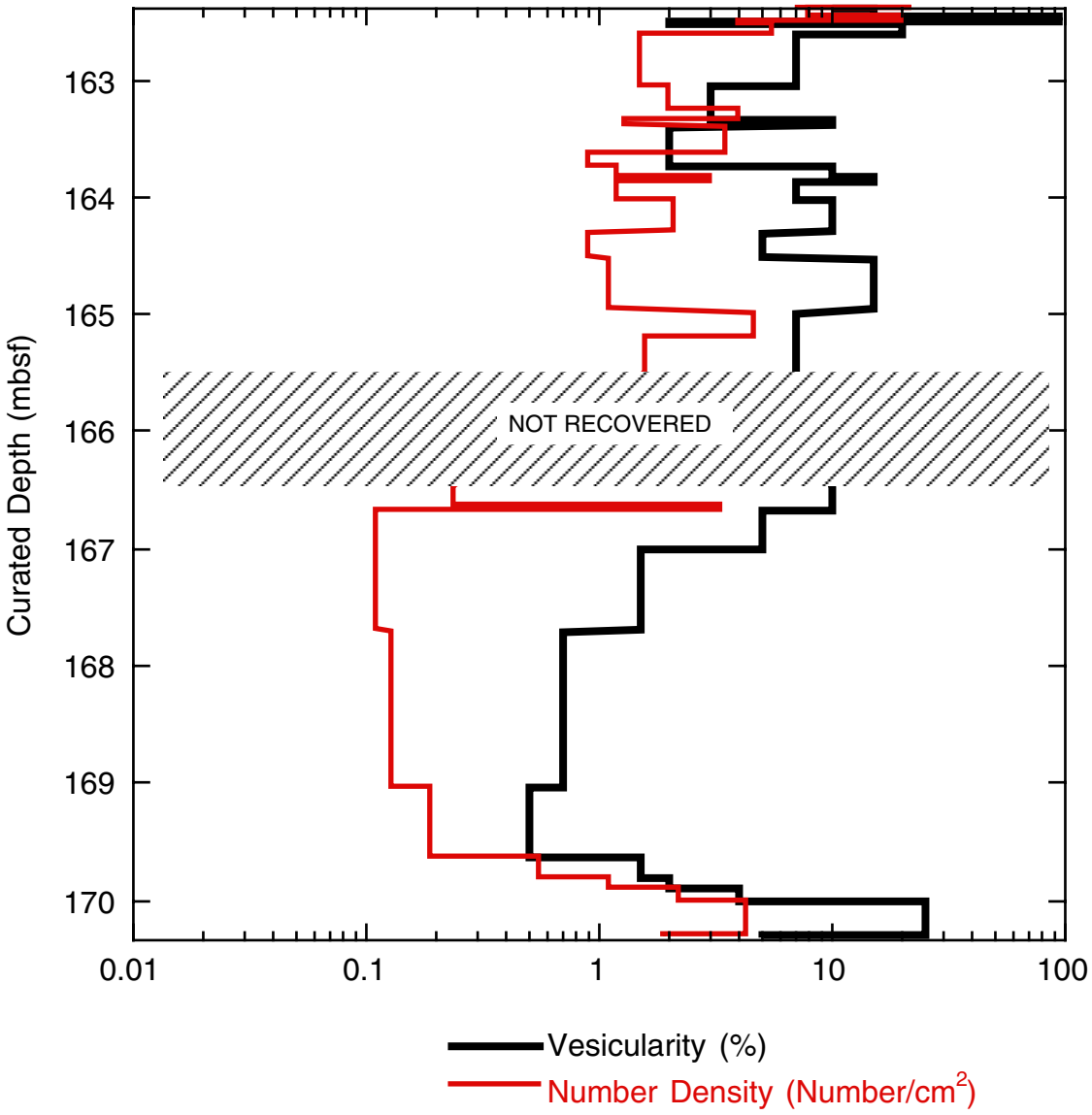

Figure F16. Close-up photograph of interval 183-1141A-21R-1, 20–34 cm, showing the transition between the vesicular upper crust and the massive interior of basement Unit 5. At this transition, note the horizontal vesicular sheet (arrows) with an undulating upper surface and flat bottom. The undulations contain large vesicles pushing up into the base of the upper crust and demonstrate that these megavesicles are derived from volatiles released during crystallization and segregation of late-stage melts.

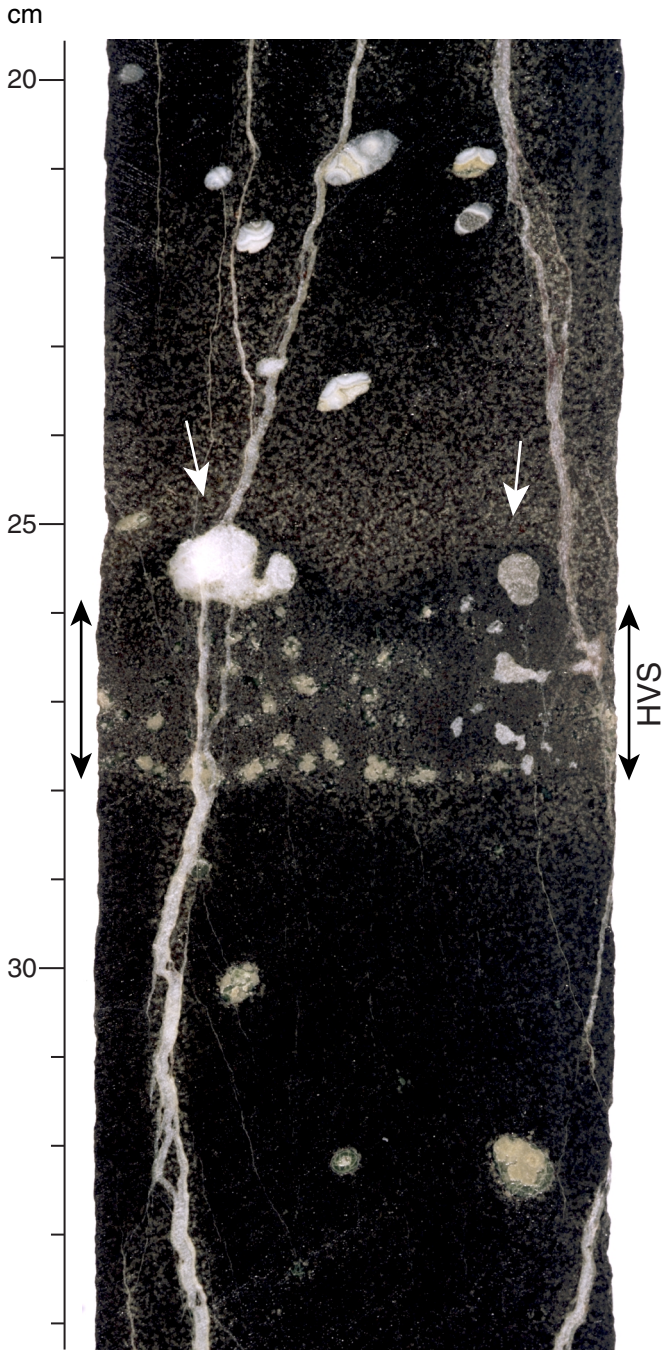

Figure F17. Close-up photograph of interval 183-1141A-21R-3, 120–140 cm, shows the change from basement Unit 5 to Unit 6. Note that the smooth undulating vesicular base of Unit 5 is highly altered, which probably obscures the small vesicles characteristic of chill zones. The top of Unit 6 seen in the photo shows some of the best preserved parts of the upper breccia. Note the subrounded clasts with subangular vesicles and the clay-filled voids.

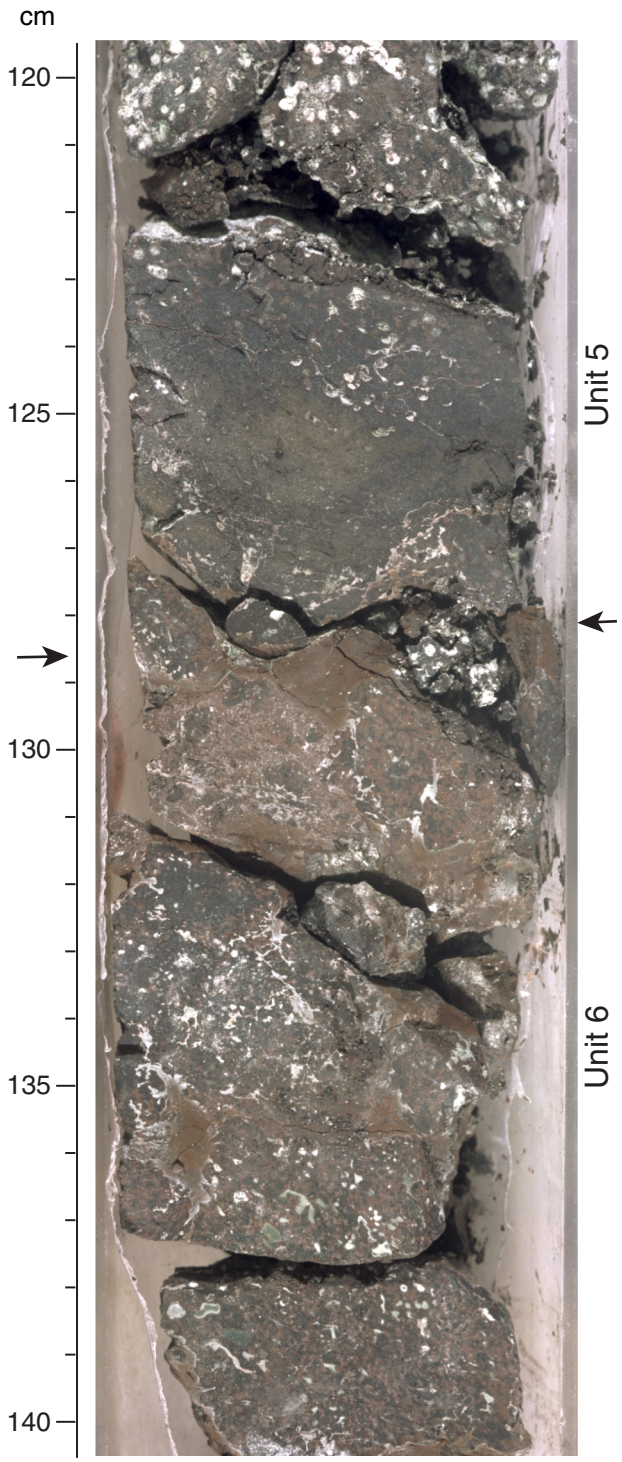

Figure F18. Vesicularity and vesicle number density as a function of depth in basement Unit 6, Site 1141. Note that data could only be gathered in small intervals within the altered breccias at the top and base of the unit.

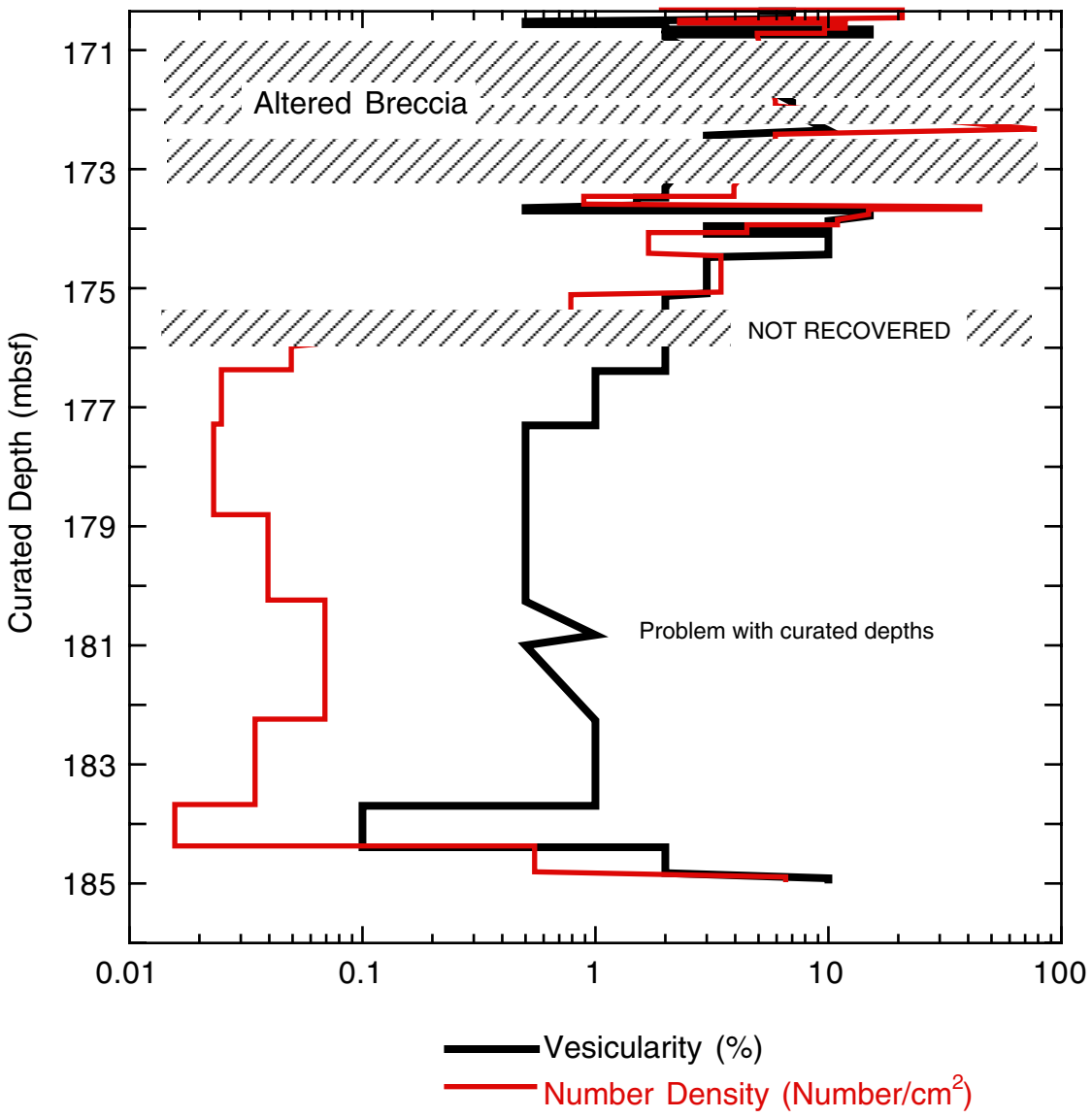

Figure F19. Close-up photograph of interval 183-1141A-22R-1, 105–120 cm, showing the best preserved textures within the flow-top breccia of basement Unit 6.

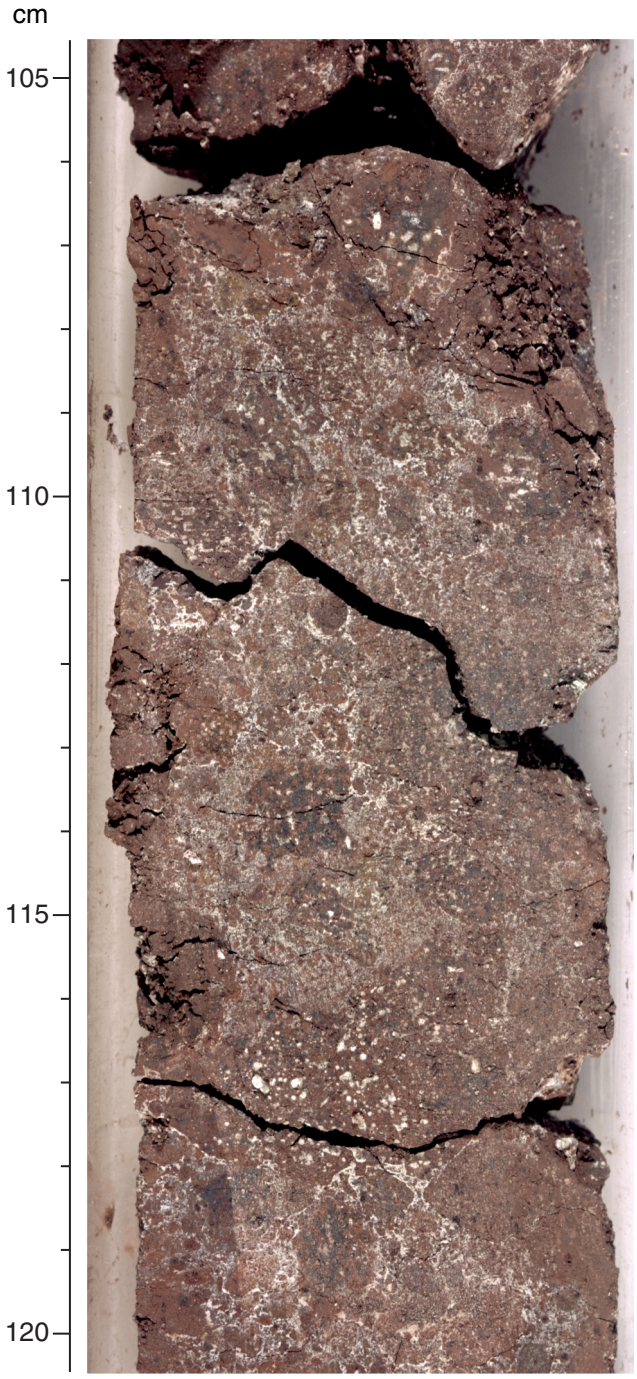

Figure F20. Close-up photograph of Sample 183-1141A-22R-3 (Piece 2, 10–24 cm) showing megavesicle horizon marking the change from the more vesicular upper part of the lava to the more massive interior of basement Unit 6. Vesicles are filled with banded agate filling and have multiple generations of light brown carbonates along their margins. Also shown is a patch of basalt with a variolitic texture altered to light pink and green clay.

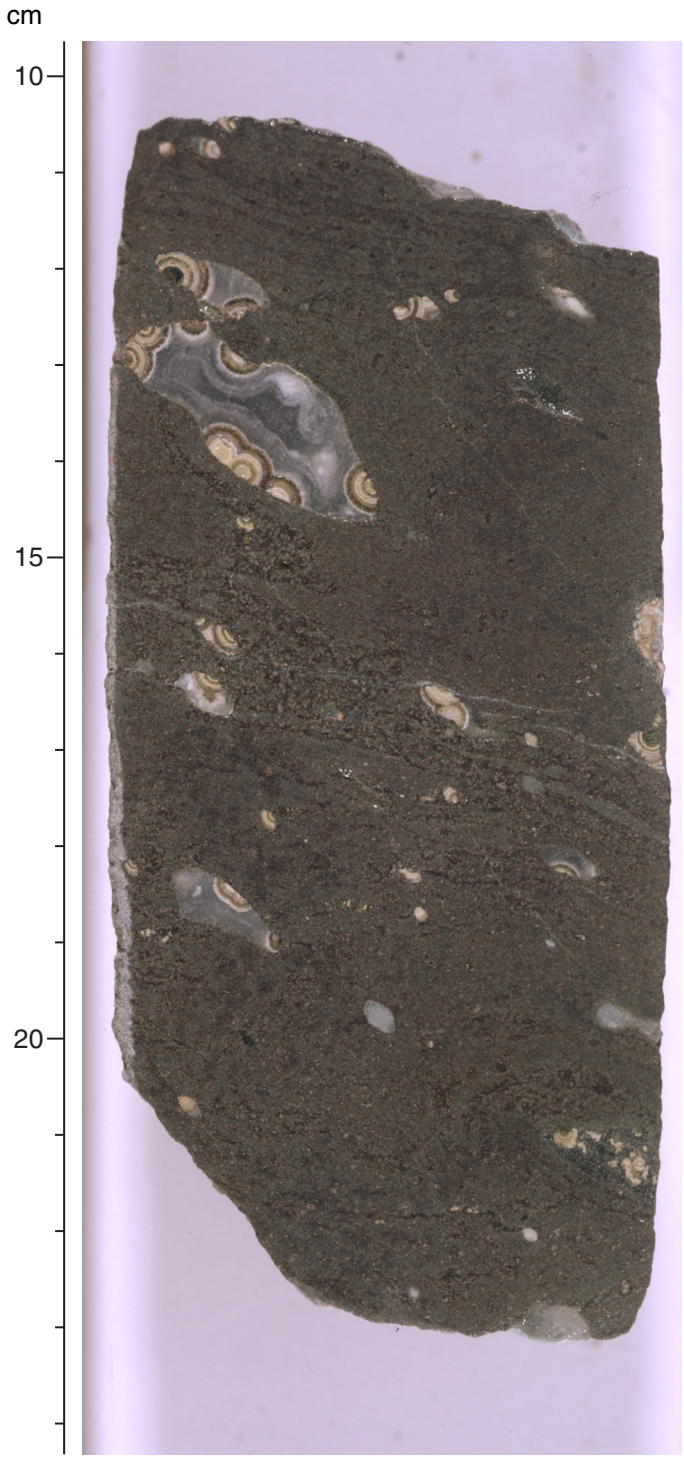

Figure F21. Close-up photograph of interval 183-1141A-22R-2, 89–101 cm, showing a zone of intermixed lavas with different groundmass textures (arrows) in the more vesicular upper part of basement Unit 6.

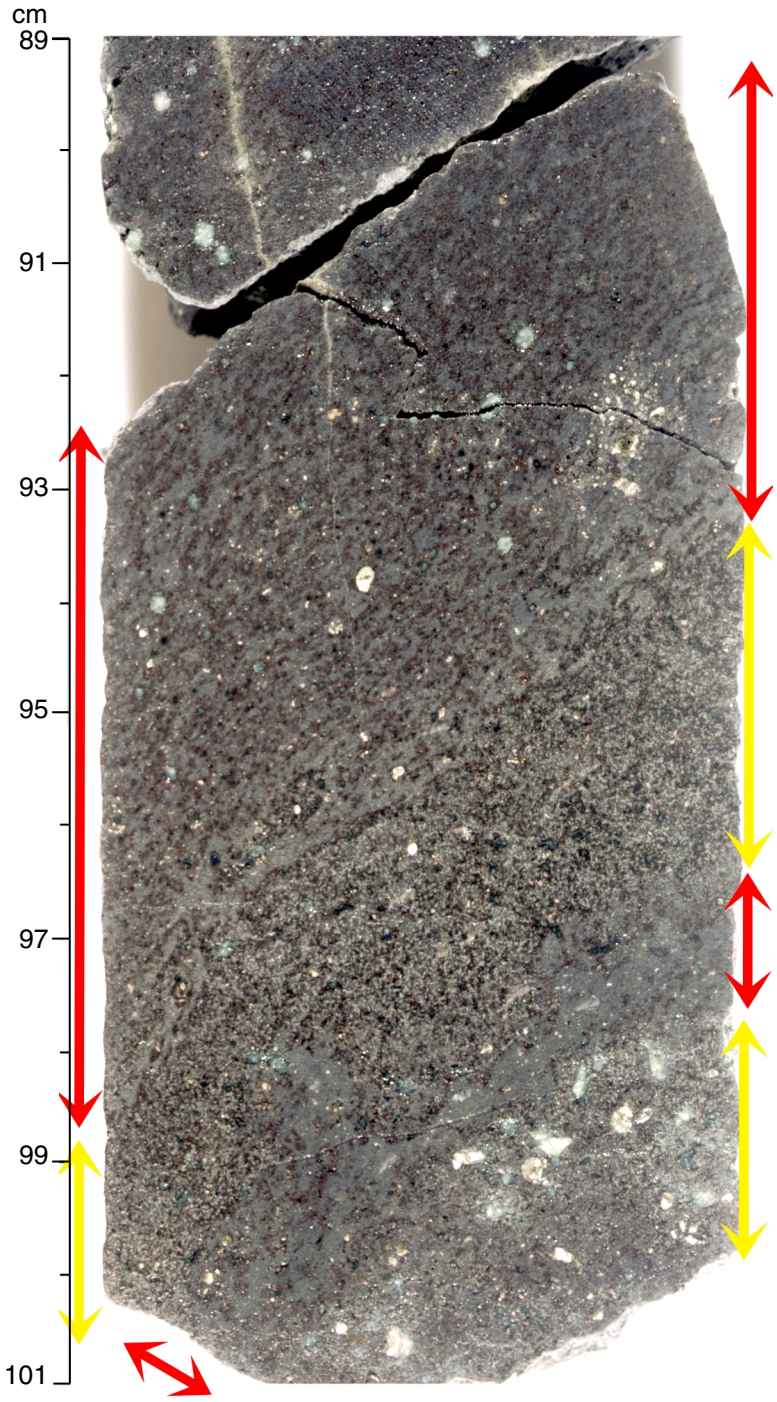

Figure F22. Close-up photograph of interval 183-1141A-22R-3, 111–119 cm, showing a zone of intermixed lavas with different groundmass textures (arrows) in the more massive interior of basement Unit 6.

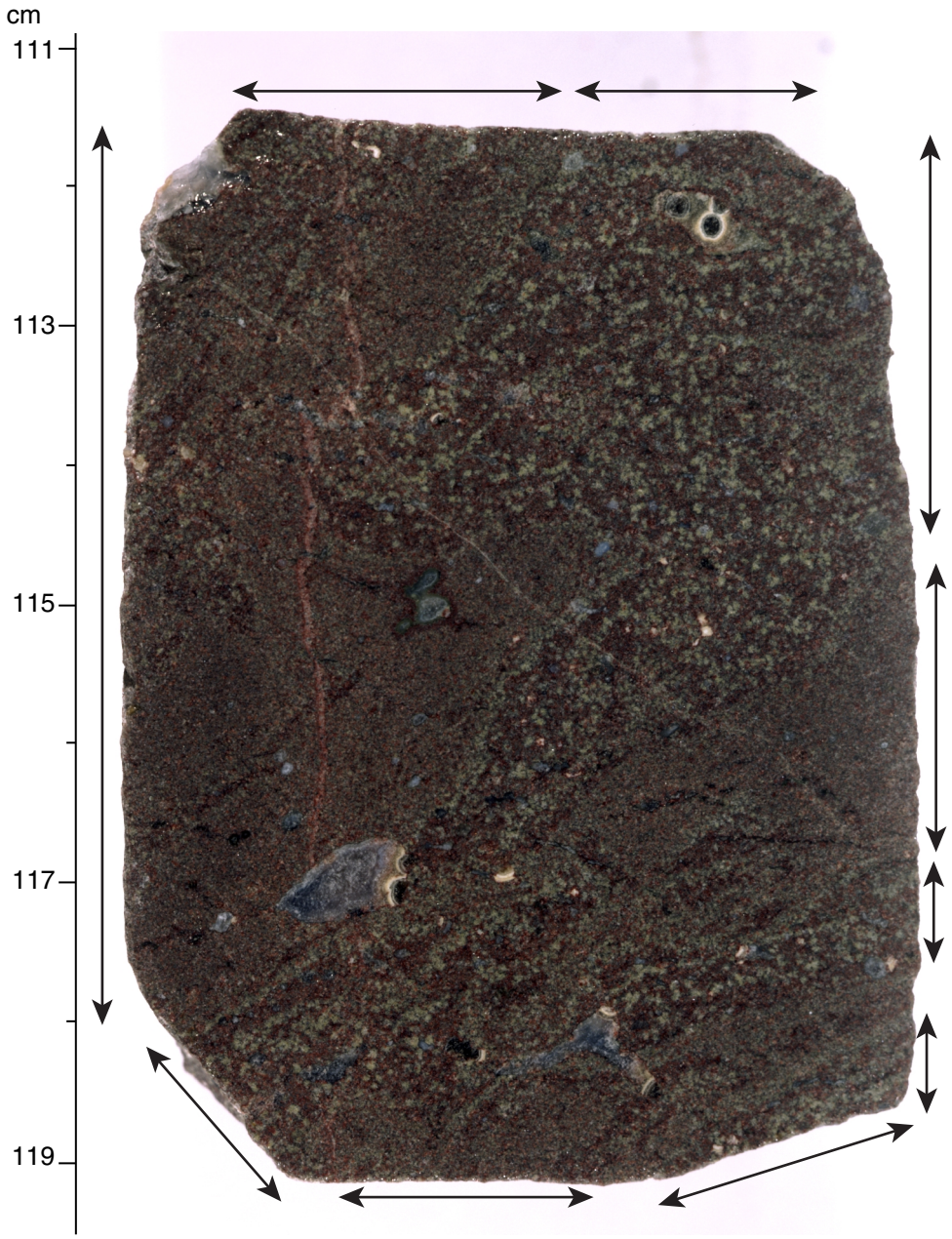

Figure F23. Close-up photograph of interval 183-1141A-23R-1, 105–115 cm, showing a sheet-like body of material with distinct groundmass interpreted to be nonvesicular segregated material.

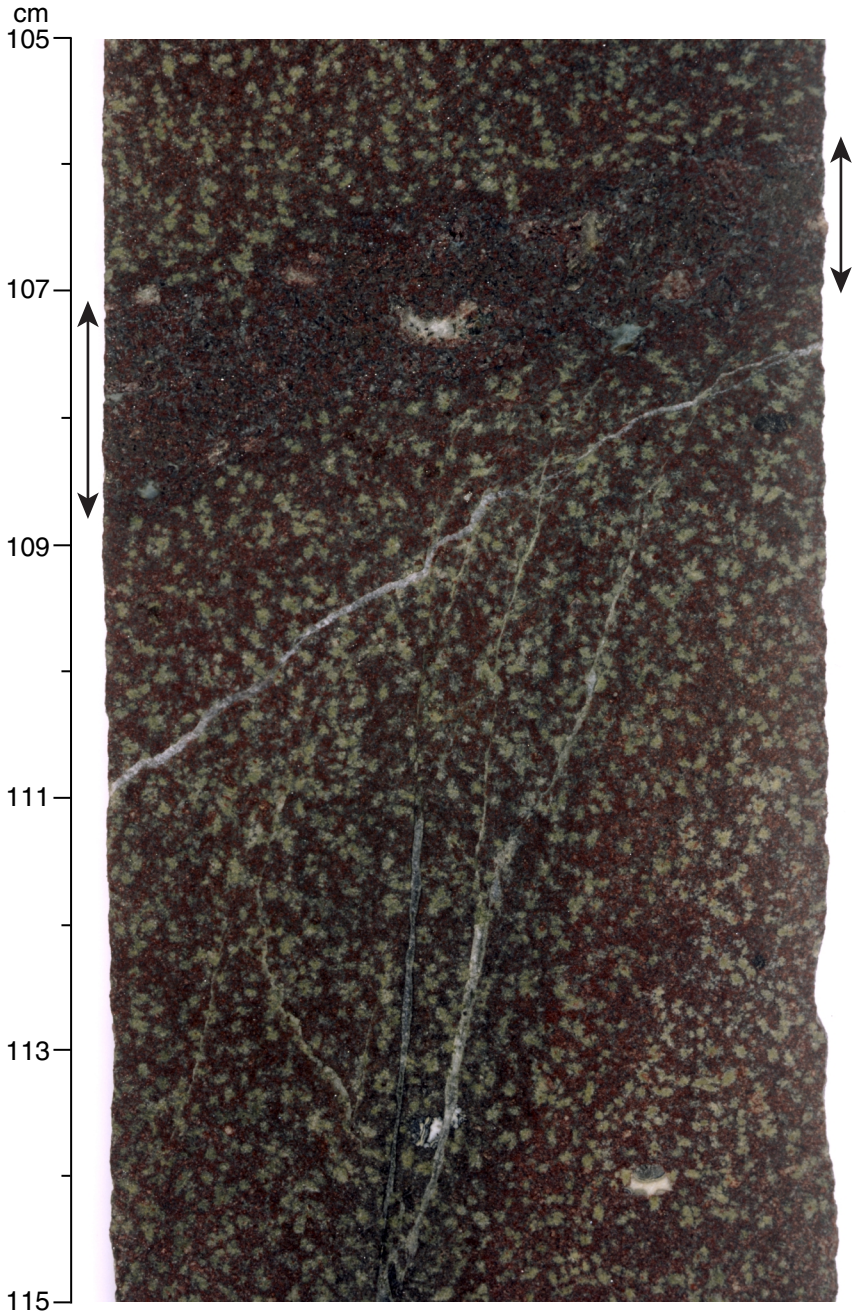

Figure F24. Close-up photograph of interval 183-1142A-3R-1, 16–24 cm, showing textures of the breccia at the top of basement Unit 2.

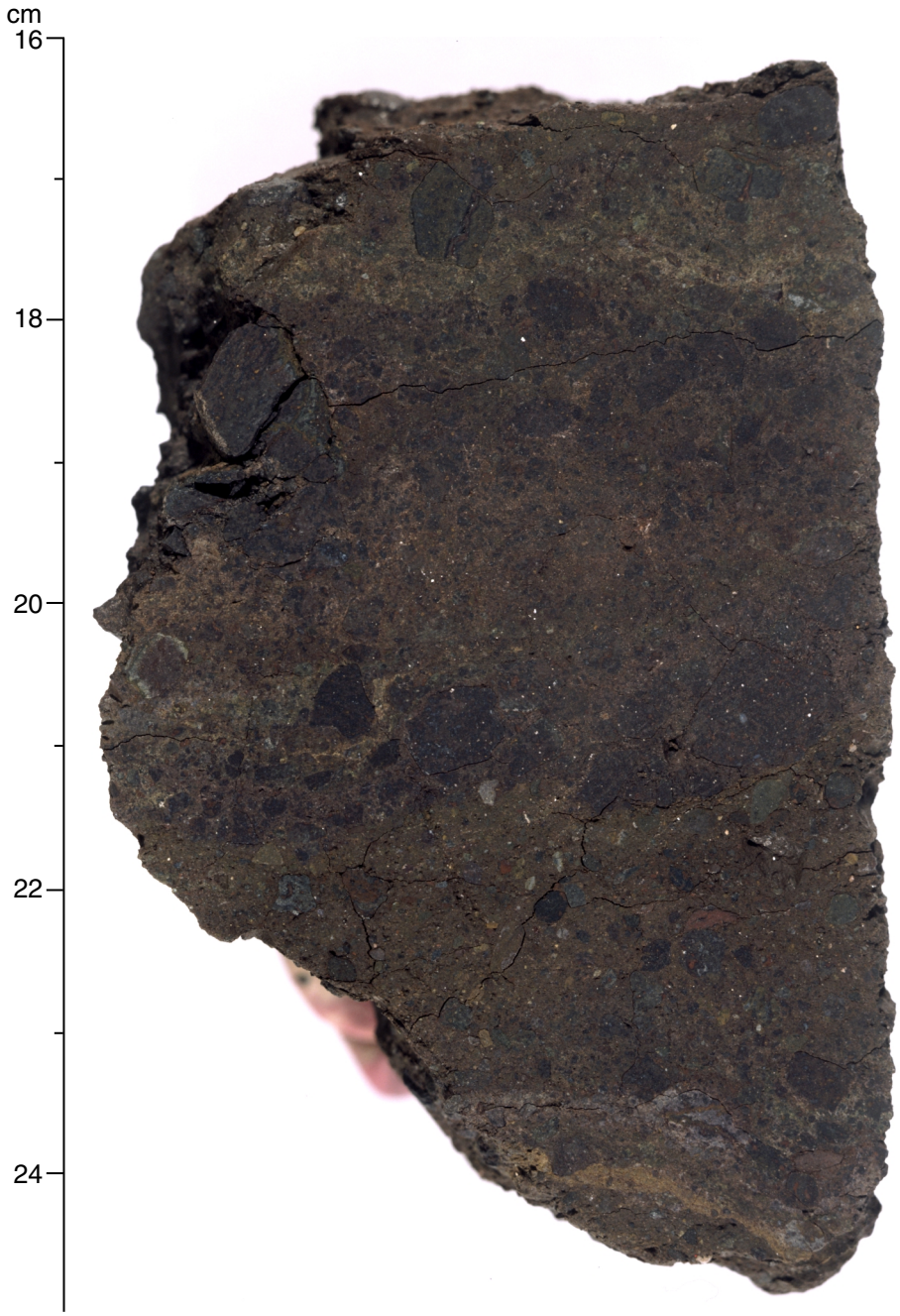

Figure F25. Close-up photograph of interval 183-1142A-3R-1, 76–83 cm, showing textures of the breccia in the middle of basement Unit 2.

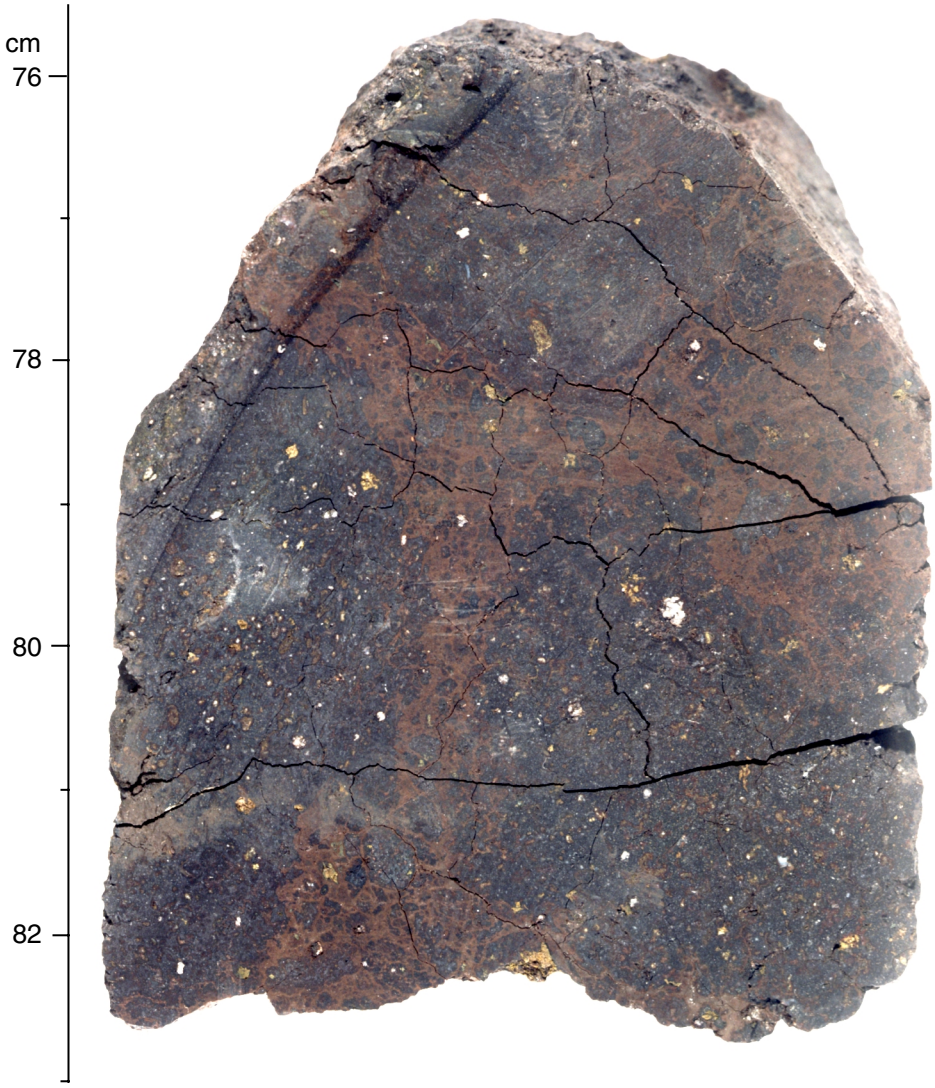

Figure F26. Close-up photograph of Sample 183-1142A-5R-1 (Piece 7, 38–52 cm), showing brittle deformation in altered (basalt?) lava forming a breccia with angular clasts.

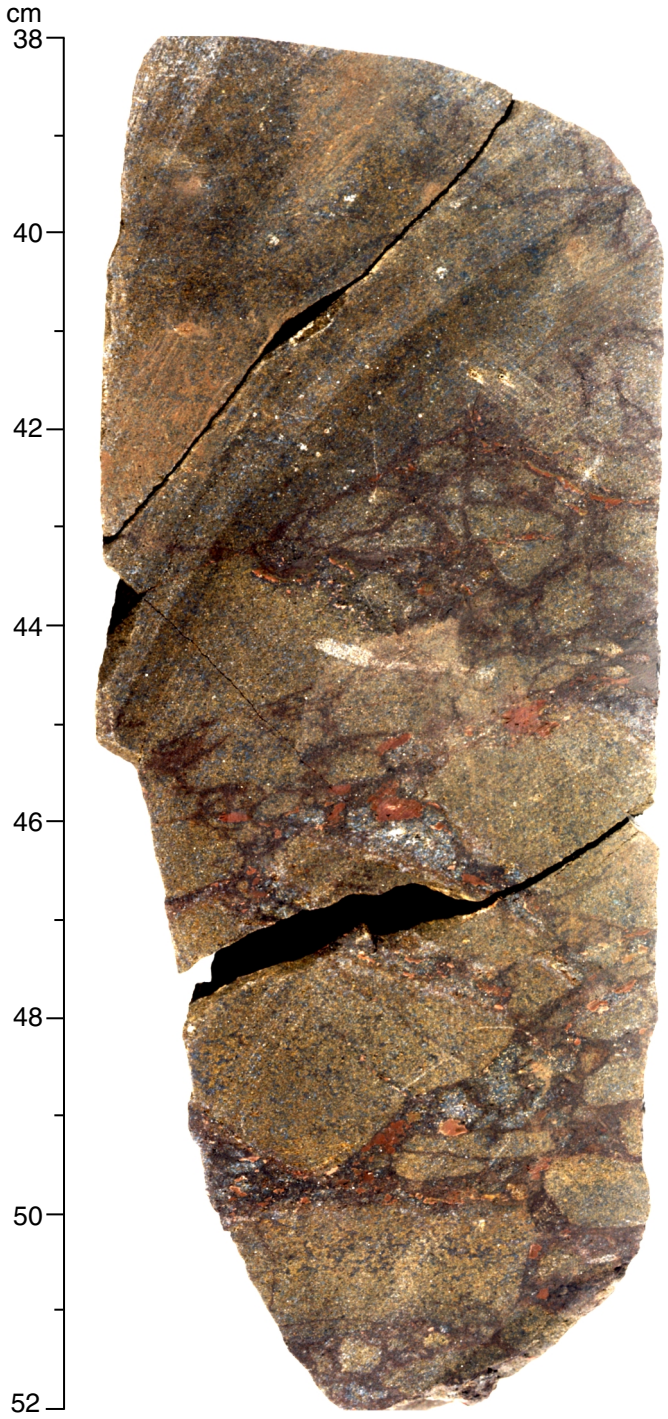

Figure F27. Close-up photograph of interval 183-1142A-5R-1, 70–80 cm, showing thin (<1 mm) elongate domains of altered domains in the mesostasis defining an internal texture in the lava.

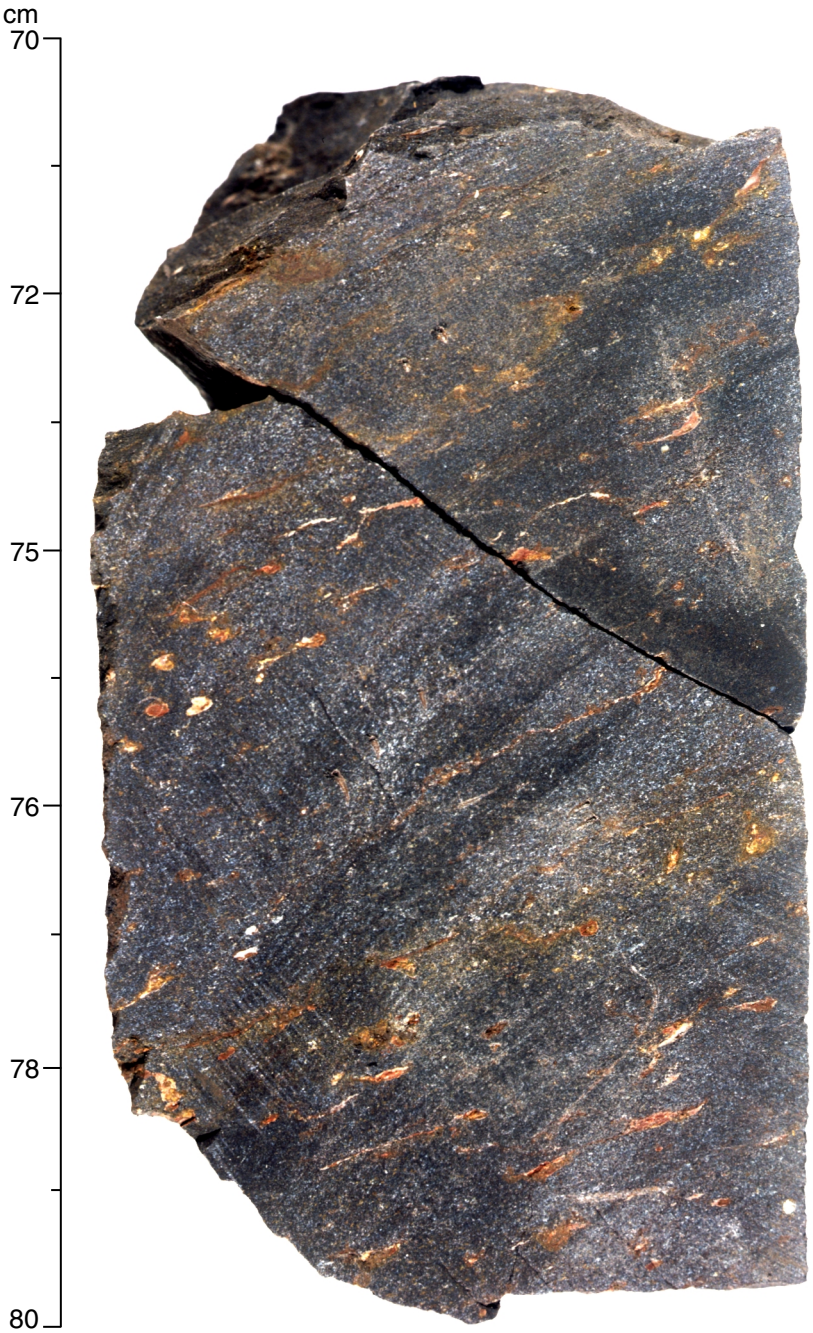

Figure F28. Close-up photograph of interval 183-1142A-5R-1, 118–126 cm, showing coalescence of thin elongate altered domains in the mesostasis forming a pseudobreccia texture.

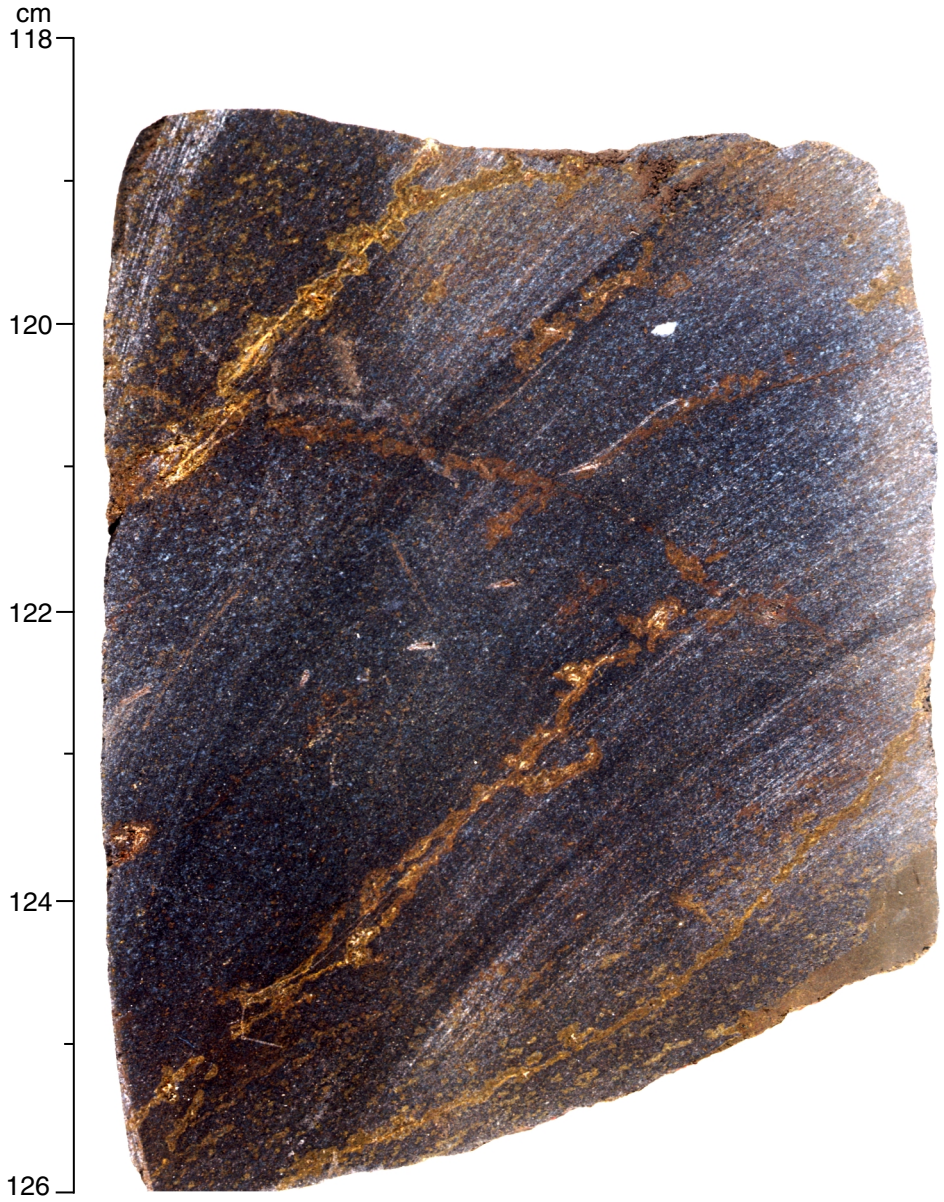

Figure F29. Close-up photograph of interval 183-1142A-5R-2, 12–23 cm, showing a breccia with elongate clasts in a red clay matrix. The degree of alteration of clasts within the breccia and larger adjacent clasts is similar. This is possibly a zone of shearing.

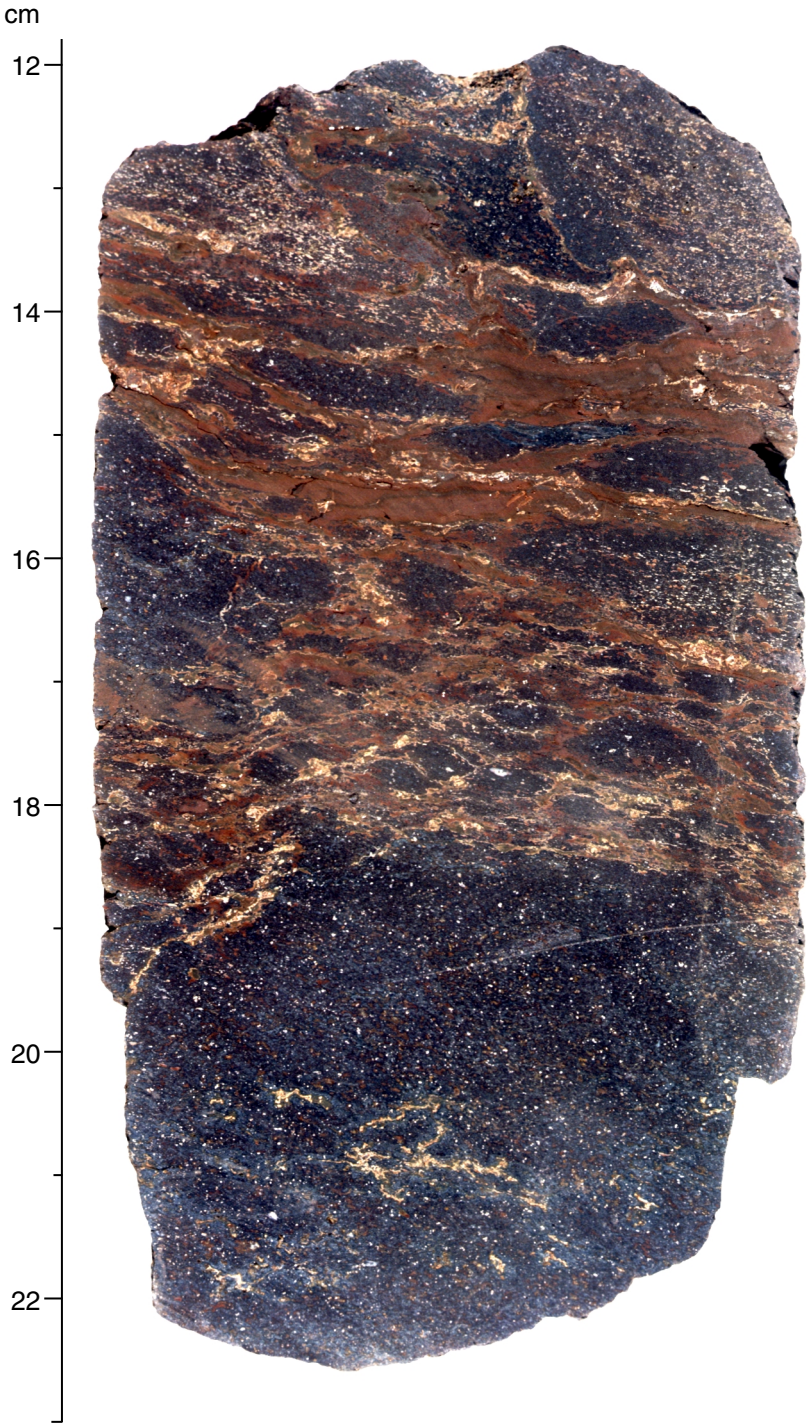

Figure F30. Close-up photograph of interval 183-1142A-6R-2, 28–40 cm, showing the red, normally graded, very coarse sand to granule-bearing clay of basement Unit 4.

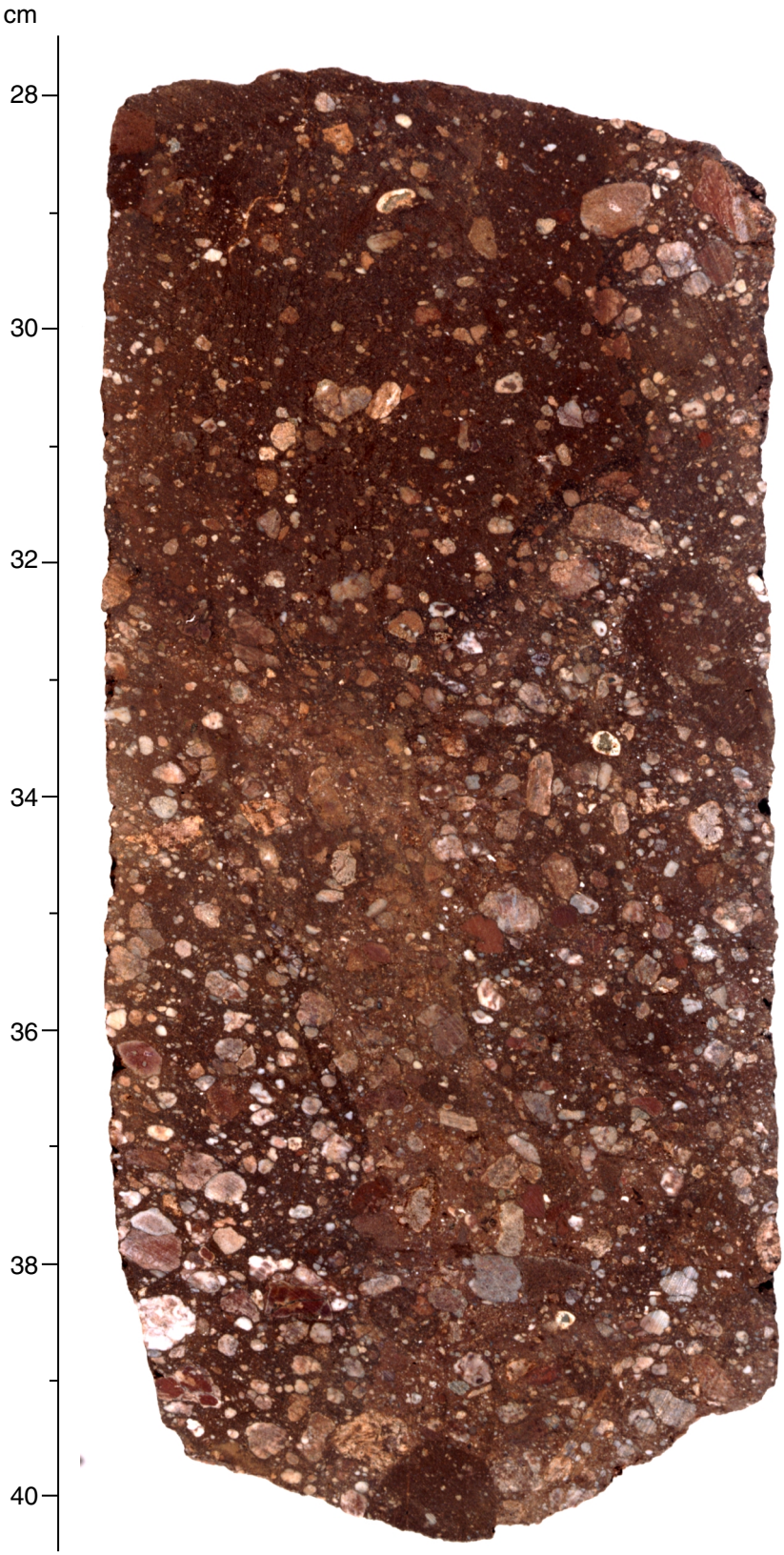

Figure F31. Close-up photograph of interval 183-1142A-7R-1, 10–20 cm, showing the red, matrix-supported, very coarse sand to granule-bearing clay of basement Unit 4.

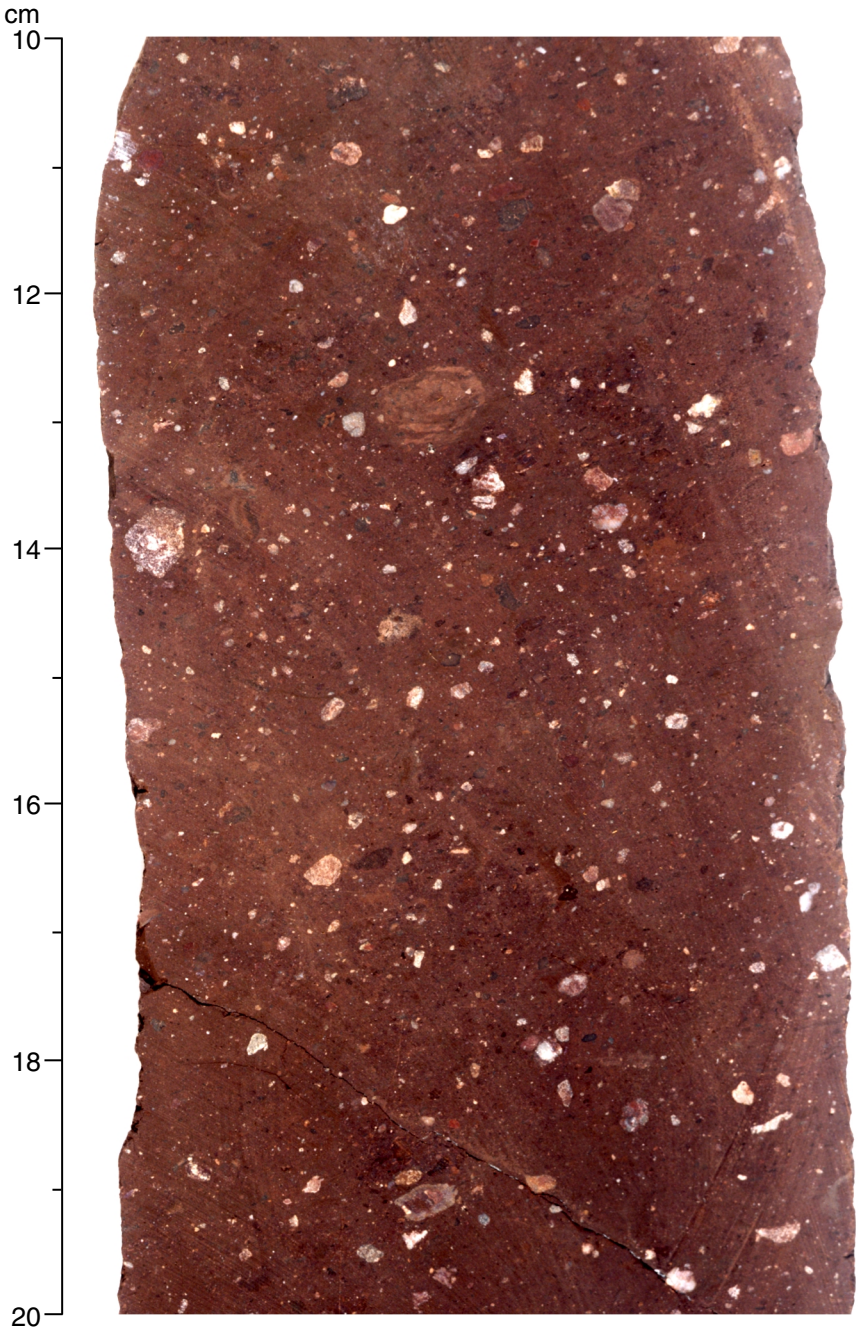

Figure F32. Close-up photograph of interval 183-1142A-7R-1, 137–148 cm, showing a breccia from Unit 5 with a large gray clast enclosed by a red granular breccia matrix (with some shearing).

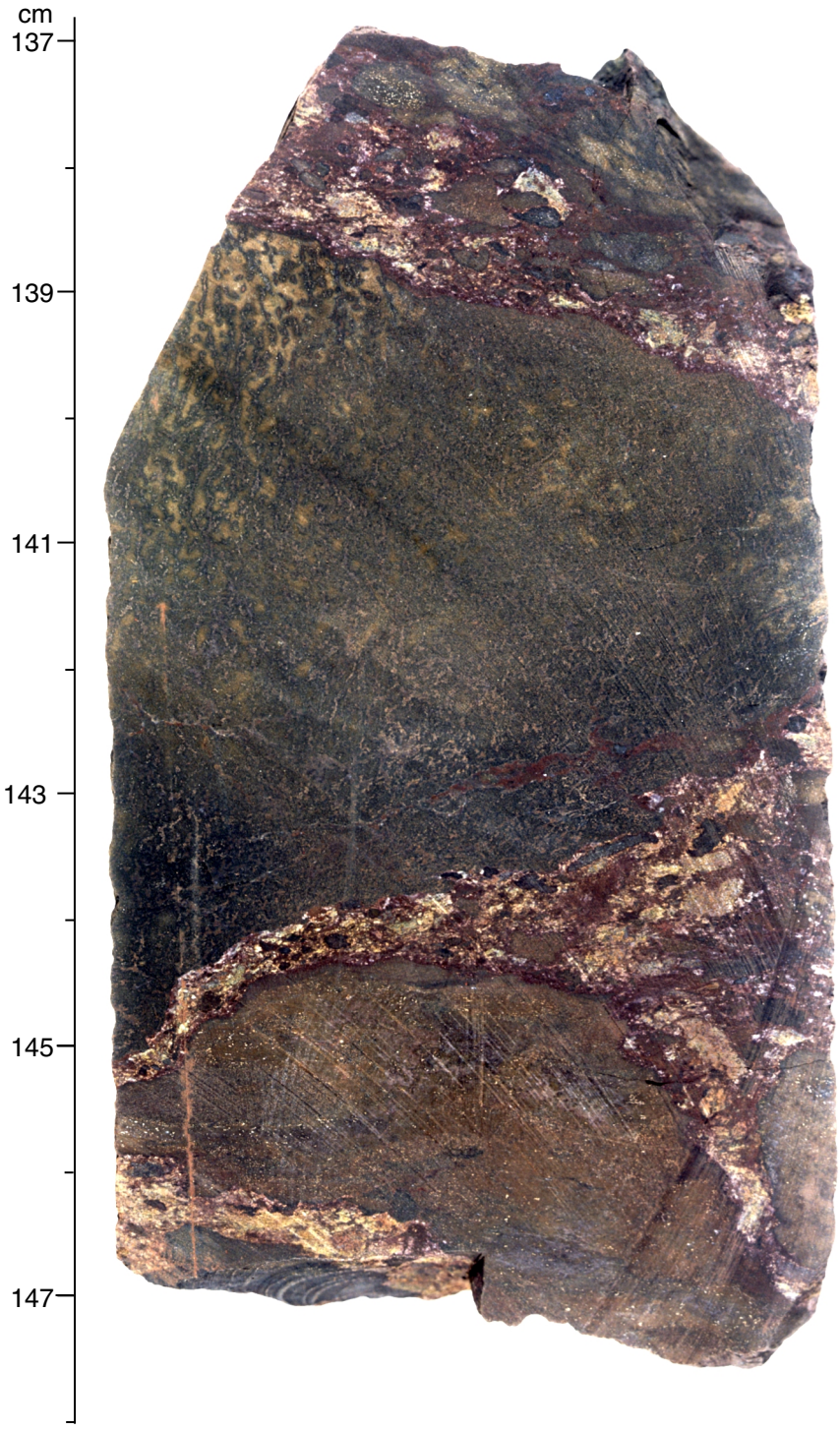

Figure F33. Close-up photograph of interval 183-1142A-7R-2, 21–40 cm, showing the dark reddish gray, highly altered breccia with some flattening of clasts in basement Unit 5. The brecciation defines a fabric in the rock.

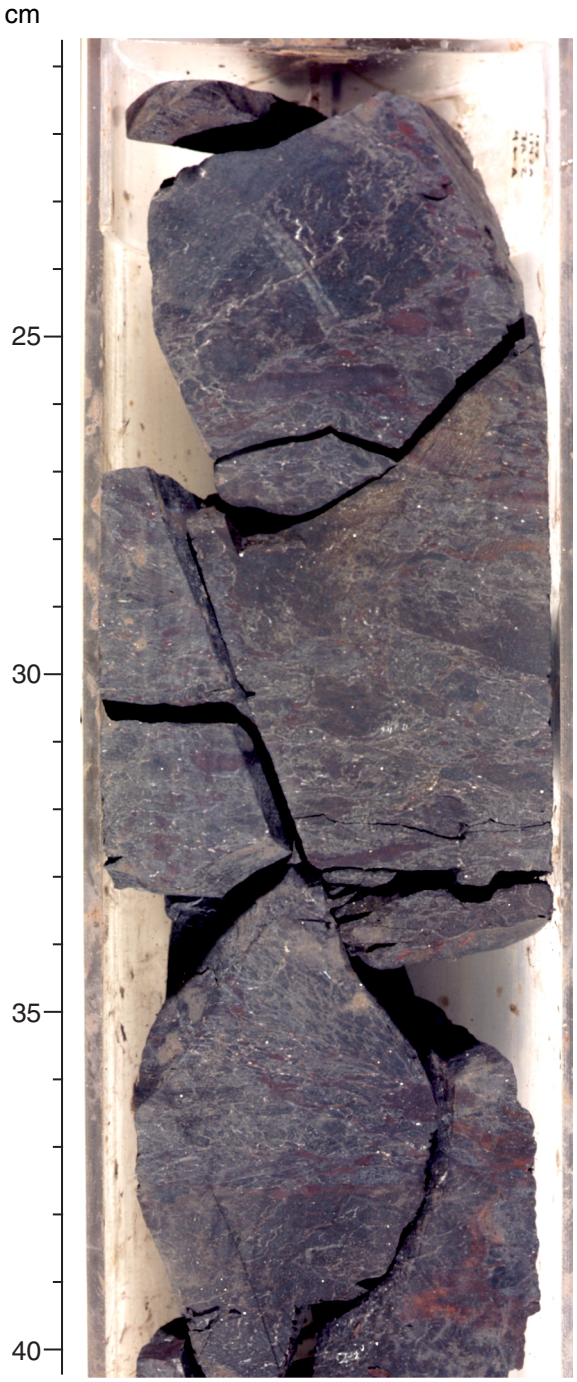

Figure F34. Color close-up photograph of Sample 183-1142A-9R-1, 71–93 cm. Light green fine-grained basalt with prominent red oxidation halo adjacent to calcite-hematite vein. The red alteration halo penetrates farther into wall rock along mesostasis bands. This feature is crosscut by a subvertical calcite vein.

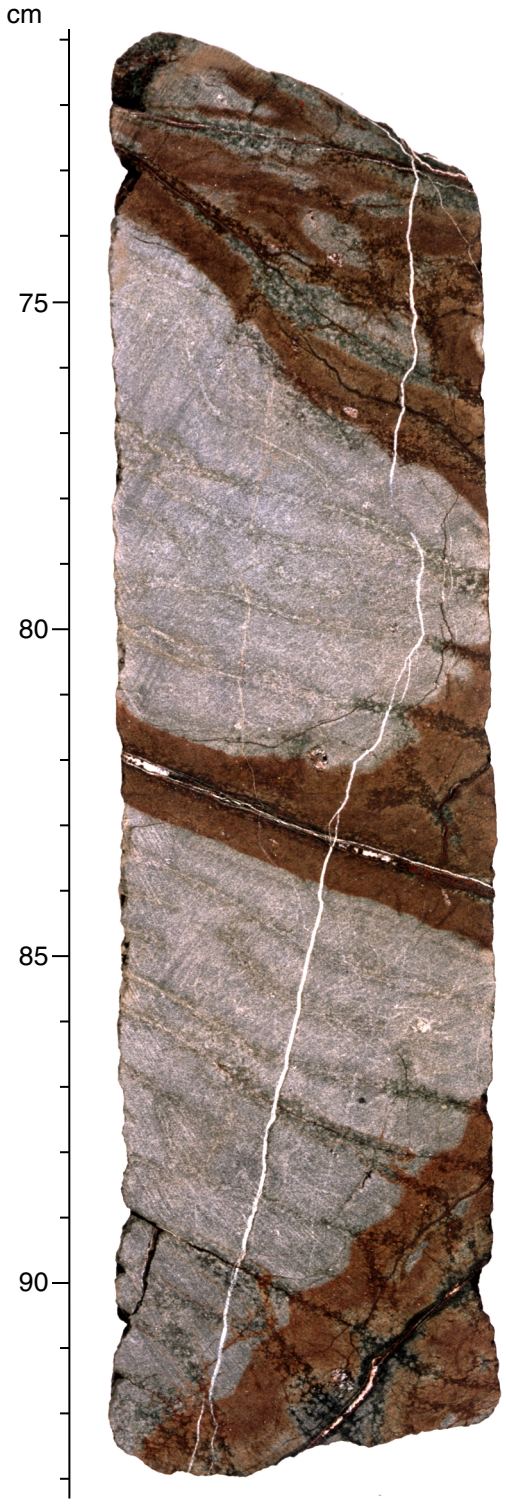

Figure F35. Color close-up photograph of Sample 183-1142A-10R-2 (Piece 5, 42–63 cm). Semicircular and linear oxidation halos crosscut and offset by subvertical calcite vein. Halo at 45–47 cm is clearly associated with vein, indicating that these alteration patterns do not necessarily imply progressive oxidation into pillow-shaped structure.

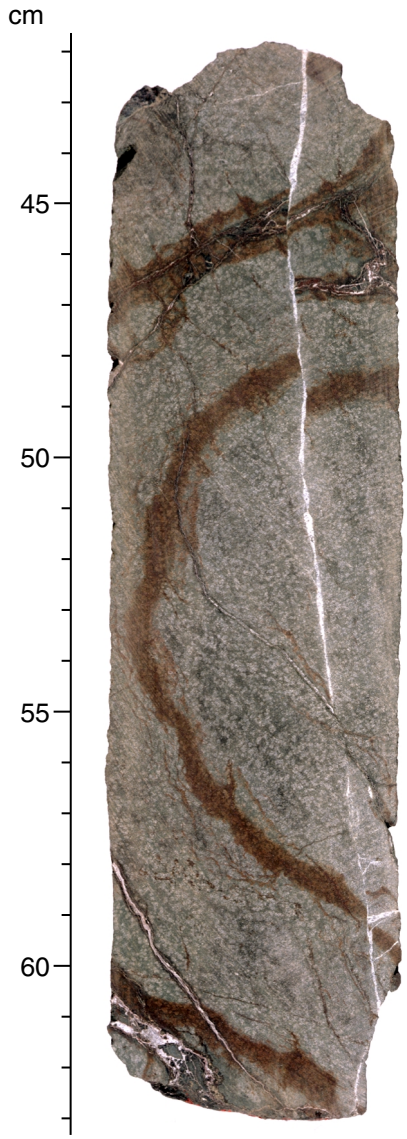

Figure F36. Close-up photograph of interval 183-1142A-9R-2, 58–68 cm, showing a possible pillow chilled margin in basement Unit 6.

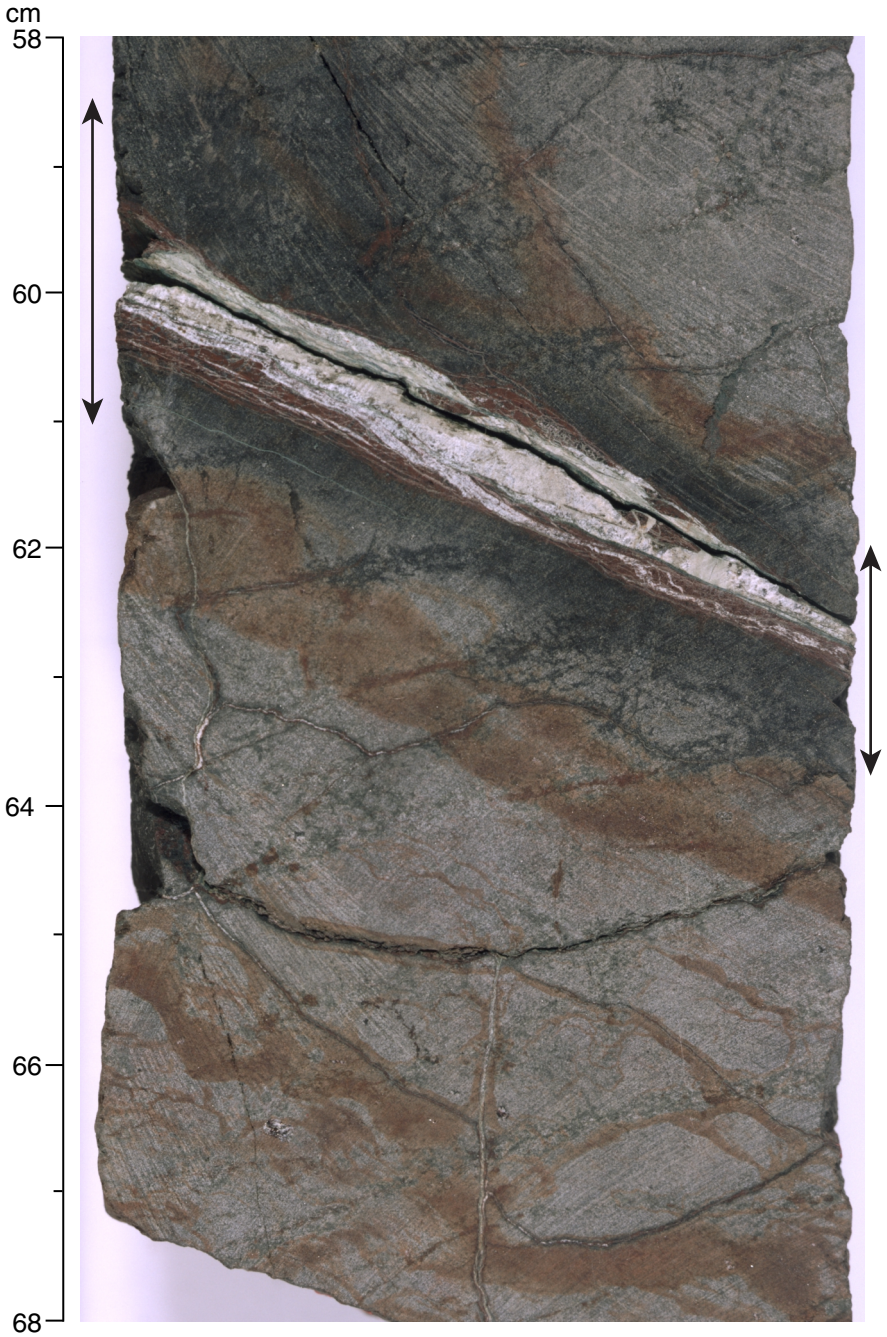

Figure F37. Color close-up photograph of Sample 183-1142A-9R-4 (Piece 1, 0–12 cm). A possible example of a glassy pillow margin with large calcite vein oriented parallel to dark green alteration zone and intersecting smaller calcite veins at approximately right angles. This is identical to the features observed in fresh glassy pillow margins in Hole 1140A. Thin-section examination of this feature, however, reveals that grain size does not decrease toward the highly altered margins, an observation that does not support the argument that these features are altered glassy pillow margins.

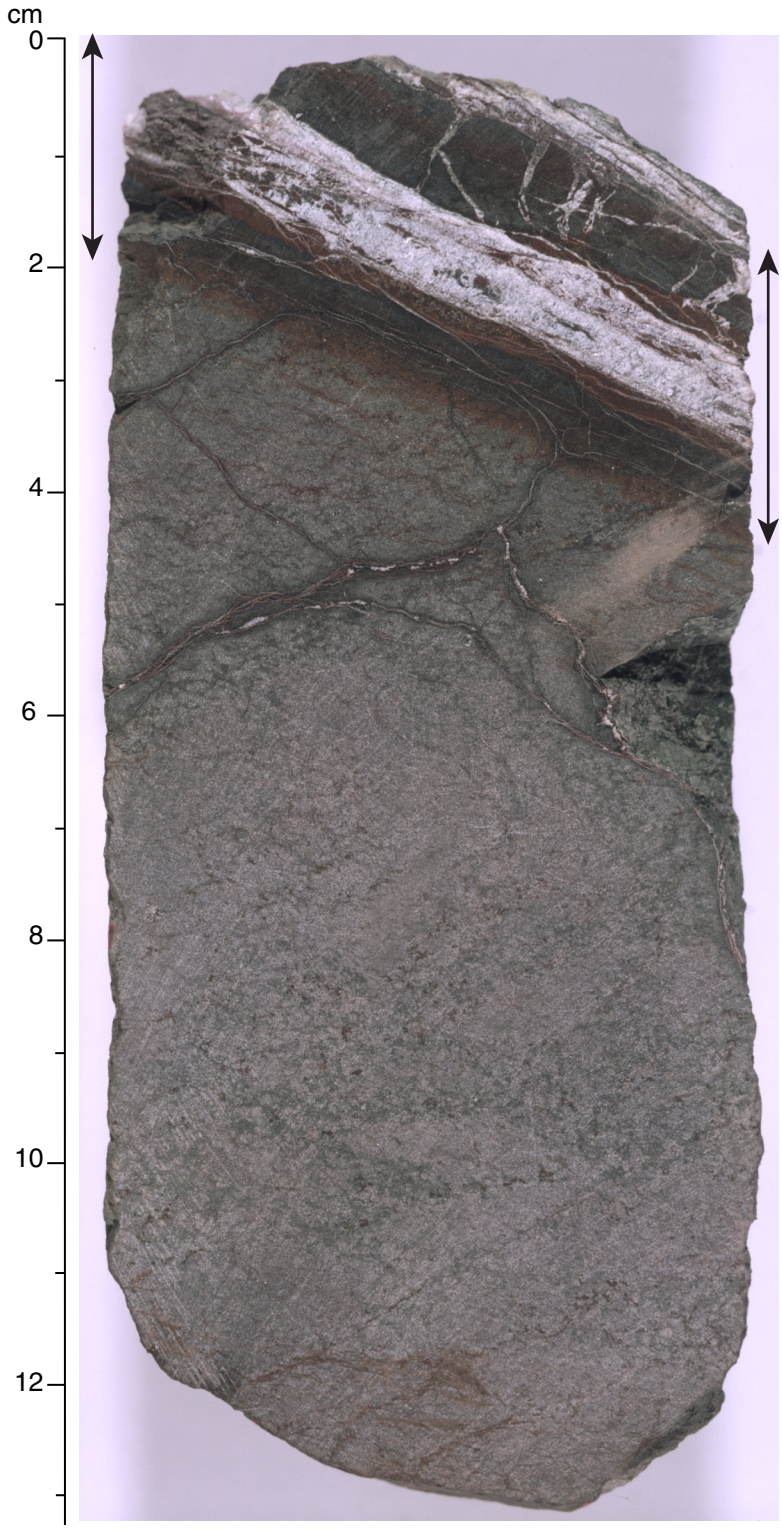

Figure F38. Interpretive log for Hole 1141A. Curated depths are used to show recovery. Structure, lithology, degree of alteration, and major phenocryst phases of basement units are summarized schematically.

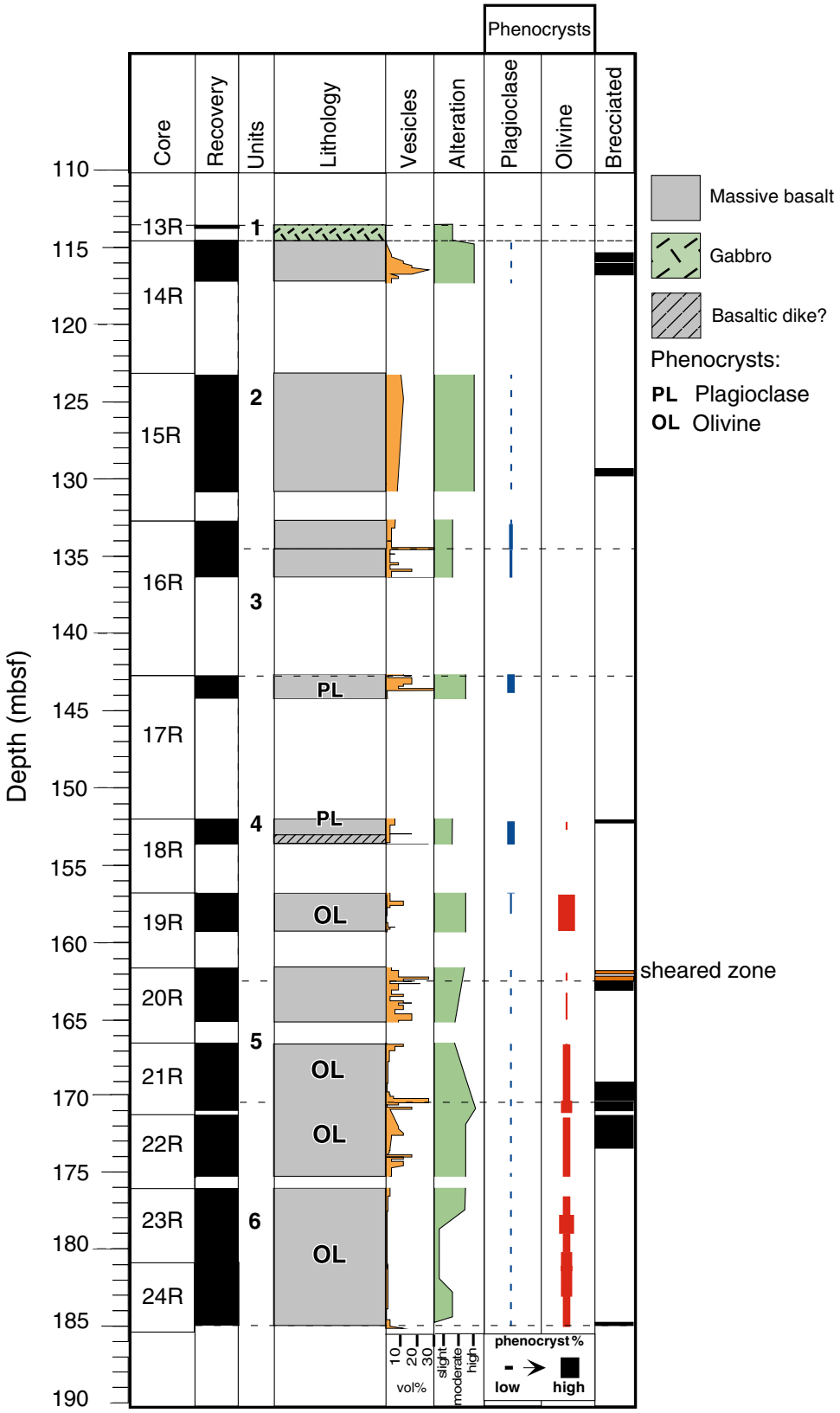

Figure F39. A, B. Two examples from Unit 3 (both in cross-polarized light) of plagioclase phenocrysts exhibiting a sieve texture (Sample 183-1141A-17R-CC, 24–27 cm).

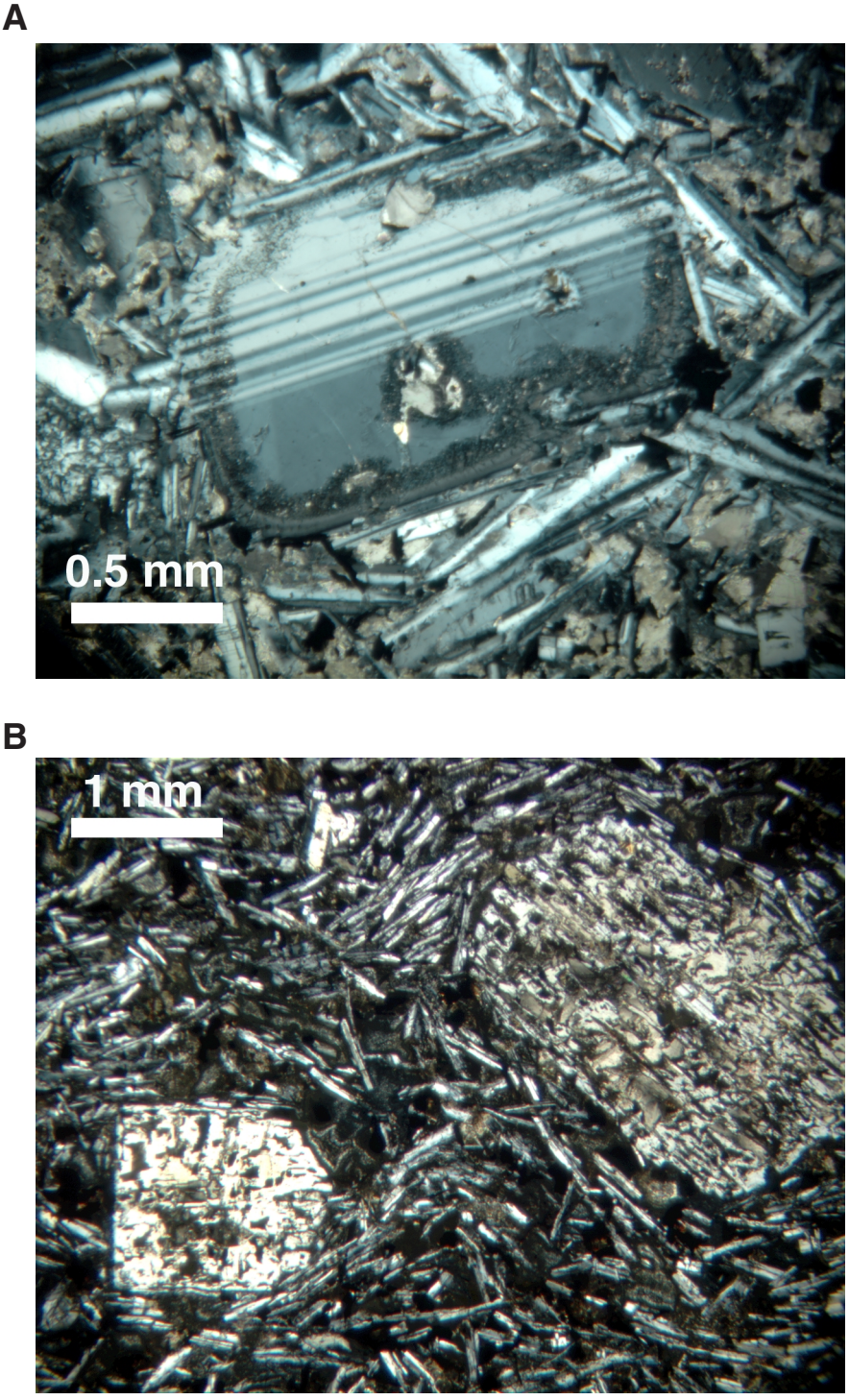

Figure F40. Altered olivine phenocryst from Unit 6 with fresh cores (183-1141A-23R-1, 46–49 cm). **A.** In plane-polarized light. **B.** In cross-polarized light.

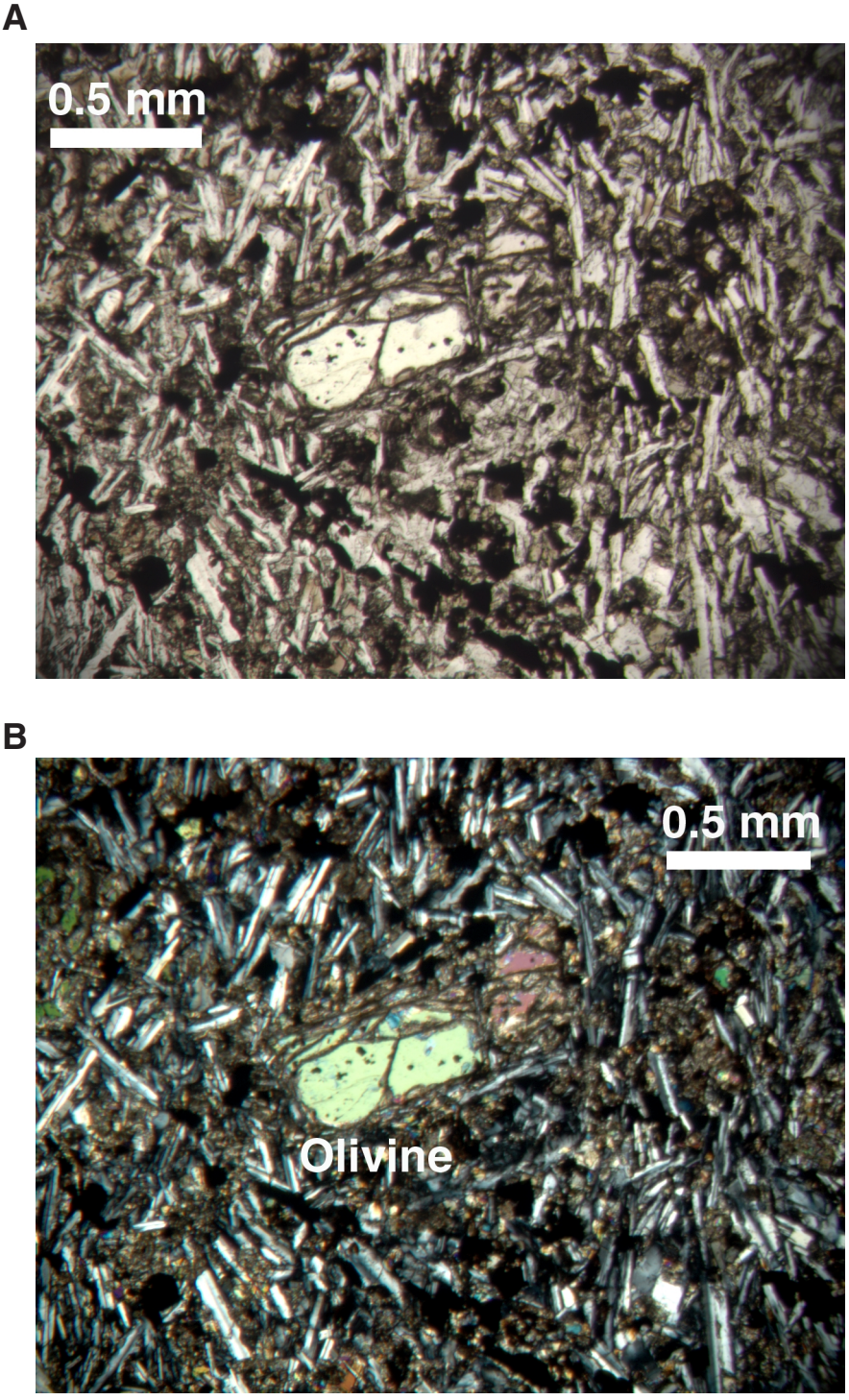

Figure F41. Subophitic texture with olivine phenocrysts, clinopyroxene, and plagioclase from Unit 6 (Sample 183-1141A-23R-2, 107–108 cm). **A.** In plane-polarized light. **B.** In cross-polarized light.

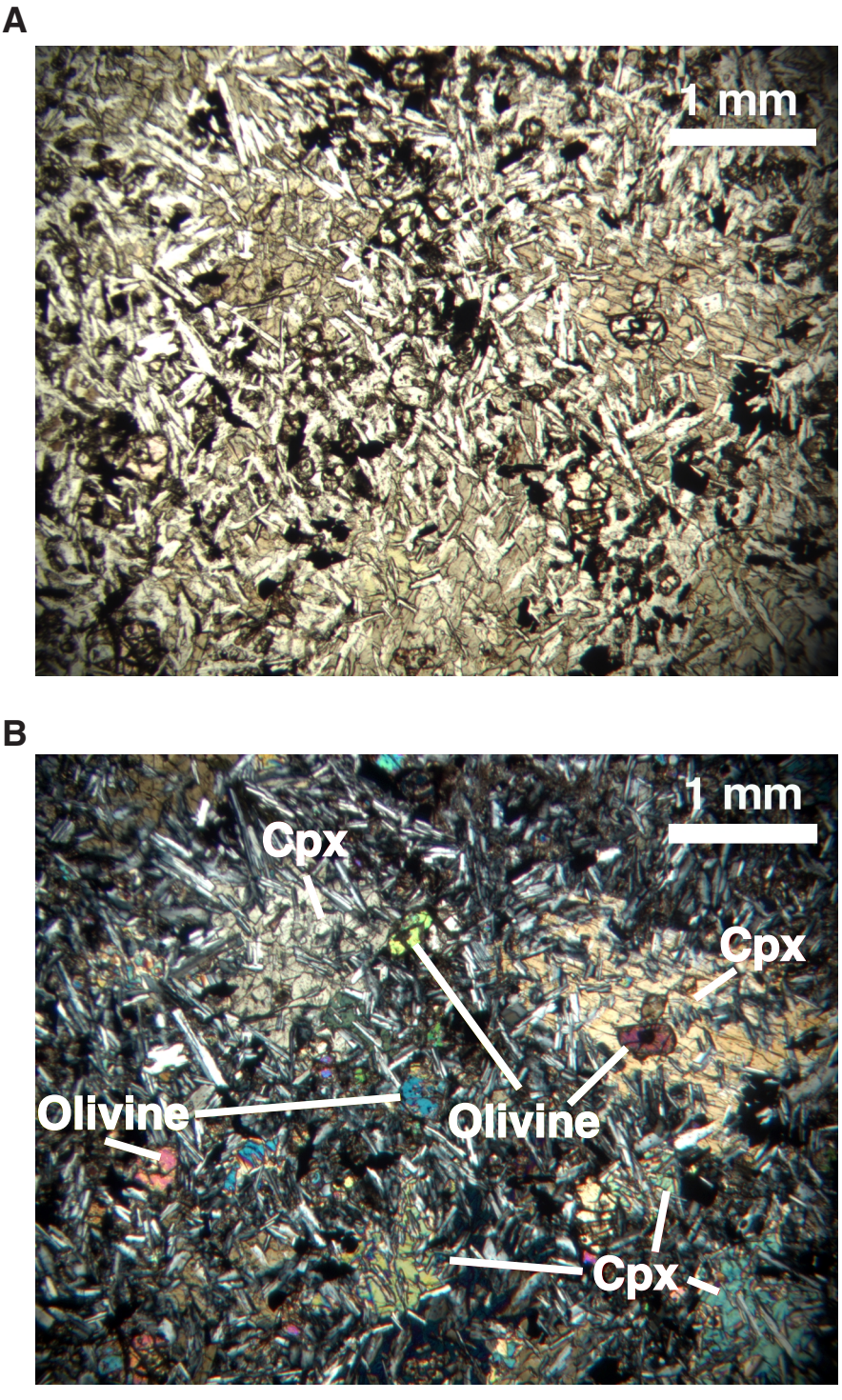

Figure F42. Carbonate pseudomorph (in cross-polarized light) of a mafic phenocryst from Unit 6 (Sample 183-1141A-22R-3, 146–148 cm).

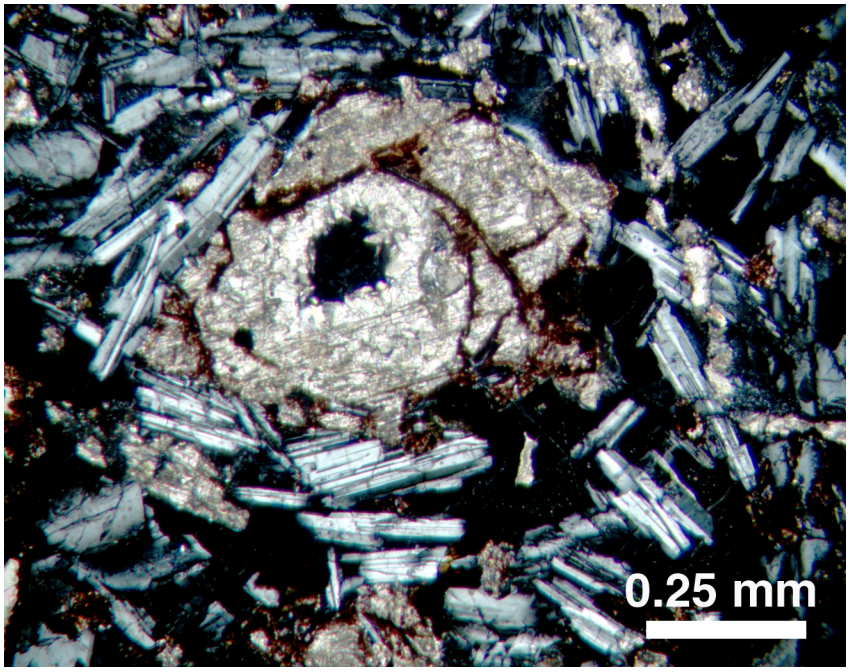

Figure F43. Two examples of crystalline goethite replacing titanomagnetite in Unit 6. **A.** Sample 183-1141A-22R-3, 146–148 cm (in plane-polarized light). **B.** Sample 183-1141A-23R-1, 106–109 cm, with carbonate (in cross-polarized light).

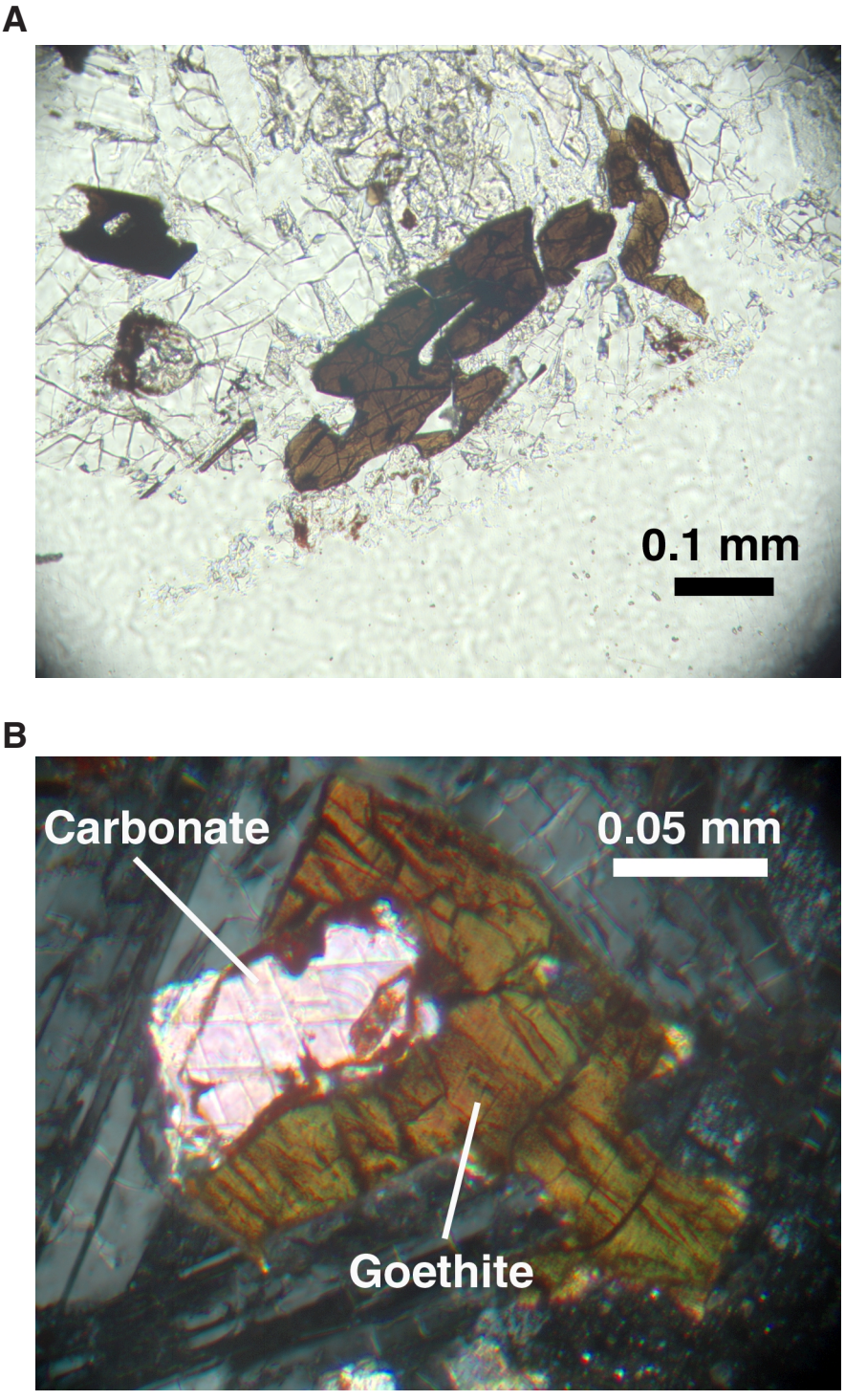

Figure F44. Interpretive log for Hole 1142A. Curated depths are used to show recovery. Structure, lithology, degree of alteration, and major phenocryst phases of basement units are summarized schematically.

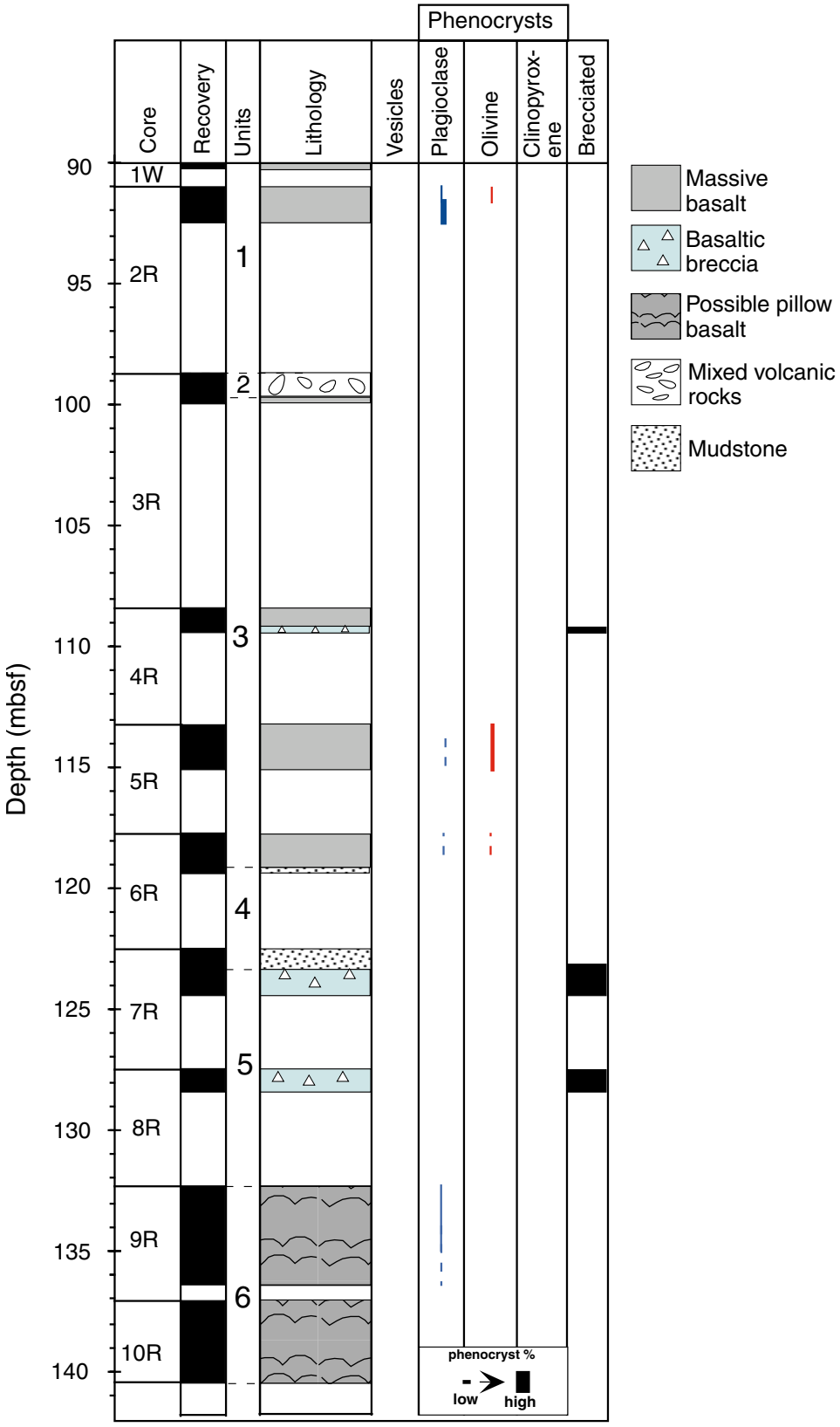

Figure F45. Corroded olivine microphenocrysts with fresh cores from Unit 1 in an intergranular groundmass (Sample 183-1142A-2R-1, 50–53 cm). **A.** In plane-polarized light. **B.** In cross-polarized light.

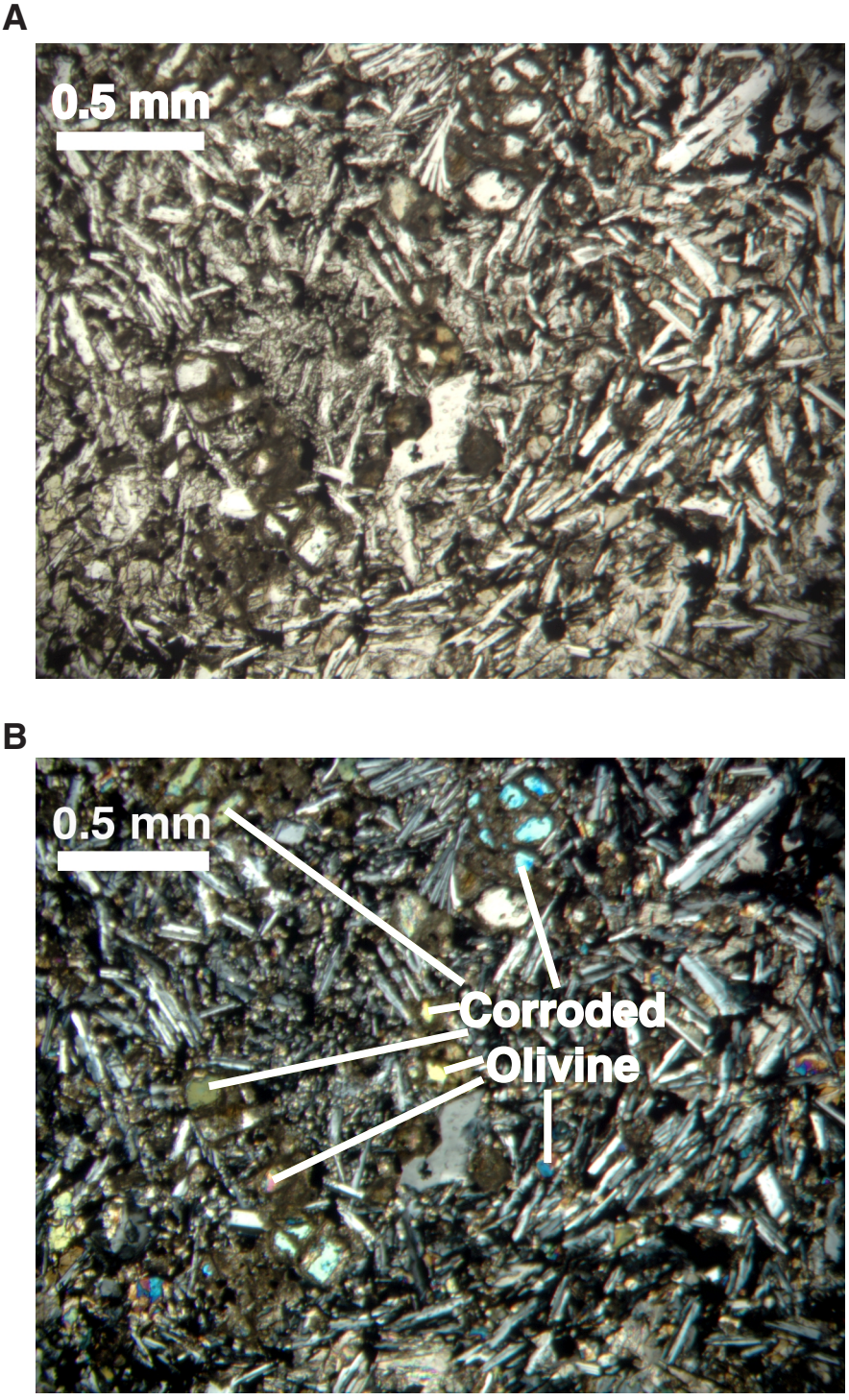

Figure F46. Sieve-textured plagioclase and altered olivine phenocrysts in an intergranular groundmass from Unit 3 (Sample 183-1142A-6R-1, 11–14 cm). **A.** In plane-polarized light. **B.** In cross-polarized light.

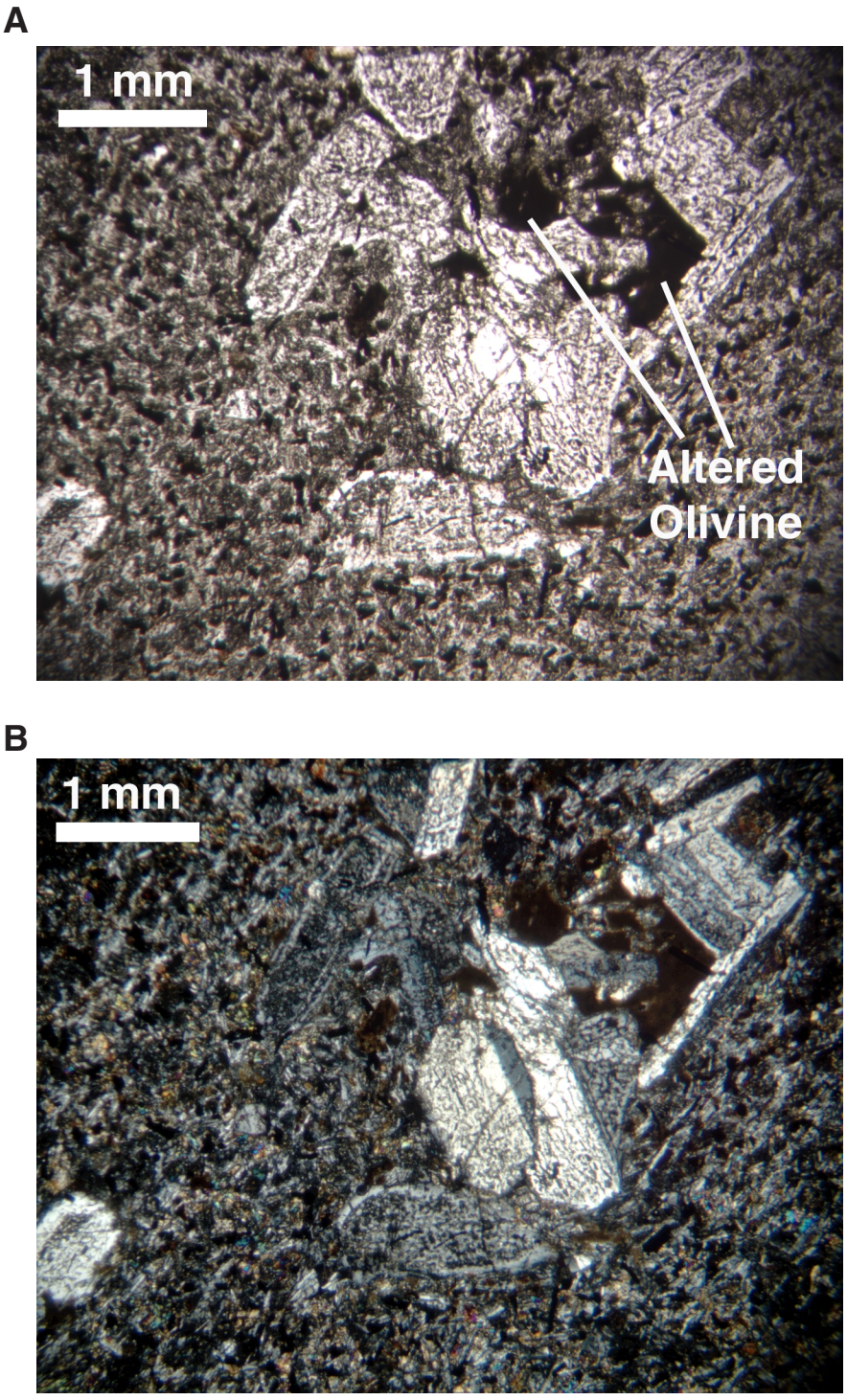

Figure F47. Altered, possibly originally glassy, pillow margin from Unit 6 (Sample 183-1142A-9R-4, 3–7 cm). **A.** In plane-polarized light. **B.** In cross-polarized light.

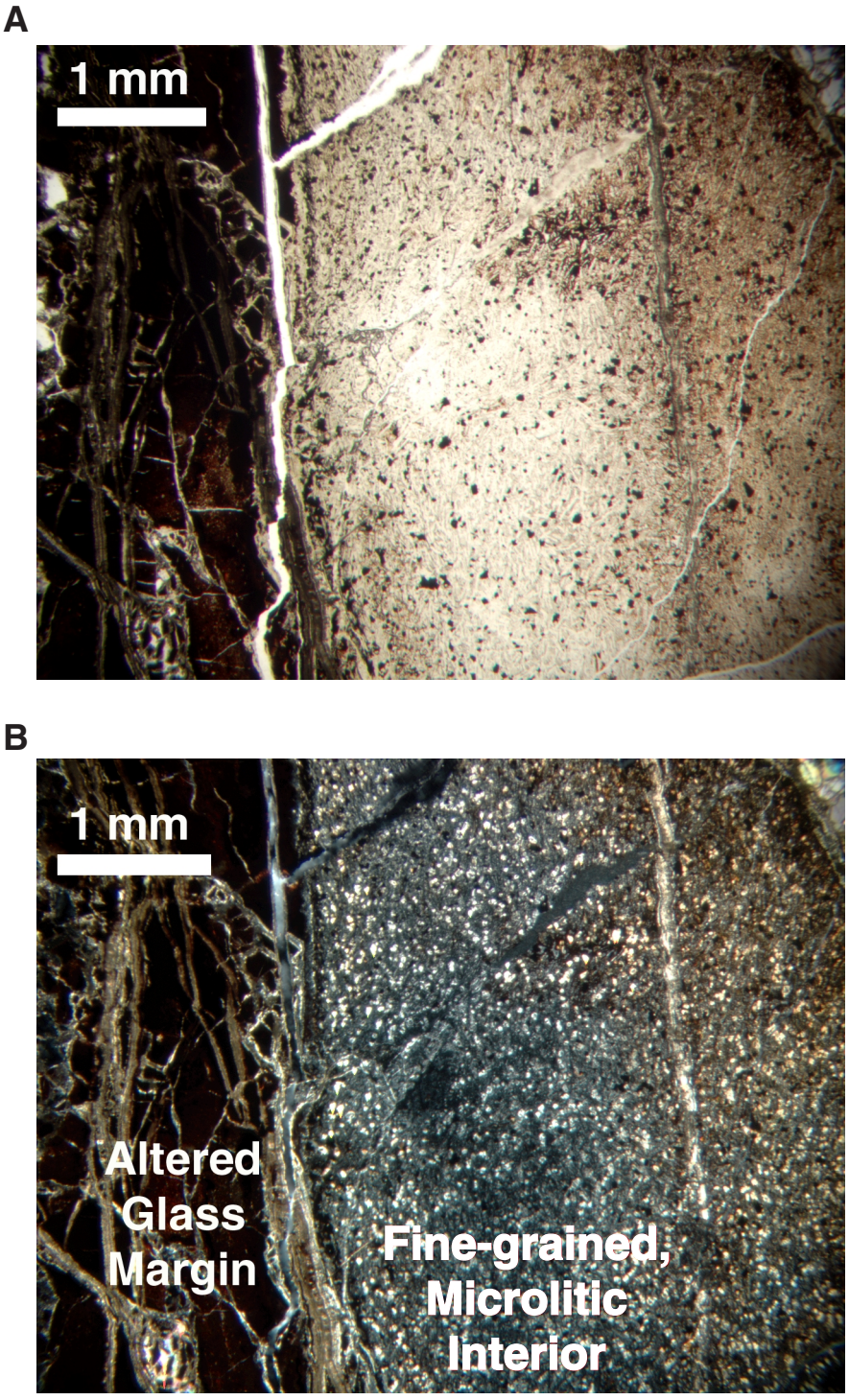

Figure F48. Interior of possible pillow lava showing corroded plagioclase phenocrysts in an intergranular groundmass from Unit 6 (Sample 183-1142A-9R-3, 108–111 cm). **A.** In plane-polarized light. **B.** In cross-polarized light.

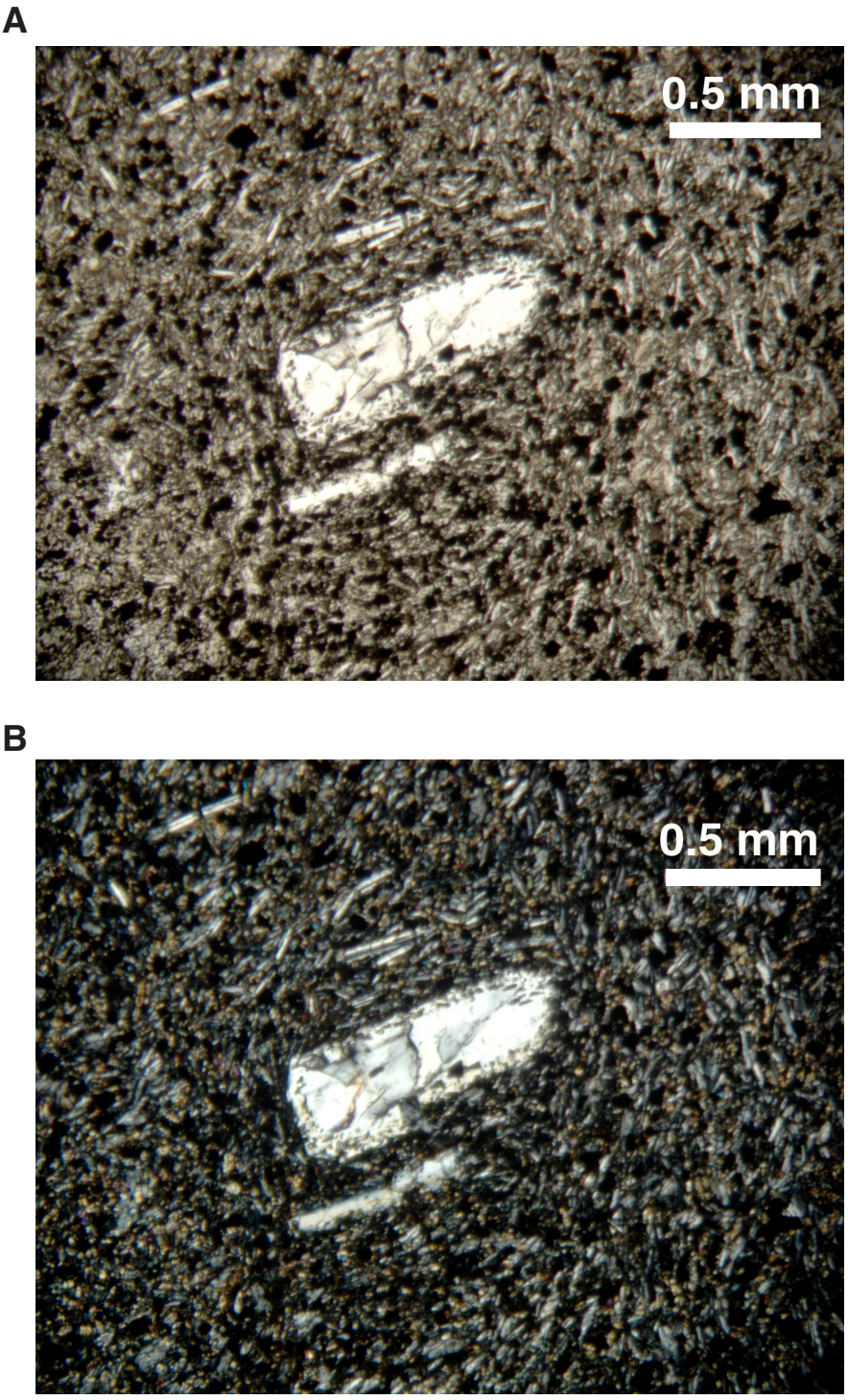

Figure F49. Sites 1141 and 1142 igneous rock compositions presented on a plot of total alkalis ($Na_2O + K_2O$) vs. SiO_2 (Le Bas et al., 1986); alkali and tholeiitic fields are distinguished by the Macdonald-Katsura (1964) line (dashed line on the figure). The basement compositions of Site 1141/1142 are compared with those from all other Leg 183 sites.

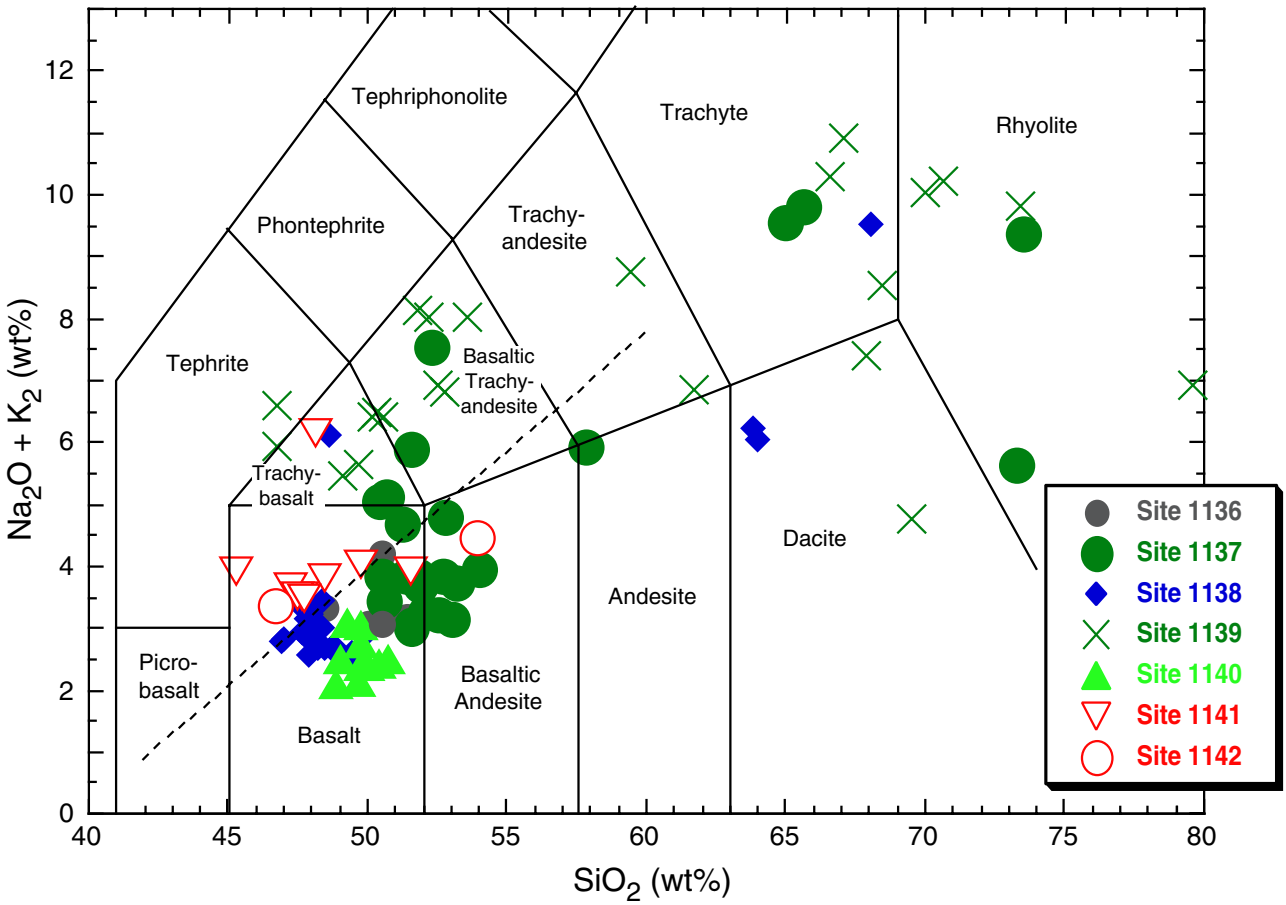

Figure F50. Downhole variations of major elements through basement Units 4–6 at Site 1141.

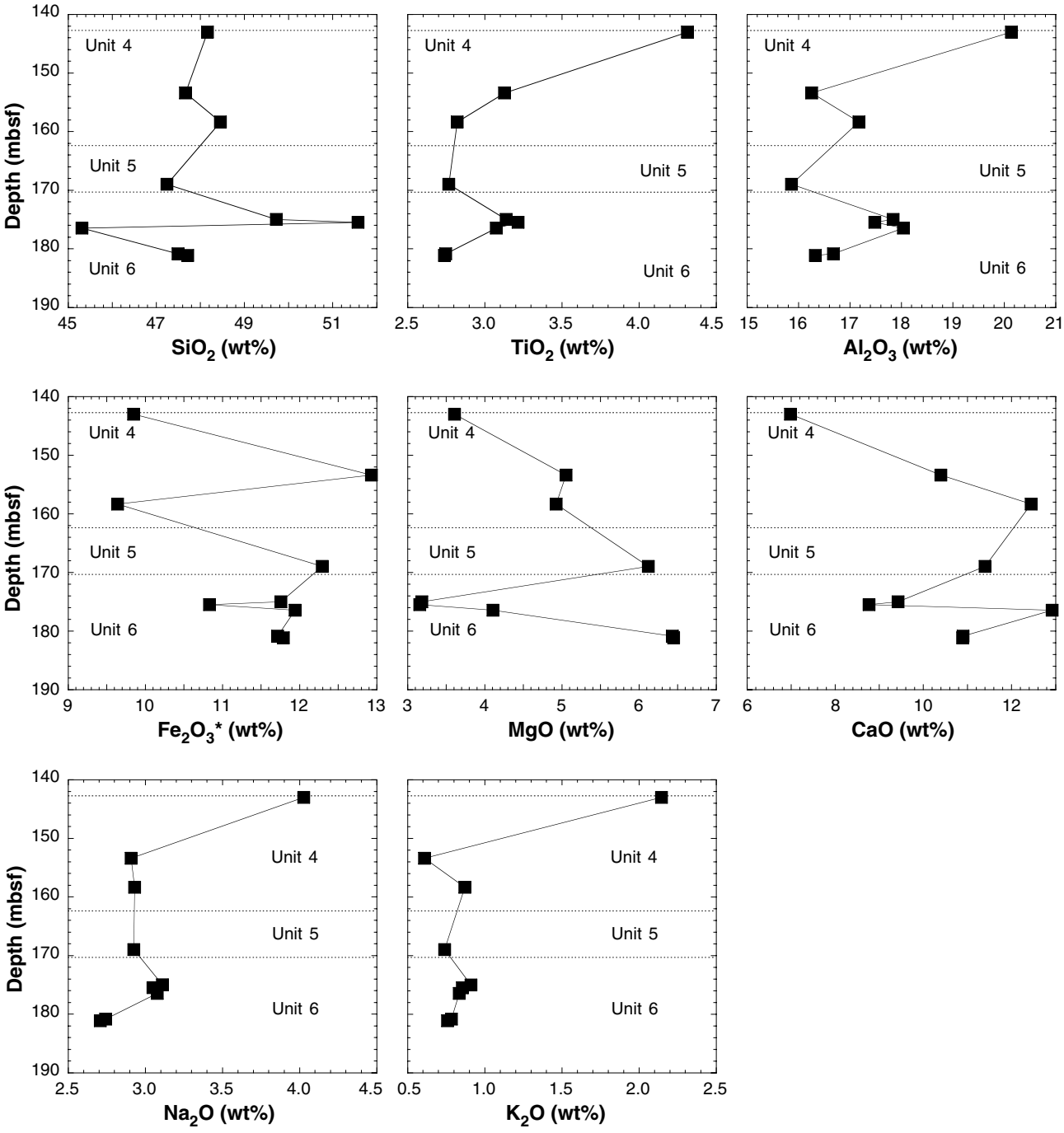

Figure F51. Downhole variations of selected minor and trace elements through basement Units 4–6 at Site 1141.

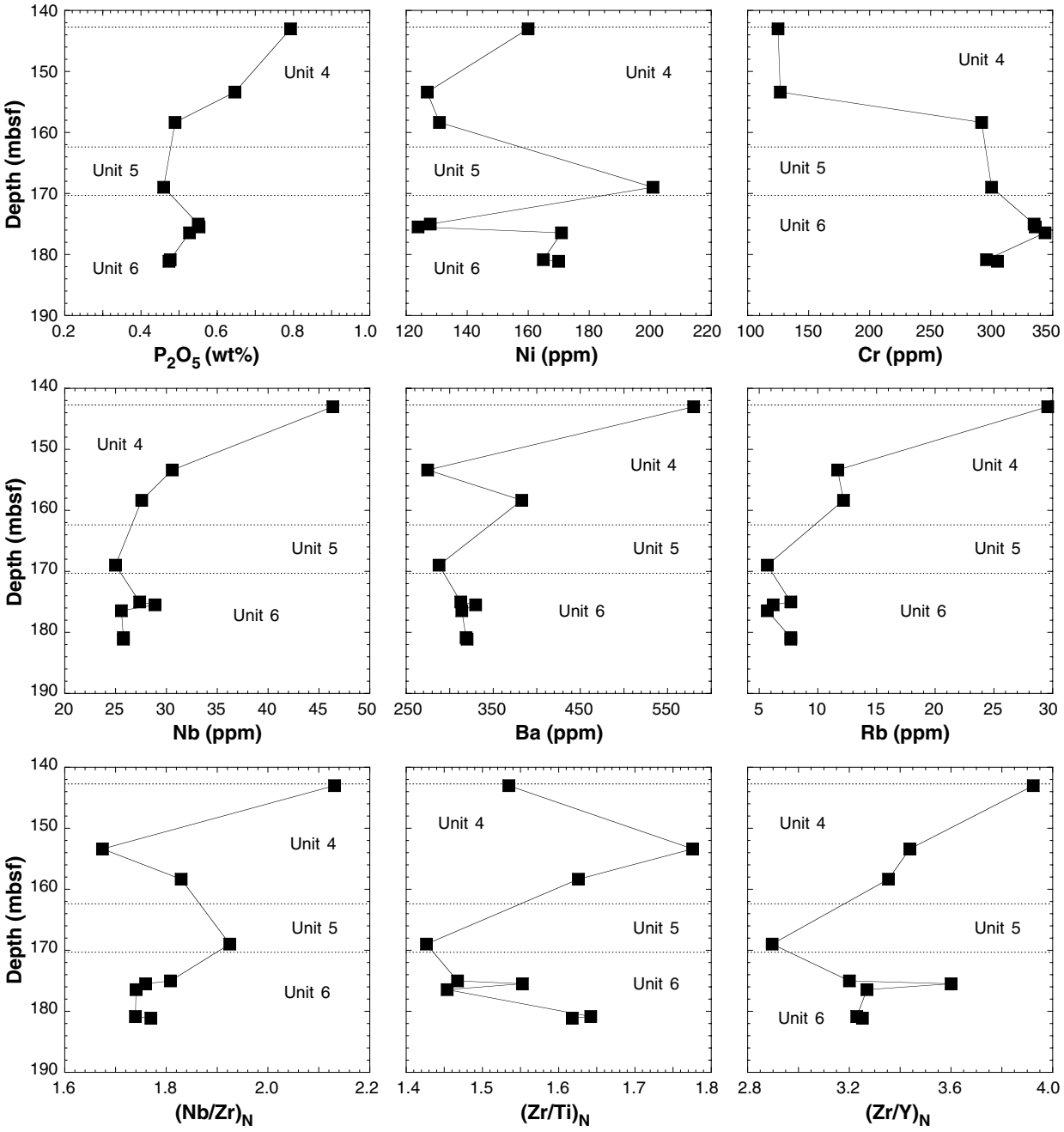

Figure F52. Major and minor element compositions of Sites 1141 and 1142 basalts (defined by the dashed field in each panel) compared with other Broken Ridge and Kerguelen Plateau basement samples.

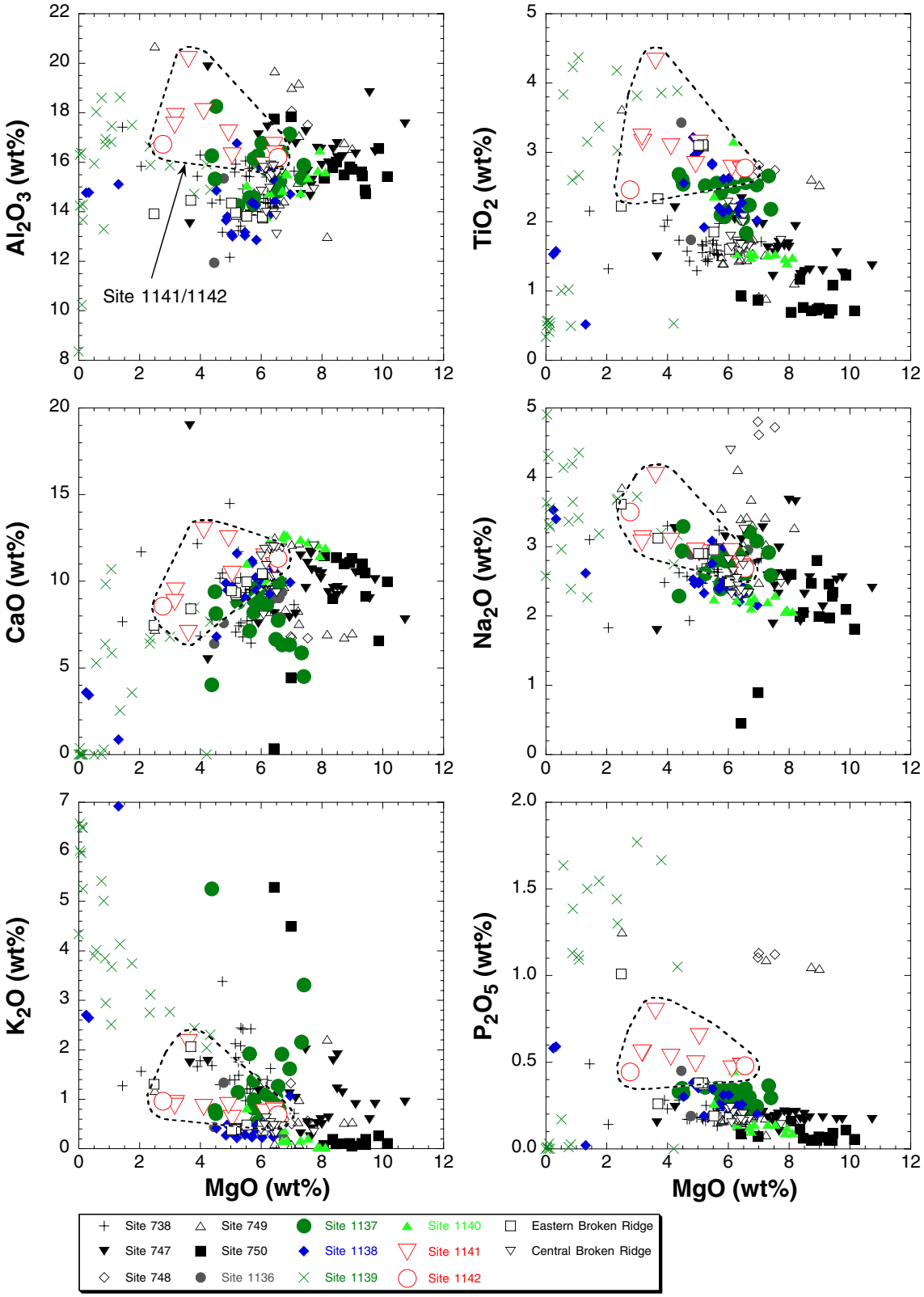

Figure F53. Trace element compositions of Sites 1141 and 1142 basalts (defined by the dashed field in each panel) are compared with other Broken Ridge and Kerguelen Plateau basement samples.

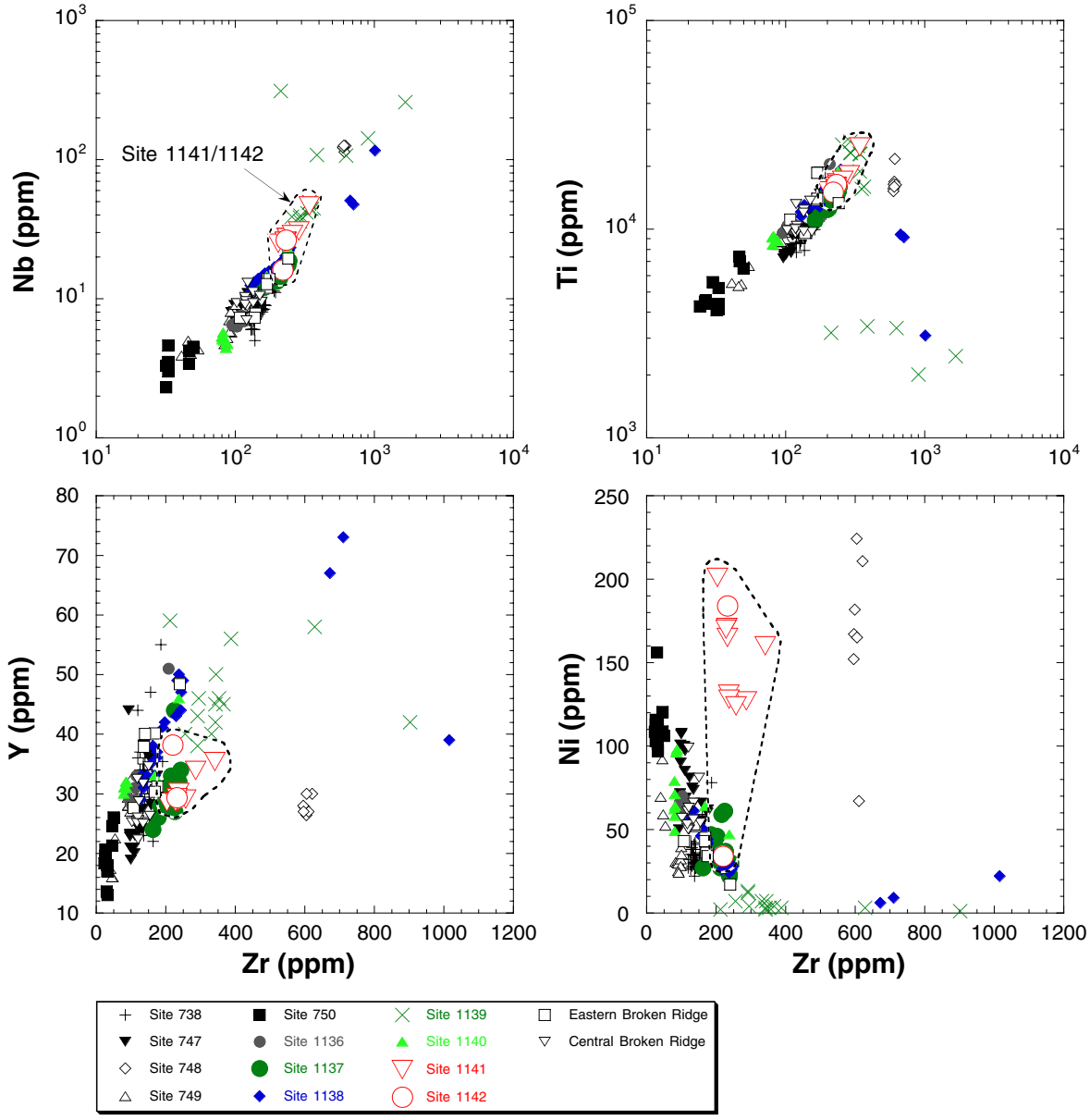

Figure F54. Variations of minor and trace element abundances with primitive mantle–normalized Nb/Zr ratio for Sites 1141 and 1142 basalts (defined by the dashed field in each panel) compared with other Broken Ridge and Kerguelen Plateau basement samples.

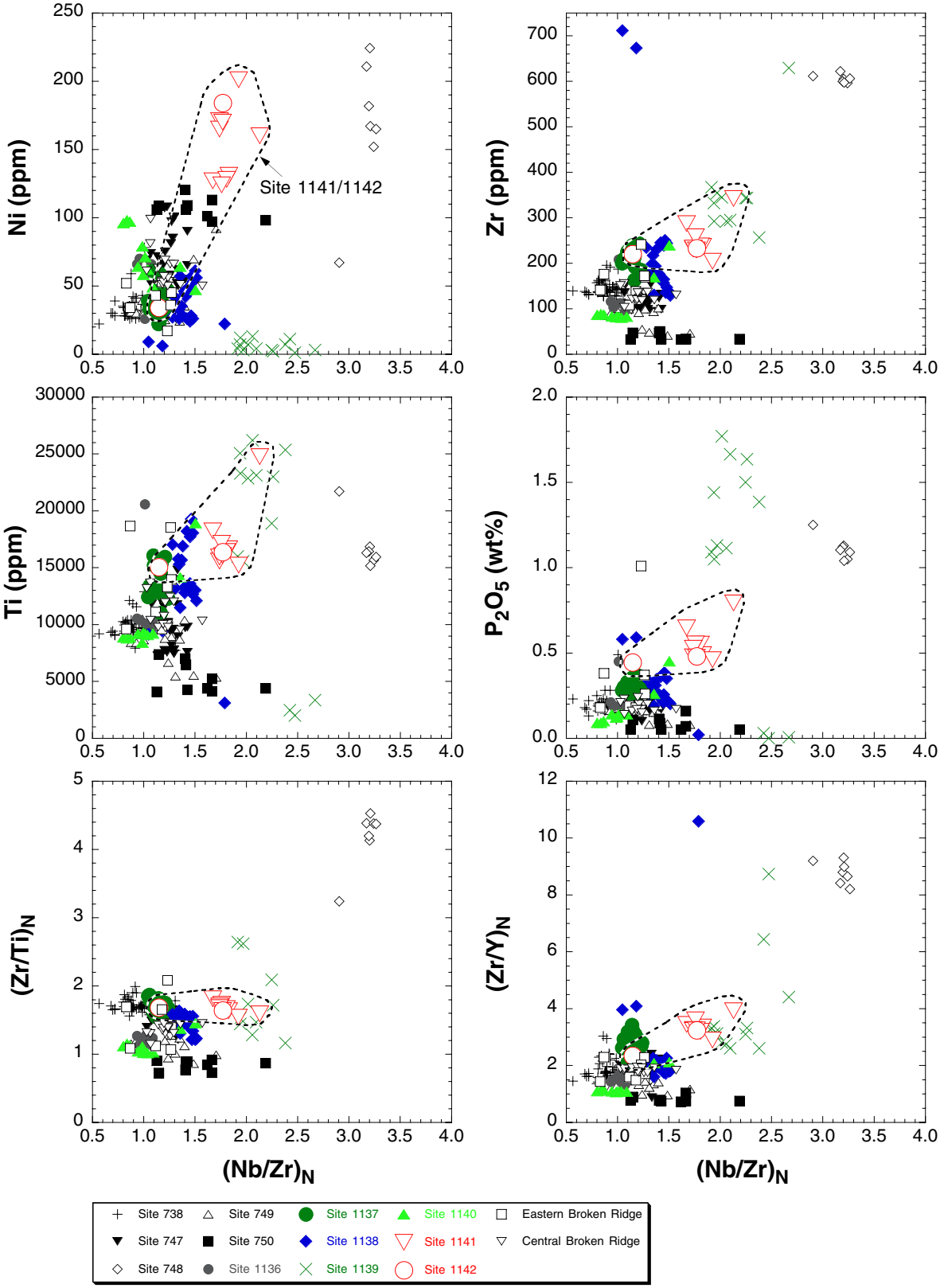

Figure F55. Primitive mantle–normalized plots of Sites 1141 and 1142 basalts. **A.** Individual profiles for each sample analyzed are defined. Site 1141 samples are depicted by a dashed line, and those from Site 1142 by a solid line. **B.** Sites 1141 and 1142 basalts are compared with dredge samples from eastern and central Broken Ridge (reported by Mahoney et al., 1995). The dredge data for central and eastern Broken Ridge are defined by the shaded fields. **C.** Three individual dredge samples with compositions plotting outside the fields defined in B are plotted for comparison with Sites 1141 and 1142 basalts and the main fields for eastern and central Broken Ridge. Normalizing values are from Sun and McDonough (1989).

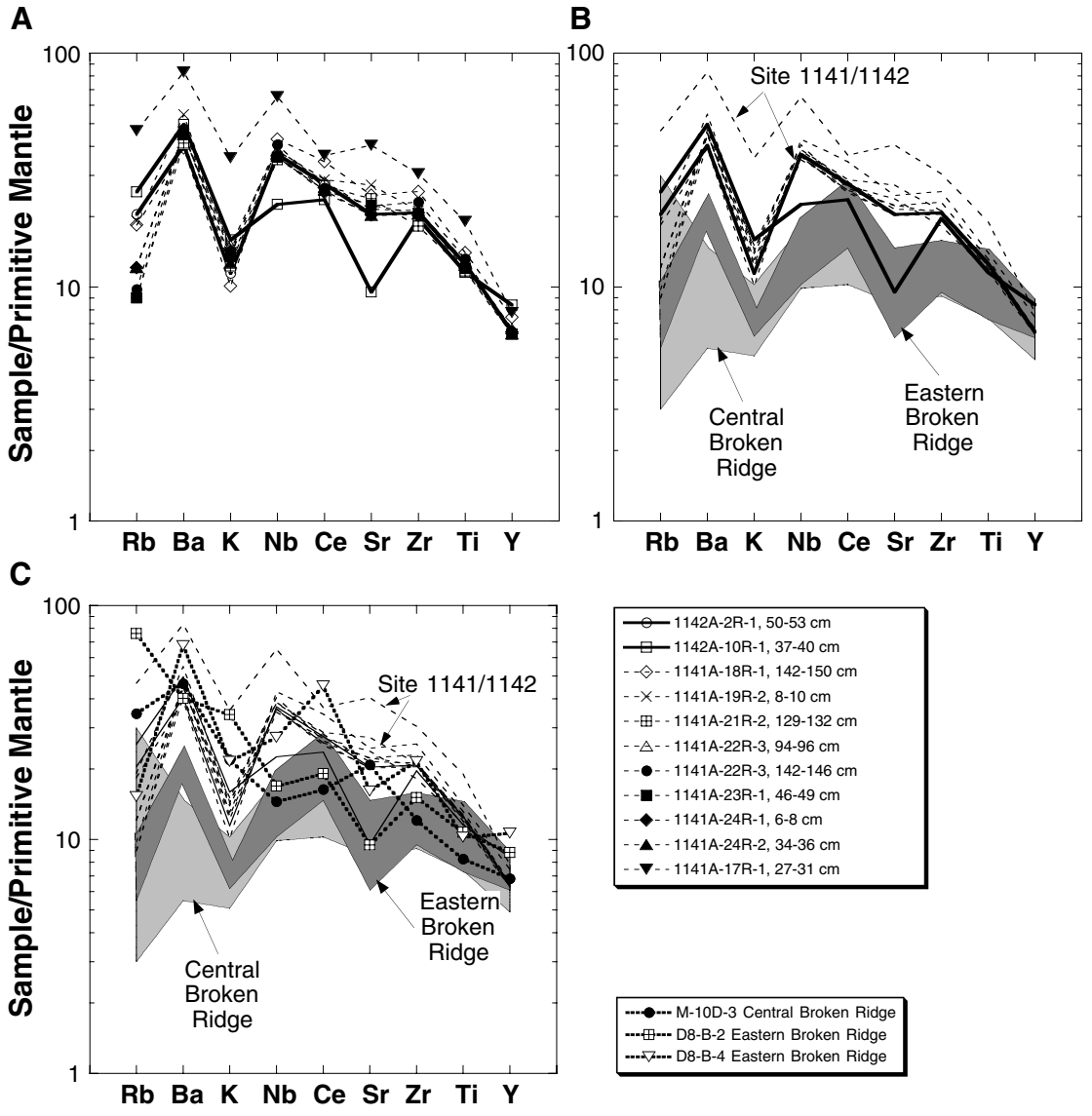

Figure F56. A. The downhole distribution of secondary minerals in Hole 1141A as determined from visual examination of macroscopic samples of drill core. Alteration: sl = slight, m = moderate, h = high, c = complete. Colors: Gn = green, G = gray, Pk = pink, Bn = brown, R = red. SiO = quartz and amorphous silica. (Continued on next page).

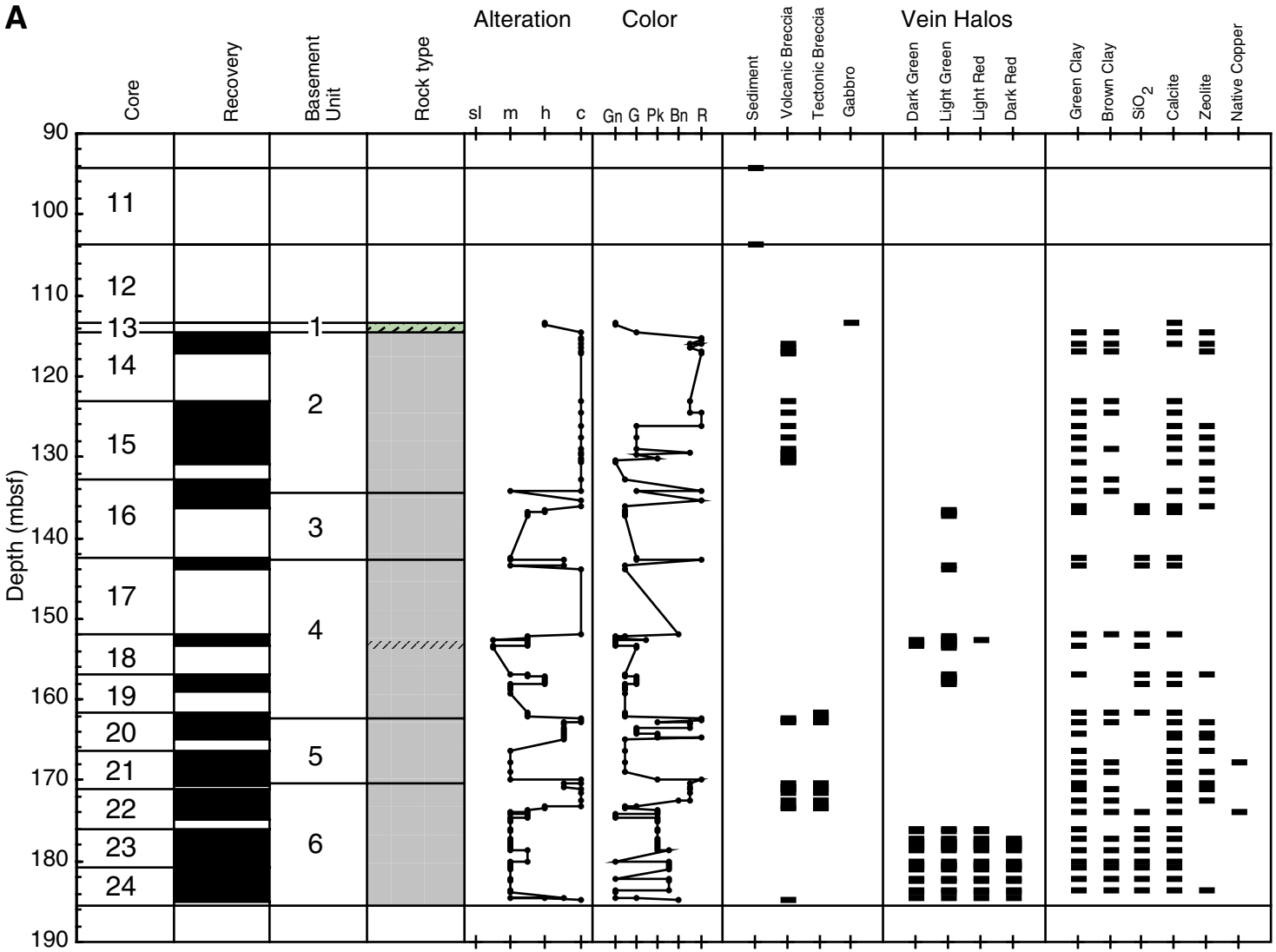

Figure F56 (continued). B. The downhole distribution of secondary minerals in Hole 1142A as determined from visual examination of macroscopic samples of drill core. Alteration: sl = slight, m = moderate, h = high, c = complete. Colors: Gn = green, G = gray, Pk = pink, Bn = brown, R = red. SiO = quartz and amorphous silica.

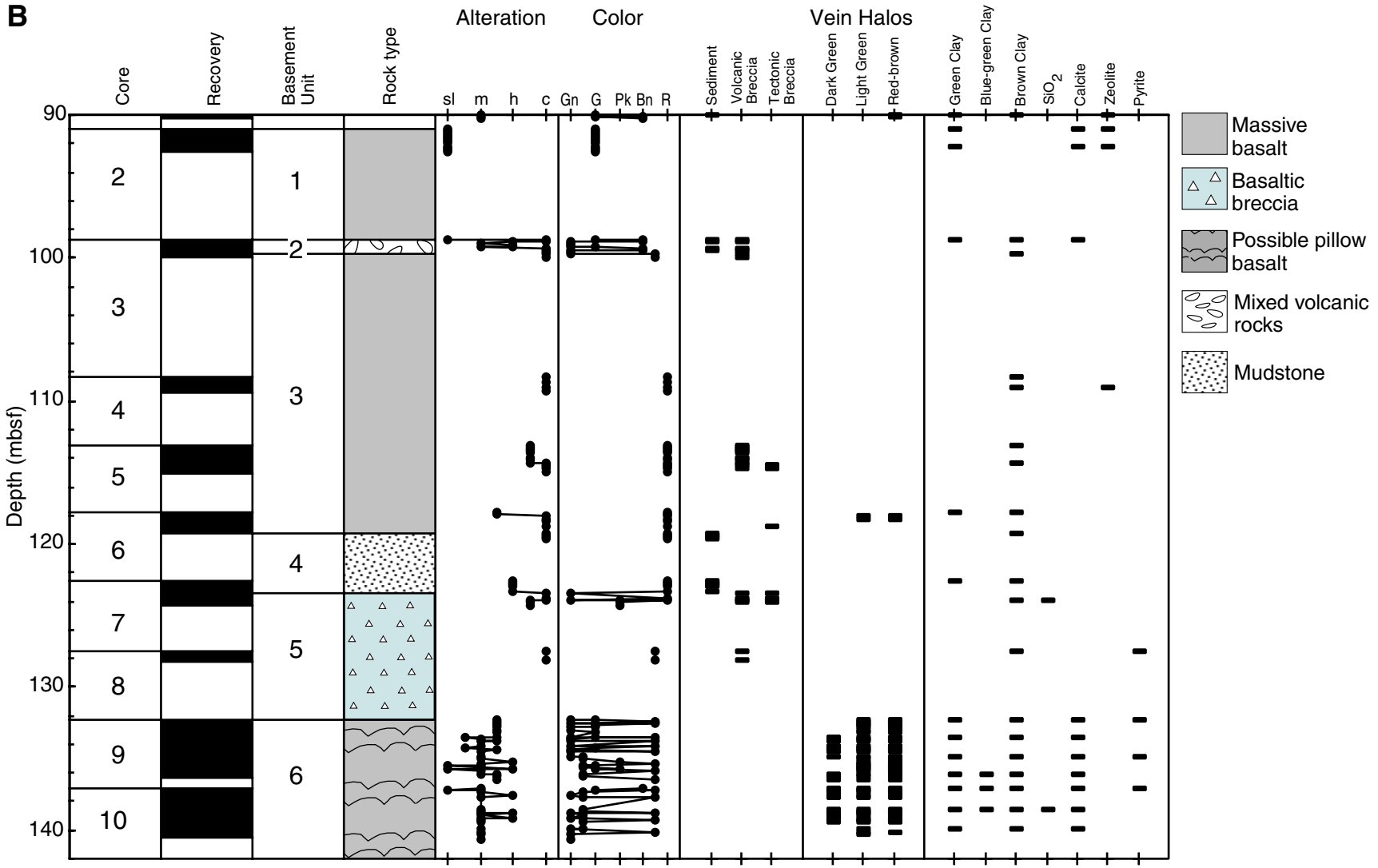

Figure F57. Color close-up photograph of interval 183-1141A-18R-1 (Piece 11B, 74–85 cm). Red alteration front crosscut by calcite veins in fine-grained light green basalt (Unit 4). Light green alteration halo associated with calcite vein replaces oxidized basalt. Also shown are vesicles with colloform textures.

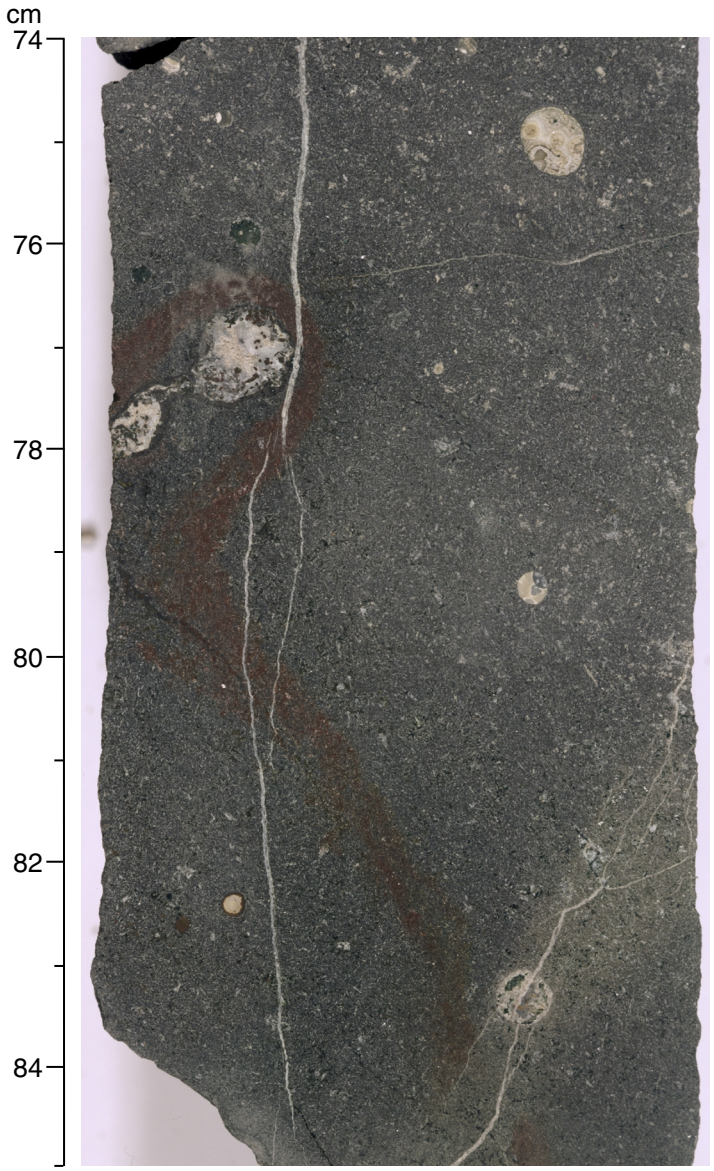

Figure F58. Color close-up photograph of interval 183-1141A-22R-1 (Piece 2, 105–120 cm). Red volcanic breccia comprising the flow top of Unit 6. Clasts are altered to red and dark brown clays and cemented by calcite and zeolite.

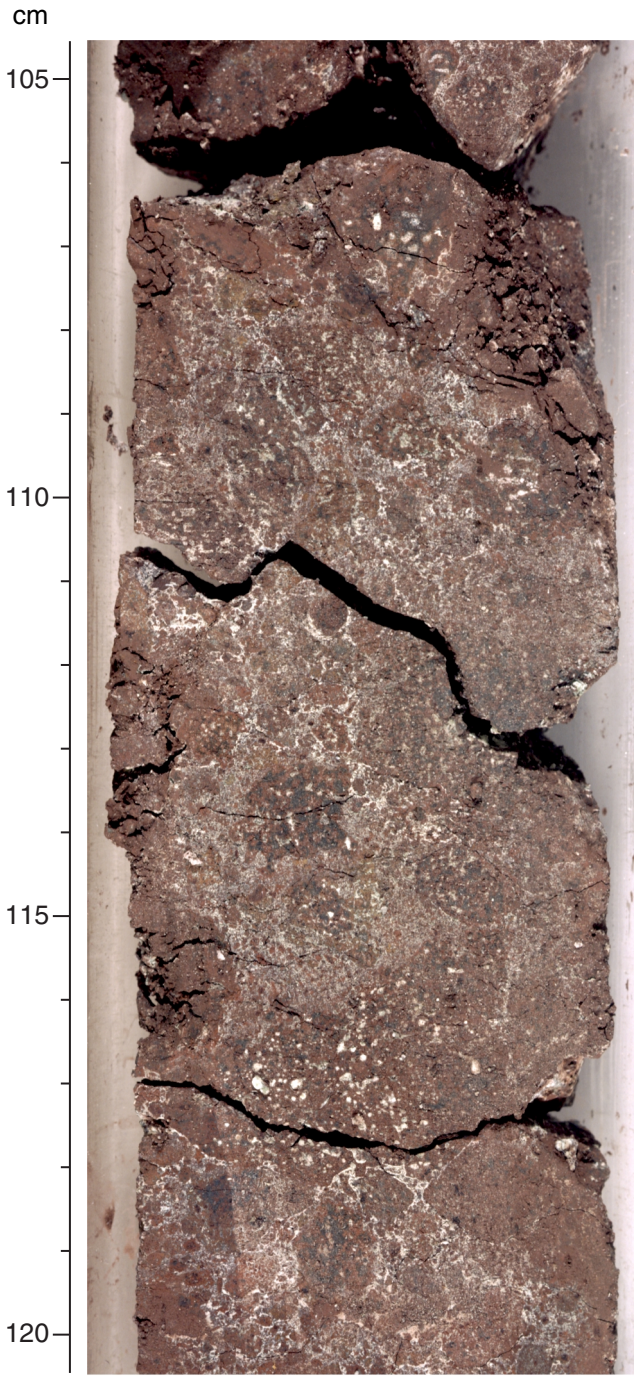

Figure F59. Color close-up photograph of interval 183-1141A-23R-1, 105–115 cm. Alteration accentuating variolitic texture in basalt (Unit 6). Plagioclase is altered to light green clay, and mafics are altered to red clay. A less altered, finer grained late stage (?) segregation is at 106–108 cm.

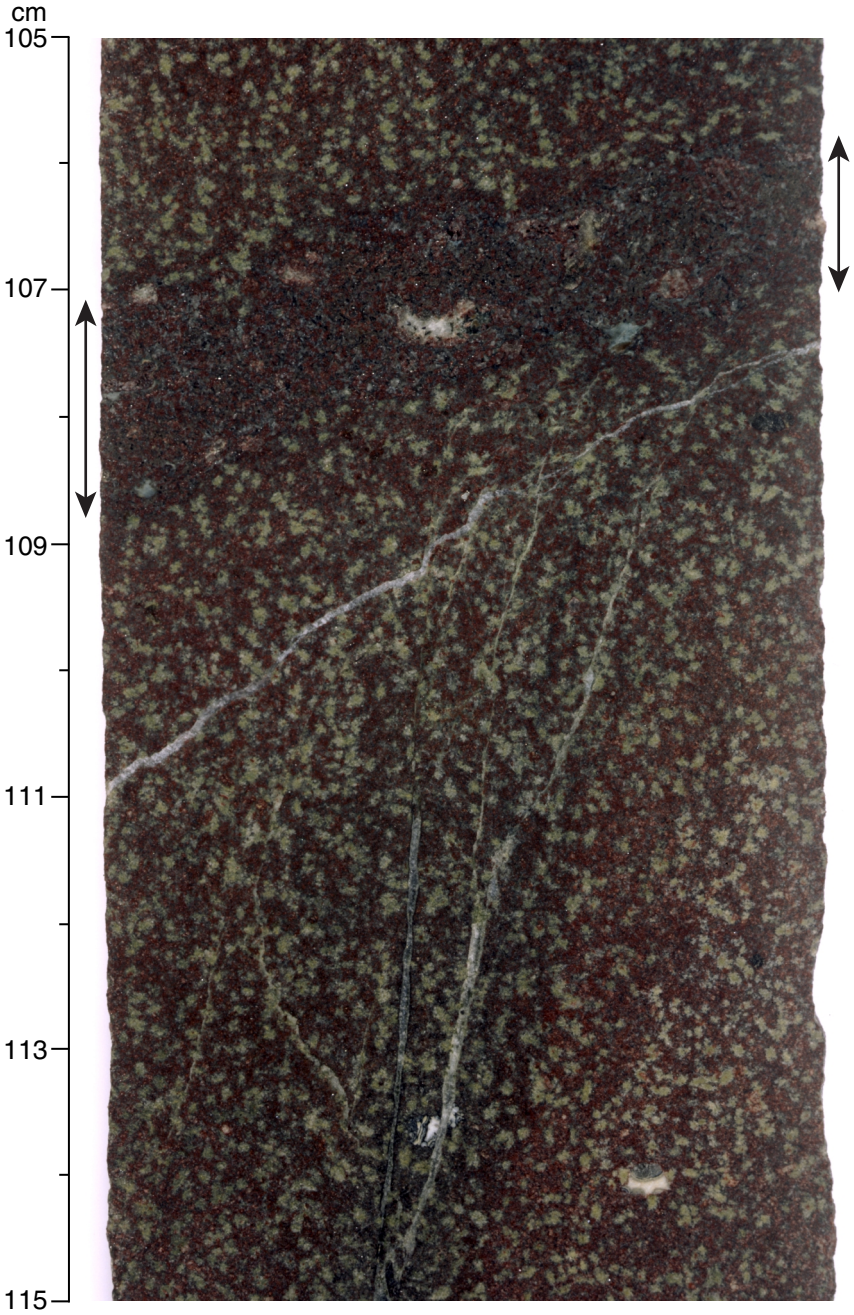

Figure F60. Color close-up photograph of interval 183-1141A-24R-1 (Piece 2H, 85–101 cm). Subvertical quartz + minor calcite vein with multiple alteration halos. Starting from the vein margin, these halos are dark green, light green, dark red, and light red, grading into dark red-gray basalt (Unit 6). The intensity of alteration in these halos decreases with distance from the vein. This complex pattern is crosscut by late calcite vein. Vesicles with colloform textures are also visible.

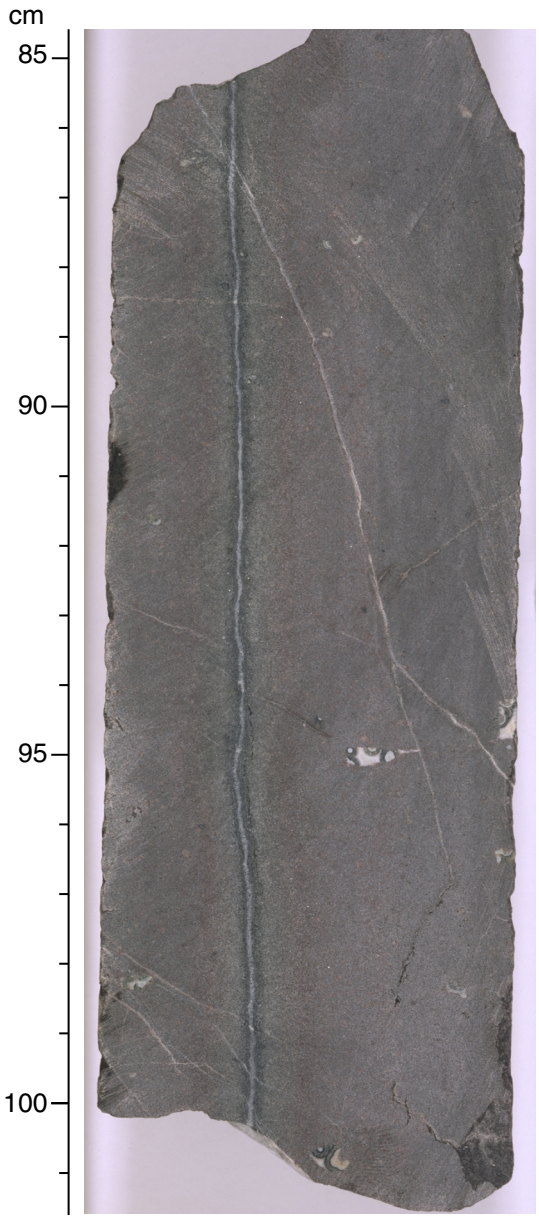

Figure F61. Color close-up photograph of interval 183-1141A-23R-2 (Piece 1, 98–120 cm). Network of calcite + quartz veins in Unit 6 with a dark green alteration halo adjacent to vein representing highly altered basalt. Light green ("bleached") and red alteration halos are found outside the dark green halo and the less altered wall rock. Brecciated wall rock in veins is also visible.

Figure F62. Color close-up photograph of Sample 183-1142A-9R-2, 56–68 cm. Calcite vein with red oxidation halo external to dark green alteration halo representing completely altered basalt (Unit 6). This and similar features look like altered glassy pillow margins, although the continuous mesostasis fabric crosscut by vein indicates that this is probably basalt altered by the veining event.

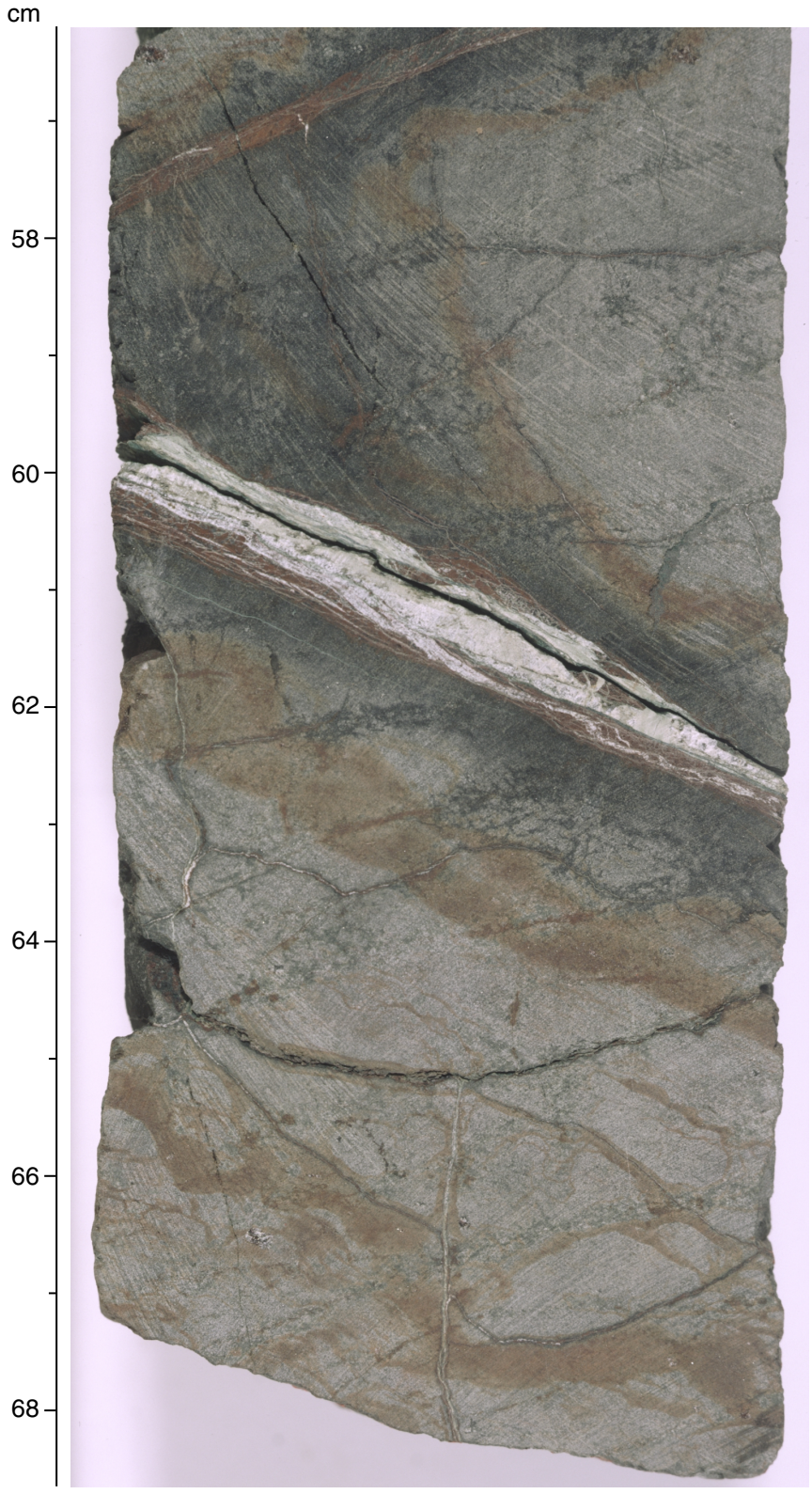

Figure F63. Example of progressive AF demagnetization of a discrete sediment sample from Hole 1141A. The intensity decay curve is plotted on the left, and the directional change is plotted on an orthogonal vector projection on the right. Magnetic directions that tend toward the origin with high median destructive fields are considered reliable. J_0 is the magnetization intensity before AF treatment.

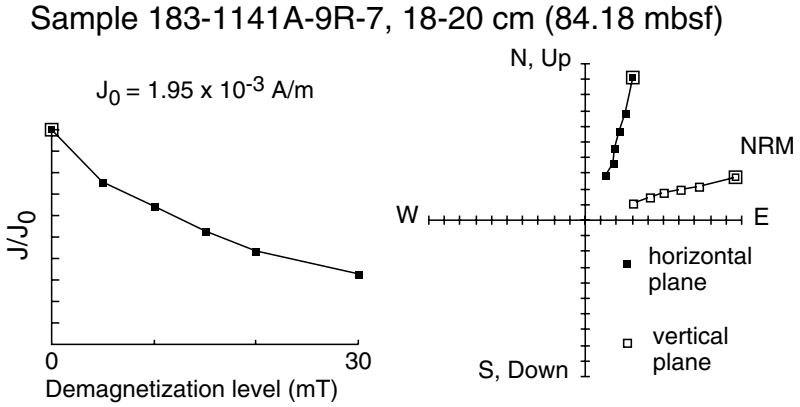

Figure F64. Hole 1141A inclination, intensity of remanent magnetization, and MST susceptibility of sediments vs. depth. Crosses and lines represent remanent magnetization before and after AF demagnetization at 20 mT, respectively. Selected inclination data (see **"Paleomagnetism,"** p. 35) used for polarity interpretations are shown by open circles. Interpreted normal and reversed geomagnetic chrons are shown by black and white rectangles, respectively. Inclinations from discrete samples are shown by solid circles. Lithologic units are shown on the right.

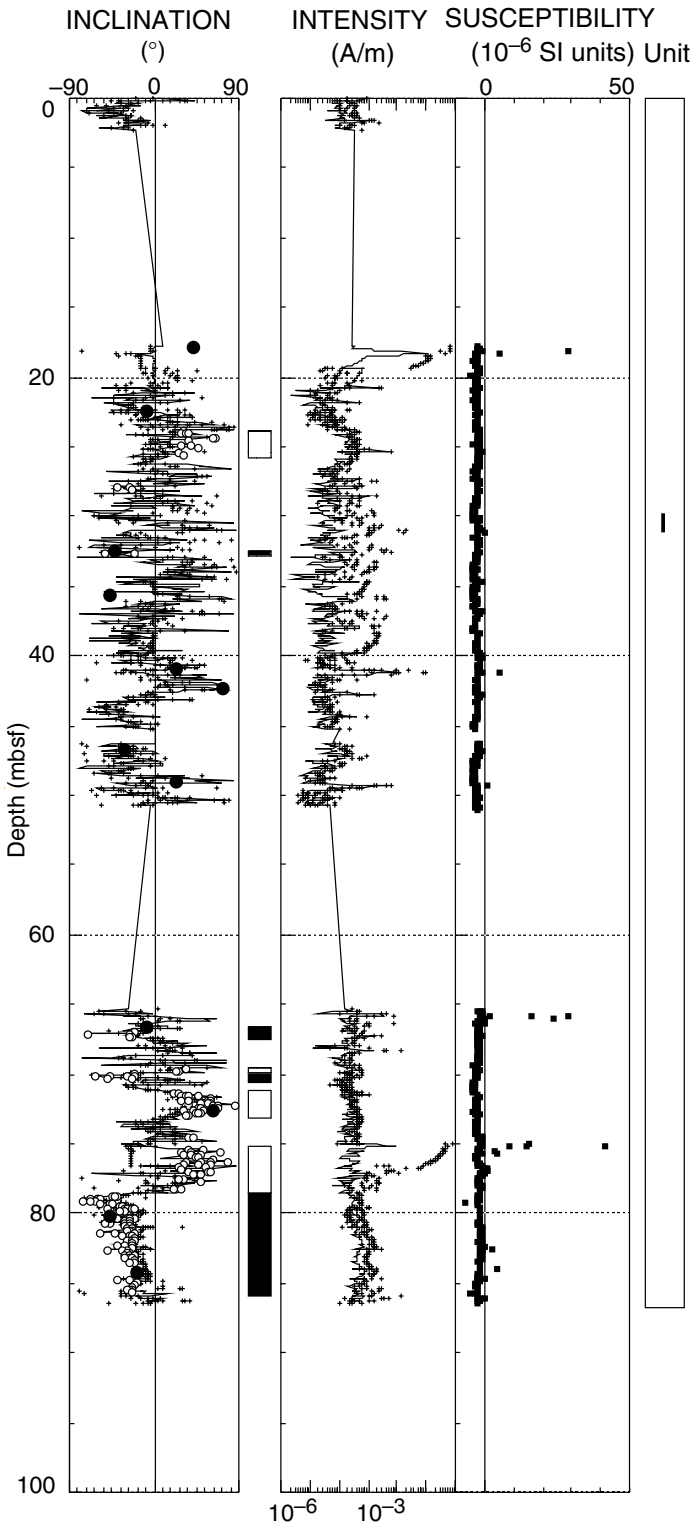

Figure F65. Average NRM intensity and MST susceptibility of each lithologic and basement unit. Large solid circles give the average values for lavas. The horizontal bars show the range between maximum and minimum values in the respective units.

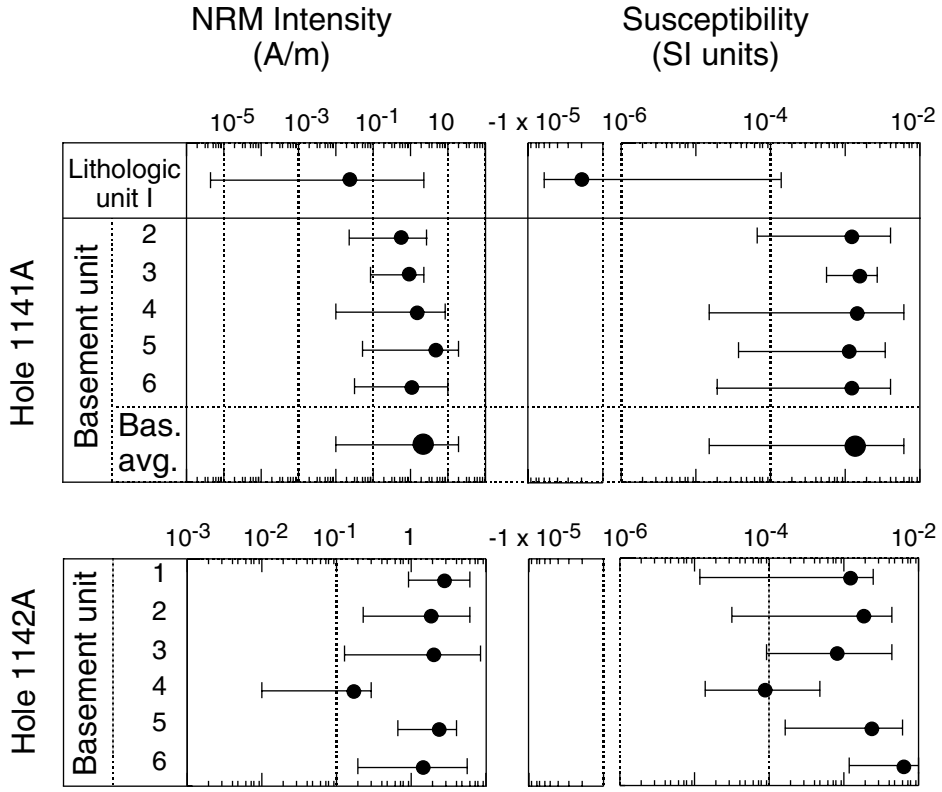

Figure F66. Hole 1141A inclination, intensity of remanent magnetization, and susceptibility of basement rocks vs. depth. Crosses and lines represent remanent magnetization before and after AF demagnetization at 40 mT, respectively. Inclinations of NRM from discrete samples are represented by solid circles. MST, AMST, and discrete-sample susceptibilities are represented by lines, crosses and open circles, respectively. Basement units are shown on the right.

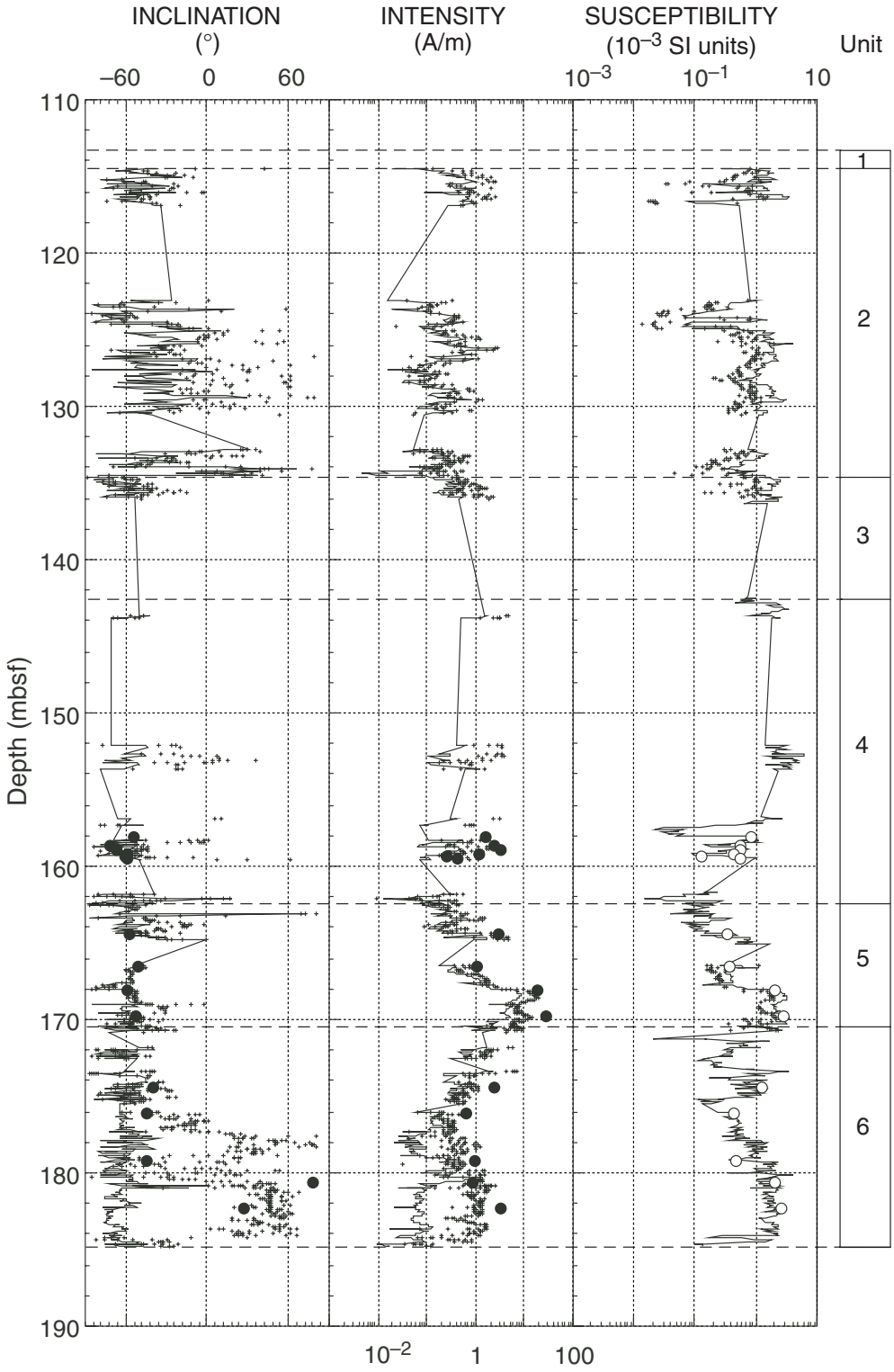

Figure F67. Examples of progressive AF demagnetization of basement archive halves. **A.** Section 183-1141A-22R-2 at 90 cm from basement Unit 6. The magnetization has a MDF of 30 mT and a single-component magnetization. **B.** Section 183-1141A-24R-2 at 77.5 cm from basement Unit 6. The magnetization has a MDF of 8 mT and a two-component magnetization. J_0 is the magnetization intensity before AF treatment.

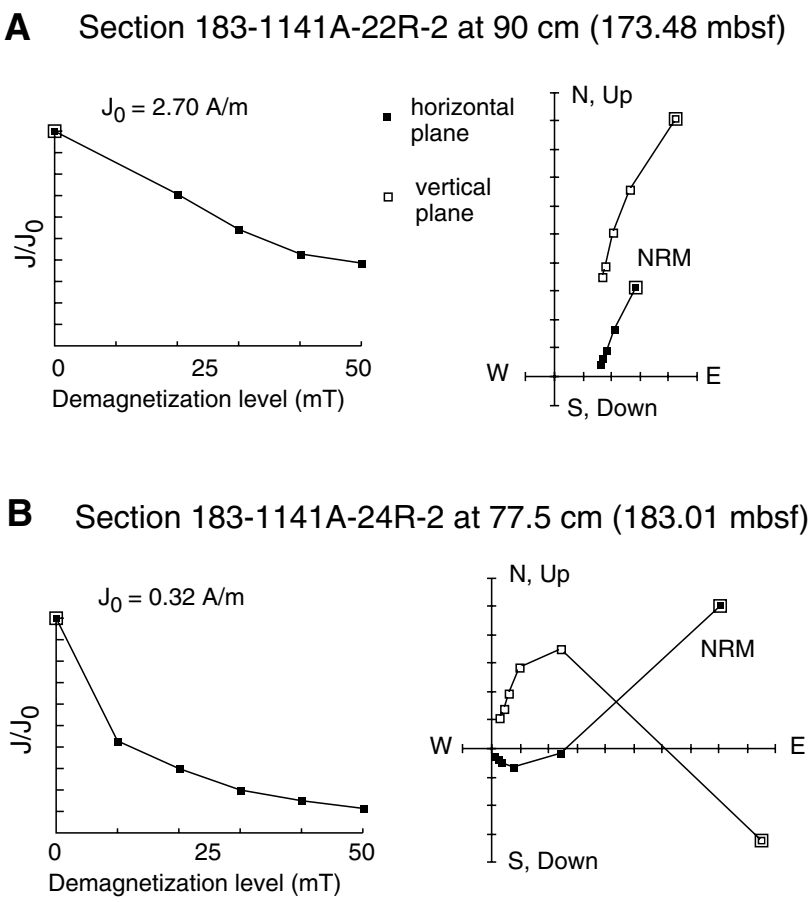

Figure F68. Hole 1142A inclination, intensity of remanent magnetization, and susceptibility of basement rocks vs. depth. Crosses and lines represent remanent magnetization before and after AF demagnetization at 40 mT, respectively. Basement units are shown on the right.

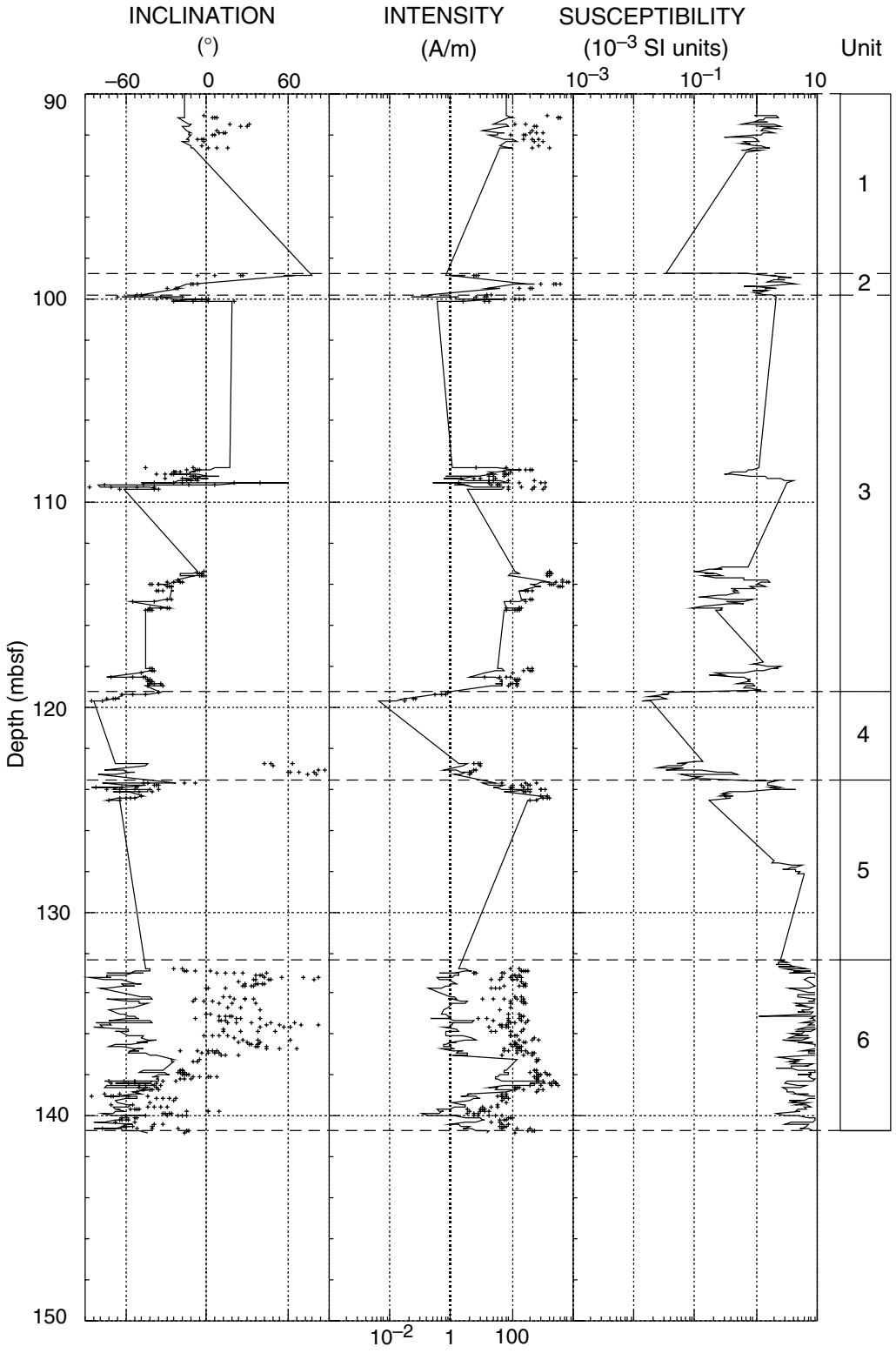

Figure F69. Examples of progressive AF demagnetization up to 50 mT of basement archive halves. **A.** Section 183-1142A-10R-3 at 65 cm from basement Unit 6. The magnetization has a MDF of 15 mT and a single-component magnetization. **B.** Section 183-1142A-5R-2 at 60 cm from basement Unit 3. The magnetization has a very high MDF. J_0 is the magnetization intensity before AF treatment.

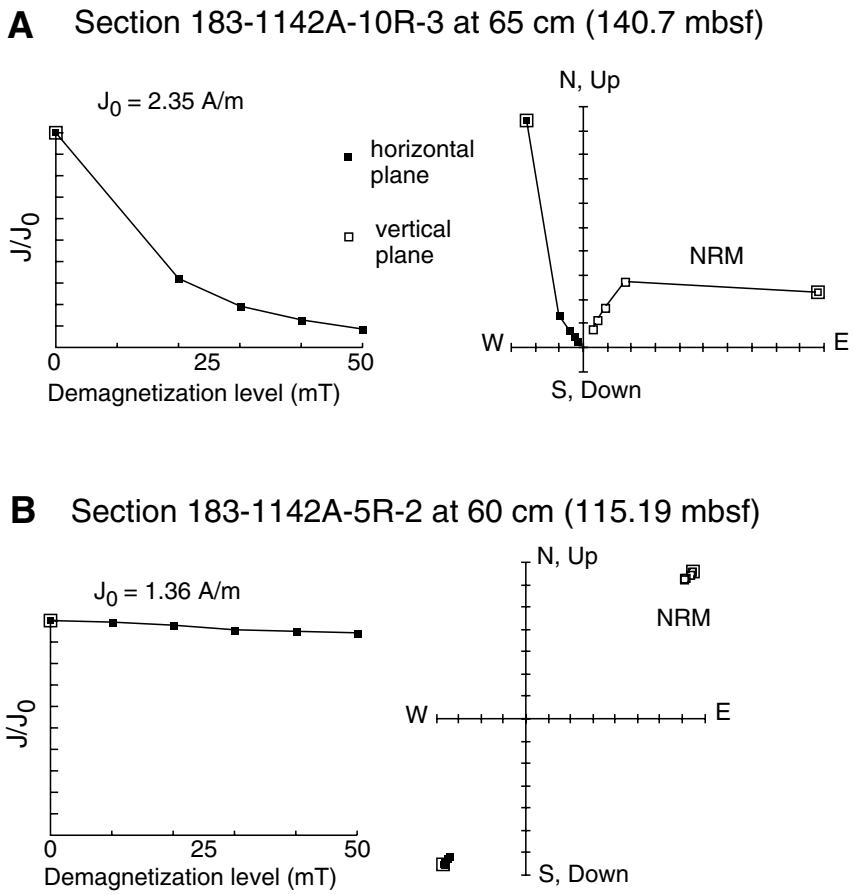

Figure F70. Downhole index properties and compressional wave velocities at Site 1141. Horizontal solid line separates the lithologic Units I and II. Lithologic units are shown on the right. Discrete determinations are (**A**) bulk density; (**B**) grain density; (**C**) porosity; and (**D**) compressional wave velocities.

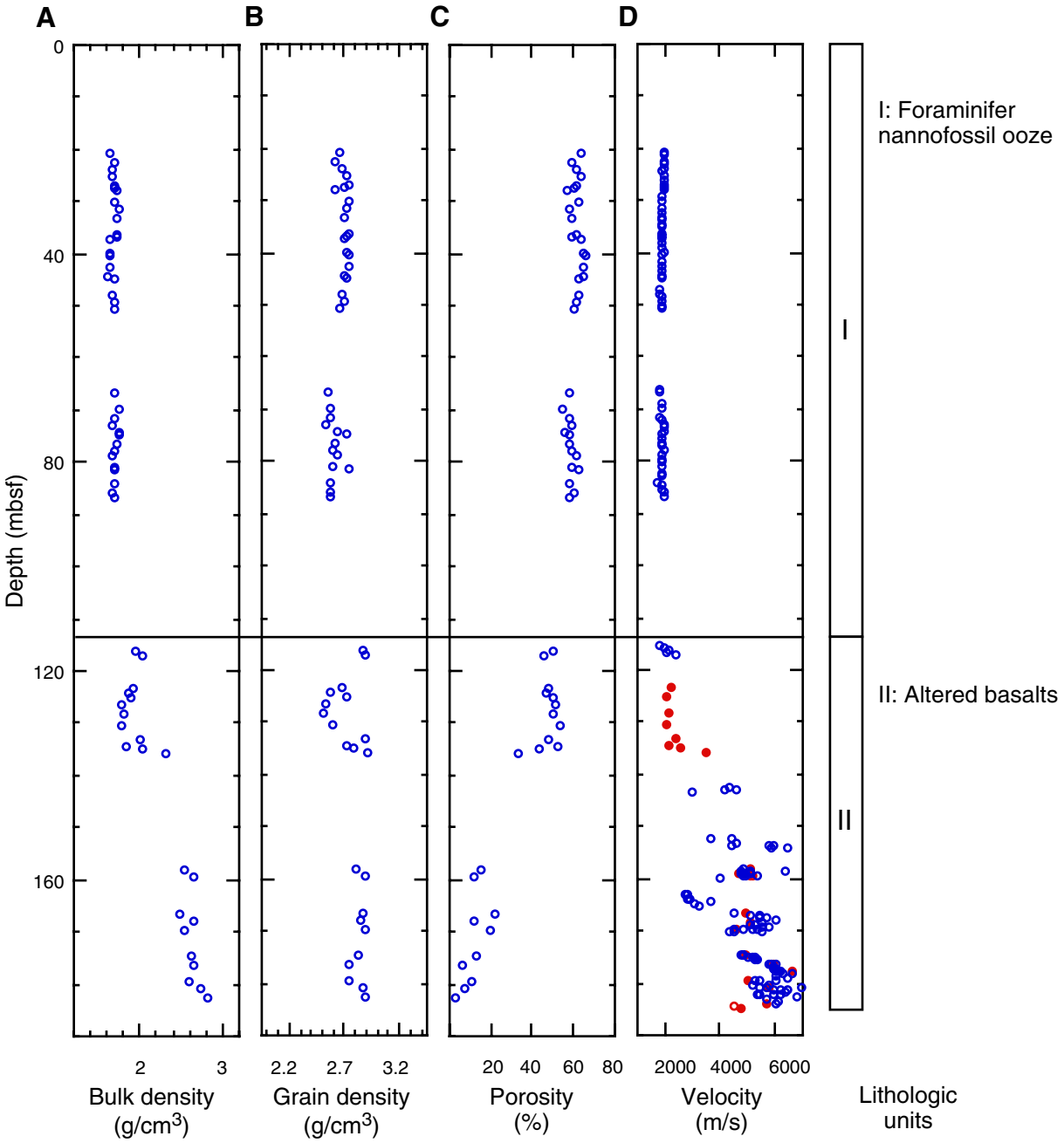

Figure F71. Downhole index properties profiles of basement Units 1–6 in Hole 1141A, including (**A**) magnetic susceptibility, (**B**) natural gamma ray, (**C**) discrete index properties bulk density, (**D**) grain density, (**E**) porosity, and (**F**) discrete velocities. Boxes to the right denote Cores 183-1141A-13 through 1141A-24, adjacent black boxes denote recovery rates, and boxes indicating basement Units 1–6 are followed by a lithologic description. Dashed gray lines indicate boundaries of the basement Units. This figure is a subset of results shown in Figures **F70,** p. 113, and **F72,** p. 115.

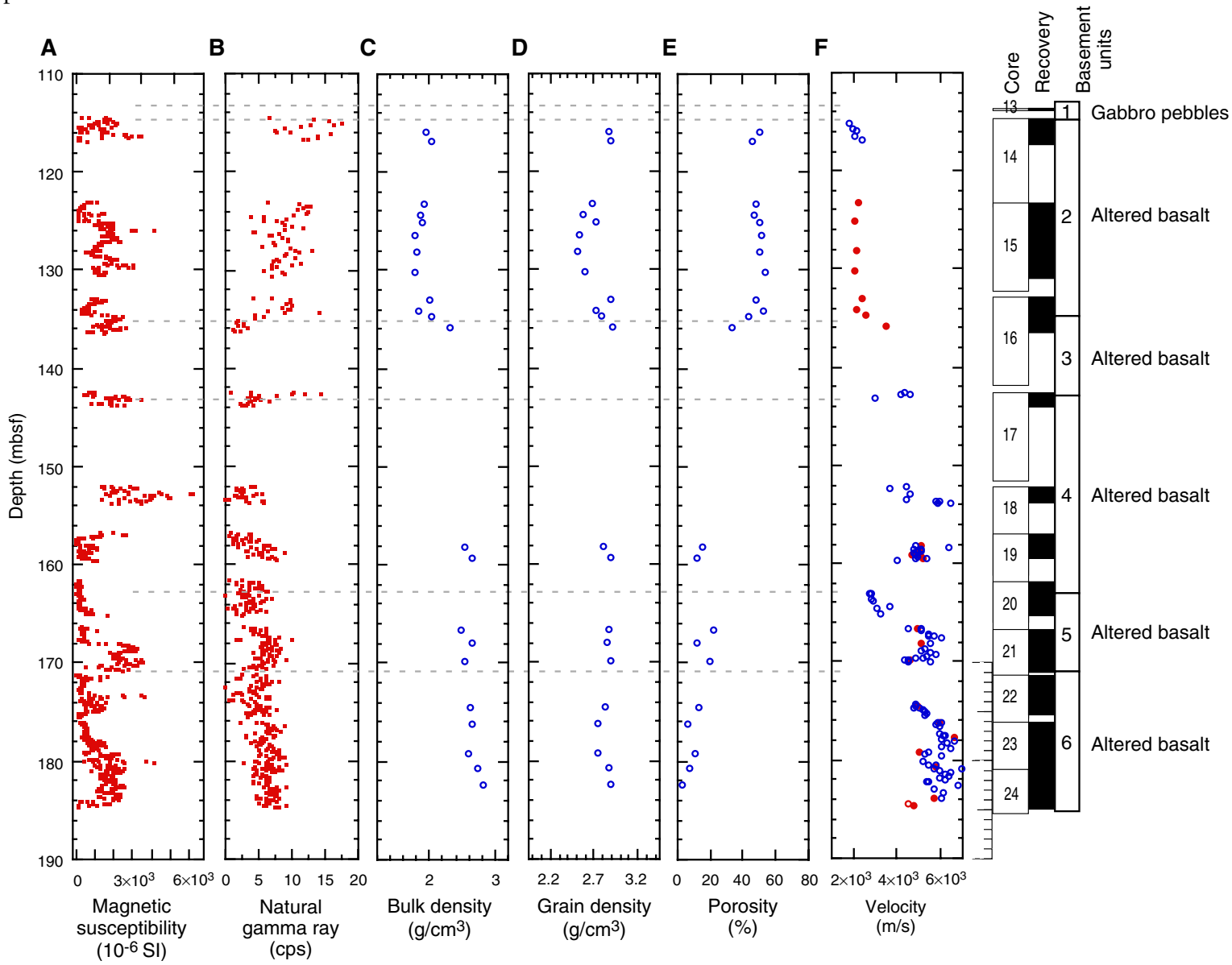

Figure F72. Downhole index properties and compressional wave velocities at Site 1142. Horizontal dashed lines separate basement Units 1–6. Lithologic units are shown on the right. Discrete determinations are (**A**) bulk density, (**B**) grain density, (**C**) porosity, and (**D**) compressional wave velocities.

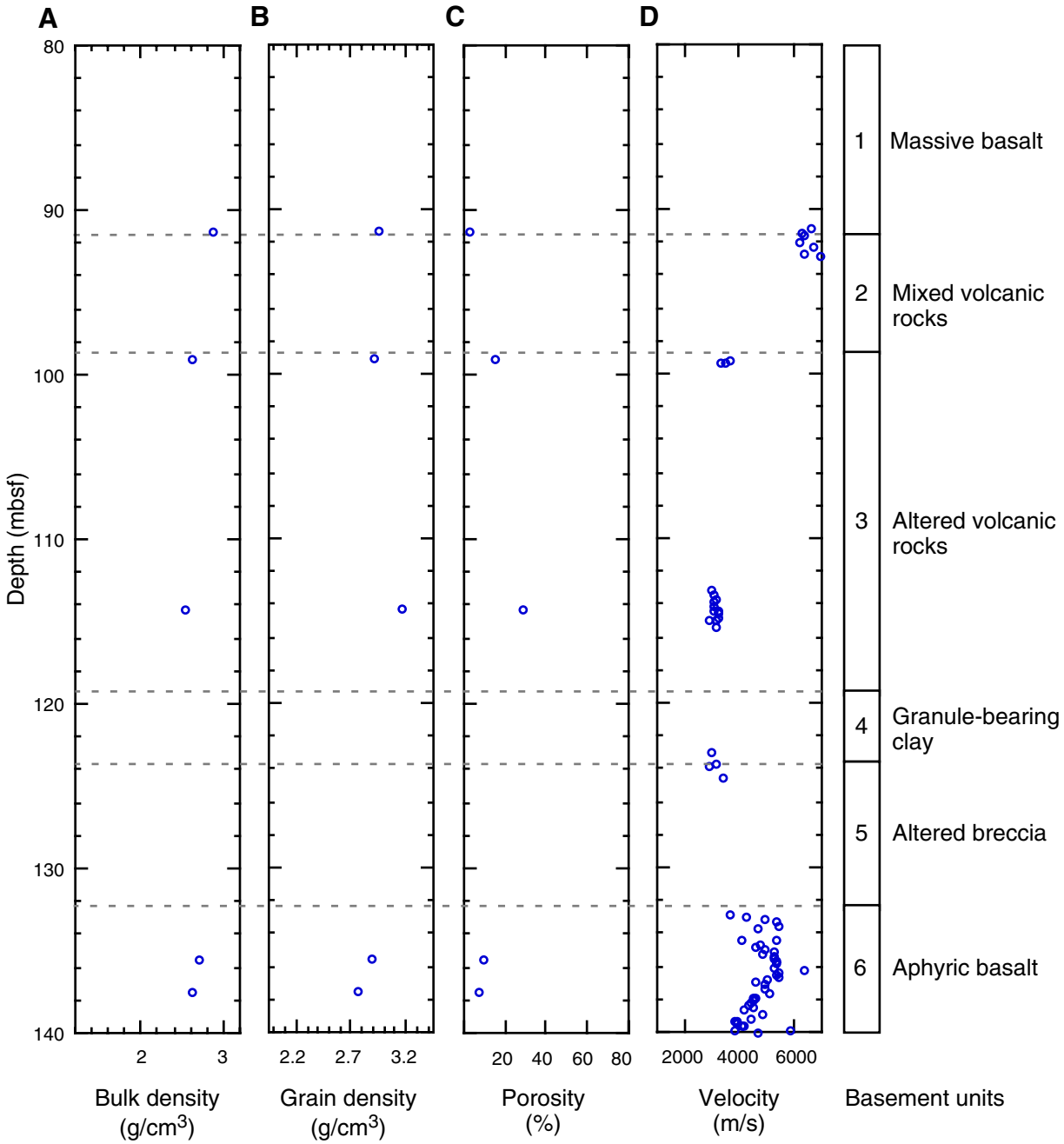

Figure F73. Downhole profiles of MST measurements along with discrete determinations from Hole 1141A, including (**A**) GRAPE bulk density and bulk density derived from discrete samples at Site 1141 (connected with solid line), (**B**) whole-core measurements of magnetic susceptibility, and (**C**) natural gamma ray. Horizontal solid line separates the lithologic units. Lithologic units are shown to the right.

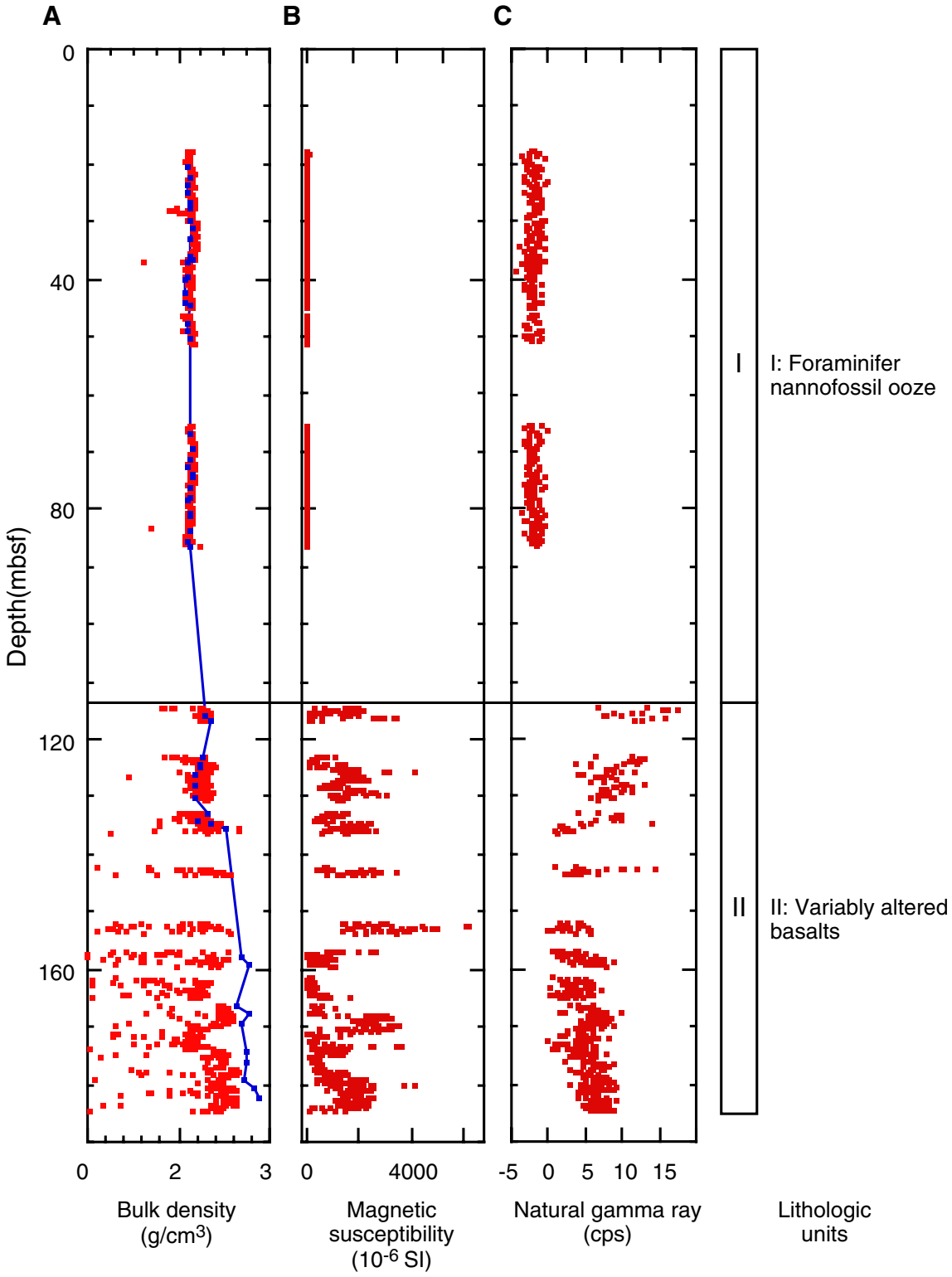

Figure F74. Downhole profiles of MST measurements from Hole 1142A, including (**A**) GRAPE bulk density, (**B**) whole-core measurements of magnetic susceptibility, and (**C**) natural gamma ray. Horizontal dashed lines separate basement Units 1–6. Lithologic units are shown to the right. Note that basalt recovered near the bottom of the washed interval (0–91.0 mbsf) has arbitrarily been plotted at ~80 mbsf.

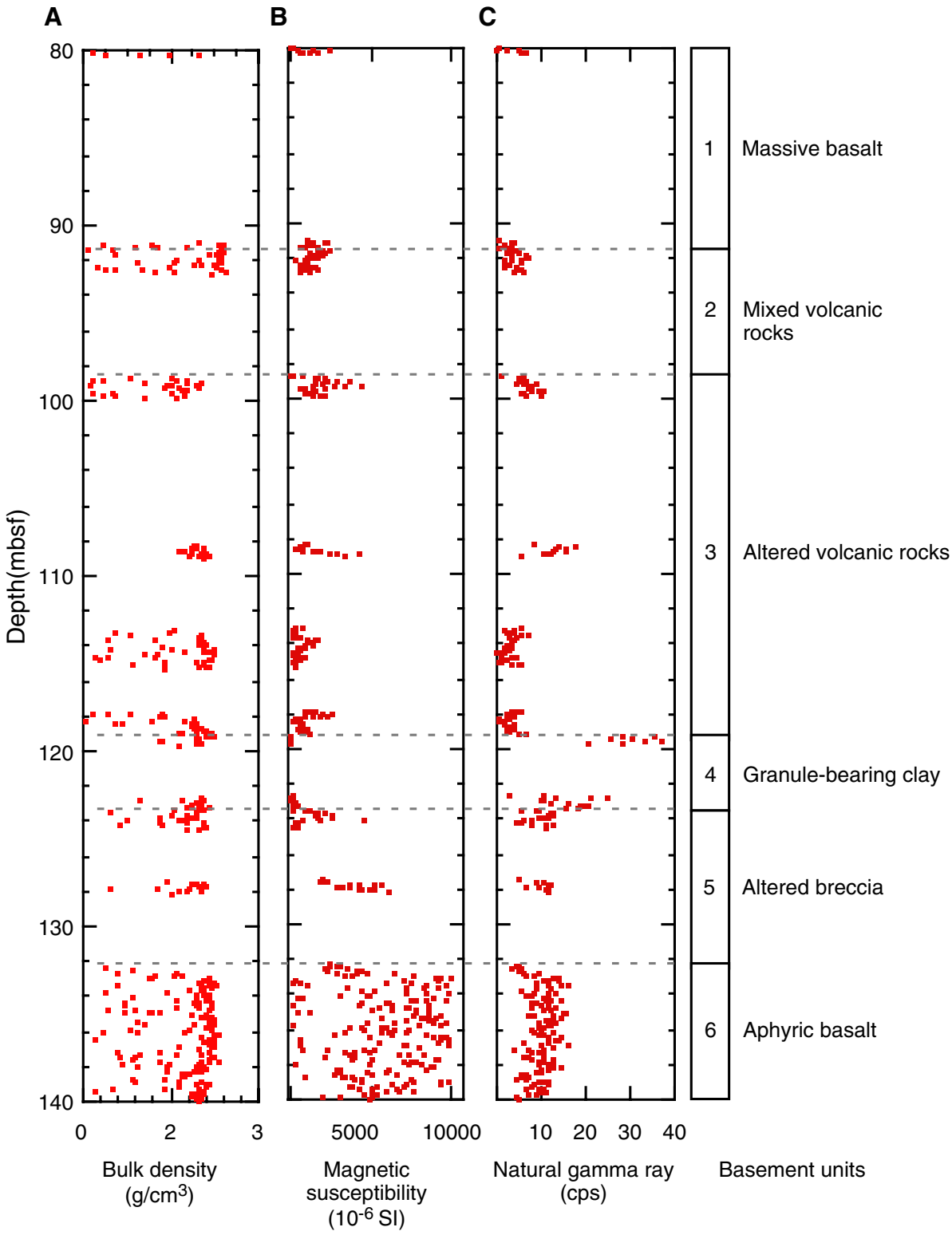

Figure F75. Site 1141 downhole profile of whole-core measurements of thermal conductivity on whole-core soft sediments and on split-core pieces of hard rocks.

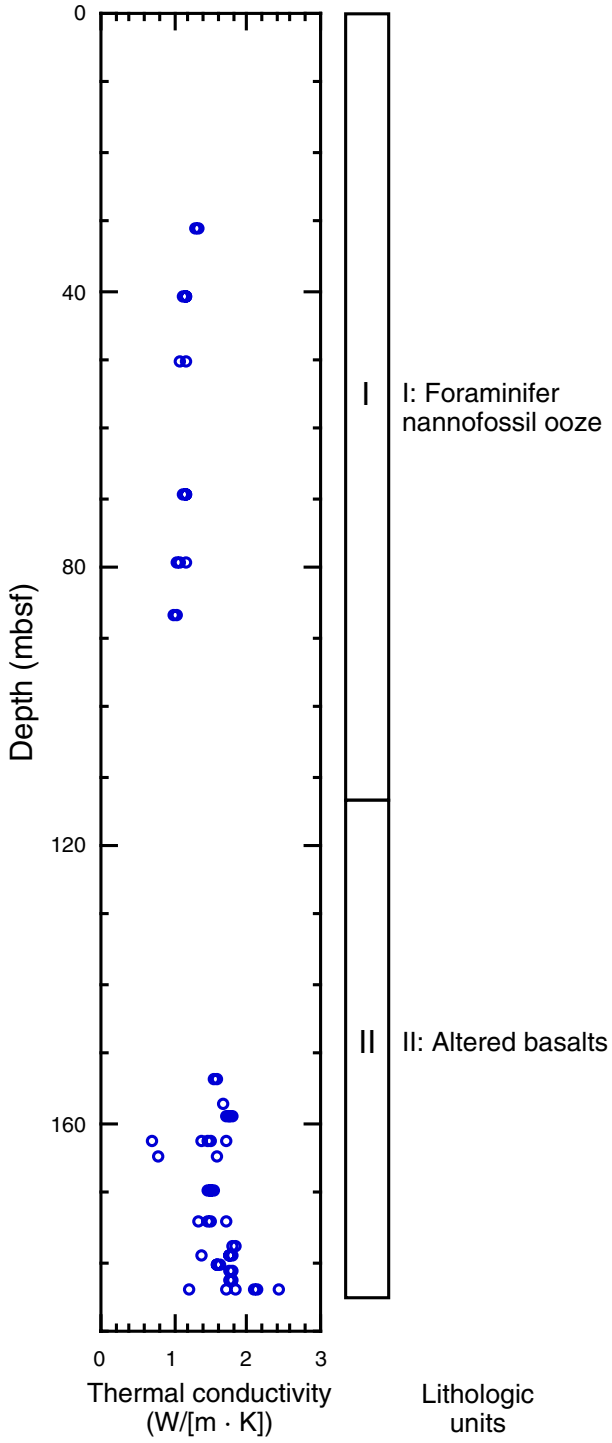

Figure F76. Site 1142 downhole profile on split-core pieces of hard rocks. Lithologic units are shown to the right. Note that basalt recovered near the bottom of the washed interval (0–91.0 mbsf) has arbitrarily been plotted at ~80 mbsf.

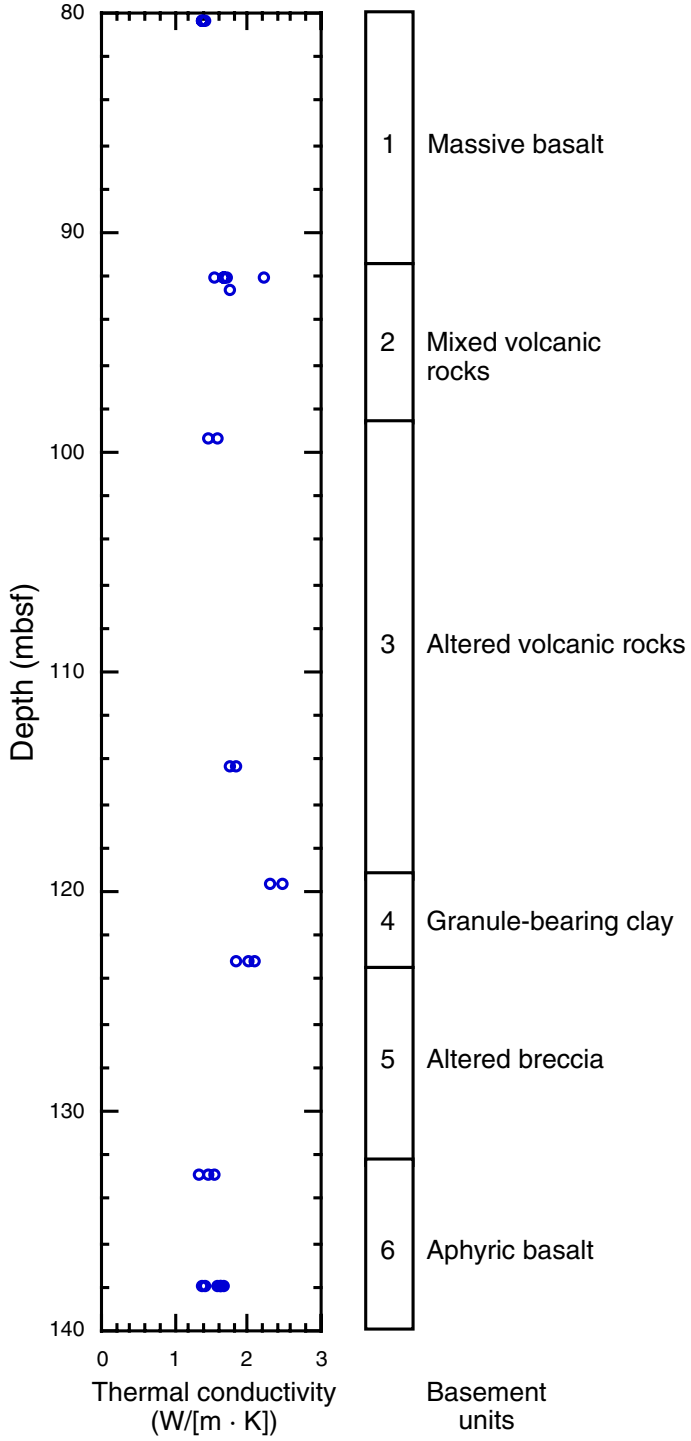

Table T1. Coring summary for Sites 1141 and 1142.

Core	Date (Feb 1999)	Time (UTC)	Depth (mbsf)	Length (m) Cored	Length (m) Recovered	Recovery (%)
183-1141A-						
1R	3	0115	0.0-8.5	8.5	2.43	28.6
2R	3	0200	8.5-17.8	9.3	0.15	1.6
3R	3	0245	17.8-27.4	9.6	9.75	101.6
4R	3	0315	27.4-36.8	9.4	9.82	104.5
5R	3	0340	36.8-46.3	9.5	8.61	90.6
6R	3	0420	46.3-55.8	9.5	5.11	53.8
7R	3	0505	55.8-65.4	9.6	0.00	0.0
8R	3	0540	65.4-75.0	9.6	9.92	103.3
9R	3	0615	75.0-84.6	9.6	9.80	102.1
10R	3	0655	84.6-94.2	9.6	1.99	20.7
11R	3	0740	94.2-103.8	9.6	0.06	0.6
12R	3	0825	103.8-113.5	9.7	0.00	0.0
13R	3	0920	113.5-114.5	1.0	0.02	2.0
14R	3	1040	114.5-123.1	8.6	2.62	30.5
15R	3	1225	123.1-132.8	9.7	7.69	79.3
16R	3	1440	132.8-142.4	9.6	3.46	36.0
17R	3	2200	142.4-152.0	9.6	1.49	15.5
18R	4	0120	152.0-156.8	4.8	1.47	30.6
19R	4	0335	156.8-161.6	4.8	2.32	48.3
20R	4	0620	161.6-166.4	4.8	3.24	67.5
21R	4	0855	166.4-171.2	4.8	4.34	90.4
22R	4	1105	171.2-176.0	4.8	3.62	75.4
23R	4	1535	176.0-180.8	4.8	4.72	98.3
24R	4	1910	180.8-185.6	4.8	4.16	86.7
25R			185.6-185.6	0.0	0.00	NA
			Totals:	185.6	96.79	52.1
183-1142A-						
1W	5	1930	0.0-91.0	91.0	0.24	0.3
2R	5	2335	91.0-98.7	7.7	1.58	20.5
3R	6	0145	98.7-108.3	9.6	1.25	13.0
4R	6	0420	108.3-113.1	4.8	1.09	22.7
5R	6	0705	113.1-117.8	4.7	1.94	41.3
6R	6	0930	117.8-122.6	4.8	1.50	31.3
7R	6	1100	122.6-127.5	4.9	1.72	35.1
8R	6	1235	127.5-132.3	4.8	0.76	15.8
9R	6	1440	132.3-137.1	4.8	4.05	84.4
10R	6	1700	137.1-141.9	4.8	3.41	71.0
			Totals*:	50.9	17.30	34.0

Notes: UTC = Universal Time Coordinated. NA = not applicable. * = totals do not include washed interval (Core 1W) core. This table is also available in **ASCII format.**

Table T2. Expanded coring summary for Holes 1141A and 1142A. (**See table note.** Continued on next two pages.)

Core	Date (Feb 1999)	Time (UTC)	Depth (mbsf)	Length (m) Cored	Length (m) Recovered	Recovery (%)	Section	Length (m) Liner	Length (m) Curated	Section depth (mbsf)	Catwalk samples	Comment
183-1141A-												
1R	3	0115	0.0-8.5	8.5	2.43	28.6						
							1	1.50	1.50	0.00-1.50		
							2	0.77	0.77	1.50-2.27	HS	
							CC(w/2)	0.16	0.16	2.27-2.43	PAL	
								2.43	2.43			
2R	3	0200	8.5-17.8	9.3	0.15	1.6						
							CC(w/CC)	0.15	0.15	8.50-8.65	PAL, HS	
								0.15	0.15			
3R	3	0245	17.8-27.4	9.6	9.75	101.6						
							1	1.50	1.50	17.80-19.3		
							2	1.50	1.50	19.30-20.80		
							3	1.50	1.50	20.80-22.30		
							4	1.50	1.50	22.30-23.80		
							5	1.50	1.50	23.80-25.30	HS	
							6	1.50	1.50	25.30-26.80		
							7	0.59	0.59	26.80-27.39		
							CC(w/7)	0.16	0.16	27.39-27.55	PAL	
								9.75	9.75			
4R	3	0315	27.4-36.8	9.4	9.82	104.5						
							1	1.50	1.20	27.40-28.60		
							2	1.50	1.50	28.60-30.10		
							3	1.50	1.50	30.10-31.60		
							4	1.50	1.50	31.60-33.10		
							5	1.50	1.50	33.10-34.60	HS	
							6	1.50	1.50	34.60-36.10		
							7	0.77	0.77	36.10-36.87		
							CC(NS)	0.05	0.05	36.87-36.92	PAL	All to PAL
								9.82	9.52			
5R	3	0340	36.8-46.3	9.5	8.61	90.6						
							1	1.50	1.50	36.80-38.30		
							2	1.50	1.50	38.30-39.80		
							3	1.50	1.50	39.80-41.30		
							4	1.50	1.50	41.30-42.80		
							5	1.50	1.50	42.80-44.30	HS	
							6	0.96	0.96	44.30-45.26		
							CC(w/6)	0.15	0.15	45.26-45.41	PAL	
								8.61	8.61			
6R	3	0420	46.3-55.8	9.5	5.11	53.8						
							1	1.50	1.50	46.30-47.80		
							2	1.50	1.50	47.80-49.30		
							3	1.50	1.50	49.30-50.80	HS	
							4	0.36	0.36	50.80-51.16		
							CC(w/4)	0.25	0.25	51.16-51.41	PAL	
								5.11	5.11			
7R	3	0505	55.8-65.4	9.6	0.00	0.0						
8R	3	0540	65.4-75.0	9.6	9.92	103.3						
							1	1.50	1.50	65.40-66.90		
							2	1.50	1.50	66.90-68.40		
							3	1.50	1.50	68.40-69.90		
							4	1.50	1.50	69.90-71.40		
							5	1.50	1.50	71.40-72.90		
							6	1.50	1.50	72.90-74.40	HS	
							7	0.65	0.65	74.40-75.05		
							CC(w/7)	0.27	0.27	75.05-75.32	PAL	
								9.92	9.92			
9R	3	0615	75-84.6	9.6	9.80	102.1						
							1	1.50	1.50	75.00-76.50		
							2	1.50	1.50	76.50-78.00		
							3	1.50	1.50	78.00-79.50		
							4	1.50	1.50	79.50-81.00		
							5	1.50	1.50	81.00-82.50	HS	
							6	1.50	1.50	82.50-84.00		
							7	0.62	0.62	84.00-84.62		
							CC(w/7)	0.18	0.18	84.62-84.8	PAL	
								9.80	9.80			

Table T2 (continued).

Core	Date (Feb 1999)	Time (UTC)	Depth (mbsf)	Length (m) Cored	Length (m) Recovered	Recovery (%)	Section	Length (m) Liner	Length (m) Curated	Section depth (mbsf)	Catwalk samples	Comment
10R	3	0655	84.6-94.2	9.6	1.99	20.7						
							1	1.50	1.50	84.60-86.10		
							2	0.44	0.44	86.10-86.54	HS	
							CC(NS)	0.05	0.05	86.54-86.59	PAL	All to PAL
								1.99	1.99			
11R	3	0740	94.2-103.8	9.6	0.06	0.6						
							CC(w/CC)	0.06	0.06	94.20-94.26		
								0.06	0.06			
12R	3	0825	103.8-113.5	9.7	0.00	0.0						
13R	3	0920	113.5-114.5	1.0	0.02	2.0						
							1	0.02	0.04	113.50-113.54		
								0.02	0.04			
14R	3	1040	114.5-123.1	8.6	2.62	30.5						
							1	1.50	1.50	114.50-116.00		
							2	0.90	0.90	116.00-116.90	HS	
							CC(w/2)	0.22	0.22	116.90-117.12	PAL	
								2.62	2.62			
15R	3	1225	123.1-132.8	9.7	7.69	79.3						
							1	1.50	1.50	123.10-124.60		
							2	1.50	1.50	124.60-126.10		
							3	1.50	1.50	126.10-127.60		
							4	1.50	1.50	127.60-129.10	HS	
							5	1.48	1.48	129.10-130.58		
							CC(w/CC)	0.21	0.21	130.58-130.79	PAL	
								7.69	7.69			
16R	3	1440	132.8-142.4	9.6	3.46	36.0						
							1	1.50	1.50	132.80-134.30		
							2	1.00	1.00	134.30-135.30	HS	
							3	0.71	0.71	135.30-136.01		
							CC(w/3)	0.25	0.45	136.01-136.46		Crushed liner
								3.46	3.66			
17R	3	2200	142.4-152.0	9.6	1.49	15.5						
							1	1.17	1.17	142.40-143.57		
							CC(w/1)	0.32	0.32	143.57-143.89		
								1.49	1.49			
18R	4	0120	152.0-156.8	4.8	1.47	30.6						
							1	1.47	1.50	152.00-153.50		
							2	0.00	0.32	153.50-153.82		
								1.47	1.82			
19R	4	0335	156.8-161.6	4.8	2.32	48.3						
							1	0.85	1.48	156.80-158.28		
							2	1.47	1.33	158.28-159.61		
								2.32	2.81			
20R	4	0620	161.6-166.4	4.8	3.24	67.5						
							1	1.44	1.46	161.60-163.06		
							2	1.50	1.47	163.06-164.53		
							3	0.00	0.67	164.53-165.20		
							CC(w/3)	0.30	0.30	165.20-165.50		
								3.24	3.90			
21R	4	0855	166.4-171.2	4.8	4.34	90.4						
							1	1.27	1.31	166.40-167.71		
							2	1.30	1.33	167.71-169.04		
							3	1.44	1.44	169.04-170.48		
							4	0.33	0.33	170.48-170.81		
								4.34	4.41			
22R	4	1105	171.2-176	4.8	3.62	75.4						
							1	0.76	1.38	171.20-172.58		
							2	1.50	1.50	172.58-174.08		
							3	1.36	1.50	174.08-175.58		
								3.62	4.38			
23R	4	1535	176.0-180.8	4.8	4.72	98.3						
							1	0.37	1.32	176.00-177.32		
							2	1.44	1.52	177.32-178.84		
							3	1.46	1.44	178.84-180.28		
							4	1.45	0.73	180.28-181.01		
								4.72	5.01			

Table T2 (continued).

Core	Date (Feb 1999)	Time (UTC)	Depth (mbsf)	Length (m) Cored	Length (m) Recovered	Recovery (%)	Section	Length (m) Liner	Length (m) Curated	Section depth (mbsf)	Catwalk samples	Comment
24R	4	1910	180.8-185.6	4.8	4.16	86.7						
							1	1.17	1.44	180.80-182.24		
							2	1.45	1.45	182.24-183.69		
							3	1.36	1.12	183.69-184.81		
							CC(w/CC)	0.18	0.18	184.81-184.99		
								4.16	4.19			
25R			185.6-185.6	0.0	0.00	NA						
			Totals:	185.6	96.79	52.1						
183-1142A-												
1W	5	1930	0.0-91	91	0.24	0.3						
							1	0.24	0.42	0.00-0.42		
								0.24	0.42			
2R	5	2335	91.0-98.7	7.7	1.58	20.5						
							1	0.08	1.49	91.00-92.49		
							2	1.50	0.36	92.49-92.85		
								1.58	1.85			
3R	6	0145	98.7-108.3	9.6	1.25	13.0						
							1	0.98	1.24	98.70-99.94		
							CC(w/1)	0.27	0.27	99.94-100.21		
								1.25	1.51			
4R	6	0420	108.3-113.1	4.8	1.09	22.7						
							1	0.74	0.74	108.30-109.04		
							CC(w/1)	0.35	0.35	109.04-109.39		
								1.09	1.09			
5R	6	0705	113.1-117.8	4.7	1.94	41.3						
							1	0.47	1.49	113.10-114.59		
							2	1.47	0.75	114.59-115.34		
								1.94	2.24			
6R	6	0930	117.8-122.6	4.8	1.50	31.3						
							1	1.50	1.46	117.80-119.26		
							2	0.00	0.49	119.26-119.75		
								1.50	1.95			
7R	6	1100	122.6-127.5	4.9	1.72	35.1						
							1	1.25	1.50	122.60-124.10		
							2	0.47	0.48	124.10-124.58		
								1.72	1.98			
8R	6	1235	127.5-132.3	4.8	0.76	15.8						
							1	0.76	0.68	127.50-128.18		
								0.76	0.68			
9R	6	1440	132.3-137.1	4.8	4.05	84.4						
							1	0.15	1.50	132.30-133.80		
							2	1.40	1.43	133.80-135.23		
							3	1.50	1.50	135.23-136.73		
							4	1.00	0.31	136.73-137.04		
								4.05	4.74			
10R	6	1700	137.1-141.9	4.8	3.41	71						
							1	0.51	1.47	137.10-138.57		
							2	1.44	1.48	138.57-140.05		
							3	1.46	0.75	140.05-140.80		
								3.41	3.70			
			Totals:	50.9	17.30	34.0						

Notes: UTC = Universal Time Coordinated. CC = core catcher (number in parenthesis indicates which section the core catcher is stored with), NS = all of the core catcher was used for paleontology sample. HS = headspace gas sample, PAL = paleontology sample, NA = not applicable. Totals do not include washed interval (Core 1W). This table is also available in **ASCII format.**

Table T3. Summary of lithologic units at Site 1141.

Lithologic unit	Basement units	Core interval	Depth (mbsf)	Thickness (m)	Age	Lithology	Interpretation
I		1R-1, 0 cm, to 11R-CC, 6 cm	0.00-103.80	103.80	Pleistocene to late or middle Eocene	Foraminifer nannofossil ooze	Pelagically deposited sediment in bathyal depths with localized redeposition by turbidity currents and debris flows, or possibly bottom-current reworking
II	1–6	13R-1, 0 cm, to 24R-CC, 18 cm	113.50-185.60	72.1	late Eocene or older	Altered basalts and basalts	Basalt flows

Table T4. X-ray diffraction results and carbonate contents expressed as $CaCO_3$ for Hole 1141A.

Core, section, interval (cm)	Depth (mbsf)	Minerals	$CaCO_3$ (wt%)
Unit I			
183-1141A-			
1R-1, 89	0.89	Calcite, aragonite (1%)	95
2R-CC, 2	8.52	Calcite	96
3R-1, 90	18.70	Calcite	96
5R-1, 90	37.70	Calcite	96
6R-1, 90	47.20	Calcite	95
9R-1, 90	75.90	Calcite	96

Note: See **"Organic and Inorganic Geochemistry,"** p. 41.

Table T5. Site 1141 basement units.

Basement unit	Rock type	Top (cm)	Curated depth (mbsf)	Curated thickness* (m)	Recovery (m)
		183-1141A-			
1	Gabbro pebbles	13R-1, 0	113.50	1.00	0.02
2	Altered basalt?	14R-1, 0	114.50	19.99	7.36
3	Altered basalt?	16R-2, 19	134.49	8.26	2.29
4	Basalt	17R-1, 35	142.75	19.64	5.92
5	Basalt	20R-1, 79	162.39	7.95	6.37
6	Basalt	21R-3, 130	170.34	15.26	13.75

Note: * = thicknesses from curated depths. Actual unit thicknesses may be ±5 m of these values.

Table T6. Site 1142 basement units.

Basement unit	Rock type	Top (cm)	Curated depth (mbsf)	Curated thickness* (m)	Recovery (m)
		183-1142A-			
1	Massive basalt	1W-1, 11	NA	NA	1.91
2	Mixed volcanic rocks	3R-1, 0	98.70	1.24	1.03
3A	Disturbed volcanic rock	3R-CC, 0	99.94	13.16	1.31
3B	Lava and volcanic breccia	5R-1, 0	113.10	4.70	1.91
3C	Lava and volcanic breccia	6R-1, 0	117.80	1.46	1.31
4	Granule-bearing clay	6R-2, 0	119.26	4.26	1.21
5	Volcanic breccia	7R-1, 92	123.52	8.78	0.87
6	Pillow? basalt	9R-1, 0	132.30	9.60	8.27

Notes: * = thicknesses from curated depths. Actual unit thicknesses may be ±5 m of these values. NA = no curated position for material in the wash core.

Table T7. Vesicle distribution in Unit 2 at Site 1141.

Core, section, interval (cm)	Vesicularity (%)	Size range (mm)	Shape
183-1141A-			
14R-1, 6-10	0	>1	
14R-1, 91-95	3	0.4-4	Round and spherical
14R-1, 122-138	10	0.6-2	Irregular to spherical, rounded
14R-1, 10-20	15	0.5-4	Irregular to spherical, rounded
14R-2, 29-35	25	0.2-15	Irregular, subangular
14R-2, 54-56	15	1-10	Equant to elongate, angular
14R-2, 57-62	3	0.1-2	Spherical to irregular, rounded
14R-2, 80-90	7	0.5-22	Equant to elongate, rounded to subangular
14R-CC, 0-22	3	0.1-2	Spherical to irregular, rounded
15R-1, 8-16	10	1-4	Rounded, near spherical
16R-1, 14-20	5	0.5-6	Irregular, subangular
16R-1, 105-112	0	<1	
16R-2, 0-19	10-25	0.3-6	Moderately spherical, rounded

Table T8. Summary of petrographic characteristics of Sites 1141 and 1142 basement units.

Unit	Core, section, piece, interval (cm)	Type of basalt	Phenocrysts (%)		Groundmass mineralogy (%)					Groundmass texture	Alteration
			Plag	Ol	Plag	Cpx	Ol	Opq	Ms		
	183-1141A-										
2	16R-2, 5-8	Sparsely plagioclase phyric	1		50	30		2	18	Intersertal to intergranular	Moderate
3	16R-CC (Piece 3B, 37-38)	Aphyric basalt	<1		50	30		2	18	Intersertal to intergranular	Moderate
	17R-1 (Piece 6, 26-29)	Sparsely plagioclase phyric	2		65	15		3	15	Intersertal to intergranular	High
4	17R-CC (Piece 1, 24-27)	Sparsely plagioclase phyric	2		50	30		3	15	Intersertal to intergranular	High
	18R-1 (Piece 18, 146-148)	Sparsely plagioclase phyric	2		50	30	10	5	5	Intersertal to intergranular	Moderate
	19R-2 (Piece 2, 13-14)	Moderately olivine phyric	<1	5	45	35		3	10	Intersertal to intergranular	High
5	21R-2 (Piece 1D, 126-128)	Sparsely olivine phyric		2	50	40				Ophitic to intersertal	Moderate
	21R-3 (Piece 1C, 93-95)	Vesicular olivine phyric	<1	2	40	40	3	10		Intersertal to intergranular	High
6	22R-2 (Piece 3A, 79-81)	Vesicular olivine phyric		3	60	10		3	20	Trachytic	Very high
	22R-3 (Piece 7, 100-101)	Sparsely olivine phyric	<1	2	40	30	10	3	15	Subophitic	High
	22R-3 (Piece 12, 146-148)	Sparsely olivine phyric		2	40	30	10	3	15	Subophitic to intergranular	High
	23R-1 (Piece 2B, 46-49)	Moderately olivine phyric		3	45	25	10	3	12	Subophitic to intergranular	High
	23R-1 (Piece 1C, 106-109)	Sparsely olivine phyric		2	40	30	10	3	15	Subophitic	High
	23R-2 (Piece 5C, 61-63)	Moderately olivine phyric		4	50	40	5	2		Subophitic	Slight
	23R-2 (Piece 11A, 107-108)	Sparsely olivine phyric	<1	2	40	40	10	3	5	Ophitic	Slight
	24R-1 (Piece 1A, 6-8)	Moderately olivine phyric		3	50	30	1	4	10	Intersertal to intergranular	Slight
	24R-2 (Piece 2A, 36-37)	Sparsely olivine phyric	<1	2	50	30		3	15	Intersertal to intergranular	Moderate
	183-1142A-										
1	2R-1 (Piece 9, 50-53)	Sparsely olivine phyric	<1	2	40	50		3	5	Intergranular	Slight
3	6R-1 (Piece 3, 11-14)	Moderately plagioclase phyric	3	<1	45	45		4	5	Intergranular	Moderate
6	9R-3 (Piece 9, 108-111)	Aphyric basalt			50	45		5	5	Trachytic, aphanitic	Moderate
	9R-4 (Piece 1, 3-7)	Glassy pillow margin	2	0	45	25		5	25	Trachytic, glassy	Very high
	10R-1 (Piece 5B, 37-40)	Aphyric basalt			60	20		4	15	Intergranular	High

Note: Plag = plagioclase, Cpx = clinopyroxene, Ol = olivine, Opq = opaque, Ms = mesostasis.

Table T9. Major and trace element XRF* data and normative mineralogy for Site 1141 and 1142 basalts.

Hole:	1141A	1141A	1141A	1141A	1141A	1141A	1141A	1141A	1141A	1142A	1142A
Core, section:	17R-1	18R-1	19R-2	21R-2	22R-3	22R-3	23R-1	24R-1	24R-2	2R-1	10R-1
Interval (cm):	27-31	142-150	8-10	129-132	94-96	142-146	46-49	6-8	34-36	50-53	37-40
Unit:	4	4	4	5	6	6	6	6	6	1	6
SiO_2	48.2	47.7	48.5	47.2	49.7	51.6	45.3	47.5	47.7	46.7	53.9
TiO_2	4.31	3.13	2.82	2.77	3.14	3.22	3.08	2.75	2.74	2.77	2.46
Al_2O_3	20.1	16.3	17.2	15.9	17.9	17.5	18.0	16.7	16.3	16.2	16.7
Fe_2O_3	9.85	12.9	9.64	12.3	11.8	10.8	11.9	11.7	11.8	11.9	9.89
MnO	0.20	0.18	0.14	0.11	0.18	0.17	0.20	0.16	0.16	0.16	0.29
MgO	3.61	5.05	4.93	6.12	3.19	3.16	4.11	6.43	6.45	6.56	2.77
CaO	6.99	10.4	12.4	11.4	9.43	8.77	12.9	10.9	10.9	11.3	8.56
Na_2O	4.03	2.91	2.93	2.93	3.11	3.05	3.08	2.74	2.71	2.69	3.50
K_2O	2.15	0.61	0.87	0.74	0.91	0.86	0.84	0.79	0.76	0.69	0.96
P_2O_5	0.79	0.65	0.49	0.46	0.55	0.55	0.53	0.48	0.47	0.48	0.44
Total:	100.23	99.83	99.93	99.93	99.90	99.68	99.92	100.15	99.99	99.45	99.50
Mg#	0.45	0.47	0.53	0.53	0.38	0.39	0.44	0.55	0.55	0.55	0.39
Nb	46.4	30.6	27.6	25.0	27.4	28.9	25.6	25.8	25.8	26.3	16.1
Zr	342	287	237	204	238	258	231	233	229	233	220
Y	35.4	33.9	28.7	28.6	30.2	29.1	28.7	29.3	28.6	29.3	38.2
Sr	852	520	576	503	454	470	473	429	427	431	201
Rb	29.6	11.7	12.2	5.7	7.7	6.2	5.7	7.7	7.7	13.0	16.2
Th	2	1	1	2	1	1	1	1	2	1	4
Pb	3	3	3	3	2	3	3	3	3	3	5
Ga	24	20	19	19	19	19	19	19	18	19	22
Zn	305	147	132	130	104	112	117	117	116	115	141
Ni	160	127	131	201	128	124	171	165	170	184	34
Cr	125	127	292	300	335	336	344	296	305	303	21
V	280	274	241	242	285	288	269	256	261	263	370
Ba	580	275	383	288	313	330	314	319	320	282	346
La	35	31	26	26	27	24	25	26	25	25	25
Ce	65	61	51	48	50	47	46	45	46	49	42
Q	0.0	0.0	0.0	0.0	3.2	7.1	0.0	0.0	0.0	0.0	7.8
Or	12.7	3.6	5.2	4.4	5.4	5.1	5.0	4.7	4.5	4.1	5.7
Ab	34.2	24.9	25.0	25.0	26.6	26.1	17.2	23.4	23.1	23.1	30.0
An	29.6	29.9	31.4	28.3	32.4	31.9	33.2	31.1	30.4	30.6	27.4
Cor	0.4	0.0	0.0	0.0	0.0	0.0	0.0	0.0	0.0	0.0	0.0
Ne	0.0	0.0	0.0	0.0	0.0	0.0	4.9	0.0	0.0	0.0	0.0
Lc	0.0	0.0	0.0	0.0	0.0	0.0	0.0	0.0	0.0	0.0	0.0
Ac	0.0	0.0	0.0	0.0	0.0	0.0	0.0	0.0	0.0	0.0	0.0
Ns	0.0	0.0	0.0	0.0	0.0	0.0	0.0	0.0	0.0	0.0	0.0
Wo (Di)	0.0	7.5	11.5	10.8	4.7	3.5	11.7	8.4	8.7	9.7	5.3
En (Di)	0.0	4.0	7.0	6.2	2.2	1.8	6.0	5.0	5.2	5.8	2.4
Fs (Di	0.0	3.3	3.9	4.0	2.4	1.7	5.4	2.9	3.1	3.4	2.8
En (Hy)	0.1	7.9	1.2	0.5	5.8	6.2	0.0	4.1	5.4	2.1	4.5
Fs (Hy)	0.0	6.4	0.7	0.3	6.4	5.9	0.0	2.4	3.2	1.2	5.2
Ol (Fo)	6.2	0.5	2.9	6.1	0.0	0.0	3.0	4.9	3.9	6.0	0.0
Ol (Fa)	3.6	0.4	1.7	4.3	0.0	0.0	3.0	3.1	2.5	3.9	0.0
Ilmenite:	8.3	6.0	5.4	5.3	6.0	6.2	5.9	5.3	5.3	5.4	4.7
Magnetite:	2.9	3.8	2.8	3.6	3.5	3.2	3.5	3.4	3.5	3.5	2.9
Apatite:	1.7	1.4	1.1	1.0	1.2	1.2	1.2	1.1	1.0	1.1	1.0
Total:	99.8	99.8	99.8	99.8	99.9	99.8	99.9	99.8	99.8	99.8	99.9

Notes: * = XRF analyses conducted after the cruise at the University of Massachusetts. Mg# = (Mg# = Mg/[Mg+Fe^{2+}]), where Fe^{2+} = 0.8 Fe total.

Table T10. X-ray diffraction (XRD) identification of alteration minerals from Hole 1141A.

Core, section, piece, interval (cm)	Description	Identification
183-1141A-		
14R-1, 19-20	White vesicle filling in completely altered basalt	Dolomite
15R-4, 125-127	White vesicle filling in completely altered basalt	Dolomite
16R-3, 48-49	Mineral in large vesicle in completely altered basalt	Quartz
17R-CC, 2-3	Mineral in large vesicle in completely altered basalt	Dolomite
18R-1 (Piece 15, 120-125)	Green mineral in vein	Calcite, albite, saponite
19R-1 (Piece 1, 1-3)	Green mineral in vein	Rhodocrosite(?)
19R-1 (Piece 6, 36-38)	Part of colloform vesicle	Rhodocrosite, calcite
20R-1 (Piece 6, 46-48)	Sheared vein mineral	Dolomite, siderite > calcite
20R-2 (Piece 11, 139-140)	Vein mineral	Dolomite, calcite
20R-2 (Piece 5, 65-67)	Vesicle filling	Dolomite
20R-3 (Piece 1, 1-2)	Fibrous while mineral in vein	Calcite >> dolomite
20R-3 (Piece 3, 15-16)	Ceramic-like vesicle filling	Siderite
20R-3 (Piece 3, 9-12)	Altered whole rock sample	Montmorillonite > saponite
22R-3, (Piece 3, 38-39)	Colloform vesicle filling	Quartz, siderite > calcite > dolomite

Table T11. Index properties data from Sites 1141 and 1142.

Core, section, interval (cm)	Depth (mbsf)	Water content (%)		Density (g/cm^3)			Porosity (%)	Void ratio
		Bulk	Dry	Bulk	Dry	Grain		
183-1141A-								
3R-2, 112-114	20.42	39.6	65.6	1.63	0.98	2.65	63.0	1.70
3R-3, 131-133	22.11	35.3	54.6	1.69	1.09	2.61	58.2	1.39
3R-4, 130-132	23.60	37.7	60.5	1.67	1.04	2.68	61.3	1.58
3R-5, 120-122	25.00	39.5	65.2	1.64	0.99	2.71	63.3	1.73
3R-6, 128-130	26.58	37.1	58.9	1.69	1.06	2.74	61.2	1.58
3R-7, 27-29	27.07	36.6	57.6	1.69	1.07	2.70	60.3	1.52
4R-1, 20-22	27.60	34.1	51.7	1.71	1.13	2.61	56.9	1.32
4R-2, 137-139	29.97	37.7	60.5	1.68	1.04	2.73	61.7	1.61
4R-3, 130-132	31.40	34.3	52.2	1.73	1.14	2.71	58.0	1.38
4R-4, 127-129	32.87	35.2	54.4	1.71	1.11	2.68	58.7	1.42
4R-6, 134-136	35.94	36.5	57.5	1.70	1.08	2.73	60.5	1.53
4R-7, 45-47	36.55	35.2	54.2	1.71	1.11	2.70	58.9	1.43
5R-1, 41-43	37.21	39.9	66.5	1.63	0.98	2.69	63.6	1.75
5R-2, 129-131	39.59	40.2	67.2	1.63	0.98	2.72	64.1	1.79
5R-3, 18-20	39.98	41.3	70.3	1.62	0.95	2.73	65.2	1.87
5R-4, 115-117	42.45	40.8	69.0	1.63	0.96	2.73	64.8	1.84
5R-5, 127-129	44.07	41.2	70.1	1.61	0.95	2.68	64.7	1.84
5R-6, 48-50	44.78	37.8	60.8	1.67	1.04	2.71	61.7	1.61
6R-1, 131-133	47.61	38.4	62.4	1.65	1.02	2.66	61.9	1.62
6R-2, 116-118	48.96	37.7	60.4	1.67	1.04	2.69	61.3	1.59
6R-3, 120-122	50.50	36.3	56.9	1.68	1.07	2.65	59.5	1.47
8R-1, 129-131	66.69	35.4	54.9	1.67	1.08	2.56	57.8	1.37
8R-3, 123-125	69.63	31.9	46.8	1.73	1.18	2.57	53.9	1.17
8R-4, 130-132	71.20	34.7	53.1	1.69	1.10	2.58	57.2	1.34
8R-5, 132-134	72.72	36.3	57.1	1.65	1.05	2.54	58.6	1.42
8R-6, 122-124	74.12	32.2	47.6	1.75	1.18	2.63	55.0	1.22
8R-7, 16-18	74.56	33.9	51.3	1.74	1.15	2.72	57.7	1.36
9R-1, 128-130	76.28	34.5	52.7	1.70	1.12	2.62	57.4	1.35
9R-2, 133-135	77.83	35.5	55.1	1.68	1.08	2.59	58.2	1.39
9R-3, 37-39	78.37	37.6	60.2	1.66	1.03	2.63	60.7	1.55
9R-4, 130-132	80.80	35.4	54.9	1.68	1.09	2.60	58.2	1.39
9R-5, 31-33	81.31	37.8	60.7	1.68	1.04	2.74	61.9	1.62
9R-6, 120-122	83.70	35.2	54.4	1.68	1.09	2.58	57.8	1.37
10R-1, 125-127	85.85	37.2	59.2	1.65	1.03	2.57	59.8	1.49
10R-2, 29-31	86.39	34.6	53.0	1.69	1.11	2.58	57.2	1.34
14R-1, 128-130	115.78	26.1	35.3	1.94	1.43	2.84	49.5	0.98
14R-2, 73-75	116.73	23.0	29.9	2.02	1.56	2.86	45.5	0.83
15R-1, 11-13	123.21	25.5	34.3	1.89	1.41	2.67	47.2	0.89
15R-1, 113-115	124.23	25.7	34.5	1.85	1.38	2.57	46.5	0.87
15R-2, 46-48	125.06	26.9	36.8	1.88	1.37	2.71	49.4	0.98
15R-3, 32-34	126.42	29.5	41.9	1.77	1.25	2.54	50.9	1.04
15R-4, 41-43	128.01	28.3	39.4	1.78	1.28	2.52	49.3	0.97
15R-5, 94-96	130.04	30.8	44.5	1.76	1.22	2.60	53.0	1.13
16R-1, 13-15	132.93	24.7	32.8	1.98	1.49	2.87	47.9	0.92
16R-1, 133-135	134.13	29.1	41.1	1.83	1.30	2.71	52.1	1.09
16R-2, 39-41	134.69	21.4	27.2	2.03	1.60	2.77	42.4	0.74
16R-3, 50-52	135.80	14.4	16.8	2.29	1.96	2.90	32.2	0.48
19R-1, 129-131	158.09	6.0	6.3	2.52	2.37	2.78	14.7	0.17
19R-2, 84-86	159.12	4.6	4.8	2.65	2.53	2.87	11.8	0.13
21R-1, 10-12	166.50	8.8	9.7	2.46	2.25	2.85	21.2	0.27
21R-2, 6-8	167.77	4.2	4.4	2.64	2.53	2.84	10.8	0.12
21R-3, 66-68	169.70	7.7	8.4	2.52	2.32	2.87	19.0	0.24
22R-3, 35-37	174.43	4.7	5.0	2.60	2.48	2.82	12.0	0.14
23R-1, 3-5	176.03	2.0	2.1	2.64	2.58	2.73	5.2	0.06
23R-2, 36-38	177.68	0.9	0.9	2.86	2.83	2.90	2.5	0.03
23R-3, 34-36	179.18	3.9	4.1	2.57	2.47	2.74	9.9	0.11
23R-4, 32-34	180.60	2.4	2.4	2.73	2.67	2.85	6.3	0.07
24R-2, 6-8	182.30	1.0	1.0	2.82	2.79	2.87	2.8	0.03
24R-3, 85-87	184.54	6.4	6.8	2.60	2.43	2.90	16.1	0.19
183-1142A-								
2R-1, 28-30	91.28	0.9	0.9	2.87	2.84	2.92	2.6	0.03
3R-1, 39-41	99.09	5.9	6.3	2.60	2.45	2.89	15.1	0.18
5R-1, 107-109	114.17	11.5	13.0	2.53	2.24	3.13	28.4	0.40
9R-3, 33-35	135.56	3.6	3.7	2.70	2.60	2.87	9.4	0.10
10R-1, 38-40	137.48	2.9	2.9	2.62	2.55	2.75	7.3	0.08

Note: This table is also available in **ASCII format.**

Table T12. Compressional wave velocity of discrete measurement, Site 1141. (See table note. Continued on next page.)

Core, section, interval (cm)	Depth (mbsf)	Direction	Velocity (m/s)
183-1141A-			
3R-2, 112	20.42	LX	1971
3R-3, 35	21.15	LX	1948
3R-3, 131	22.11	LX	1905
3R-4, 45	22.75	LX	1897
3R-4, 129	23.59	LX	1937
3R-5, 49	24.29	LX	1882
3R-5, 121	25.01	LX	1896
3R-6, 44	25.74	LX	1910
3R-6, 129	26.59	LX	1971
3R-7, 28	27.08	LX	1911
4R-1, 21	27.61	LX	1963
4R-2, 39	28.99	LX	1867
4R-2, 128	29.88	LX	1871
4R-3, 128	31.38	LX	1871
4R-3, 132	31.42	LX	1856
4R-4, 38	31.98	LX	1863
4R-4, 128	32.88	LX	1828
4R-5, 41	33.51	LX	1823
4R-5, 112	34.22	LX	1815
4R-6, 33	34.93	LX	1836
4R-6, 135	35.95	LX	1834
4R-7, 46	36.56	LX	1869
5R-1, 43	37.23	LX	1873
5R-1, 128	38.08	LX	1862
5R-2, 54	38.84	LX	1872
5R-2, 130	39.60	LX	1892
5R-3, 19	39.99	LX	1885
5R-4, 17	41.47	LX	1843
5R-4, 118	42.48	LX	1825
5R-5, 44	43.24	LX	1812
5R-5, 128	44.08	LX	1820
5R-6, 50	44.80	LX	1843
6R-1, 54	46.84	LX	1804
6R-1, 133	47.63	LX	1796
6R-2, 33	48.13	LX	1854
6R-2, 117	48.97	LX	1809
6R-3, 54	49.84	LX	1820
6R-3, 122	50.52	LX	1813
8R-1, 63	66.03	LX	1807
8R-1, 123	66.63	LX	1777
8R-3, 35	68.75	LX	1815
8R-3, 123	69.63	LX	1814
8R-4, 129	71.19	LX	1801
8R-5, 44	71.84	LX	1840
8R-5, 130	72.70	LX	1896
8R-6, 48	73.38	LX	1900
8R-6, 123	74.13	LX	1897
8R-7, 16	74.56	LX	1861
9R-1, 23	75.23	LX	1856
9R-1, 129	76.29	LX	1873
9R-2, 17	76.67	LX	1891
9R-2, 134	77.84	LX	1902
9R-3, 39	78.39	LX	1868
9R-3, 125	79.25	LX	1827
9R-4, 14	79.64	LX	1856
9R-4, 132	80.82	LX	1836
9R-5, 128	82.28	LX	1885
9R-6, 25	82.75	LX	1842
9R-6, 122	83.72	LX	1669
9R-7, 35	84.35	LX	1824
10R-1, 50	85.10	LX	1840
10R-1, 126	85.86	LX	1905
10R-2, 31	86.41	LX	1961
14R-1, 51	115.01	LX	1723
14R-1, 112	115.62	LX	1937
14R-1, 130	115.80	LX	2084
14R-2, 30	116.30	LX	1994
14R-2, 75	116.75	LX	2353
15R-1, 12	123.22	CZ	2213
15R-2, 47	125.07	CZ	2035
15R-4, 42	128.02	CZ	2135
15R-5, 95	130.05	CZ	2013
16R-1, 16	132.96	CZ	2321
16R-1, 134	134.14	CZ	2099
16R-2, 40	134.70	CZ	2494
16R-3, 51	135.81	CZ	3422
17R-1, 10	142.50	X	4293
17R-1, 22	142.62	X	4138
17R-1, 32	142.72	X	4517
17R-1, 66	143.06	X	2937
17R-CC, 36	152.00	X	4386
18R-1, 20	152.20	X	3614
18R-1, 80	152.80	X	4591
18R-1, 135	153.35	X	4359
18R-2, 5	153.55	X	5751
18R-2, 14	153.64	X	5945
18R-2, 20	153.70	X	6388
18R-2, 29	153.79	X	5788
19R-1, 128	158.08	X	4808
19R-1, 130	158.10	MX	5079
19R-1, 136	158.70	X	5049
19R-2, 6	158.34	X	6330
19R-2, 15	158.43	X	5100
19R-2, 23	158.51	X	4689
19R-2, 34	158.62	X	4880
19R-2, 36	158.64	MX	4939
19R-2, 55	158.83	X	4692
19R-2, 67	158.95	MX	4677
19R-2, 68	158.96	X	4821
19R-2, 85	159.13	MX	5031
19R-2, 95	159.23	X	4917
19R-2, 105	159.33	X	5339
19R-2, 113	159.41	X	4838
19R-2, 115	159.43	MX	5177
19R-2, 125	159.53	X	3991
20R-1, 135	162.95	X	2690
20R-1, 142	163.02	X	2754
20R-2, 50	163.56	X	2818
20R-2, 60	163.66	X	2839
20R-2, 120	164.26	X	3596
20R-2, 140	164.46	X	3021
20R-3, 20	165.00	X	3196
21R-1, 8	166.48	X	4484
21R-1, 10	166.50	MX	4896
21R-1, 21	166.61	X	5076
21R-1, 31	166.71	X	5028
21R-1, 65	167.05	X	5410
21R-1, 80	167.20	X	5424
21R-1, 98	167.38	X	5623
21R-1, 115	167.55	X	5978
21R-2, 25	167.96	X	5442
21R-2, 30	168.01	MX	5086
21R-2, 86	168.57	X	5246
21R-2, 101	168.72	X	5041
21R-2, 124	168.95	X	5464
21R-3, 12	169.16	X	5709
21R-3, 29	169.33	X	5316
21R-3, 42	169.46	X	5137
21R-3, 54	169.58	X	4774
21R-3, 61	169.65	X	4455
21R-3, 65	169.69	MX	4540
21R-3, 75	169.79	X	4276
21R-3, 83	169.87	X	4472
21R-3, 95	169.99	X	5505
22R-3, 22	174.30	X	4817

Table T12 (continued).

Core, section, interval (cm)	Depth (mbsf)	Direction	Velocity (m/s)
22R-3, 32	174.40	X	4833
22R-3, 36	174.44	MX	4913
22R-3, 48	174.56	X	4701
22R-3, 60	174.68	X	5016
22R-3, 70	174.78	X	5160
22R-3, 84	174.92	X	5230
22R-3, 115	175.23	X	5350
22R-3, 135	175.43	X	5217
23R-1, 4	176.04	MX	5944
23R-1, 8	176.08	X	5957
23R-1, 20	176.20	X	5786
23R-1, 33	176.33	X	5715
23R-1, 43	176.43	X	5916
23R-1, 125	177.25	X	5872
23R-2, 8	177.40	X	6149
23R-2, 20	177.52	X	6042
23R-2, 37	177.69	MX	6580
23R-2, 40	177.72	X	6022
23R-2, 66	177.98	X	6621
23R-2, 80	178.12	X	6267
23R-2, 120	178.52	X	6013
23R-2, 144	178.76	X	6439
23R-3, 28	179.12	X	5398
23R-3, 29	179.13	MX	4947
23R-3, 41	179.25	X	5240
23R-3, 57	179.41	X	6018
23R-3, 128	180.12	X	5122
23R-4, 6	180.34	X	5703
23R-4, 20	180.48	X	5426
23R-4, 33	180.61	MX	5740
23R-4, 56	180.84	X	5648
23R-4, 67	180.95	X	5940
24R-1, 4	180.84	X	6902
24R-1, 40	181.20	X	6436
24R-1, 50	181.30	X	6128
24R-1, 75	181.55	X	6287
24R-1, 100	181.80	X	5925
24R-1, 120	182.00	X	6132
24R-1, 130	182.10	X	5335
24R-1, 140	182.20	X	5362
24R-2, 20	182.44	X	6753
24R-2, 56	182.80	X	5671
24R-2, 94	183.18	X	6038
24R-3, 5	183.74	MX	5660
24R-3, 10	183.79	X	6031
24R-3, 73	184.42	X	4482
24R-3, 86	184.55	MX	4700

Notes: Type of samples is denoted by prefix: L = split-core section with core liner, C = oriented cubes, M = oriented minicore, and no prefix = split core sections without core liner. The directions of the velocity measurements are represented by X (into the core) and Z (along the core). This table is also available in **ASCII format.**

Table T13. Compressional wave velocity of discrete measurements, Site 1142.

Core, section, interval (cm)	Depth (mbsf)	Direction	Velocity (m/s)
183-1142A-			
2R-1, 14	91.14	X	6566
2R-1, 43	91.43	X	6212
2R-1, 55	91.55	X	6290
2R-1, 102	92.02	X	6170
2R-1, 120	92.20	X	6684
2R-2, 15	92.64	X	6320
2R-2, 33	92.82	X	6917
3R-1, 46	99.16	X	3635
3R-1, 54	99.24	X	3272
3R-1, 60	99.30	X	3453
5R-1, 2	113.12	X	2921
5R-1, 35	113.45	X	3023
5R-1, 50	113.60	X	3099
5R-1, 78	113.88	X	2996
5R-1, 100	114.10	X	3034
5R-1, 123	114.33	X	3242
5R-1, 129	114.39	X	3010
5R-1, 146	114.56	X	3211
5R-2, 14	114.73	X	3181
5R-2, 31	114.90	X	3126
5R-2, 40	114.99	X	2839
5R-2, 70	115.29	X	3133
7R-1, 40	123.00	X	2940
7R-1, 108	123.68	X	3128
7R-1, 123	123.83	X	2888
7R-2, 36	124.46	X	3339
9R-1, 50	132.80	X	3598
9R-1, 65	132.95	X	4218
9R-1, 80	133.10	X	4884
9R-1, 89	133.19	X	5286
9R-1, 123	133.53	X	5396
9R-1, 134	133.64	X	4610
9R-2, 55	134.35	X	4034
9R-2, 64	134.44	X	5319
9R-2, 83	134.63	X	4741
9R-2, 94	134.74	X	4582
9R-2, 114	134.94	X	4865
9R-2, 130	135.10	X	5204
9R-2, 140	135.20	X	4793
9R-3, 13	135.36	X	5227
9R-3, 26	135.49	X	5202
9R-3, 40	135.63	X	5297
9R-3, 59	135.82	X	5351
9R-3, 85	136.08	X	5260
9R-3, 97	136.20	X	6369
9R-3, 115	136.38	X	5405
9R-3, 125	136.48	X	5282
9R-3, 135	136.58	X	5436
9R-3, 148	136.71	X	5015
9R-4, 10	136.83	X	4988
9R-4, 18	136.91	X	4571
9R-4, 26	136.99	X	4908
10R-1, 18	137.28	X	4865
10R-1, 45	137.55	X	5041
10R-1, 74	137.84	X	4591
10R-1, 82	137.92	X	4493
10R-1, 90	138.00	X	4429
10R-1, 110	138.20	X	4387
10R-1, 120	138.30	X	4268
10R-1, 140	138.50	X	4482
10R-2, 5	138.62	X	4130
10R-2, 38	138.95	X	4824
10R-2, 53	139.10	X	4424
10R-2, 68	139.25	X	3825
10R-2, 73	139.30	X	3903
10R-2, 85	139.42	X	3907
10R-2, 100	139.57	X	4062
10R-2, 107	139.64	X	4093
10R-2, 125	139.82	X	3789
10R-2, 130	139.87	X	5783
10R-2, 140	139.97	X	4676
10R-3, 12	140.17	X	4550
10R-3, 20	140.25	X	4290
10R-3, 40	140.45	X	4734
10R-3, 44	140.49	X	4627
10R-3, 52	140.57	X	4669
10R-3, 60	140.65	X	4255
10R-3, 67	140.72	X	4460
10R-3, 72	140.77	X	4378

Note: The velocity measurements are on split-core sections without core liner, and the direction is X (into the core). This table is also available in **ASCII format.**

Table T14. Thermal conductivity values for Sites 1141 and 1142.

Core, section, interval (cm)	Depth (mbsf)	Thermal conductivity (W/[m·K])
183-1141A-		
4R-3, 75	30.85	1.28
5R-3, 75	40.55	1.13
6R-3, 75	50.05	1.09
8R-3, 75	69.15	1.12
9R-3, 75	78.75	1.07
10R-2, 30	86.40	0.98
18R-2, 10-24	153.67	1.54
19R-1, 5-18	156.92	1.66
19R-2, 70-86	159.06	1.74
20R-1, 99-120	162.70	1.33
20R-3, 11-28	164.73	1.15
21R-3, 52-68	169.64	1.48
22R-2, 139-150	174.03	1.47
23R-2, 30-40	177.67	1.80
23R-2, 140-150	178.77	1.64
23R-4, 2-9	180.34	1.57
24R-1, 20-35	181.08	1.76
24R-2, 14-27	182.45	1.75
24R-3, 1-14	183.77	1.88
183-1142A-		
2R-1, 92-105	91.99	1.71
2R-2, 9-17	92.62	1.74
3R-1, 56-66	99.31	1.49
5R-1, 119-125	114.32	1.80
6R-2, 28-40	119.60	2.37
7R-1, 44-52	123.08	1.98
9R-1, 58-67	132.93	1.42
10R-1, 76-86	137.91	1.54

Note: This table is also available in **ASCII format.**

Table T15. Carbon, nitrogen, sulfur, and hydrogen analyses of sediments and altered volcanic rocks from Site 1141.

Core, Type, Section	Depth (mbsf)	$CaCO_3$ (wt%)	IC (wt%)	OC (wt%)	N (wt%)	S (wt%)	H (wt%)
183-1141A-							
1R-1	0.88-0.89	94.54	11.35	0	0.01	0	0.07
2R-CC	8.51-8.52	95.66	11.48				
3R-1	18.69-18.70	95.93	11.52				
5R-1	37.69-37.70	95.68	11.49	0	0.01	0.01	0.03
6R-1	47.19-47.20	95.01	11.41				
9R-1	75.89-75.90	96.14	11.54	0	0.01	0.02	0.02
14R-1	115.39-115.40	0.37	0.05	0.02	0.00	0	0.71
15R-1	123.99-124.00	1.98	0.24	0	0.01	0	0.74

Notes: Samples from Sections 183-1141A-1R-1 through 9R-1 are sediments; samples from Sections 14R-1 and 15R-1 are highly altered basalts. This table is also available in **ASCII format.**